DOCTOR OF PHILOSOPHY

Pipe-Soil Interaction on a Clay Seabed

Morrow, Damian

Award date:
2016

School of Engineering, Physics and Mathematics
Department of Civil Engineering

Pipe-Soil Interaction on a Clay Seabed

Damian Morrow

A dissertation submitted for the
degree of Doctor of Philosophy
to the University of Dundee
April 2016

Declaration

This is to certify that the candidate is the author of the thesis; that, unless otherwise stated, all references cited have been consulted by the candidate; that the work of which the thesis is a record of has been done by the candidate, and that it has not been previously accepted for a higher degree.

Damian R Morrow (candidate)

Dr Andrew Brennan (supervisor)

Acknowledgements

While undertaking this research project I have had the support of two supervisors, Dr Fraser Bransby for the first period of this study and Dr Andrew Brennan for the later period. I would like to acknowledge the support of both supervisors and thank them for their suggestions and review of analysis results throughout the course of this study. I would also like to thank Andrew for his review of this thesis prior to submission.

This research project was undertaken on a part time basis in conjunction with consultancy work in offshore geotechnics. I would like to thank the numerous people I have worked with other this period for their understanding and encouragement, as well as making it easier to undertake this study then otherwise could have been the case. In a wider sense, I would also like to thank a large number of people I have worked with in the offshore industry over the years colleagues, mentors, clients, etc, for making this an interesting industry to work in and an area where I wanted to undertake research.

I would like to thank my family and friends for their interest and encouragement.

Finally I would like to thank the various students and staff who I have met during my period studying at the University of Dundee. I owe them thanks, whether it was for an interesting discussion, on, or off topic, or just some friendly chat and someone to head out for a drink with.

Abstract

Subsea pipelines form an integral part of the infrastructure associated with offshore oil and gas developments. These pipelines fulfil a range of functions from linking extraction wells to other subsea infrastructure to transporting products onshore, or to a central processing facility. Ancillary pipelines may also be present for gas or water injection to the reservoir or transporting additives.

Pipelines are typically installed directly onto the seabed and, in the absence of significant drivers to undertake burial operations, they may remain on the seabed for the remainder of their design life. This is typically the case for deepwater developments. Subsea pipelines are subjected to a wide range of load cases including, self weight, installation loads, thermal and pressure driven expansion and hydrodynamic loading. Design of pipeline systems to accommodate these load cases requires an understanding of pipe-soil interaction.

This thesis reports the results of a research study investigating pipe-soil interaction on a clay seabed, as relevant to the design of subsea pipeline systems. This study has utilised numerical analysis techniques based on the finite difference code FLAC to investigate a range of problem definitions. These problem definitions include pipelines subject to both vertical loading (V) and combined vertical and horizontal (V-H) loading. Factors such as variation in interface conditions, large strain and large displacement effects, soil unit weight effects and variation in shear strength conditions were considered in these problem definitions. Reliability based analysis techniques have also been used to investigate both V and V-H loading problem definitions.

The analyses and investigations undertaken as part of this study generally achieved the following; reproduction and validation of earlier research with additional interpretation, extension of problem definitions to deeper pipeline embedment depths and investigation of pipe-soil interaction problem definitions that have not previously been considered. Reliability based analysis techniques have also provided some interesting insights into the impact of soil shear strength variation as well as providing a fundamental link between safety factors and probability of failure. Application to design practice of this, and similar studies, has been considered as part of this thesis and potential areas for future research have also been suggested.

Keywords: pipe-soil interaction, subsea pipelines, clay, numerical analysis.

Contents

List of Figures

List of Tables

Notation

Note; within Chapter 2 (Literature Review) notation has been modified from that used in the original references. These changes have been made to improve clarity within this chapter, as well as maintaining a consistent system of notation throughout this study and thesis.

A	Fitting coefficient (correlation for pipeline penetration under V load)
A_c	Pipeline contact area e.g. Brennodden and Stokkeland (1992)
a	Fitting coefficient (for V_{max} correlation)
B	Fitting coefficient (correlation for pipeline penetration under V load)
b	Fitting coefficient (for V_{max} correlation)
C_{lat}	Empirical lateral resistance coefficient, see Dendani and Jaeck (2007a)
c	Fitting coefficient (for H_{max} correlation)
CoV	Coefficient of variation
CoV_{Vmax}	Coefficient of variation of V_{max}
c_v	Coefficient of consolidation
D	Diameter of a pipeline - Note this convention refers to the outside diameter (OD) of the pipeline including the thickness of any coating material
d	Fitting coefficient (for H_{max} correlation)
E	Young's modulus
E_a	Fitting coefficient
E_b	Fitting coefficient
$F_{S\mu}$	Mean factor of safety
F_v	Vertical force corrected for displaced soil weight e.g. Brennodden and Stokkeland (1992)
F_a	Fitting coefficient
F_b	Fitting coefficient
f	Fitting coefficient for parabolic skew parameter correlation e.g. $\beta 1$
G	Shear modulus

$\hat{G}$	Dimensionless group $\hat{G} = s_u/(D.\gamma')$ e.g. Verley and Lund (1995)
H	Horizontal load
H_L	Horizontal load within a local coordinate system, sloping seabed.
H_{max}	Maximum capacity under horizontal loading
h	Fitting coefficient for parabolic skew parameter correlation e.g. $\beta 1$
h_0	H_{max} to V_{max} ratio e.g. Hodder and Cassidy (2010)
I_F	Fragility index
K	Bulk modulus
k	Gradient of shear strength increase with depth e.g. for a linear increasing shear strength gradient
k_{max}	Empirical lateral resistance coefficient e.g. Brennodden and Stokkeland (1992)
k_n	Pipe-soil interface normal stiffness
k_s	Pipe-soil interface shear stiffness
L	Pipeline length
M	Moment load
MC	Monte Carlo analysis method
N	Number of simulation e.g. MC analysis
N_c	Soil shear strength bearing capacity factor
N_{cV}	Soil shear strength resistance factor for vertical loading e.g. Merifield et al. (2009)
N_{cH}	Soil shear strength resistance factor for horizontal loading e.g. Merifield et al. (2009)
N_F	Number of failures within a number of simulations e.g. MC analysis
N_{swV}	Soil unit weight resistance factor for vertical loading e.g. Merifield et al. (2009)
N_{swH}	Soil unit weight resistance factor for horizontal loading e.g. Merifield et al. (2009)
P_F	Probability of Failure
R	Resistance to displacement
R_H	Horizontal component of resistance to displacement
$R_{H,residual}$	Residual horizontal resistance to displacement e.g. Lee et al. (2012)
R_{SW}	Soil unit weight component of resistance

R_V	Vertical component of resistance to displacement
$\hat{S}$	Dimensionless group $\hat{S} = V/(D.s_u)$ e.g. Verley and Lund (1995)
S_s	Softening Index, see Cheuk (2005)
S_t	Soil sensitivity i.e. soil undrained shear strength divided by the soil remoulded undrained shear strength.
s_u	Soil undrained shear strength
s_{u0}	Soil undrained shear strength at seabed/mudline i.e. z=0
$S_{u,1D}$	Soil undrained shear strength at a depth of one pipeline diameter
s_{uzp}	Soil undrained shear strength at pipeline embedment depth z_p
$s_{u\mu}$	Mean soil undrained shear strength, with respect of a statistical distribution of shear strength within reliability based analysis
s_{uct}	Soil shear strength associated with the peak of a shear strength crust
s_{ui}	Soil-pipe interface undrained shear strength
$s_{u,ave}$	Average shear strength, see Dendani and Jaeck (2007a)
$s_{u,operational}$	Operational shear strength, see Cheuk (2005) and Equation [2.6]
$s_{u,peak}$	Peak shear strength, see Cheuk (2005)
u	Horizontal displacement
V	Vertical load
V_0	Vertical load axis interaction for current plastic potential e.g. Hodder and Cassidy (2010)
V_L	Vertical load within a local coordinate system, sloping seabed.
V_{max}	Maximum capacity under vertical loading
V_S	Volume of soil e.g. displaced by a given pipeline embedment
V_{S_add}	Additional soil volume e.g. from extend solution Equation [4.13]
V_{S_tot}	Total volume of soil displaced by a pipeline
V_t	Vertical uplift capacity e.g. Hodder and Cassidy 2010
V1, V2	Vertical reference loads e.g. for calculation of I_F, Equation [6.1]
V_2/V_1	Overloading ratio, see White and Dingle (2011)
v	Vertical displacement
x	Horizontal direction within numerical analysis or a graph axis

y	Vertical direction within numerical analysis or a graph axis
z	Depth
z_p	Pipeline embedment depth
z_c	Depth range/thickness of shear strength crust
z_{cp}	Depth of shear strength crust peak
$z_{p,initial}$	Initial pipeline embedment prior to lateral displacement, see White and Dingle (2011)
$\hat{w}$	$\hat{w} = z/D$
ψ	Angle of seabed slope
α	Pipeline roughness e.g. Merifield et al. (2008) 1 = rough 0 = smooth
Γ	Angle of sector of a circle
Γ_r	Angle of sector of a circle in radians
β	Parabolic skew parameter for V-H stability envelopes
β_R	Reliability Index
β_1	Parabolic skew parameter for V-H stability envelopes
β_2	Parabolic skew parameter for V-H stability envelopes
β_m	Empirical lateral resistance coefficient e.g. Brennodden and Stokkeland (1992)
γ'	Effective soil unit weight e.g. submerged unit weight
Δ_z	Finite difference mesh zone size
Δ_δ	Displacement distance
δ	Pipeline displacement angle
δ_L	Pipeline displacement angle in local coordinate space e.g. sloping seabed.
δ_{LS}	Pipeline displacement angle in V-H load space
δ_{SW}	Angle of soil wedge for soil unit weight equation for <0.5D
θ	One half of pipeline penetration arc length - arsin(1-z/r) - e.g. Brennodden and Stokkeland (1992)
ν	Poisson's ratio
ρ_S	Soil submerged density

σ'_n	Normal stress on a pipe-soil interface.
σ_{Vmax}	Standard deviation of V_{max}
$\sigma_1,\sigma_2,\sigma_3$	Major, intermediate and minor stress.
$\bar{\upsilon}$	Displacement velocity
$\bar{\upsilon}_L$	Displacement velocity within a local coordinate system, sloping seabed.
μ	Friction coefficient e.g. $\mu = H/V$
μ_{Vmax}	Mean V_{max}
ϕ	Standard normal cumulative function

1 Introduction

1.1 Background

Subsea pipelines play an important role in the development of offshore oil and gas fields with pipeline systems forming an integral part of the subsea infrastructure required for this development. A network of infield pipelines link extraction wells and subsea structures with larger diameter export pipelines transporting products onshore, or to a central offshore facility such as an FPSO (Floating Production Storage and Offloading vessel) or a platform. As part of the pipeline system ancillary pipelines may also be present, providing water or gas injection to the reservoir to improve product recovery. Additional ancillary pipelines can also be used to transport additives for functions such as dewatering or wax inhibition.

During installation subsea pipelines are typically laid directly onto to the seabed. In some cases there may be stability, protection or insulation requirements and the pipeline will be buried with various trenching tools (e.g. Finch et al., 2000, Morrow and Larkin, 2007). However, in the absence of drivers for burial the pipeline will remain on the seabed for the course of its design life, as is typically the case in deep water developments (Bruton et al., 2006, Perinet and Fraser, 2006).

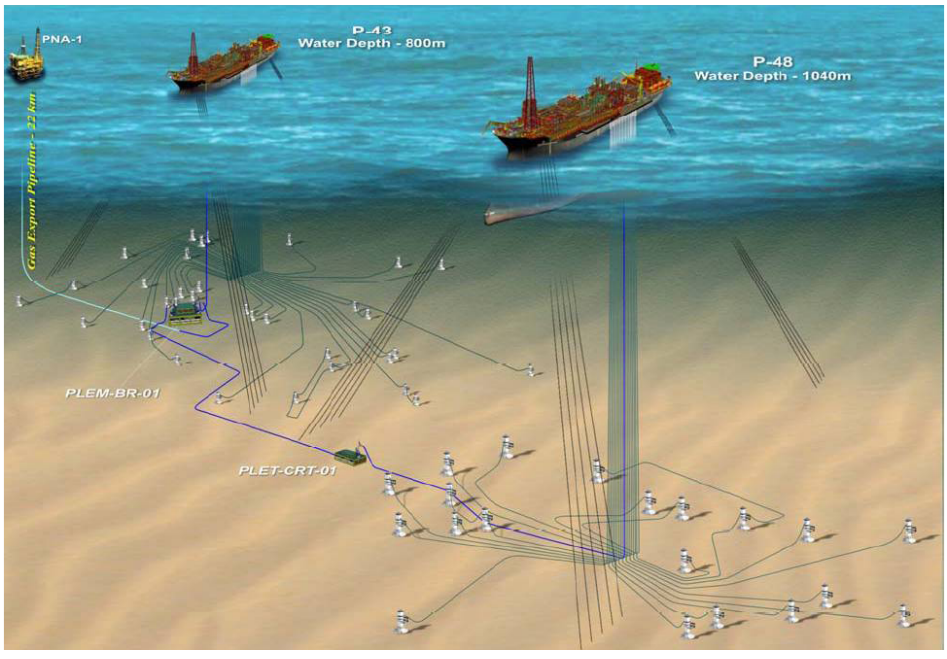

Figure 1.1 *- A schematic field layout for the Barracuda and Caratinga development, Brazil, South America (Messias-Dos-Santos, 2005).*

Figure 1.1 shows the Barracuda and Caratinga projects situated offshore Brazil, South America, an example of the large amount of pipeline infrastructure associated with a typical deep water development. These two Brazilian projects combined have 415 km of pipeline and 236 km of umbilical (Messias-Dos-Santos, 2005). Another example is the Greater Plutonio development situated in a water depth of 1500 m, offshore Angola, West Africa, see Figure 1.2. Greater Plutonio has over 150 km of pipelines and 107 km umbilical (Oldfield, 2008).

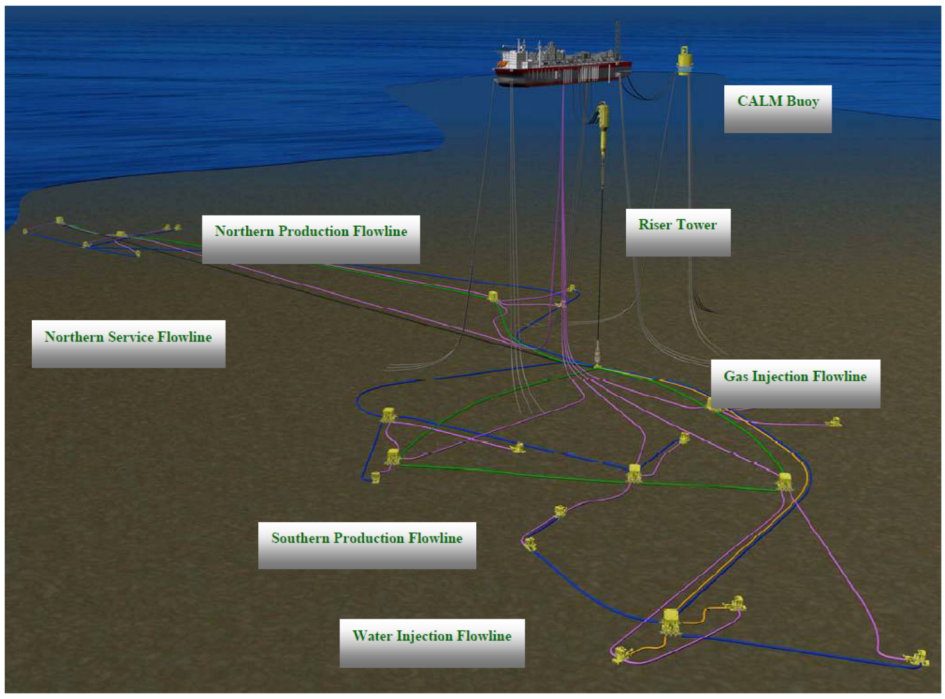

Figure 1.2 *- Schematic of the Greater Plutonio field architecture, offshore Angola, West Africa (Campbell, 2008).*

During installation and through the course of their design life, pipelines resting on the seabed are subjected to a range of load cases arising from both internal and externally sources. This loading will generally fall into one of the following categories;

- Self weight loading
- Installation loads
- Thermal and pressure driven expansion
- Hydrodynamic loading

These load cases may occur in isolation or in combination and may be temporary or sustained over a period of time. Loading may also vary over time, for example

with flooding of the pipeline, changes in operating conditions, or increases in hydrodynamic loading during storm events. Understanding how a pipeline behaves under these load cases and designing pipeline systems that can accommodate these load cases requires an understanding of pipe-soil interaction, the interaction between the pipeline and the seabed that it rests upon and in many cases penetrates into.

Perhaps the most obvious load case on a pipeline is self weight loading on a flat seabed. Although this appears to represent a relatively simple case there are some additional complexities, primarily arising from the cylindrical geometry of the pipeline and the variable contact area during penetration into the seabed. A clear difference when comparing a pipeline subjected to self weight loading and a classical foundation analysis is the lack of control or certainty over the geometry of the problem, with some degree of penetration into the seabed a common feature (White and Cathie, 2010).

For some oil and gas developments sections of the pipeline system, such as the export pipeline, may have to be installed on a sloping seabed, there may even be cases when whole development area is located on a sloping seabed. Figure 1.3 shows the example of the West Nile Delta and the challenges associated with development on a steep delta front (Evans et al., 2007). For this development area water depths range from 100 m to over 1000 m over a short distance, with associated steep seabed slopes. The active delta front is also associated with very soft normally consolidated clay soils.

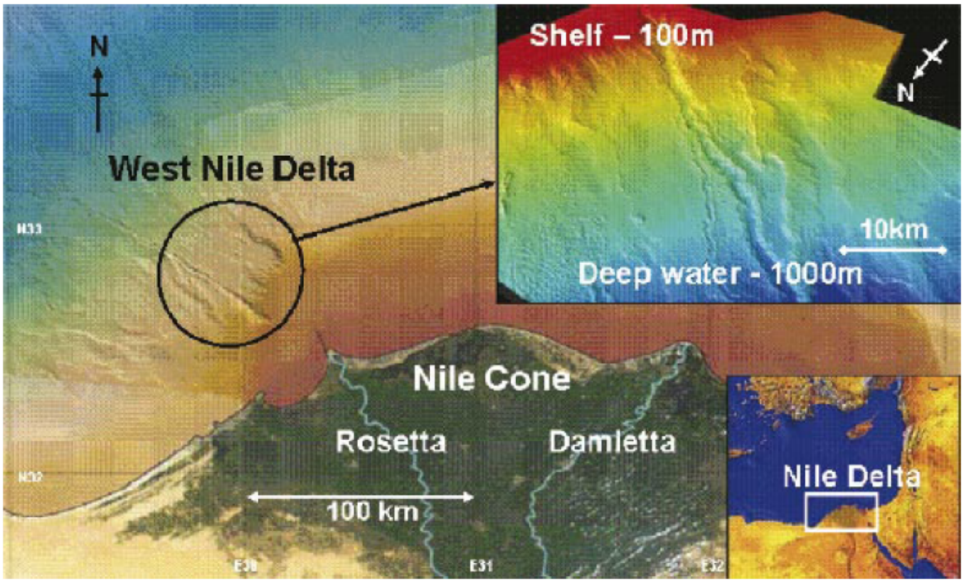

Figure 1.3 *- The West Nile Delta development area (Evans et al., 2007).*

During pipeline installation forces associated with the motion of the pipe-lay vessel can be transmitted down the pipeline catenary to a section of the pipeline on the seabed. Vertical loading in excess of the pipeline self weight can occur, with the loading often expressed as a multiple of the pipeline's self weight. Horizontal loading can also be transmitted to the pipeline by lateral movement of the lay-vessel, in particular when the pipeline is installed on a curved lay route. (Lund, 2000, Palmer, 2008)

Pipelines are typically laid at, or close to, ambient sea-bottom temperature. Following commissioning of the pipeline system these pipelines are required to transport high pressure and high temperature liquids or gasses. This temperature and pressure increase, from the installation conditions to operating conditions, results in expansion of the pipeline material e.g. steel. Radially and over a short section of pipeline this expansion may be relatively insignificant. However, axially, along the pipeline route, this expansion can be cumulative resulting in large displacements and, or, large constrained forces. Depending on the expansion characteristics of the pipeline and pipe-soil interaction this thermal and pressure driven expansion may result in pipeline walking or lateral buckling, both of which are potentially undesirable (Carr et al., 2006, Parsloe et al., 2006). Thermal and pressure driven expansion can also be considered within the context of the trend towards increasing wellhead temperature and pressure with the development of high pressure high temperature (HPHT) fields. Loading applied to pipelines due to thermal and pressure driven expansion is considered by some to be one of the biggest challenges in deep water field development (Perinet and Fraser, 2006). Mebarkia (2006) provides an overview of some of the pipe-soil interaction related challenges faced in developing a deepwater HPHT fields.

Assessment of the stability of a pipeline under hydrodynamic loading is a standard requirement during the design of a pipeline system. This assessment requires consideration of the loads applied to a pipeline by waves and currents in conjunction with the ability of the pipeline to resist these forces. The pipeline penetration into the seabed and the pipeline's subsequent resistance to horizontal displacement are fundamental aspects of this stability assessment. Pipeline penetration into the seabed plays a dual role, both increasing lateral resistance and reducing hydrodynamic loading due to a reduction in the area of pipeline above seabed level. This dual role increases the importance of being able to accurately assess penetration of a pipeline under vertical loading. (Zeitoun et al., 2008, Tornes et al., 2009)

While the focus of this study is on rigid pipelines within the oil and gas industry, there are a range other broadly similar cylindrical objects in comparable environments. This includes other applications in the oil and gas industry along with potential application within other industries, such as utility infrastructure and renewable energy applications. Within subsea oil and gas developments there is a range of other infrastructure with similarities to pipelines, for example electro-hydraulic umbilical's, flexible pipelines, jumpers and spools. Smaller near shore pipelines, or pipelines in lakes and rivers, may also be used by the utility industries. Offshore power cables also have comparable geometries. In addition to applications in oil and gas industries, power cables are subject to an increasing focus with current developments in offshore renewable energy. There may also be analogies in the telecommunications industry, with offshore telecom cables. While the research presented here is not necessarily fully applicable to these other applications it may provide a reasonable framework to progress further research in these fields.

As noted in this chapter, and further detailed in the literature summarised in Chapter 2, pipe-soil interaction is an important aspect of subsea pipeline design for the pipeline systems used in the offshore oil and gas industry. This study has investigated pipe-soil interaction on clay seabed using numerical analysis techniques, extending understanding of a number of aspects of pipe-soil interaction relevant to a range of pipeline design issues. Guidance is provided on the application of these findings to design practice including the use of reliability based analysis techniques.

1.2 Study Aims and Objectives

The aim of this study is to investigate pipe-soil interaction for sub-sea pipelines resting on a clay seabed, improving understanding of pipeline behaviour for a wide range of conditions relevant to the design of subsea pipeline systems. This will be undertaken using numerical and reliability based analysis techniques. The principal objectives of this study are;

- Provide a summary of previous research related to pipe-soil interaction on a clay seabed.
- Investigate pipelines subjected to vertical loading. Initial analyses focus on problems that have been investigated to some extent by previous researchers, before extending analyses into areas such as a deeper

pipeline embedment, the effect of pipe-soil interface conditions and the influence of inhomogeneous shear strength conditions, such as linear increasing shear strength gradients and shear strength crusts.

- Investigate the behaviour of pipelines subjected to combined vertical and horizontal loading, as described by the maximum horizontal capacity and stability envelopes in vertical and horizontal load space. Initial analyses focus on problems where some previous research has been undertaken, prior to extending analyses into areas such as deeper pipeline embedment, the effect of linear increasing shear strength gradients and the influence of a seabed slope. Large displacement behaviour is also considered.

- Place analysis of pipe-soil interaction on a clay seabed into a reliability based analysis framework. This increases the applicability to design practice of the correlations and observations produced as part of this study and links safety factors for a selection of design problems with a probability of failure.

- Review how the findings of this study can be incorporated into design practice.

- Summarise the conclusions of this study and provide suggestions on potential areas for future research.

1.3 Thesis Structure

The previous sections in this chapter have provided background information on this study and a summary of the study objectives; this introductory chapter will close by providing an overview of the structure of this thesis and the content of the following chapters.

Chapter 2 Literature Review - provides further introduction and background to pipe-soil interaction on clay seabed with a literature review of research of this and related topics. This literature review is divided into a number of subsections addressing different areas of the literature. These subsections include Physical Modelling (*Section 2.2*), Numerical and Analytical Methods (*Section 2.3*) and Pipe-soil Interface Properties (*Section 2.4*). For context a brief review of the Occurrence of Clay Seabed is provided (*Section 2.5*). A review of Reliability Based Design Methods (*Section 2.6*) is

provided within the context of the study objective to place pipe-soil interaction into a reliability based framework. Summary and Discussion of the literature is provided at the end of this chapter (*Section 2.7*)

Chapter 3 Methodology - presents the methodology utilised in this study. This chapter is subdivided into several sections. Following an initial introduction the problems analysed in this study are described in Problem Definition (*Section 3.2*). The Numerical Analysis Methodology used in this study is summarised in *Section 3.3*. Additional sections address the Interpretation Framework and Correlation Methodology (*Section 3.4*) and the methodology used for Reliability Based Design Methods (*Section 3.5*).

Chapter 4 Pipeline Subjected to Vertical Loading - represents the first results chapter of this thesis. This chapter reports the results of analyses into a pipeline subjected to a Vertical (V) load, including the general case of the maximum capacity under Vertical loading (V_{max}) for a range of pipeline embedment depths. The first problem analysed is the case of a pipeline on a Homogenous Shear Strength Weightless Seabed (*Section 4.2*). This section also includes comparisons between this analyses and previous research. Following this idealised case a range of additional factors are considered including The Influence of Large Strain Effects (*Section 4.3*), The Effect of Interface Conditions (*Section 4.4*), The Effect of Soil Unit Weight (*Section 4.5*) and The Effect of a Variation in Shear Strength (*Section 4.6*). Two different categories of variation in shear strength are considered, linear increasing shear strength gradients and shear strength crusts. Summary and discussion is provided at the end of this chapter.

Chapter 5 Pipelines Subjected to Combined V-H Loading - leading on from the previous chapter the results for analyses into more complex pipeline load cases are reported in this chapter, with the consideration of combined Vertical and Horizontal (V-H) loading. Following an initial introduction, the first problem considered is the case of a pipeline on a Homogenous Shear Strength Weightless Seabed (*Section 5.2*). This section includes comparisons with previous research. Results are then reported for analyses into The Effect of a Variable Shear Strength Profile (*Section 5.3*), with various linear increasing shear strength gradients considered. Analysis investigating Pipelines Subjected to V-H Loading on a Sloping Seabed is reported in *Section 5.4*. There is also consideration of Large Displacement

Behaviour (S*ection 5.5*) followed by a summary and discussion of the results reported in this chapter.

Chapter 6 Reliability Analysis - reliability based analysis is first applied to the case of a single pipeline subjected Vertical (V) loading *(Section 6.2)*. This is then extended to a more general vertical loading case with Reliability Based Analysis of V_{max} (*Section 6.3*). Extension of reliability based analysis techniques to V-H loading is first investigated with Reliability Based Analysis of H_{max}, where H_{max} is the maximum capacity under horizontal loading (*Section 6.4*). Following on from analysis of H_{max} reliability based analysis is applied to full V-H stability envelopes (*Section 6.5*). Discussion of the results presented in this chapter is provided in *Section 6.6*.

Chapter 7 Conclusions - this chapter concludes the thesis. The study conclusions are summarised (*Section 7.1*) prior to consideration of how the findings and methods used within this study can be applied to design practice (*Section 7.2*). Potential areas for future research are also identified in *Section 7.3*.

2 Literature Review

2.1 Introduction

Pipe-soil interaction on clay seabed has been an area of active research for several decades with literature stretching back to at least the early 1970's. Early in this period the body of literature was relatively sparse, both in volume and scope. However, more recently the volume and breadth of literature has increased significantly. For example White and Cathie (2010) draw attention to the significant amount of research undertaken between their review paper in 2010 and an earlier review of pipeline geotechnics undertaken by Cathie et al. (2005). More recent studies have taken advantage of advances in physical modelling techniques, such as centrifuge testing, and advances in numerical analysis techniques, software and hardware. Pipe-soil interaction is now a well enough established topic to be considered within recently published textbooks on marine geotechnics e.g. Dean (2009), Randolph and Gourvenec (2011).

While a significant body of literature now exists, including literature published during the course of this study, there are still a number of areas of research that would benefit from further investigation. Some of these areas are addressed within this thesis, see Section 1.2 for a summary of the objectives of this study. Potential areas for further research are also noted in Chapter 7. Where appropriate comparisons will be made between the results of previous researchers and the results of this study.

Approaches adopted to consider pipe-soil interaction typically fall into two categories;

- Physical Modelling
- Numerical and Analytical Methods

A physical modelling approach to pipe-soil interaction on a clay seabed typically consists of testing the behaviour of a model pipeline in conjunction with measurements of seabed geotechnical properties. Variations of this approach include laboratory based testing, laboratory based testing in a centrifuge apparatus and field testing. Empirical relationships can be produced from the results of this model testing, which can potentially be used as design equations. Literature within this category is summarised in Section 2.2.

Various numerical and analytical techniques have been applied to pipe-soil interaction problems. For example finite element analysis and limit analysis techniques have been used to investigate various problems. Analysis typically involves a degree of simplification with idealisation of geometry and, or, simplifications in the soil constitutive model adopted. Numerical and analytical studies typically comprise large suites of analyses allowing relationships to be identified and design equations to be developed. Literature in this area is summarised in Section 2.3.

This review will also consider literature related to pipe-soil interface properties (Section 2.4) and a summary of occurrence and properties of clay seabed (Section 2.5). A review of reliability based analysis techniques is provided in Section 2.6.

2.2 Physical Modelling

Some of the earliest research into pipe-soil interaction using model testing is described by Lyons (1973). Small-scale model tests, full scale model tests and some early finite element analysis was used to consider the stability of pipelines on a clay and a sandy seabed. This study focussed on stability of pipelines under hydrodynamic loading following an initial embedment into the seabed under self weight. Model testing was used to investigate resistance to vertical penetration, for a given weight of pipeline, followed by resistance to lateral displacement.

Testing for the clay seabed conditions within Lyons (1973) was limited to the large scale model tests, which used a section of 9 inch (~225mm) and 16 inch (~400mm) diameter pipeline. The experimental apparatus, shown in Figure 2.1, was relatively unsophisticated and is likely to have become a limiting factor if a more comprehensive testing program was attempted. For example an uplift is applied in conjunction with lateral displacement, additionally this uplift angle is not constant and will increase with increasing lateral displacement. The clay used to model the seabed soils was described as having a shear strength of 45 pounds a square foot (~2 kPa) and slightly wet of its liquid limit, a very soft clay. In addition to a limited testing scope, interpretation of the results within Lyons (1973) was very limited and no design methods were proposed. In common with some later model tests (e.g. Wantland et al., 1979), the lateral displacement distance used in testing was relatively small and it is not clear if peak resistance was reached in all tests. One of the principal conclusions of this research was that a single "Coulomb friction analysis" was not valid for lateral stability on soft

clay, recognising even within early research some of the complexities of pipe-soil interaction on clay seabed and the inappropriateness of a friction factor based approach.

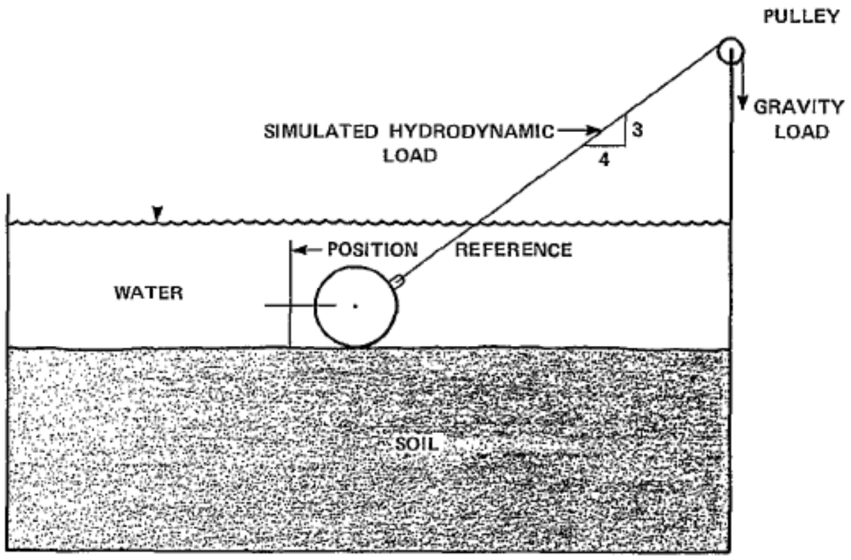

Figure 2.1 *- Experimental apparatus used by Lyons (1973).*

Wantland et al. (1979) reported the results of further reduced scale laboratory based model testing along with some reduced scale field testing; similar data and further interpretation was presented in Wantland et al. (1982). Figure 2.2 shows the arrangement used to undertake this field testing as reported in Wantland et al. (1979). It is clear that this basic arrangement has its limitations. For example it would appear that at larger displacement an inappropriate rolling failure mode could develop. Wantland et al. (1979) presented results for vertical penetration to a predetermined embedment depth and subsequent lateral resistance to displacement see Figure 2.3. The notation next to each line indicates the depth of embedment normalised by pipeline diameter referred to as B, foundation breadth, e.g. B/6 and 1B.

Wantland et al. (1979) interpreted resistance to vertical penetration with a simple strip footing bearing capacity formulae, where the width of the footing was taken as the projected width of the embedded pipeline. A range of bearing capacity factors were presented from the model test results, exhibiting an increasing trend in resistance with depth. Interpretation of lateral resistance was relatively limited and, in common with Lyons (1973), it may have been beneficial

to increase the lateral displacement distance for the deeply embedded pipelines to ensure peak capacity was reached, see Figure 2.3.

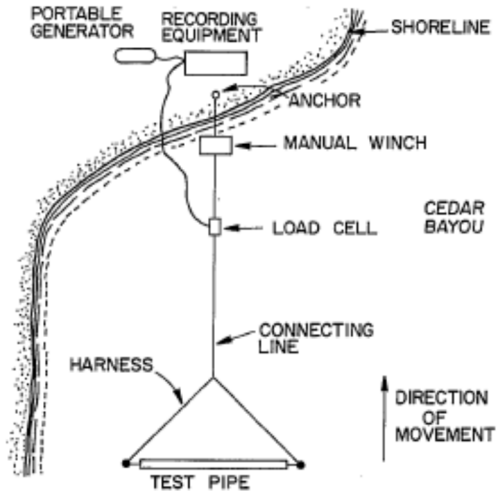

FIG. 6 - LOADING ARRANGEMENT FOR FIELD TESTS.

Figure 2.2 *- Experimental arrangement for field testing (plan view), as used by Wantland et al. (1979).*

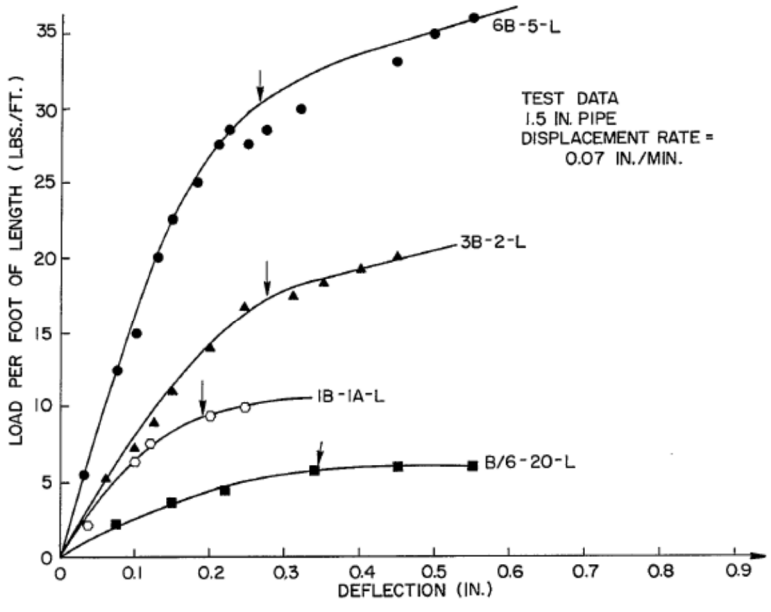

FIG. 10 - LOAD - DISPLACEMENT RELATIONSHIPS FOR A SERIES OF LABORATORY TESTS.

Figure 2.3 *- Resistance to lateral displacement from laboratory testing, as undertaken by Wantland et al. (1979).*

Following on from earlier field based testing Lambrakos (1985) provides details of a more sophisticated field based testing program. This testing program was ship based, removing the requirement for near shore operations. The pipeline section was also contained within an instrumented vehicle, see Figure 2.4. This arrangement presumably increased control over the test conditions. The vehicle was towed along both clay and sandy seabed with a measurement of tow force, this was presented as a tow force graphs, the speed of the vehicle was also detailed. Although the equipment used to undertake this research appeared to be an improvement over previous work, reporting of results and interpretation was very limited. Pipeline penetration was not measured during testing, or given consideration. Interpretation for both clay and sand seabed was in terms of a friction coefficient (i.e. $\mu = H_{max}/V$). There was also little consideration given to the geotechnical properties of the seabed, with conditions classified as generic sandy or clay seabed. Some broad guidance on a range of friction coefficients (μ) for clay and sandy seabed were given within this paper. However, applicability to other seabed conditions, or indeed other combinations of pipeline weight or diameter, is unclear.

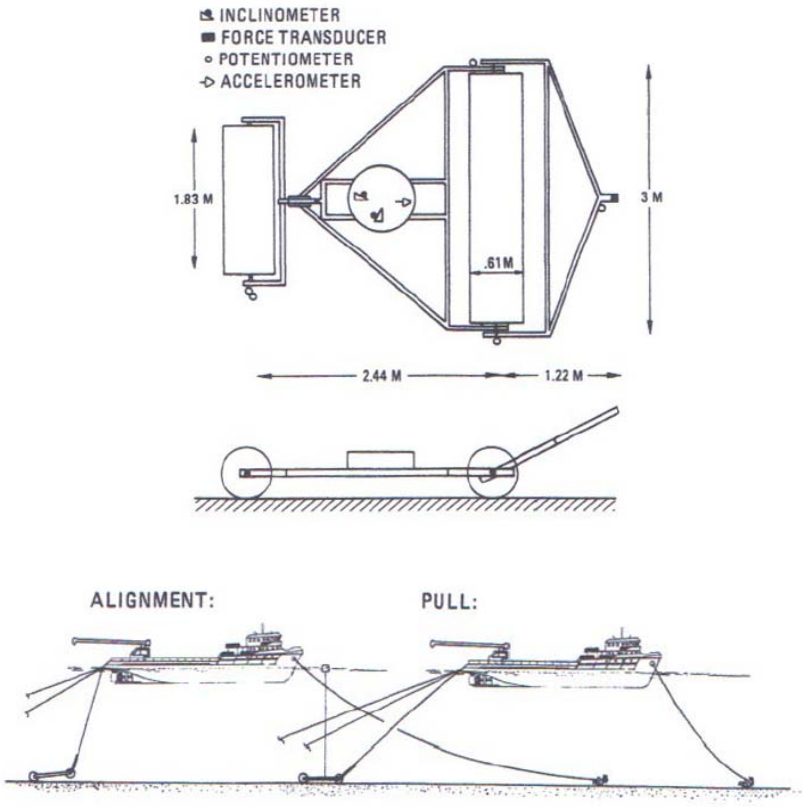

Figure 2.4 *- Test vehicle and testing arrangement described by Lambrakos (1985).*

During the mid-1980s it is understood that a large programme of full-scale model testing was undertaken at SINTEF in Norway on behalf of the American Gas Association. These studies are sometimes referred to as the PIPESTAB project. Initially this testing remained confidential, however the methodology and later results and interpretation were reported over a series of papers in the 1980's and into the early 1990's. Brennodden et al. (1986) gave details of the test apparatus and an overview of the test program. Some results were also presented in this paper. However, reporting was limited and no detailed interpretation was provided. The relatively sophisticated test apparatus used in these studies is shown in Figure 2.5.

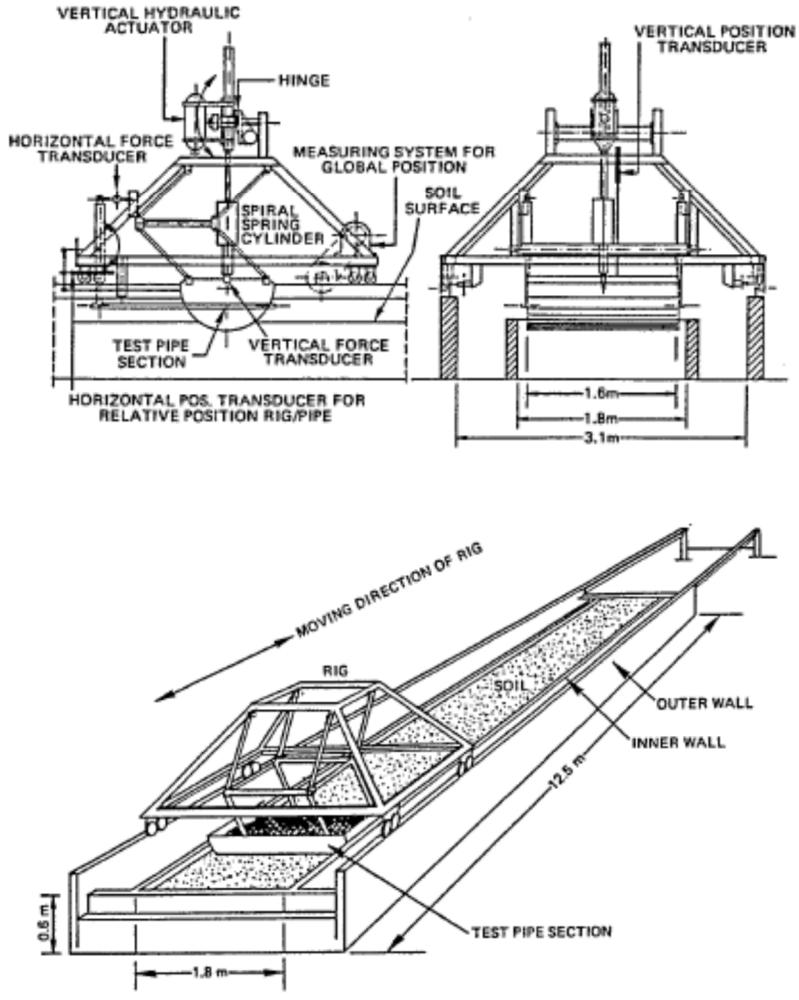

Figure 2.5 *- Pipe-soil interaction test apparatus from Brennodden et al. (1989).*

Some further results from these studies was presented by Wagner et al. (1987), some interpretation was also provided. Detailed interpretation and empirical relationships that could be used in design were later reported in Brennodden et al. (1989) and Brennodden and Stokkeland, (1992).

Testing at SINTIF was based on full scale large diameter pipelines with a diameter of 0.5 m to 1.0 m, presumably to consider the behaviour of large diameter export lines and trunk lines. The testing programme involved filling the test tank with sand prepared to various relative densities, soft clay or stiff clay. Vertical penetration, with and without vertical cycling, was measured for a range of conditions. Subsequent lateral resistance to displacement was then measured following this initial penetration. Axial resistance was also considered in some tests. Final interpretation of this test program was used to produce a series of empirical equations, for example Equation [2.1] from Brennodden and Stokkeland, (1992) could be used to predict pipeline penetration into a clay seabed. This equation was produced by fitting to the test data and includes a simple correction to allow for the submerged unit weight of soil. It should be noted that this relationship may be based on a relatively small number of tests with clays from a limited geographical area, i.e. offshore Norway.

$$[\mathbf{2.1}] \qquad \frac{F_V}{(r.s_u)} = 4\,(1+\theta)\cos\theta + \frac{4z_p}{r}$$

Where;

F_v = Soil weight corrected vertical force i.e. R_V - ($\gamma'.V_s$)

γ' = Effective soil unit weight

V_s = Volume of displaced soil for a given pipeline penetration

R_V = Resistance (vertical component) i.e. bearing capacity

s_u = Soil undrained shear strength

θ = One half of penetration arc length i.e. arcsin (1- z_p/r)

z_p = Pipeline penetration

r = Pipeline radius i.e. r = D/2

D = Pipeline diameter

The design method proposed by Brennodden et al. (1989) and Brennodden and Stokkeland (1992) initially required a prediction of pipeline penetration, e.g. using Equation [2.1], lateral resistance was then estimated from this initial

penetration. Within this methodology lateral resistance was derived using a friction coefficient approach; an empirical equation was then used to predict peak and lateral resistance, as shown in Equation [2.2]. The adopted friction coefficient was assigned based on a broad characterisation of soil type, e.g. a sandy or clay seabed, and can also be viewed as being empirical.

$$[\mathbf{2.2}] \qquad H_{max} = k_{max}\left(\mu.W_s + \beta_m.s_u.\frac{A_c}{D}\right)$$

Where;

H_{max} = Maximum capacity under horizontal loading
k_{max} = Empirical later coefficient (0.8 was suggested)
μ = Friction coefficient (0.2 was suggested for very soft clay)
V = Vertical load e.g. submerged pipe weight
β_m = Empirical coefficient (1.47 was suggested)
s_u = Undrained shear strength of soil
A_C = Pipeline-soil contact area
D = Pipeline diameter

An additional equation in a similar form, but with reduced coefficients, was proposed to predict residual lateral resistance at large displacements. Axial resistance was interpreted in terms of an alpha factor approach, i.e. contact area derived from predicted penetration multiplied by soil shear strength with a reduction for interface factors captured within an alpha term. This α factor was considered to be empirical and to range from a peak value to a lower residual value for larger displacements.

Other physical modelling studies of note in this period were the investigations into vertical penetration of a pipeline under cyclic vertical loading, described by Dunlap (1990), and investigations into vertical penetration under cyclic lateral loading described by Morris et al. (1986). Both studies considered very soft clay, with $s_u \approx$ 1-2 kPa. Both load controlled and displacement controlled tests were reported. A rationale for investigating very low strength clays was not provided. However, presumably cases with a larger pipeline penetration into the seabed were considered of particular interest. Additionally there may have been advantages in preparing clay of this strength in the laboratory.

After this period of relatively active research in the area of pipe-soil interaction model testing Verley and Lund (1995) compiled a review of much of the

available test results from this period, both the testing referenced previously in this section and other testing not available in the public domain. This testing was reinterpreted and series of empirical equations were proposed. This included a method to predict pipeline penetration under vertical load, see Equation [2.3], and a method for estimating lateral resistance to displacement for a given pipeline penetration, see Equation [2.4].

$$[\mathbf{2.3}] \qquad \left(\frac{z_p}{D}\right) = 0.0071\left(\hat{S}.\hat{G}^{0.3}\right)^{3.2} + 0.062\left(\hat{S}.\hat{G}^{0.3}\right)^{0.7}$$

$$[\mathbf{2.4}] \qquad \frac{H_{max}}{D.s_u} = 4.13\hat{G}^{-0.392}\left(\frac{z_p}{D}\right)^{1.31}$$

Where;

z_p = Depth of pipeline embedment
D = Pipeline diameter
$\hat{G}$ = s_u /(D.γ')
$\hat{S}$ = V /(D.s_u)
V = Vertical load e.g. submerged pipe weight
s_u = Shear strength of clay
γ' = Effective soil unit weight
H_{max} = Horizontal component of soil resistance

Equation [2.4] addresses soil resistance due to pipeline embedment and requires addition of a horizontal resistance due to a "frictional" component. No specific guidance is given for this, although Cheuk (2005) suggests μ = 0.2 is utilised in this design method, where μ is a friction coefficient applied to the submerged pipeline weight. The use of this design value is also consistent with Brennodden and Stokkeland (1992). Verley and Lund (1995) also provided additional results and equations for the development of vertical penetration due to cyclic vertical motion of a given amplitude. Within Verley and Lund (1995) there appears to be significant scatter between the summarised data and the empirical fitting equations. Additionally these equations do not seek to bound or otherwise describe and quantify this scatter. There are also a number of restrictions in the use of these equations, both stated and implied, arising from the range of pipeline diameters tested, soil conditions and loading used in the model tests.

Willis and West (2001) described the results of some interesting full scale harbour based model tests, although these are more relevant to steel catenary risers (SCR) then pipelines. This testing investigated penetration of a riser under

large repetition cyclic vertical load using relatively sophisticated test equipment mounted to a quay wall. Interpretation of these results into a pipe-soil interaction model for assessing SCR fatigue was given in Bridges et al. (2004). This model could be incorporated into design software to account for riser-soil interaction and changes in riser-soil interaction in association with the large numbers of vertical loading cycles. Bridges et al. (2004) indicated this could have significant implications for riser fatigue assessments when compared to simpler soil models.

There was something of a resurgence in model testing for pipelines on clay seabed from around mid-2000 to the present day. Simple empirical equations derived from this model testing was seemingly a popular approach to this design problem. Much of this work was in association with the SAFEBUCK Joint Industry Project (JIP); although initially confidential there is now a significant amount of information on this testing in the public domain. Some of the model testing undertaken for SAFEBUCK JIP is described in greater detail by Cheuk (2005). This testing included full scale model testing and what appears to be the first application of centrifuge testing to the problem. The centrifuge testing was undertaken in a small drum centrifuge and is also described in Cheuk and Bolton (2006). Figure 2.6 shows the apparatus within the drum centrifuge, with the model pipeline section towards the centre left of the image.

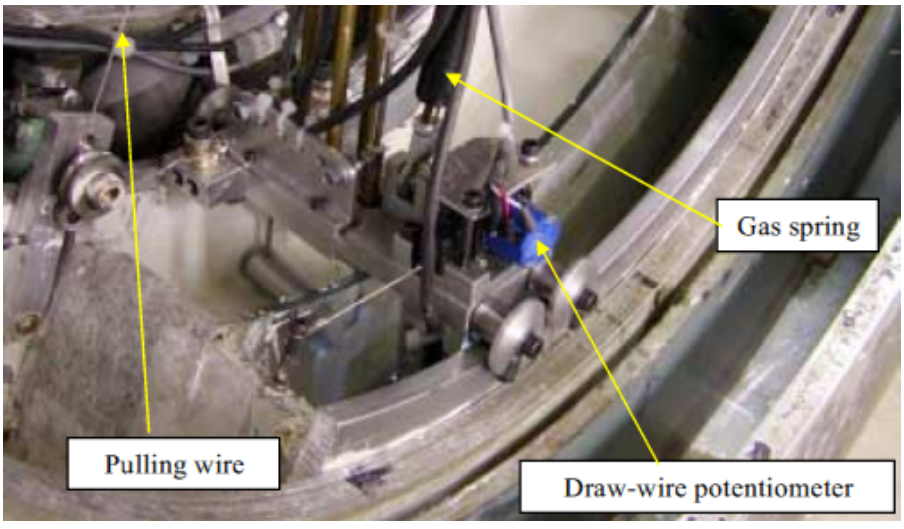

Figure 2.6 *- Model pipeline drum centrifuge test apparatus from Cheuk (2005).*

Cheuk and Bolton (2006) suggested good agreement between the centrifuge testing and the full scale model testing, with the test conditions applied to reduced scale pipeline section under increased gravitational forces seemingly replicating the conditions for a full scale model. There were also advantages in terms of sample preparation with the increase in gravitational forces within the centrifuge test apparatus allowing rapid consolidation of a model clay seabed from a kaolin slurry.

Cheuk (2005) provided design equations from the test results reported within his study. Equation [2.5] gives an upper and lower bound estimate on pipeline penetration under vertical loading. Equation [2.5] is formulated in terms a reduced shear strength parameter, $s_{u,operational}$, which is described by Equation [2.6]. Equation [2.7] estimates lateral resistance to displacement.

$$[\mathbf{2.5}] \qquad \frac{1}{64}\left(\frac{V}{L.D.s_{u,operational}}\right) < \frac{z_p}{D} < \frac{1}{32}\left(\frac{V}{L.D.s_{u,operational}}\right)$$

$$[\mathbf{2.6}] \qquad s_{u,operational} = \frac{s_{u,peak}}{\sqrt{S_s}}$$

$$[\mathbf{2.7}] \qquad \frac{H_{max}}{L.D.s_{u,peak}} = 3.8\sqrt{\frac{2z_p}{D}} - 0.08\left(\frac{V}{L.D.s_{u,peak}}\right)^2$$

Where;

V	= Vertical load e.g. submerged pipeline weight
L	= Length of pipeline
D	= Pipeline diameter
$s_{u,operational}$	= See Equation [2.6]
z_p	= Pipeline embedment
$s_{u,peak}$	= Peak undrained soil shear strength
S_s	= Softening index parameter
H_{max}	= Maximum capacity under horizontal loading

The softening index parameter used in Equation [2.6] is empirical and was taken by Cheuk (2005) as 1.3 for kaolin clay and 1.75 for the West African soils tested.

Bruton et al. (2006) discussed the findings of the SAFEBUCK JIP and provided alternative design equations to those presented by Cheuk (2005). These equations are presumably a reinterpretation of the testing from Cheuk (2005) although they may also incorporate additional testing. An equation to predict initial pipeline penetration was given, see Equation [2.8], along with equations to estimate peak and residual lateral horizontal resistance, Equations [2.9] and [2.10] respectively.

$$[\mathbf{2.8}] \qquad \left(\frac{z_p}{D}\right) = \frac{S_t}{15}\left(\frac{V}{D.s_{uzp}}\right)^2$$

$$[\mathbf{2.9}] \qquad H_{max} = 0.2\,.V + \frac{3}{\sqrt{\frac{s_{uzp}}{\gamma'.D}}}\,.\,\frac{z_p}{D}$$

$$[\mathbf{2.10}] \qquad \frac{R_H}{V} = 1 - 0.65\left[1 - exp\left(0.5\,\frac{S_{u,1D}}{\gamma'.D}\right)\right]$$

Where;

z_p = Pipeline penetration (referred to as initial pipeline embedment)
D = Pipeline diameter
S_t = Soil sensitivity
V = Vertical load
s_{uzp} = Shear strength at pipeline embedment depth (invert level)
H_{max} = Maximum capacity under horizontal loading (referred to as breakout)
γ' = Effective soil unit weight
R_H = Horizontal resistance
$s_{u,1D}$ = Soil shear strength at a depth of one pipeline diameter

Bruton et al. (2006) described the relationship between Equation [2.9] and [2.10] in terms of peak horizontal resistance typically being reached at less than 0.5D. A reduction in resistance to residual resistance at approximately 3 to 5 D is then noted. It is suggested that the use of the $s_{u.invert}$ term in Equation [2.8] allows for variations in shear strength with depth be accounted for, in particular linear increasing shear strength. Although as shear strength variation and the form of this variation (e.g. linear increasing, shear strength crusts, etc) is not specifically accommodated in this empirical equation, the generality of this approach should be questioned. In a similar way, the shear strength parameter

$s_{u,1D}$ in the lateral resistance equation may also lack generality and could be specific to a particular set of conditions and pipeline characteristics.

Following on from Cheuk (2005) and Bruton et al. (2006) further full scale model testing was undertaken, particularly at the Norwegian Geotechnical Institute (NGI). This is referred to in Langford et al. (2007) and Dendani and Jaeck (2007b), similar material is also presented in Dendani and Jaeck (2007a) and Dendani and Jaeck (2008). Apparatus for undertaking this testing was largely the same as used for the earlier PIPESTAB testing, e.g. Brennodden et al. (1989). Interpretation of these model tests was in terms of existing empirical equations referenced in this section, as well as numerical analysis studies referenced in Section 2.3. The principal addition reported in this work was further guidance on expected changes in lateral resistance at larger lateral displacement, see Figure 2.7. This extends the concept of a residual resistance to a specific load displacement relationship for larger displacements. For comparison purposes this relationship and the relationship reported by Bruton et al. (2006) are also shown in Figure 2.7

A simplified expression was also proposed to estimate horizontal resistance to displacement, see Equation [2.11], e.g. as presented in Dendani and Jaeck (2007b).

$$[\mathbf{2.11}] \qquad R_H = 0.2V + C_{lat}.s_{u,av}.z_p$$

Where;

R_H = Resistance to horizontal displacement
V = Vertical load e.g. submerged pipeline weight
C_{lat} = Empirical lateral resistance coefficient
$s_{u,ave}$ = Average soil shear strength
z_p = Depth of pipeline embedment

A value of 2.3 was recommended for C_{lat} for pipeline embedded to a depth greater than 0.2D, which was suggested as common for pipelines in deep water West African soils.

a)

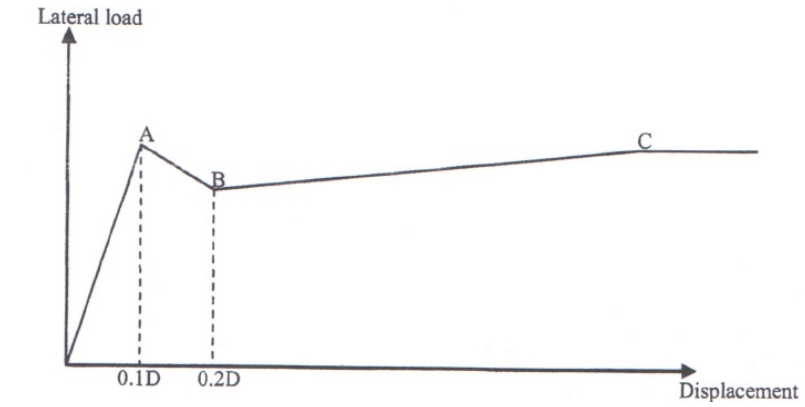

b)

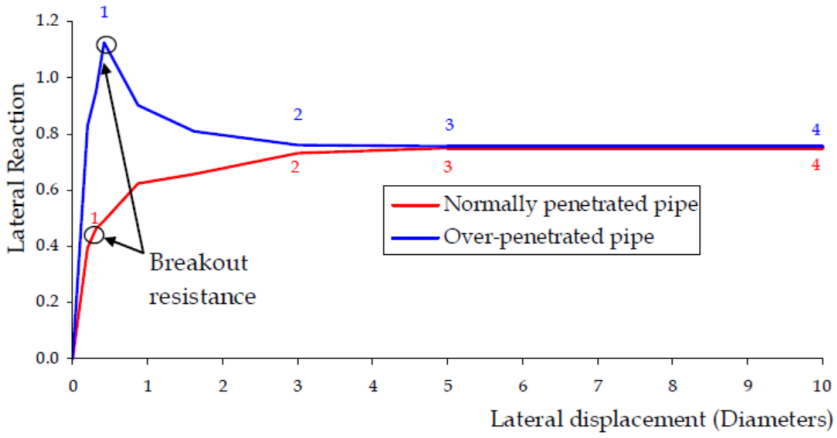

Figure 2.7 *- Lateral displacement behaviour a) Dendani and Jaeck (2007b) and b) from Bruton et al. (2006).*

Dendani and Jaeck (2007a) provided estimates of displacement distance to peak resistance and a residual lateral resistance, Figure 2.7a, based on the NGI testing. However, it can been seen that this differs somewhat from the estimates previously discussed by Bruton et al. (2006), see Figure 2.7b with peak resistance at up to 0.5D and residual at 3-5D. Additionally in their design recommendations Dendani and Jaeck (2007a) provide a relatively broad ranges of behaviour; peak horizontal resistance based on Equation [2.11], post peak resistance of 50-90% of peak and a residual resistance at larger displacements of 70-150% of peak.

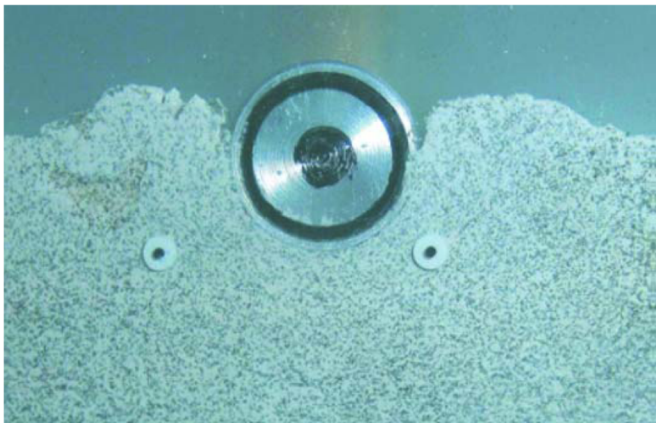

Figure 2.8 *- Model pipeline from Dingle et al. (2008).*

Further to Cheuk (2005) and Cheuk and Bolton (2006) additional use was made of centrifuge testing to investigate pipe-soil interaction on clay seabed. Dingle et al. (2008) investigated pipeline penetration and subsequent lateral displacement. An image of the model pipeline after a phase of vertical penetration can be seen in Figure 2.8. This testing program include the use of particle image velocimetry (PIV), e.g. as described in White et al. (2003), to investigate displacement behaviour and possible failure mechanisms. Interpretation of this testing included comparisons with recent numerical results for Vertical (V) loading e.g. Merifield et al. (2009), although these comparisons did not extend to Horizontal (H) loading or V-H stability envelopes.

Details of a centrifuge test program was reported by White and Dingle (2011) with the stated aim to produce a simplified method of estimating lateral resistance to displacement. It was noted that Equation [2.12] correlated to the test results by approximately 15%, with fitting coefficients of a= 2.8 and b = 0.75. Equations [2.13] was suggested as possible design methods, including consideration of the over penetration ratio noted by Bruton et al. (2006) and Dendani and Jaeck (2007b), referred to as overloading ratio by White and Dingle (2011). It was however noted that although simple this approach was potentially less robust then a design method that considers the pipeline displacement trajectory. It was also noted the design methods were purely empirical, with generality and the applicability to various conditions or pipeline characteristics not, as yet, demonstrated.

$$[\mathbf{2.12}] \qquad \frac{R_H}{s_u.D} = a\left(\frac{z_p}{D}\right)^b$$

$$[\mathbf{2.13}] \qquad \frac{R_H}{s_u D} = \frac{V}{s_u D}\left[0.3 + 2\left(\frac{z_{p,intial}}{D}\right)\frac{1}{\sqrt{V_2/V_1}}\right]$$

Where;

R_H = Horizontal resistance to displacement
s_u = Undrained shear strength of soil
D = Pipeline diameter
a = Empirical correlation coefficient
b = Empirical correlation coefficient
z_p = pipeline embedment depth
V = Vertical load e.g. pipeline weight
$z_{p,initial}$ = initial pipeline embedment depth prior to later displacement
V_2/V_1 = Overloading ratio reference load 2 divided by reference load 1

Hodder et al. (2008) reports a series of reduced scale model tests with Hodder and Cassidy (2010) reporting similar tests undertaken in a centrifuge. Of particular note in these two studies is the use of a more advanced test methodology within a more robust interpretative framework.

Instead of trying to model individual pipeline displacement or loading scenario, swipe tests with vertical displacement control were used to approximately define a yield surface. These swipe tests consisted of an initial phase of vertical displacement, to a target pipeline embedment, followed by lateral displacement with the vertical displacement fixed. The loads on the pipeline during these tests were measured and logged. Probe tests were also used to define a flow rule, with the pipeline displaced laterally at various constant vertical loads. This was similar to the numerical analysis methodologies used by Bransby and Randolph (1998) to investigate foundation capacity, for example with swipe tests to define a yield surface. However, Bransby and Randolph (1998) defined probe tests as displacement controlled analysis with a fixed horizontal and vertical displacement ratio, i.e. a fixed angle, which is the convention and method adopted in this study. The yield surface defined by this type of model testing can be viewed as a pipeline stability envelope with the flow rule used to describe post yield behaviour. A parabolic yield surface was fitted to the experimental data. This was based on a two dimensional simplification of the parabolic equation used by Martin (1994) and Martin and Houlsby (2001). Various modifications can be

made to the general form of this equation, for example to allow for tensile capacity, or uplift loads. Equations [2.14] and [2.15] show the version presented in Hodder and Cassidy (2010). For Equations [2.14] and [2.15] Hodder and Cassidy (2010) suggested skew parameters of $\beta_1=\beta_2=0.75$ represented a reasonable fit to their swipe tests. These were kept constant to a depth of 1.5D. A form of parabolic stability envelope has also been utilised in interpreting numerical analysis, and is discussed in further detail in Section 2.3, e.g. Merifield et al. (2008). Reinterpretation to account for the large amount of soil remoulding associated with steel catenary risers was presented in Hodder et al., (2013).

$$[\mathbf{2.14}] \qquad \frac{H}{h_0 V_{max}} - \beta\left(\frac{V}{V_{max}} - \frac{V_t}{V_{max}}\right)^{\beta_1}\left(1 - \frac{V}{V_{max}}\right)^{\beta_2} = 0$$

$$[\mathbf{2.15}] \qquad \beta = \frac{(\beta_1+\beta_2)^{\beta_1+\beta_2}}{\beta_1^{\beta_1}\beta_2^{\beta_2}\left[1-\left({}^{V_t}/_{V_{max}}\right)\right]^{\beta_1+\beta_2}}$$

Where;

H	= Horizontal load on the pipe
H_{max}	= Peak horizontal capacity
V_0	= Vertical load axis interaction for current plastic potential
h_0	= ratio of H_{max} to V_{max}
V_t	= Vertical uplift capacity
V	= Vertical load on pipe
β_1, β_2, β	= Skew parameters that control the geometry of the envelope

Reduced scale model testing was also reported by Lee et al. (2011) with further testing and more detailed interpretation in Lee et al. (2012). This model testing includes swipe and probe tests to investigate a pipeline subjected to V-H loading. Investigations of V loading with the same apparatus was previously reported in Lee et al. (2008). Lee et al. (2012) also included the results of numerical analysis, which is discussed in the next section. Interpretation was within a stability envelope framework and consideration was given to pre-loading during installation by investigating various overloading ratios. It was noted that at small displacement behaviour could be described with stability envelopes. Then, depending on the overloading ratio the pipeline may undergo ride-in or ride-out

behaviour at larger displacement. It was observed that at larger displacements most tests trended towards a residual resistance to horizontal displacement. A fitting relationship was proposed for this residual resistance, see Equation [2.16].

$$[\mathbf{2.16}] \qquad \frac{R_{H,residual}}{s_u . D} = 4.5 \left(\frac{z_p}{D}\right)^{0.64}$$

Where;

$R_{H,residual}$ = Horizontal resistance to displacement
s_u = Undrained shear strength of soil
D = Pipeline diameter
z_p = pipeline embedment depth

A further recent development of interest with respect field testing is the Smartpipe project. This involves what is essentially in-situ model testing using a subsea testing apparatus that can be placed on the seabed at a deepwater development location. This system can be used to perform project specific model tests for use in design. This system was first described by Hill and Jacob (2008). Figure 2.9 shows a schematic of this apparatus. It is expected that this equipment will be used for specific projects with test data remaining confidential. However, a small amount of test data for an unnamed site has been recently released with a focus on axial pipeline resistance, e.g. White et al. (2011).

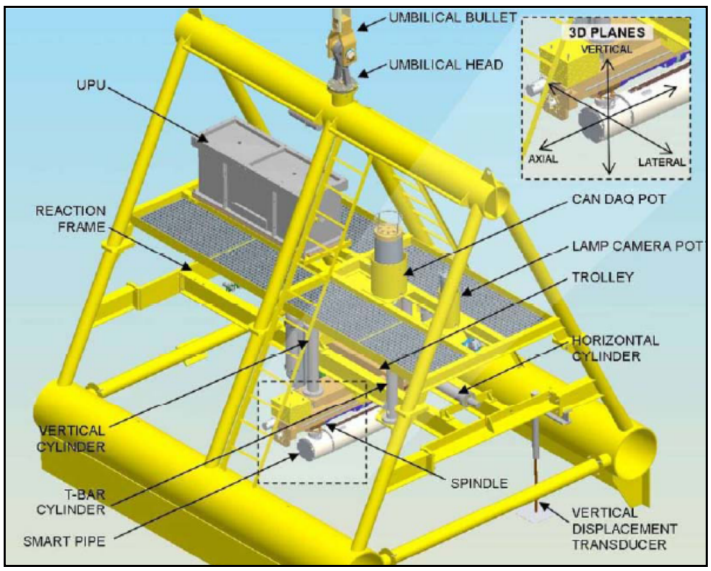

Figure 2.9 *- Smartpipe in-situ test apparatus, from Hill and Jacob (2008).*

So far all reference to model testing has been for the case of a flat seabed. Until recently there appears to have been no consideration of the effect of a sloping seabed using physical modelling techniques. Gao et al. (2011) utilised laboratory based model testing to consider this issue, however only for a sandy seabed. Additionally Gao et al. (2011), in common with most model testing referred to here, does not use a stability envelope framework for interpretation, instead focusing on a friction coefficient approach and resistance models similar to Brennodden et al. (1989). This research is not directly applicable to this study. However, it may be relevant if future researchers wish to investigate pipeline behaviour on a sloping clay seabed using model testing techniques. It is recommended that a stability envelope approach is adopted for interpretation of future model testing.

This section has provided an overview of the application of physical modelling techniques to investigate pipe-soil interaction on a clay seabed. This has provided historical context and background information for this study. Further discussion and a summary of the most relevant aspects of this section will be provided in Section 2.7. Comparisons between this study and previous research will also be made in later chapters.

2.3 Numerical and Analytical Methods

Pipe-soil interaction on clay seabeds has been investigated using a range of numerical and analytical techniques. Some of the first work in this area was the finite element analysis described by Lyons (1973). The analysis reported from this study was a very early example of the application of finite element analysis to geotechnical problems and had a number of short falls compared to more recent applications of this method. For example there were some significant simplifications in the geometry of the problem, presumably due to limitations in the analysis methodology. This included the pipeline not being embedded, or wished in place, into the soil mesh. Instead loads are transferred to the soil mesh by a series of interface elements across a given width. A relatively coarse mesh was also used in analysis. An example mesh from Lyons (1973) is shown in Figure 2.10.

Despite the issues highlighted it would appear there was good agreement between this finite element analysis and the model testing undertaken in this study, as previously described in Section 2.2, see Figure 2.10b. It was also

suggested by Lyons (1973) that the Coulomb friction model was not valid for pipes on a soft clay seabed.

Other early work in this area using numerical methods was Karal (1977). This paper provided a summary of a relatively large parametric study using upper bound limit analysis techniques. This study investigated pipeline penetration under vertical load and subsequent lateral resistance to displacement under horizontal loading. Example failure mechanisms were presented and a simple interpretation framework similar to early model testing. However, reporting of results was not comprehensive and no specific design guidance was given.

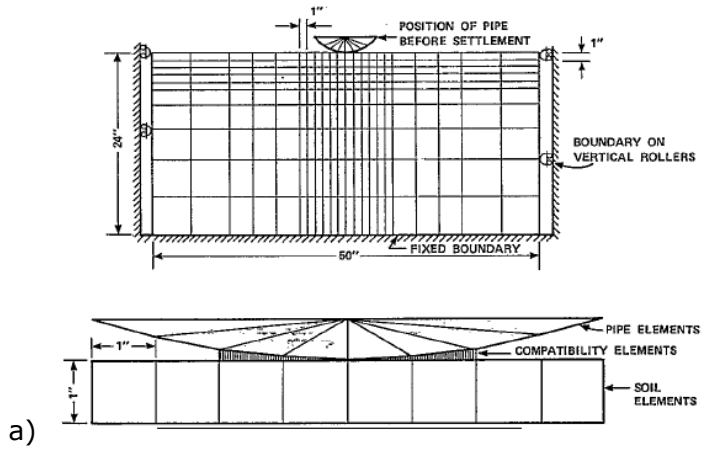

a)

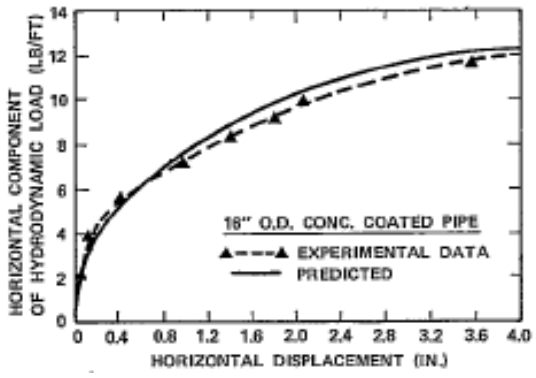

b)

Figure 2.10 *- a) Example finite element mesh from Lyons (1973) and a comparison between the model testing and the finite element testing b).*

There was a period of relatively little research using numerical and analytical techniques to investigate pipe-soil interaction until the research reported by Schotman and Stork (1987). Schotman and Stork (1987) noted that advances in computer technology at this time presented an opportunity to undertake finite

element analysis of this problem. Of particular note in this early study was the interpretation framework, which appears to be the first use of V-H stability envelopes and discussion of load paths with respect to these envelopes. See example stability envelope in Figure 2.11. The focus of this paper was on providing an overview of the analysis techniques and no comprehensive design guidance was provided.

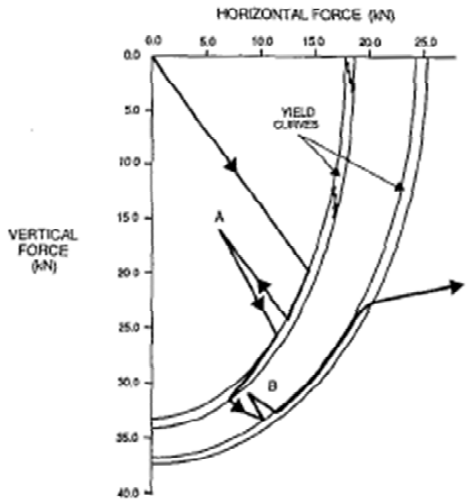

Figure 2.11 *- Yield surfaces in V-H load space (Schotman and Stork, 1987).*

Murff et al. (1989) presented upper and lower bound limit analysis solutions for pipeline penetration under vertical loading into a cohesive soil. The proposed upper bound solution was more rigorous then the previous mechanisms proposed by Karal (1977), especially for deeper penetration. Murff et al. (1989) considered penetration up to 0.5D, with analyses giving a difference between the lower and upper bound methods of approximately 10% for a rough interface pipeline and around 25 % for a smooth interface pipeline. Issues such as soil heave, shear strength gradient and seabed slope were discussed although comprehensive analysis for all these cases was not fully developed or presented. The equations and analysis methods presented by Murff et al. (1989) are relatively inaccessible as design tools being mathematically complex and in some cases, such as for the upper bound, it is not possible to evaluate the solutions for all cases. Later authors such as Dendani and Jaeck (2007a) suggest approximate fitting equation to these analyses.

Aubeny et al. (2005) undertook relatively detailed investigations into penetration of a pipeline into a clay seabed under Vertical (V) loading with a large suite of

finite element analyses. Embedment depths of up to five pipeline diameters were considered within a plane strain idealisation. These analyses used a small strain methodology and the pipeline was "wished in place". The assumption of a vertical sided trench and no soil backflow was used for embedment depths greater than half a pipeline diameter. These analyses considered a uniform strength weightless clay seabed.

In addition to a uniform soil shear strength case Aubeny et al. (2005) undertook a limited amount of analyses to investigate the effect of shear strength increase with depth. The approach adopted was to bound the problem between the uniform strength case already analysed and an infinite shear strength gradient. The practicalities of how this was undertaken within the finite element analysis methodology is not detailed. However, it is presumed for a given pipeline embedment depth a very steep shear strength gradient was applied. For this shear strength gradient to be steep it is also assumed there is a zero shear strength intercept at mudline assigned. While economic in terms of analyses required, this approach does not necessarily bound the full range of pipeline behaviour. A more comprehensive analysis of this problem is undertaken within this study.

In addition to making comparisons between their finite element analyses and previous plastic limit analyses Aubeny et al. (2005) also produced an equation to estimate vertical resistance to penetration. This was undertaken by fitting a power law equation to the results of the finite element analyses. This form of power law relationship and the associated dimensionless groups appear to be a useful approach to considering this problem, and similar problems, and are adopted by later researchers as well as this study. This power law equation is reproduced in Equation [2.17]. Some of the correlation coefficients recommended by Aubeny et al. (2005) are presented Table 2.1. Note correction of the typo in the depth range from the original paper.

$$[\mathbf{2.17}] \qquad \frac{V_{max}}{s_{uzp}.D} = a\left(\frac{z}{D}\right)^{b}$$

Where;

V_{max} = Maximum capacity under vertical loading
s_{uzp} = Soil strength at pipeline embedment depth
D = Pipeline diameter

a, b, = Correlation coefficients

z_p = Depth of pipeline embedment

Aubeny et al. (2005) had difficulties in fitting Equation [2.17] to both shallow (<0.5D) and deep behaviour (>0.5D) and proposed slightly different coefficients for these two different depth ranges.

Strength Gradient	Pipeline Roughness	$z_p/D < 0.5$	$z_p/D > 0.5$
0	Smooth	a = 5.42	a = 5.16
		b = 0.29	b = 0.21
	Rough	a = 7.41	a = 6.35
		b = 0.37	b = 0.15
∞	Smooth	a = 4.44	a = 4.62
		b = 0.17	b = 0.21
	Rough	a = 6.02	a = 5.95
		b = 0.20	b = 0.15

Table 2.1*: Correlation coefficients from Aubeny et al. (2005).*

Barbosa-Cruz and Randolph (2005) reported the results of more complex finite element analysis using the RITSS techniques (Remeshing and Interpolation Techniques at Small Strain). This analysis technique allowed some large strain effects to be accounted for, such as soil berm formation during pipeline penetration, removing the need for a wished in place methodology and the associated assumptions. Soil unit weight was also considered in these analyses, although not within the context of a comprehensive parametric study. Interpretation of analysis results included the use of a dimensionless bearing capacity term (N_C), similar to that used for classical bearing capacity analysis where $N_c = V/D.s_u$. V is vertical load, D is pipeline diameter and s_u is the soils undrained shear strength. The number of analyses in this study was relatively small and each analysis appeared to be very computationally intensive. No specific design recommendations were presented in this paper, although this work was developed further by later researchers e.g. Hodder and Cassidy (2010).

With increasingly more complex approaches to pipe-soil interaction the issue is raised on how these approaches are incorporated into design practice. Cassidy (2006) discussed the use of force resultant macro elements to implement complex pipe-soil interaction behaviour within structural finite element programs. The behaviour of these macro elements is determined by the geotechnical specialist, based on techniques such as numerical analysis or model testing; accurate behaviour can then be captured within the structural analyses without the requirement for complex pipe-soil interaction to be determined directly within these analyses.

Yu and Konuk (2007) presented the results of a series of 2D and 3D finite element analysis. The scope of this analysis and design recommendations were limited. This research did demonstrate the feasibility of complex 3D analysis. However, the requirement for this analysis was not demonstrated over plane strain analysis. This analysis was undertaken in a general purposes structural finite element software package and this may have been an attempt to combine the geotechnical aspects of the problem and analysis of structural pipeline design requirements within a single analysis. The principal conclusion of this study was the authors concerns over the accuracy and appropriateness of simple spring based, or friction based, models commonly used in design practice for considering pipe-soil interaction in pipeline structural design.

The relatively active period of research previously mentioned with respect to physical modelling techniques was mirrored in numerical and analytical techniques, with a significant body of research published recently. Merifield et al. (2008) reported a large parametric study using small strain finite element analysis to investigate pipeline behaviour under Vertical (V) loading and when subjected to combined Vertical and Horizontal (V-H) loading. For V loading a power law equation was fitted to analysis results, as previously utilised by Aubeny et al. (2005) see Equation [2.17]. The authors found reasonable agreement between their analyses and this earlier work. The correlation coefficients they suggested for use with Equation [2.17] are given in Table 2.2. All analysis undertaken by Merifield et al. (2008) was limited to a pipeline embedment less than, or equal to, half a pipeline diameter (0.5D) and a uniform shear strength weightless seabed soil. The similarities between the coefficients proposed by Merifield et al. (2008), as summarised in Table 2.2, and those previously summarised in Table 2.1 for Aubeny et al. (2005) can be noted. Graphical comparisons between these two studies, as well as analysis undertaken for this study, are presented in Chapter 4.

Pipeline Roughness	a	b
Rough	7.40	0.40
Smooth	5.66	0.32

***Table 2.2**: Correlation coefficients for V loading from Merifield et al. (2008).*

Merifield et al. (2008) also provided an approach to consider combined V-H loading on a pipeline by fitting a parabolic stability envelope to Finite Element analyses results. This stability envelope is in the same general form used by Martin (1994) and Martin and Houlsby (2001), also see Equation [2.14] and [2.15] from Hodder and Cassidy (2010). The Merifield et al. (2008) version of this equation is reproduced in Equation [2.18] and [2.19]. The parabolic skew parameters β_1 and β_2 were correlated to embedment depth, as shown in Equations [2.20] and [2.21]. V_{max}, maximum resistance to vertical loading is calculated from Equation [2.17] using the coefficients in Table 2.2, as previously discussed. H_{max}, maximum resistance to horizontal loading, for a given embedment, is calculated from Equation [2.22].

$$[\mathbf{2.18}] \qquad \frac{H}{H_{max}} = \beta \frac{V}{V_{max}}^{\beta_1} \left(1 - \frac{V}{V_{max}}\right)^{\beta_2}$$

$$[\mathbf{2.19}] \qquad \beta = \frac{(\beta_1 + \beta_1)^{(\beta_1+\beta_2)}}{\beta_1^{\beta_1}.\beta_2^{\beta_2}}$$

$$[\mathbf{2.20}] \qquad \beta_1 = (0.8 - 0.15\alpha)\left(1.2 - \frac{Z_p}{D}\right)$$

$$[\mathbf{2.21}] \qquad \beta_2 = 0.35\left(2.5 - \frac{Z_p}{D}\right)$$

$$[\mathbf{2.22}] \qquad \frac{H_{max}}{V_{max}} = \left(0.48 - \frac{\alpha}{25}\right)\left(\frac{Z_p}{D}\right)^{\left(0.46 - \frac{\alpha}{25}\right)}$$

Where;

H = Horizontal load, location on the stability envelope
V = Vertical load, location on the stability envelope
H_{max} = Maximum capacity under horizontal loading
V_{max} = Maximum capacity under vertical loading
α = Pipe surface roughness factor, set to 0 for smooth 1 for rough

z_p = Pipeline embedment depth

D = Pipeline diameter

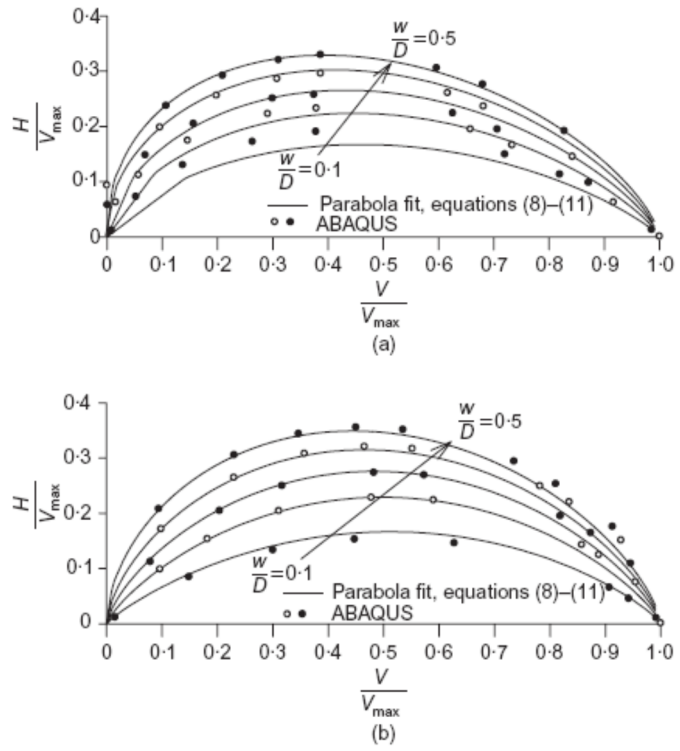

Figure 2.12 *- Stability envelopes produced by Merifield et al. (2008).*

Examples of the stability envelopes produced by Merifield et al. (2008) are shown in Figure 2.12. Note; w/D is equivalent to z_p/D i.e. dimensionless pipeline embedment depth in terms of pipeline diameter. Both Vertical (V) load and Horizontal (H) load are expressed in dimensionless form with respect to maximum capacity under V loading (V_{max}).

Bransby et al. (2008a) and Bransby et al. (2008b) reported the results of two small finite element analysis studies into pipelines subjected to vertical and combined vertical and horizontal loading. A limited number of analysis cases compared large strain and small strain analysis methods noting some differences due to large strain effects. The effect of soil unit weight with respect to vertical loading was also considered, with the conclusion that at large strain the additional capacity due to soil weight could reasonably be approximated from a "buoyancy" term assuming no soil heave. The scope of these studies were relatively limited with these aspects investigated in greater detail by Merifield et al. (2009).

Further refinement of the upper bound plasticity solution for a pipeline under vertical loading and an extension to combined vertical and horizontal loading was presented by Randolph and White (2008). A pipeline embedment depth range from 0.025 D to 0.5D was considered. At a pipeline embedment depth of >0.1D the solution proposed for V loading undercut the previous solution reported by Murff et al. (1989) and can therefore be considered a more refined solution. This was the first example of an upper bound solution to V-H loading. Cheuk et al. (2008) also undertook upper bound calculations at a similar time. Both V and combined V-H loading were considered. For V loading a correlation in the same form as Equation [2.17] was proposed, see correlation coefficients in Table 2.3. This correlation was within approximately 10% of the upper bound solution for V loading presented in this paper and as can be expected, as an upper bound solution, they produce a greater resistance then the coefficients previously presented in Table 2.1 and 2.2

Pipeline Roughness	a	b
Rough	8.10	0.43
Smooth	5.85	0.32

Table 2.3*: Correlation coefficients for V loading from Cheuk et al. (2008).*

A further investigation into pipelines subjected to vertical loading was undertaken by Lee et al. (2008). A cylindrical and square shape were analysed in plane strain using a limit analysis methodology, Discontinuity Layout Optimisation (Smith and Gilbert, 2007). These shapes were analysed from a shallow embedment to a depth where it was indicated a deep seated failure mechanism was occurring, with a steady value of the bearing capacity factor N_c. Of particular interest in this study was the use of an open slot shaped trench, without backflow, for pipeline embedment depths >0.5D an analysis assumption that was consistent with the model testing undertaken as part of this study. However, as this model testing was reduced scale bench top testing, as oppose to centrifuge testing, care would be needed with this assumption for full scale deeper embedment depths and, or, lower shear strength clays.

Merifield et al. (2009) used large strain finite element analysis techniques to investigate some of the factors not addressed in their previous paper, Merifield et al. (2008). The effect of soil unit weight at small and large strain was also considered.

Merifield et al. (2009) includes presentation of analysis in a format analogous to that commonly used for conventional foundation design, with separate terms describing the contribution of soil shear strength and soil unit weight to bearing capacity when subjected to vertical loading, see Equation [2.23]. A similar approach was adopted for horizontal resistance, see equation [2.24]. While this is an interesting contribution, especially for large strain analysis cases, this represents a less robust approach then a full V-H stability envelope. Merifield et al. (2009) concludes that if it is assumed that the stability envelopes maintain the same geometry as the small strain envelopes previously described in Merifield et al. (2008) then it would simply be a matter of scaling these envelope based on the revised large strain values of V_{max} and H_{max}. However, this assumption is not validated in the study. Additionally large strain behaviour does not include ride-in and ride-out behaviour at larger displacements and as with the previous study analysis was limited to a pipeline embedment depth of less than 0.5D.

$$[\mathbf{2.23}] \qquad \frac{V_{max}}{D} = N_{cV}.s_u + N_{swV}.\gamma'.z_p$$

$$[\mathbf{2.24}] \qquad \frac{H_{max}}{D} = N_{cH}.s_u + N_{swH}.\gamma'.z_p$$

$$[\mathbf{2.25}] \qquad N_{cV} = a\left(\frac{z_p}{D}\right)^b$$

$$[\mathbf{2.26}] \qquad N_{cH} = a\left(\frac{z_p}{D}\right)^b$$

Where;

V_{max}	= Maximum capacity under vertical loading
H_{max}	= Maximum capacity under horizontal loading
D	= Pipeline diameter
N_{cV}, N_{cH},	= Bearing capacity factors, soil strength
N_{swV}, N_{swH},	= Bearing capacity factors, soil unit weight
s_u	= Soil undrained shear strength
γ'	= Effective soil unit weight i.e. submerged unit weight
z_p	= Pipeline embedment depth
a, b,	= Correlation coefficients see Table 2.2 and Table 2.3

In Equation [2.23] and [2.24] the resistance term associated with soil shear strength (N_{cV}, N_{cH}) are described by the power law fitting coefficients shown in

Equation [2.25] and [2.26]. For V loading these fitting coefficients are the same as those previously summarised in Table 2.2. The coefficients for H loading are shown in Table 2.4. It is indicated that resistance to H loading at shallow pipeline embedment depths is less than for V loading, which is reflected in the coefficients presented in Table 2.4 as compared to those previously summarised in Table 2.1 and 2.2.

Pipeline Roughness	a	b
Rough	3.26	0.82
Smooth	2.72	0.78

Table 2.4*: Correlation coefficients for H loading at small strain, from Merifield et al. (2009). V loading coefficients as per Merifield et al. (2008), see Table 2.2.*

At small strain the soil unit weight terms (N_{swV}, N_{swH}) are relatively simple. N_{swV} is the volume of soil removed by wishing the pipeline in place, analogous to an Archimedes or buoyancy effect. N_{swH} is based on the volume of soil associated with an equilateral triangle with a side equivalent to the pipeline embedment depth.

Merifield et al. (2009) also used Equations [2.23] and [2.24] to describe resistance to vertical or horizontal resistance at large strain. For the large strain case the correlation coefficients in Equation [2.25] and [2.26] are changed, with the modified coefficients presented in Table 2.5. Merifield et al. (2009) also presented a graphical comparison between this large strain V loading case and previous small strain analysis reported Merifield et al. (2008). This comparison indicated a trend where at shallow embedment depths large strain conditions produced a greater resistance to V loading. As embedment depth increased the difference between large strain and small strain conditions reduces, until at 0.5D the results are similar. This trend can also be seen in a comparison between the fitting relations from Table 2.2 and Table 2.5.

In addition to an increase in the soil strength terms for these equations there is also an increase in resistance due to soil unit weight, in association with soil heave. Merifield et al. (2009) provides a method to estimate the size of the soil heave zone and account for this by applying a multiplier to the small strain soil unit weight terms.

Pipeline Roughness	Vertical		Horizontal	
	a	b	a	b
Rough	7.1	0.33	3.0	0.58
Smooth	5.3	0.25	2.7	0.64

***Table 2.5**: Correlation coefficients for V and H loading at large strain from Merifield et al. (2009).*

Various further work was undertaken using the RITSS approach, as previously used by Barbosa-Cruz and Randolph (2005). However, much of this work was demonstration of the technique to a range of problems rather than parametric studies with specific guidance to design. One of the more recent examples of this work was by Chatterjee et al. (2010), who demonstrated the use of an advanced constitutive model that accounted for strain rate effects as a pipeline penetrated into the seabed under vertical loading. It is not clear if the results of this analysis would differ significantly from a simpler analysis that uses an appropriate shear strength that characterised the anticipated strain rate effect e.g. from appropriate geotechnical laboratory or in-situ testing.

Recently there has been some focus on consolidation of the soil around a pipeline following embedment. This may be associated with a small amount of vertical settlement under self weight loading following pipeline installation. However, the principal area of interest was related to axial pipeline displacement and the changes in soil properties during consolidation. Gourvenec and White (2010) and Krost et al. (2011) presented the results of coupled (mechanical and fluid) finite element analysis into this problem. Krost et al. (2011) also included some comparisons with Smartpipe test data.

Chatterjee (2012) presented the results of a study that used numerical modelling techniques to investigate pipe-soil interaction. This thesis was primarily composed of previously published work comprising four journal papers and one conference paper. Chatterjee et al. (2012a) considered the effect of strain rate on pipeline penetration, similar to Chatterjee et al. (2010). Chatterjee et al. (2011) and Chatterjee et al. (2012b) addressed resistance to lateral resistance under combined vertical and horizontal loading. Chatterjee et al. (2012b) presents alternative fitting parameters for V-H stability envelopes. These analyses appear to be quite computationally intensive and only a limited number of variables are considered. For example a validation case to fit numerical analysis data to the results of Dingle et al. (2008) is considered with

parameters set to address the specific physical modelling conditions. Further analysis cases are constrained to a limited number of variables i.e. a single fixed pipe-soil interface roughness, a single shear strength gradient, single soil sensitivity, etc. These analyses do not represent a detailed parametric study and related design guidance.

In addition to the reduced scale model testing described in the previous section Lee et al. (2012) also reported the results of some numerical analysis using Discontinuity Layout Optimisation. Both vertical and combined loading were investigated. Large strain effects were estimated by changing the seabed profile, e.g. adding soil heave effects, and good agreement between the numerical analysis and the model testing was noted.

Martin and White, (2012) presented the results of an extremely large parametric study that used finite element limit analysis to investigate pipe-soil interaction on a clay seabed. This study comprised more than 10,000 analysis cases and used a wished in place, small strain, analysis methodology. Penetration under vertical load was investigated, including soil unit weight effects. At pipeline embedment depths greater than 0.5D soil cover was added in analysis, burying the pipeline. Uplift resistance was also considered, as appropriate for pipeline upheaval buckling. An open slot trench was not considered. A range of cases in combined vertical and horizontal loading were analysed including the effect of unit weight and some shear strength gradients. All analysis considered a range of interface properties, a smooth pipeline interface, a rough interface with a tension capacity and a rough interface without a tension capacity. A lot of the discussion in this paper focussed on pipeline upheaval buckling i.e. uplift capacity with soil backfill. Results were presented as a series of plots and no fitting relationship was proposed, albeit these plots could always be digitised for use in design.

This section has provided an overview of numerical and analytical techniques that have been used to study pipe-soil interaction on clay seabed. As with model testing described in the previous section, this has provided background and context to analysis undertaken in this study. A number of design equations have been presented in this section, which in some cases can usefully be compared to analysis results in this thesis, see Chapter 4 onwards. Further discussion and summary of this section is provided in Section 2.7.

2.4 Pipe-soil Interface Properties

The interaction between soil and a range of manmade materials has been of interest to geotechnical engineers for some time due to the relevance to soil structure interaction problems. An example of early research in this area is the interface shear box tests undertaken by Potyondy (1961). More recent work was undertaken by Rao et al. (2000) and Lemos and Vaughan (2000). This later research included guidance on relating resistance at an interface to the physical roughness of this interface, although factors such as the normal stresses at the interface were not discussed. These studies also had limitations in that they investigated a limited number of soils and materials.

Pipe-soil interface properties are noted to be important e.g. White and Randolph (2007) and Hill and Jacob (2008), amongst others. However, it can also be noted that from the literature described so far in this chapter that limited consideration is given to this property for studies that use a physical modelling methodology, see Section 2.2. Similarly with numerical analysis methodologies, analysis considers the theoretical bounds to a problem, a perfectly smooth or rough interface conditions, rather than investigating interface behaviour in detail.

There is a limited amount of literature that directly considers interface behaviour between pipeline coating material and a clay soil at reasonable test conditions i.e. low effective stress. This type of testing requires specialist testing apparatus, with two principal approaches adopted. Najjar et al. (2003) and Najjar et al. (2007) used a tilt table apparatus, as shown in Figure 2.13. This apparatus has a thin layer of reconsolidated soil on the test surface, gravity loading is then used to induce sliding of an interface material over the soil i.e. failure in shear. A failure is based on visual observations, rather than any instrumentation. Kuo et al. (2010) used a low mechanical friction shear apparatus referred to as a Cam-shear test, see Figure 2.14. This apparatus is similar to a standard shear box apparatus, but uses a circular sample, low friction parts and sensitive instrumentation to measure the small loads produced during this type of test.

It would appear that only Najjar et al. (2007) provides test results with respect to undrained pipeline coating to soil interface testing, even then there are significant limitations in scope of testing and the equipment used. The other studies noted here address resistance as a friction coefficient i.e. a drained model. Najjar et al. (2007) presented results for a limited number of tests suggesting failure in shear at approximately $s_u/\sigma'_n = 0.30$, where s_u is the soil undrained shear strength and σ'_n is the effective normal stress at the soil

interface i.e. the contact pressure at the interface. In the absence of a method of measuring the strength of the reconsolidated clay in this equipment it was concluded that this interface behaviour related to an alpha factor of approximately 1, a rough interface. This conclusion was based on the s_u/σ'_n ratio being similar to that expected for the strength of normally consolidated clay i.e. the strength of the reconsolidated material in these tests is fully mobilised in shear. However, Najjar et al. (2007) also suggested that they would expect the interface strength ratio (α) to reduce at higher soil over consolidation ratio, hence higher shear strength clays may behave with lower interface roughness. Although it should be noted they did not provide a technical basis for this assertion and it was not addressed in their testing program.

An additional complexity related interface conditions could also be excess pore pressures at, or close to, the interface, for example as discussed by Krost et al. (2011). It is also not clear how representative the pipeline coating used in studies described in this section are relative to the range of pipelines installed or how representative the clay used are of seabed soils.

Figure 2.13 *- Tilt table apparatus, from Najjar et al. (2003).*

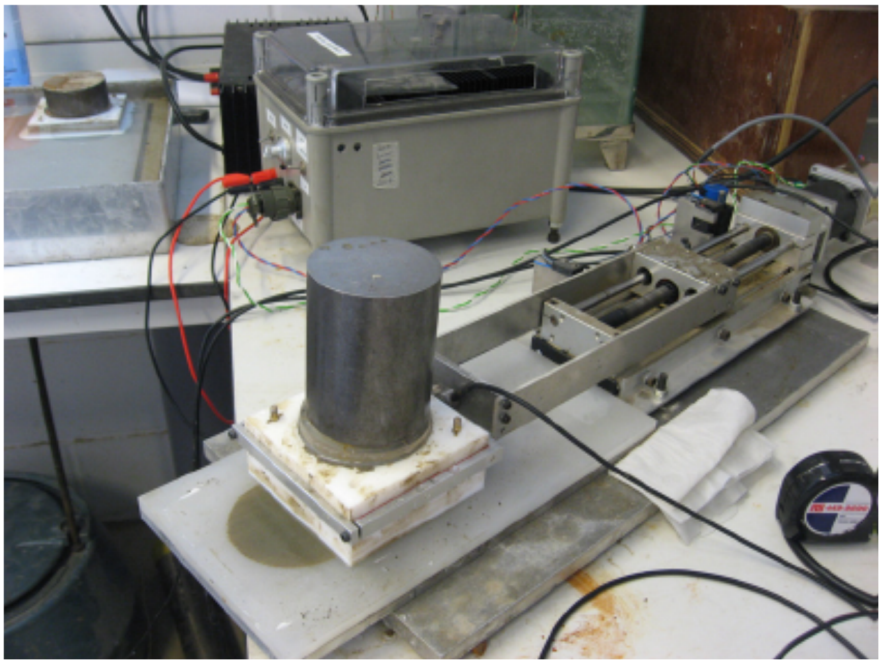

Figure 2.14 *- Cam-shear apparatus, from Kuo et al. (2010).*

At this time it does not appear from the available literature that it is possible to relate pipe-soil interface behaviour in the element tests described here, or the behaviour in model test described earlier in this chapter, to specific interface conditions in numerical analysis. However, one of the objectives of this study is to investigate the influence of a wider range of interface roughness using numerical analysis techniques. To accomplice this a parametric study will be undertaken to better understand the effect of interface behaviour between the bounds of rough and smooth interface behaviour for a pipeline subjected to vertical loading, see Chapter 4.

2.5 Occurrence of Clay Seabed

Early research into the occurrence and properties of clay seabed largely focused on mineralogy. For example Biscaye (1965) and Heath and Pisias (1979) report the results of extensive studies investigating geographic occurrence and origin of clay minerals. A summary of historical research was also provided in these studies. While these studies did not address geotechnical issues and can be considered as relatively peripheral to this thesis, this research does highlight the

widespread occurrence of clay minerals in seabed soils in the world's oceans. For example see Figure 2.15 from Biscaye (1965).

More recently information has been published on the geotechnical properties of clay seabed from various areas of the world, areas where oil and gas infrastructure is already in place or may be installed in the future. While individually these data sources do not present a full global picture, in combination these support the widespread occurrence of very soft clay seabeds.

Puech et al. (2005) describes a database of very soft clay properties from 10 sites in water depths of between 400 m and 1500 m, offshore West Africa. These sites are located in Nigeria, Equatorial Guinea, Congo and Angolan waters. Variation in soil shear strength depth was discussed, including linear increasing shear strength gradients and shear strength crusts. It was noted that the ratio of vertical effective stress to shear strength ratio was typical high, as high as 1 at shallow depth reducing to 0.4 to 0.5 below 10 m. This was contrasted with more typical values of 0.25 for this ratio, including clays in the Gulf of Mexico. However, these higher values for this West African setting are also associated with lower values of submerged unit weight. Shear strength gradients for these West African sites were noted to be in the range of 1.5 kPa/m to 2.0 kPa/m. This was compared with Gulf of Mexico clays, which it was suggested were typically closer to 1.5 kPa/m. Clay sensitivity, the ratio of intact and remoulded soil shear strength, for these sites was noted to typically be in the range of 2 to 5 and largely independent of depth.

Shear strength crusts in West Africa were discussed in further detail by Ehlers et al. (2005) and Kuo et al. (2010). Detailed and quantitative description of these shear strength crusts is limited. However, the geometry and strength of several similar shear strength crusts are reported in Kuo et al. (2010). These examples are also presented in Figure 2.16. Both uniform shear strength conditions and variation in shear strength in the form of linear increasing shear strength gradients and shear strength crusts are investigated in this study.

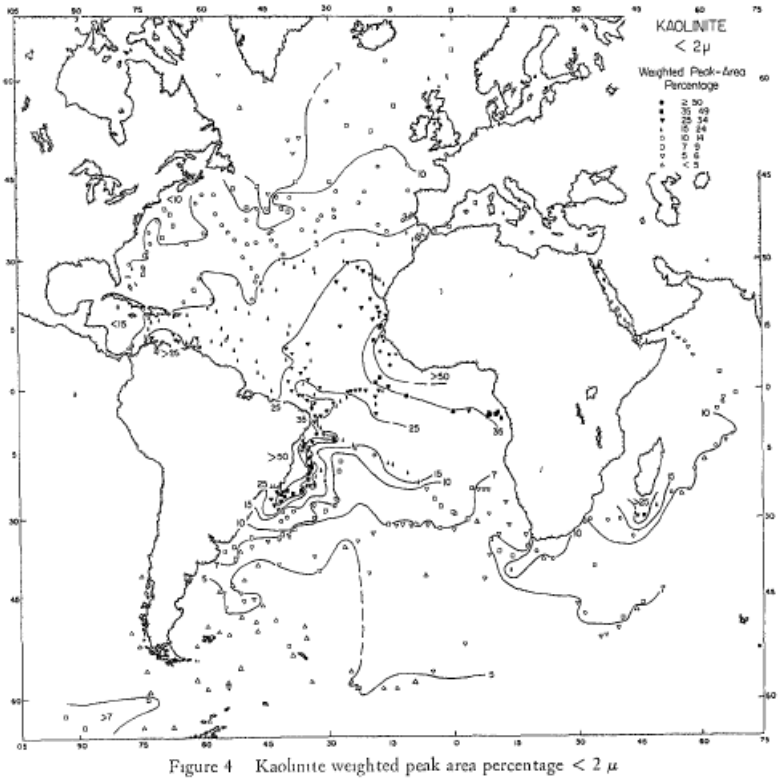

Figure 4 Kaolinite weighted peak area percentage < 2 μ

Figure 2.15 *- Occurrence of kaolinite, (Biscaye, 1965).*

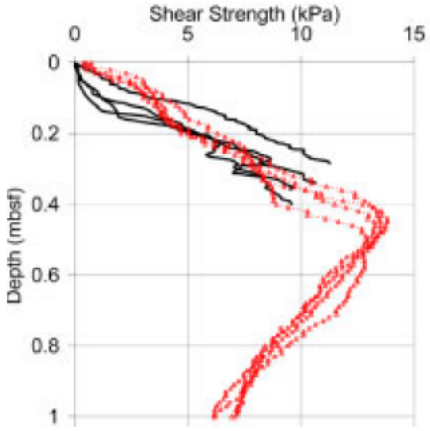

Figure 2.16 *– Example of several similar shear strength crust, (Kuo et al., 2010).*

Further details of the occurrence and properties of very soft clay in the Gulf of Mexico soft clays are given in Quiros and Little (2003) and Yun et al. (2006). Quiros and Little (2003) considered soils over a water depth range of

approximately 180m (600 ft) to 1300 m (4300 ft) and also noted the presence of steep slopes of 15°, or more. Similar slope angles were noted in other areas of the world, for example as referred to by Evans et al. (2007) on the West Nile Delta, offshore Egypt. Yun et al. (2006) provided various correlations to geotechnical properties. This included correlation between soil undrained shear strength and shear wave velocity. A correlation between water content and soil strength was also proposed. Observations were made on the ratio of vertical effective stress to soil undrained shear strength, with a value of 0.22 suggested as typical. This is similar to the value of 0.25 suggested by Puech et al. (2005) for Gulf of Mexico soils.

Further literature provides details of soil conditions in specific locations. However, studies that consider a global occurrence or a wide range of geotechnical properties are less common. One exception is Degroot et al. (2012), which further emphasises the widespread occurrence of very soft clay seabeds. This study summarises geotechnical parameters from 14 offshore developments ranging from the Caspian Sea, Gulf of Mexico and West Africa, to the UK and Norwegian sectors of the North Sea. However, citing sample disturbance as an issue, the focus of this study is largely on remoulded soil shear strength. Limiting the use of this study with respect to providing general guidance on typical seabed soil shear strength, as relevant to the issues considered in this thesis.

Low shear strength clay seabed in the North Sea tend to be in shallower water than some of the other examples noted here. There is a body of literature discussing the occurrence of soft clays within the context of pockmarks features in the North Sea. For example Hovland (1979) addresses the Norwegian sector of the North Sea and Judd (2001) considers pockmark within the soft clays of the Witch Ground, within the UK Sector of the North Sea. Higher shear strength clay seabed are also found in the North Sea, with their higher strength linked to over consolidation associated with glacial events. However, these clays typically occur in association with a sand veneer rather than being present at the seabed in contact with surface lain pipelines. An overview of these soils is presented in Johnson et al. (1993)

A high level summary of the occurrence of clay seabed has been provided in this section, highlighting a widespread and global occurrence. This has provided context for the relevance of considering pipe-soil interaction on a clay seabed, in particular for lower shear strength clays. The absence of comprehensive

guidance on typical geotechnical properties adds further weight to the approaches adopted later in this study, whereby analysis results and associated correlations are reported in terms of dimensionless soil shear strength parameters e.g. $V_{max}/s_u.D$.

2.6 Reliability Based Design Methods

A range of reliability based design methods are available that can be applied to pipe-soil interaction problems. As part of this study a review of these methods was undertaken. This review addressed three principal approaches to reliability based analysis, as follows;

- Monte Carlo Simulation
- Spreadsheet based methods e.g. first order reliability based methods
- Random Field Numerical Analysis

As part of this review consideration was also given to approaches used by previous researchers to investigate similar problems.

Reliability based design methods have been applied to a wide range of geotechnical problems. However, it has been suggested that their use is less widespread in geotechnical engineering then in other engineering discipline, such as structural engineering, (Phoon et al., 2003) (Phoon, 2008). Additionally, out with use in research studies, there may be reluctance in adopting these methods in design practice. There are a range of studies that address onshore design problems with a smaller number considering offshore design issues, for example application to several areas of offshore geotechnics is summarised in Gilbert et al. (2005), Gilbert et al. (2010) and McCarron (2011). A related area of research is when reliability based methods are used to assess the load cases applied to a structure and its foundations, for example waves impacting with a jack up platform (Cassidy et al., 2003).

No specific example of the application of reliability methods to pipe-soil interaction on a clay seabed was noted in this literature review. White and Cathie (2010) suggested reliability based analysis was limited to the structural aspects of pipeline design, although subsequently they did make passing mention to the use of Monte Carlo analysis in design practice by Advanced Geomechanics.

Monte Carlo analysis comprises a simulation technique whereby a system behaviour is defined by an equation, or series of equations, e.g. a deterministic bearing capacity for a strip footing, or a relationship for pipeline penetration into the seabed. The stochastic variables, such as soil undrained shear strength (s_u), are defined by a statistical distribution. The simulation is run a large number of times with the stochastic variables for each simulation produced from a computer generated random number, or pseudo random number, and the defined statistical distribution for these stochastic variables. With a sufficiently large number of simulations the results of these simulations are representative of the stochastic system behaviour. See Section 3.5.3 for the methodology used to implement Monte Carlo analysis in this study. Fenton and Griffiths (2008) note that Monte Carlo analysis has the advantage that its use is not dependent on a stochastic analytical solution being available. Or, within the context of this study, the accuracy of any stochastic solution that is postulated. Monte Carlo analysis also has the advantage of acting as validation to any stochastic analytical solution proposed for a problem, with various studies using Monte Carlo methods in this role, for example Low and Phoon (2002). The principal disadvantage of a Monte Carlo method is the computational effort involved. For further details of how Monte Carlo analysis is used in this study see Section 3.5.

A range of spread sheet based analytical solutions of various degrees of complexity are referred to in the literature. Some of this complexity relates to the geometry of the failure surface and the number of geotechnical parameters that are simultaneously considered e.g. undrained shear strength, soil unit weight, friction angle. Low and Phoon (2002) and Low (2005) present a method that integrates with an optimisation process using Excel solver, accommodating a curved failure surface in a problem domain defined by a range of geotechnical parameters. Relatively complex performance, or capacity, functions are incorporated into these methods including combined Vertical (V) and Horizontal (H) loading, but not V-H stability envelopes. A range of simpler analytical methods are also available, with the method selected for this study based on Phoon (2004). This simpler method based on Phoon (2004) required formulating the chosen risk premise into a one dimensional reliability space. With further modification and care in formulating the risk premise complex performance, capacity, functions could also be used including V-H stability envelopes.

Studies using random fields numerical analysis were reviewed to investigate if this could be a useful technique for this study. An example of random field finite element analysis from Fenton et al. (2003) is shown in Figure 2.17. In this figure

the different shading for the elements represents a variation in a geotechnical parameter e.g. shear strength, settlement parameters, etc.

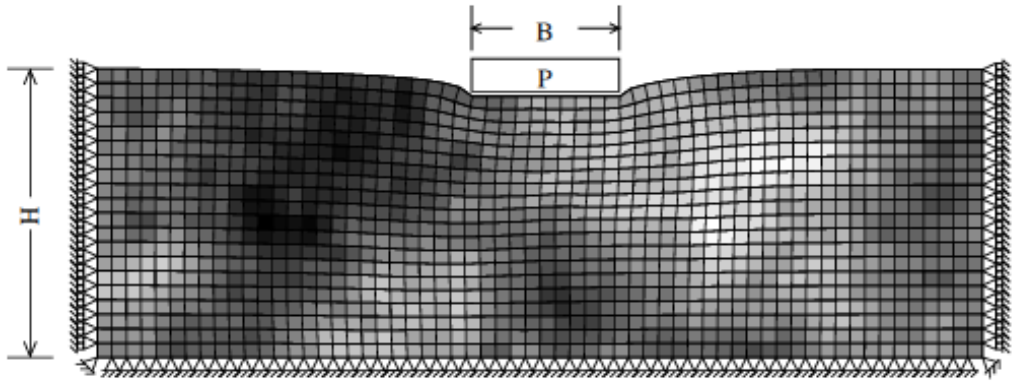

Figure 2.17 *- Random field finite element analysis (Fenton et al., 2003).*

One parameter considered in random field methods, which is not specifically considered in the previous two approaches, is the spatial correlation length. In simplified terms this is defined as the distance over which a parameter, such as soil shear strength varies. This forms part of the function that controls the parameter variation shown in Figure 2.17.

There is limited information on the typical spatial correlation length of geotechnical properties such as soil undrained shear strength and seemingly no literature addressing this for offshore soil. However, in studies where this parameter is used the dimension is significantly larger than a pipeline diameter. For example Griffiths and Fenton (2001) undertake a parametric study with the smallest dimension of spatial correlation as half the width of a strip foundation up to four times the foundation width. Cassidy et al. (2013) applies anisotropy to the spatial correlation length but the distances were still large (20 m horizontal and 1 m vertically). The large difference between the spatial correlation length and a pipeline diameter suggests for this problem variation is primarily occurring out of plane, for a plane strain analysis. This formed part of the rationale for not using random field numerical methods within this study. For further details discussion in the Methodology chapter, in particular Section 3.2.4 problem definition and Section 3.5 where the reliability based analysis methodology used in this study is discussed.

As noted previously, some literature addresses reliability analysis with consideration of V-H loading. However, the only example of the use of a V-H stability envelope was a recent study reported by Cassidy et al. (2013). In this study a large number of random field analyses were used to define points in Vertical (V), Horizontal (H) and Moment (M) load space. The yield surface derived from this analysis formed a probability based stability envelope, no mention was made of the plastic potential surface or post-failure behaviour.

Having addressed the analysis method a fundamental consideration in reliability based analysis is the statistical representation of the geotechnical parameters used in analysis, for example soil undrained shear strength (s_u). Commonly used representations of s_u are a Normal distribution and a Log Normal distribution. Consideration was given to both distributions with a Normal distribution selected, see Section 3.5 for further details. Simplified analytical methods are available for both distributions, for example Kulhawy and Phoon (2002) uses a log normal distribution and Phoon (2004) presents a method using a normal distribution.

Fenton and Griffiths (2008) notes that a log normal distribution is more commonly used for geotechnical analysis, citing that a normal distribution implies a small number of negative values, for example of s_u, where as a log normal distribution cannot have a value of less than zero. While a negative value of s_u is a conceptual problem, if this is simply viewed as another failure condition then this ceases to be a practical problem. While Fenton and Griffiths (2008) express a preference for a log normal distribution, they also note that analysis undertaken using log normal distribution without a significant degree of skew produces very similar results to a normal distribution. USACE (1997) suggest in the absence of detailed site specific data a normal distribution represents the most appropriate way to proceed. Little information on an appropriate distribution for offshore clay soils was found in this literature review. However, it was noted from Westgate et al. (2010) that field data on pipeline penetration appeared to show the form of a normal distribution, see Figure 2.17, or at least a log normal distribution with minimal skew.

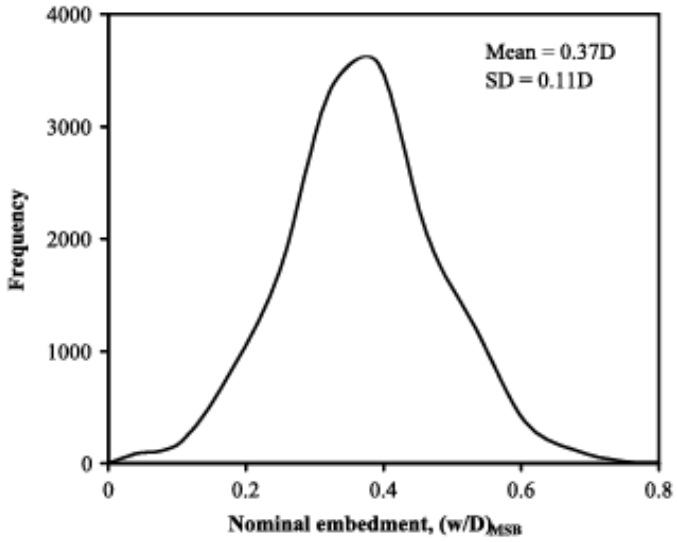

Figure 2.18 *- Distribution of pipeline embedment from Westgate et al. (2010).*

Reliability analysis is undertaken as a parametric study, therefore a range of coefficient of variation (CoV) are used with a normal distribution. The values of CoV adopted were reviewed and compared to the literature, such as Phoon and Kulhawy (1999) and Phoon (2004). Values of CoV of between 0.10 and 0.20 were used in this study, see Chapter 6 for further details. This range encompasses the lower and middle part of the typical range for a number of methods of measuring s_u. This was considered reasonable for this study as it is expected both high quality laboratory and in-situ testing will be available for offshore sites. Additionally the geological setting for normally consolidated and low over consolidation ratio clays is expected to have a lower degree of variation then the onshore clay deposits typically considered in this literature.

2.7 Summary and Discussion

Both a physical modelling approach to pipe-soil interaction on a clay seabed and a numerical and analytical approach has been addressed in this literature review. Pipe-soil interface properties and the occurrence of clay seabed have also been considered. Background literature has been provided to reliability based analysis techniques, as relevant to the use of this type of analysis in this study.

This literature review has provided an introduction to the topic of pipe-soil interaction on a clay seabed, as well as giving context and assisting in developing the objectives of this study as summarised in Section 1.2. It can be seen from a review of this chapter and Section 1.2 there are potential opportunities to compare the results of this study with the work of previous researchers. These comparisons will be summarised in Chapter 4 and Chapter 5, as relevant to a pipeline under Vertical (V) and combined Vertical and Horizontal (V-H) loading respectively.

In considering the potential for comparison between this study and previous research initial attention was given to physical modelling studies. It was noted that a number of previous researchers have tried to make similar comparisons and that issues have arisen with these comparisons, as illustrated in Figure 2.19 and Figure 2.20

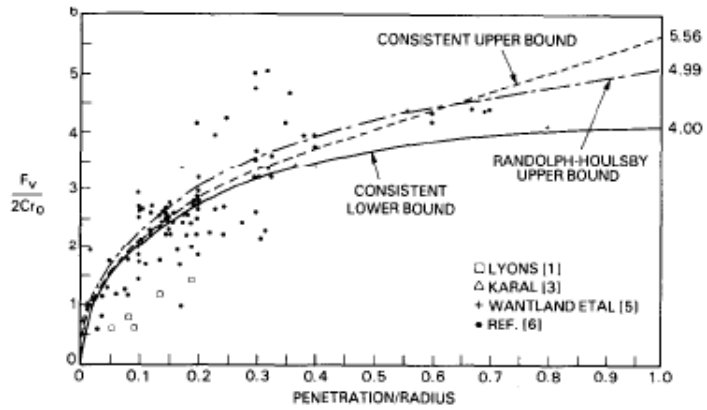

Figure 2.19 *- Comparison between plastic limit solutions and physical modelling data for pipeline penetration, from Murff et al. (1989).*

Figure 2.19 shows a comparison between a dimensionless resistance factor (equivalent to $R/s_u.D$) under vertical load and depth of penetration (z/r) to a depth of 0.5D. Resistance calculated from plastic limit upper and lower bound solutions are plotted in Figure 2.19. The data points in this figure are model test results from earlier research by Lyons (1973), Karal (1977), Wantland et al. (1979) and Wagner et al. (1987). A significant amount of scatter can be noted between the model test results and the analytical solutions. It can also be noted that the scatter is either side of the analytical solutions.

Figure 2.20 illustrates a similar point. However, in this case a number of the design equations are actually derived from model test data e.g. Verley and Lund,

(1995), Bruton et al. (2006). Similar large amounts of scatter are noted between these relationships and the model test data. Note; in Figure 2.20 the y axis is a resistance term equivalent to $R/s_u.D$, the x axis is for penetration z_p/r.

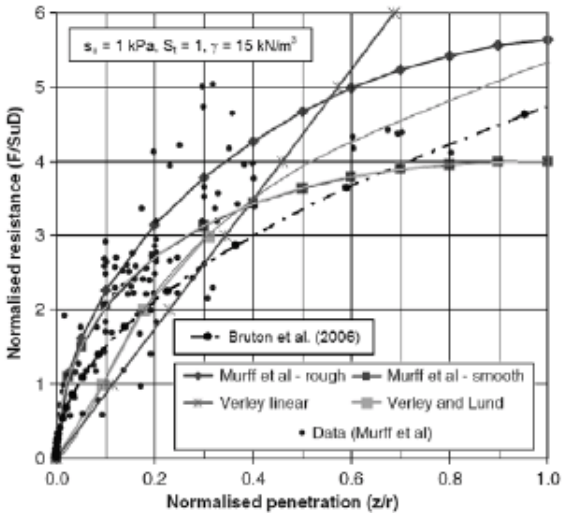

Figure 2.20 *- Comparison between various design equations and model test data, from Langford et al. (2007).*

There is limited attention to the issues raised in Figure 2.19 and 2.20 in the literature. However, it has important implications on the relevance of comparing the results of this study with model test data.

It has been noted that the scatter of the model test data is either side of the proposed relationships, an offset to one side or the other of these relationships might imply a systematic failure to address a particular factor. McCarron (2008) made an interesting observation with regards to recent centrifuge based model testing. It was noted that even for relatively advanced centrifuge testing the error in measuring the soil shear strength could be as much as 30-50%, or more. There is limited information on how shear strength measurements were obtained for earlier testing. However, it can only be assumed that this issue is similar or worse. An error, or scatter, in shear strength measurements used to derive fitting relationships would explain the scatter noted in Figure 2.19 and 2.20. This review supports some of the advantages of using a numerical analysis approach to investigating pipe-soil interaction on a clay seabed, at least in developing the initial interpretive framework and for parametric studies.

Field based model testing has been described in this literature review. While complex and presumably expensive to implement, this shows some promise, especially for site specific investigations. Unfortunately within the public domain there does not seem to be much data from this approach to physical modelling. Similar issues to that noted for laboratory based physical modelling, or worse, are expected in developing an interpretative framework from field based testing. This may not be as important if a range of anticipated pipeline movements can be addressed on a site specific basis. However, for wider relevance, interpretive models based on numerical analysis offer the most promising approach to addressing this data, especially if the uncertainty over shear strength measurements can be quantified and integrated into this model.

Scope for comparison between this study and previous research using numerical and analytical methods is a lot more promising then for physical modelling. Of particular note, with respect to Vertical (V) loading of a pipeline, are the design equations proposed by Aubeny et al. (2005) and Merifield et al. (2008). Accounting for large strain factors the analysis reported Merifield et al. (2009) is also expected to be useful for comparison purposes. For combined Vertical (V) and Horizontal (H) loading the stability envelopes proposed Merifield et al. (2008) are relevant. The large strain approach detailed by Merifield et al. (2009) has a number of limitations with respect to V-H loading, as noted in this chapter, and this research is expected to be less useful for comparison purposes. The limitation in the scope of more recent numerical analysis of V-H loading, e.g. roughness or shear strength gradient, limits their use for comparison with this study.

Literature related to pipe-soil interface properties has been reviewed and summarised in this chapter. Unfortunately there is insufficient information to assess how pipeline coating and soil will interact, either for physical modelling or more importantly within the context of this study in numerical analysis. This study will initially follow the approach used by previous researchers to bound the problem with a rough and smooth interface condition adopted in numerical analyses. These analyses will then be extended to a parametric study investigating intermediate conditions between these bounds. This will provide new information on pipeline behaviour between the extremes of a rough and smooth interface condition as well as demonstrating the potential to refine the analysis process to the properties of specific pipeline coating materials with further research.

The global occurrence of clay seabed, in particular very soft clay seabed, has been highlighted, providing context to the relevance of investigating pipeline behaviour on a clay seabed.

Reliability methods have been reviewed, providing useful background to this study. In particular with respect to choice of a shear strength distribution. For further details of the analysis method adopted see Chapter 3.

3 Methodology

3.1 Introduction

A range of physical modelling and numerical techniques have been used by previous researchers to investigate pipe-soil interaction on a clay seabed. There are advantages and disadvantages associated with both approaches. However, in reviewing the most recent work in this area, in conjunction with the objectives of this study, it was decided that numerical analysis techniques offered the most promising approach for this study.

Some of the advantages of the numerical analysis methodologies outlined in this chapter include;

- The ability to rapidly investigate a range of variables and undertake parametric studies. This could include different pipeline embedment depths, variation in geotechnical properties or in the case of combined Vertical (V) and Horizontal (H) loading a range of displacement vectors to define a V-H stability envelope. The absence of wide ranging parametric studies for problems such as interface behaviour and shear strength gradient have previously been highlighted in Chapter 2.
- Precise control over analysis conditions. For example geotechnical properties or interface properties can be easily defined as specific values.
- Readily compared to analysis by previous researchers, in particular previous numerical analysis.
- The ability to decouple aspects of the problem, such as quantifying the individual effect of properties such as soil shear strength and soil unit weight.
- Correlations and design methodologies are defined in terms of measurable geotechnical properties.
- Analysis results are readily integrated with reliability analysis techniques.

In addition, by using a well established commercial numerical analysis code the calculation methodologies used in this study have already been validated for other geotechnical problems.

Disadvantages of these numerical analysis techniques, when compared to physical modelling methodologies, largely relate to the possibility of some aspect of soil behaviour not being captured, or fully captured, within analysis. In this respect experimental methods could be advantageous for site, or project,

specific testing. However, for a more general and wide ranging study the advantages of numerical analysis techniques were considered to outweigh any disadvantages.

This chapter is divided into three sections. Section 3.2 provides an overview of the problems being considered. Section 3.3 discusses details of the numerical analysis methodology used within the finite difference code FLAC to undertake analysis for these problem definitions. The interpretation framework and correlation methodology is summarised in Section 3.4. Application of reliability based analysis methods to the results of this study are detailed in Section 3.5.

3.2 Problem Definition

3.2.1 Vertical Loading

For a subsea pipeline resting on the seabed Vertical (V) loading is likely to be an important consideration. The presence of any other load cases aside, a V load component from pipeline self weight can invariably be expected. Pipeline behaviour under V loading forms a logical first step to considering pipe-soil interaction on a clay seabed and is the first aspect considered within this study.

The following aspects of a pipeline subjected to V loading are considered in this study;

- A pipeline at shallow embedment, less than half a pipeline diameter (D), on a homogenous shear strength weightless seabed.
- A pipeline at deeper embedment, from 0.5D to 1.0D, on a homogenous shear strength weightless seabed.
- Larger strain and large displacement effects for a pipeline subjected to vertical loading.
- The effect of pipe-soil interface conditions.
- The influence of soil submerged unit weight (γ').
- The effect of a non-uniform soil shear strength, including linear increasing shear strength gradients and shear strength crusts.

A pipeline subjected to vertical loading on a sloping seabed is also considered in this study. However, the effect of variation in slope angle is more appropriately considered within a full combined Vertical and Horizontal (V-H) loading framework, therefore this problem is addressed later in the thesis in conjunction with other V-H loading problems.

A problem definition for the case of a pipeline subjected to vertical loading is shown in Figure 3.1. This definition is applicable to a shallow pipeline embedment, <0.5D, and is based on a homogenous shear strength weightless seabed at small strain.

A pipeline with an outside diameter D is embedded into a clay seabed to a depth z_p. This is a "wished in place" small strain approach to the problem within a two dimensional, plane strain, idealisation. For all the analysis undertaken in this study the pipeline is treated as a rigid body.

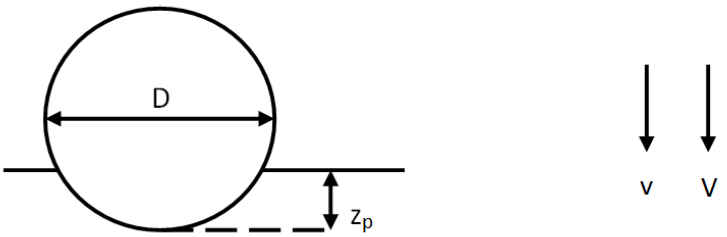

Figure 3.1 *- Problem definition - small strain V loading case for a pipeline at a shallow embedment depth (<0.5D).*

The pipeline in Figure 3.1 is subjected to a vertical displacement (v) with calculation of the resistance (R) in response to this displacement. This is a displacement controlled analysis and produces equivalent results to applying a V load to the pipeline, while providing some advantages as an analysis methodology, see Section 3.3. Analysis is progressed to provide the maximum value of R, for a given embedment depth. This is analogous to the maximum capacity under V loading, V_{max}. Analysis can be undertaken for a series of embedment depths to provide information on the variation in V_{max} with pipeline embedment depth.

For deeper embedment depths, beyond 0.5D, a problem definition is shown in Figure 3.2. This problem definition is largely the same as that previously shown in Figure 3.1. However, at an embedment depth greater than 0.5D the pipeline shoulders go below the seabed surface (mudline). For this small strain definition in a cohesive soil the soil above the pipeline shoulders is considered as a vertical wall, forming a slot into which the pipeline is wished in place.

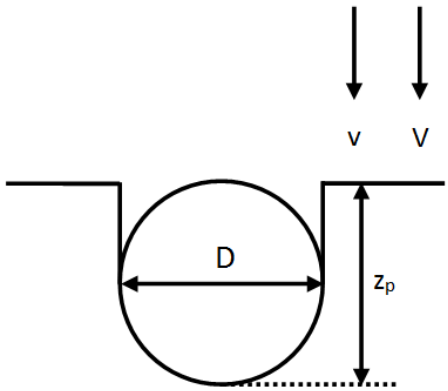

Figure 3.2 *- Problem definition - small strain V loading case for a pipeline at a deeper embedment depth (>0.5D).*

In addition to a wished in place small strain problem definition a large strain approach can also be used to investigate large displacement effects, as shown in Figure 3.3. Analysis is commenced with the pipeline above the seabed, or just in contact with the seabed. From its starting position a pipeline of diameter D, is subject to a vertical displacement (v) with measurement of resistance (R). Within a large stain analysis methodology the mesh geometry is free to move in response to applied forces. In this problem the penetration of the pipeline into the seabed will displace soil, resulting in soil heave adjacent to the pipeline. As with the previous problems R is analogous to the capacity under V loading. In this case, following a small initial elastic displacement, R is representative of a continuous profile of V_{max}. There is no requirement for a different problem definition for pipeline embedment depths >0.5D as the seabed will form into an appropriate profile above the pipeline shoulder as part of the analysis process.

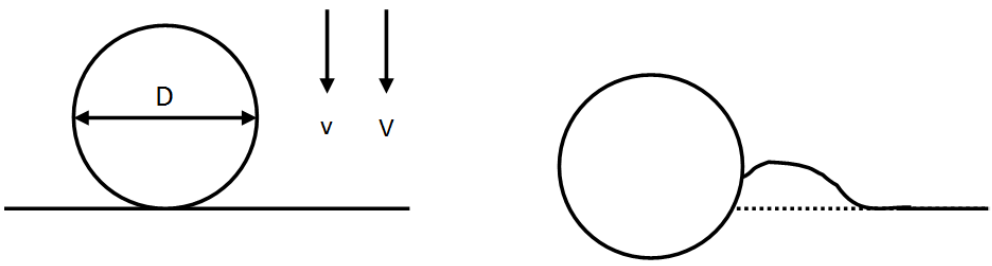

Figure 3.3 *- Problem definition - pipeline subjected to vertical (V) loading using a large strain analysis methodology.*

The comparison between small strain analysis and the problem definition shown in Figure 3.3 is also of interest as it provides a link between larger parametric studies that adopt a small strain assumption and the behaviour expected in the field.

The problem definitions shown in Figure 3.1, Figure 3.2 and Figure 3.3 all consider the case of a homogenous shear strength weightless soil. This shear strength refers to undrained soil shear strength (s_u) and is relevant to displacement or loading rates that provoke an undrained soil response. On a clay seabed this can be expected to cover a wide range of displacement or loading rates. For example undrained behaviour can be described by a $\bar{\upsilon}.D/c_v$ ratio, as referred to by House et al. (2001) and Houlsby and Cassidy (2011). Here $\bar{\upsilon}$ is taken as a velocity term, for example vertical displacement velocity, D is a diameter or drainage path length term and c_v is the soil coefficient of consolidation. On a clay seabed c_v is typically very small, for example as noted by Robinson and Allam (1998). Therefore undrained behaviour is applicable to a very wide range of pipeline displacement velocities on a clay seabed.

At undrained loading rates the principal geotechnical parameters of interest for the seabed soils are undrained shear strength (s_u) and submerged unit weight (γ'). With the soil is treated as an elasto-plastic material in this study, elastic parameters also have to be assigned i.e. Young's modulus (E) and Poisson's ratio (ν), or alternatively bulk modulus (K) and shear modulus (G). As the principal interest is in V_{max} and plastic collapse load, these elastic properties are a less important consideration compared to parameters influencing plastic behaviour. However, it can be noted that elastic properties will have some influence at the very shallowest pipeline embedment depths, prior to the onset of extensive plastic flow, and that they may become more important in higher shear strength soils and, or, for very light pipelines.

For analysis undertaken as part of this study undrained behaviour is governed by the choice of constitutive model and associated geotechnical parameters assigned. The actual displacement velocity assigned in analysis is selected based on factors such as numerical stability rather than any influence on soil behaviour.

Pipe-soil interface conditions are expected to influence the V loading problems being considered. In terms of a problem definition interface conditions can be viewed as being bounded by two extremes, a rough interface or a perfectly

smooth interface. The problems shown in Figures 3.1, Figure 3.2 and Figure 3.3 were all analysed with a rough and smooth interface condition. Variation between these two cases could also be considered. In the literature there is little attention given to the behaviour of these intermediate cases.

A rough interface has shear strength equal to, or greater than, the surrounding soil and generally provides an upper bound to a problem. With a rough pipe-soil interface the ability to accommodate shear forces exceeds or equals that of the adjacent soil, with any shear displacement transferred to the adjacent soil mass. Elastic parameters for a rough interface also exceed, or equal, those of the soil, hence elastic displacements will also be transferred to the soil mass. For further details of configuration of interface properties see Section 3.3.

A perfectly smooth interface is the opposite bound to the interface behaviour problem then a rough interface. A smooth interface is when the interface cannot accommodate any shear forces, allowing free movement of the soil past the interface with no resistance generated by this movement. A smooth interface also has no elastic stiffness in shear.

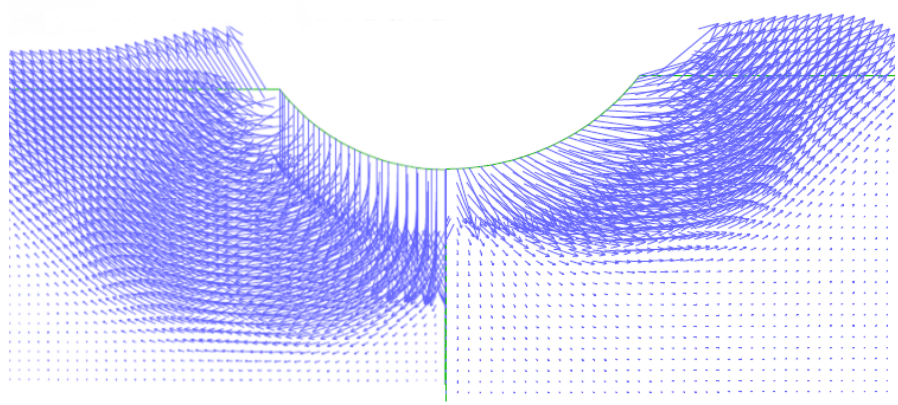

a) b)

Figure 3.4 *- Calculated soil displacement presented as a vector plot for a vertically displaced pipeline with a rough (a) and smooth (b) pipe-soil interface.*

Figure 3.4 presents the calculated soil displacement for a vertically displaced pipeline with a rough and smooth pipe-soil interface. Note these plots do not represent the same analysis. Two analyses have been mirrored against each other, using image processing techniques, in order to aid comparison. The

direction of the soil displacement adjacent to the pipe-soil interface is of particular interest and illustrates the interface properties previously defined. It can be seen that the soil adjacent to the rough interface, on the left, is displaced in the direction of the pipeline displacement i.e. vertically. The soil adjacent to the smooth interface, on the right, is not constrained and shows displacement vectors at a range of angles to the interface depending on the depth below mudline and associated pipeline geometry. The influence of interface conditions on the geometry of failure mechanism can also be seen in this example, this is discussed further in Chapter 4.

In addition to the rough and smooth interface condition, investigations were undertaken into interface conditions between these bounds. One approach to defining this problem is to consider the interface shear strength (s_{ui}). This interface strength can be expressed as a ratio of the soil undrained shear strength (s_u), producing the dimensionless group s_{ui}/s_u. A rough interface would be $s_{ui}/s_u=1.0$, or 100 % of the soil shear strength, and a smooth interface would be $s_{ui}/s_u=0$, or 0 % of the soil shear strength. Additional interface properties can be defined by this method and investigated in analysis e.g. s_{ui}/s_u = 0.25, 0.50, 0.75, where the interface strength is 25 %, 50 % and 75 % of the soil undrained shear strength respectively. This approach provides a convenient notation for considering this problem as well as being a logical way to implement the problem within the numerical analysis software.

Elastic parameters for the pipe-soil interface are not expected to significantly influence this problem, with plastic flow at the interface and in the surrounding soil mass governing the maximum capacity aspects of the problem. Even at the shallowest embedment depths, which for consideration of interface variation are out with the scope of this study, the interface stiffness is a secondary consideration to the stiffness of the soil mass. There is no information on the stiffness properties of pipe-soil interfaces in the literature. However, determining an appropriate interface stiffness for a fully rough and perfectly smooth interface, as used for much of this study, follows a clear rationale. For the rough interface the properties of the interface are the same as the surrounding soil mass, therefore the same stiffness as the soil can be assigned. A larger stiffness would also not impact this problem, with displacement occurring in the soil mass immediately adjacent to the interface. For the perfectly smooth interface there is zero stiffness in shear in conjunction with no resistance from a plastic shear failure mode.

For intermediate interface conditions, as investigated in this study, two approaches to interface stiffness could be adopted. The influence of these two approaches is expected to be confined to a limited influence over the mobilisation distance to peak capacity, rather than influencing the peak capacity as governed by the plastic properties of the soil and the interface. The first approach is to keep the interface stiffness the same as the soil for all but the perfectly smooth interface condition. The second approach is to scale the interface stiffness relative to the interface strength, reflecting the approach used to derive elastic parameters for the soil mass. This later approach is considered a more rational approach. For example, the strength of the interface will often have been influenced by factors that will also impact the stiffness properties of the interface, such as the presence of partially remoulded clay at the pipe-soil interface and/or excess pore pressures. The approach of scaling interface stiffness relative to interface strength has been adopted in this study.

Having considered the problem definitions in Figure 3.1 and Figure 3.2 with a weightless clay seabed an alternative problem definition was considered where the seabed has a defined submerged unit weight. For these calculations a density is assigned to the soil and gravitational forces are applied as part of the calculation process. By comparing this with the previous problem definition the effect of soil weight can be quantified. Submerged unit weight will be treated as homogenous and invariant with depth in this problem definition.

The problem definition shown in Figures 3.1 and 3.2 assumes a homogenous shear strength soil. Variations from this case can also be investigated. One of these variations is a linearly increasing shear strength gradient, with the problem definition for this case shown in Figure 3.5. A pipeline of diameter D is embedded to a depth z_p. The undrained shear strength s_u varies with depth, z. The shear strength at the seabed, mudline, is assigned the notation s_{u0} and the shear strength at the pipeline embedment depth is s_{uzp}.

Within the context of foundation bearing capacity, a linear increasing shear strength gradient is conventionally expressed in terms of the strength at the soil surface and a factor that describes the increase with depth, e.g. $s_{u0} + k.z$, where s_{u0} is the strength at the soil surface and k is the gradient of strength increase with depth z. This may then normalised by the foundation width. Examples of this approach include Davis and Booker (1973), DNV (1992) and BSI (2003).

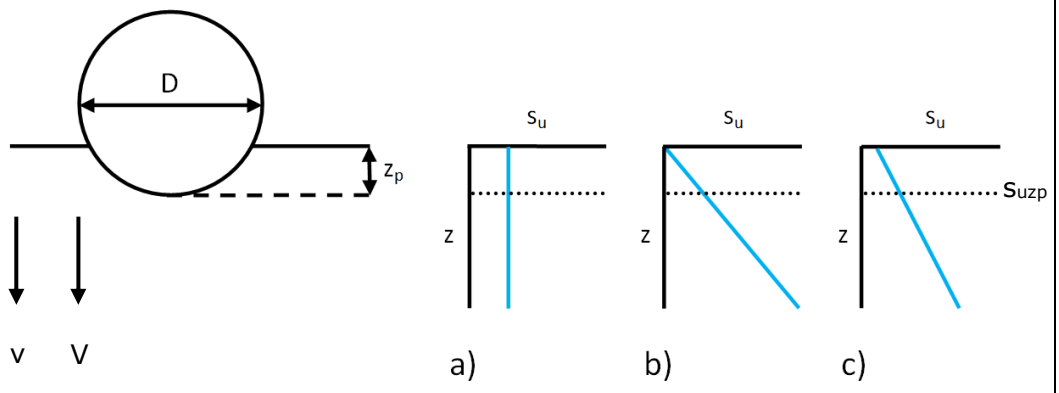

Figure 3.5 *- Problem definition - seabed soils with a linear increasing shear strength gradient.*

While this approach is reasonable, and widely used, its advantages largely lean towards the design of a specific surface pipeline on a specific shear strength gradient. It is more cumbersome to use in a general solution for foundations with a range of embedment depths in the presence of a range of shear strength gradients e.g. a general solution for a pipeline on a seabed with a linear increasing shear strength gradient. It is also more cumbersome to use with a reference shear strength at the pipeline embedment depth, e.g. s_{uzp}, as is useful for pipe-soil interaction problems. An alternative approach has been developed and is adopted in this study.

Figure 3.5 a to c presents plots that help describe the alternative definition of a linear increasing shear strength gradient adopted in this study. Figure 3.5 a) represents the uniform shear strength case, b) is the case of a linear increasing shear strength gradient with a zero shear strength intercept at mudline. Figure 3.5 c) represents a linear increasing shear strength with a non-zero strength intercept at mudline. The problem of a linear increasing shear strength gradient varies between a zero shear strength intercept at mudline and the uniform shear strength case, to the case where the strength intercept at mudline is equal to the strength of rest of the soil. Variation between these two cases can be expressed in terms of the shear strength intercept at mudline, s_{u0}, relative to the shear strength at the base of the pipeline for a given pipeline embedment depth, s_{uzp}. So for example s_{u0}/s_{uzp} = 1, or 100%, is the uniform strength case, and s_{u0}/s_{uzp} = 0 or 0% is the case with zero strength at mudline. An intermediate case would be s_{u0}/s_{uzp} = 0.5 or 50% where the strength intercept at mudline is half the strength at the pipeline embedment depth. A range of cases between 0

and 100% can be investigated. Analysis of shear strength gradients will be confined to small strain problems within this study.

A more complex variation in shear strength is a shear strength crust as described by Ehlers et al. (2005) and Puech et al. (2005) and further investigated in Kuo and Bolton (2009) and Kuo et al. (2010). While it may be possible to undertake site specific analysis for a given shear strength crust, for example directly using the result of in-situ testing such as T-bars within the numerical analysis, a more generalised approach is to represent the crust as a series of linear shear strength gradients, see Figure 3.6.

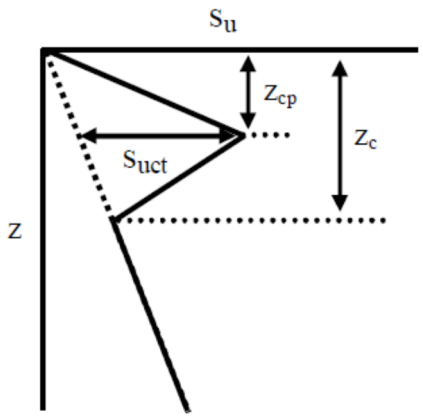

Figure 3.6 *- Linear representation of a shear strength crust.*

A shear strength crust is a relatively complex variation of undrained shear strength, s_u, with depth, z. These crusts would appear to be found in association with a linear increasing shear strength gradient. Within this study a crust is described in terms of a departure from an underlying linearly increasing shear strength gradient. The underlying strength gradient has a zero strength intercept at mudline for the cases considered in this study. The thickness of the crust, z_c, is defined as the depth range of the departure away from the underlying shear strength gradient.

The crust can then be defined by two linear strength gradients, one positive and the second negative, and the depth of the shear strength crust peak, z_{cp}. The crust peak shear strength, at a depth z_{cp}, can also be defined as the departure from the underlying gradient s_{uct}, either as a percentage increase or multiple of the strength on the underlying gradient. Within this study z_{cp} is taken as being 50% of the thickness of the crust. A range of crust magnitudes can be investigated, as described by a range of values of s_{uct}. For a given crust

geometry a range of pipeline embedment depths can also be considered. Analysis of shear strength crusts will be confined to small strain problem definition within this study.

3.2.2 Combined Vertical and Horizontal Loading

In addition to the case when a subsea pipeline is subjected to Vertical (V) loading a pipeline resting on a clay seabed can also be subjected to Horizontal loading (H), resulting in a more complex combined V-H load case. The following aspect of a pipeline subjected to V-H loading are considered in this study;

- The maximum horizontal capacity (H_{max}) of a pipeline at a range of embedment depths, up to one pipeline diameter (D), on a homogenous strength weightless seabed.
- Calculations of the V-H stability envelopes at a range of embedment depths, up to one pipeline diameter (D), on a homogenous strength weightless seabed.
- Large displacement effects under combined V-H loading.
- The effect of a linear increasing shear strength gradient on maximum horizontal capacity (H_{max}) for a range of embedment depths up to 1.0D.
- The effect of a linear increasing shear strength gradient on the V-H stability envelopes for a range of embedment depth up to 1.0D.
- The influence of a sloping seabed on V-H stability envelopes.

A problem definition for a pipeline subjected to combined V-H loading at shallow depth is presented in Figure 3.7.

A pipeline of diameter D is embedded to a depth z_p of <0.5D on a homogenous shear strength weightless seabed. A small strain "wished in place" plain strain problem definition is adopted. The pipeline is treated as a rigid object with a perfectly smooth pipe-soil interface condition.

This pipeline is subjected a combined vertical (v) and horizontal displacement (u) to give displacement at a velocity $\bar{\upsilon}$ and a displacement angle δ. The vertical and horizontal components of resistance, R_V and R_H, are calculated and analysis is progressed to peak resistance. For a pipeline displaced horizontally (0°) the maximum value of R_H is equivalent to the maximum capacity under H loading, H_{max}. For other displacement vectors the maximum value of R_V and R_H for a particular analysis is equivalent to a termination point on the pipelines V-H stability envelope.

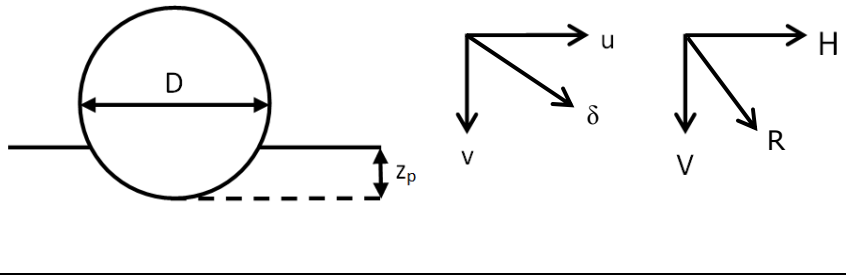

Figure 3.7 *- Problem definition - small strain combined V-H loading of a pipeline at a shallow embedment depth (<0.5D).*

As with the pipeline subjected to vertical loading in the previous section; below 0.5D an alternative problem definition is needed to account for the pipeline shoulders being below seabed level. This is shown in Figure 3.8. As with the vertically loaded pipeline the V-H loaded pipeline is wished in place into a slot with vertical walls.

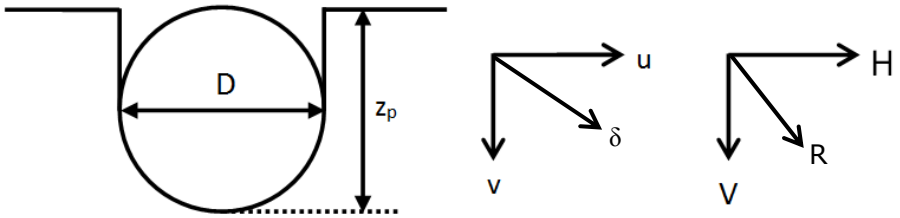

Figure 3.8 *- Problem definition - small strain combined V-H loading of a pipeline at a deeper embedment depth (>0.5m).*

Figures 3.7 and Figure 3.8 have been based on a small strain problem definition. As with the problem definition in for V loading, see Figure 3.3, there is also a large strain, large displacement, case. However, while a problem definition similar to Figure 3.3 may be of interest for V-H loading a potentially more important behaviour is ride-in and ride-out behaviour at large displacement. This concept is illustrated in Figure 3.9. While the presence of soil heave can be expected to influence the resistance to H loading ride-in and ride-out behaviour can result in both an increase and decrease in resistance with lateral displacement. It is also expected to be associated with a steady state value of

resistance at larger displacement. In this problem definition this behaviour is modelled with a series of small strain V-H stability envelopes and their plastic potential surface.

A pipeline may be subjected to a V load greater than self weight during the installation process. Following installation the pipeline self weight load case will sit in a larger stability envelope. Two example scenarios are shown in Figure 3.9. Figure 3.9 a) is the case when installation forces were only slightly more than self weight. For this case the self weight V load is around 80% of the V_{max} for the installation case. When a large enough H load is applied, such as the load path shown by the green arrow, the load case intersects the edge of the stability envelope. At this point the pipeline will start to move. In Figure 3.9 a) a displacement vector is shown in purple from the point where the green load path reaches the V-H stability envelope. This indicates the direction of initial movement. From this it can be seen that the pipeline will penetrate further into the seabed, ride-in behaviour. As the pipeline rides into the seabed the increase in pipeline embedment will lead to an increase in the size of the V-H stability envelope e.g. see Figure 3.9 c). If the H load case is large enough it is expected displacement will continue and a steady state value of pipeline embedment and resistance will be reached, at large displacement.

Ride-out behaviour in this problem definition is potentially more significant as this will result in a reduction in resistance to H loading, in association with a reduction in embedment depth, at large displacement, see Figure 3.9 b). For this case the forces associated with installation were a multiple of self weight. In this example the pipeline self weight is approximately 40% of the V_{max} associated with installation. As the H load case shown by the green arrow is applied the load path intersects with the upper part of the stability envelope. The purple displacement vector shown here illustrates how pipeline embedment depth will initially reduce as a result of this load case, the pipeline rides out. As the pipeline embedment depth reduces the size of the V-H stability envelope contracts (see Figure 3.9 c). Again, it is expected a steady state value of pipeline embedment and resistance to H loading will be reached at large displacement.

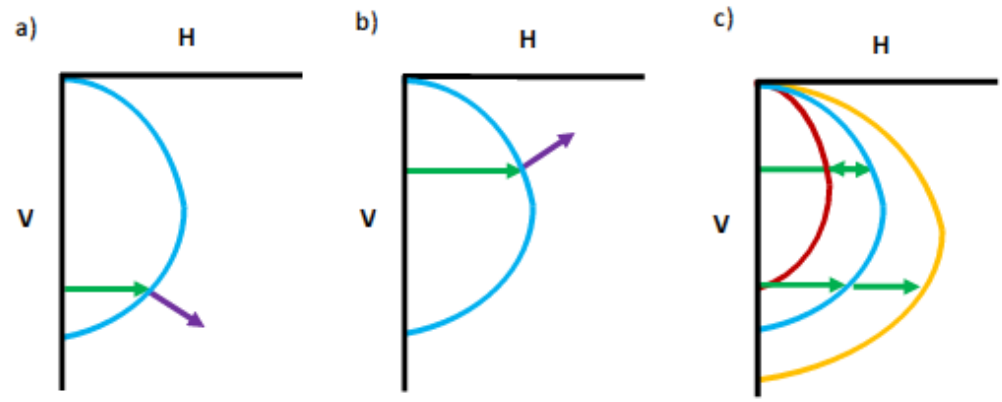

Figure 3.9 *- Problem definition - ride-in (a) and ride-out (b) behaviour at large displacement, changes in envelope geometry are shown (c)*

The effect of a linear increasing shear strength gradient on a pipeline subjected to V-H loading has also been investigated. The problem definition for this case is shown in Figure 3.10.

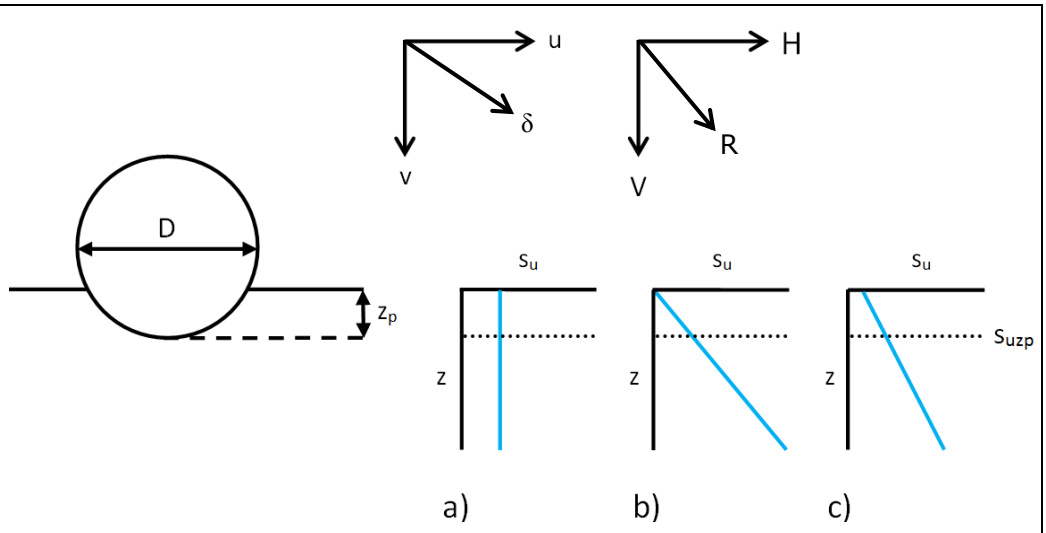

Figure 3.10 *- Problem definition - seabed soils with a linear increasing shear strength gradient.*

The problem definition for a linearly increasing shear strength gradient is the same as previously described in Figure 3.5. These shear strength gradients are defined by the s_{u0}/s_{uzp} ratio with a range of cases analysed and compared with the homogenous shear strength case. On a seabed with a linear increasing shear

strength gradient the pipeline is subjected to combined v and u with calculation of R_V and R_H. H_{max} is calculated for these conditions followed by the full V-H stability envelope.

All previous problem definitions have been based on a flat seabed. Figure 3.11 considers the case of an in plane slope of angle ψ. A pipeline of diameter D is embedded to a depth z_p, with z_p defined parallel to the slope. This pipeline is then subjected to combined vertical (v) and horizontal (u) displacement with calculation of resistance. As with previous problem definitions, peak resistance at various pipeline displacement angles (δ) were used to define V_{max}, H_{max} and additional points on the pipeline VH stability envelope. This methodology was developed to produce stability envelopes for a wide range of slope angles with a weightless seabed. Limited investigations were also undertaken into the case of a seabed slope with consideration of soil unit weight.

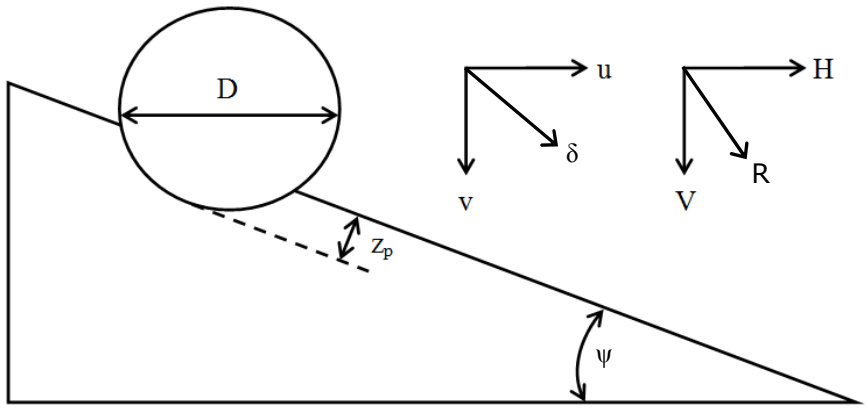

Figure 3.11 *- Problem definition - small strain combined VH loading of a pipeline on a sloping seabed.*

3.2.3 Reliability Based Design Methods

The problem definitions described so far within this chapter have been based on deterministic models. In this study reliability based design techniques have also been used to investigate pipe-soil interaction problems within a stochastic framework. These reliability based design problems are largely the same as the problem definitions previously detailed in this chapter. The principal difference is that the soil undrained shear strength, s_u, is now treated as a stochastic variable rather than being a single deterministic value. The reference shear strength for these problems is the mean undrained shear strength $s_{u\mu}$, which has a defined

statistical distribution. A normal distribution of s_u has been adopted in this study with a range coefficients of variation (CoV) analysed.

The following aspects of reliability based design are considered in this study;

- Pipeline penetration into the seabed when subjected to a Vertical (V) load.
- Reliability based analysis of maximum Vertical capacity (V_{max}) for a range of pipeline embedment depths, up to one pipeline diameter (D), on a homogenous strength weightless seabed.
- Reliability based analysis of maximum Horizontal capacity (H_{max}) for a range of pipeline embedment depths, up to one pipeline diameter (D), on a homogenous strength weightless seabed.
- Extension of reliability based techniques to V-H stability envelopes.

Reliability based techniques are applied to the various resistance models described earlier in this chapter e.g. V_{max}, H_{max}, or V-H stability envelopes. Implicit in this approach is an important aspect of the problem definition. Shear strength as the stochastic variable not only has a statistical distribution but also spatial variability (as described Section 2.6). Using the resistance models from the deterministic case implies that this spatial variability is large relative to the pipeline diameter. In other words, the spatial variability is considered to occur out of plane (along the pipeline length) for these plane strain analyses and does not influence the resistance model. This is considered reasonable given the small diameter of pipelines and the geological setting for subsea clays. The spatial variability along the pipeline length may also be large relative to the product stiffness. However, if this is not the case this would need to be addressed by the pipeline designer within the structural design. For example by allowing transfer of some load through the pipeline from areas of low resistance to areas of higher resistance.

One of the simplest problem definitions within a stochastic framework is penetration into the seabed of a pipeline under Vertical (V) load. For this problem definition the vertical load is assumed to be a well understood variable, such as self weight or a multiple of self weight due to installation forces. V is treated as a deterministic value. The pipeline diameter is also treated as a deterministic value. It is expected D will normally be measurable and well understood. This problem definition consists of a single case, where a pipeline of diameter D and one vertical load V is analysed. A smooth pipe-soil interface condition is used. The soil model is a weightless soil with a mean homogenous

undrained shear strength ($s_{u\mu}$) treated as the stochastic variable with a defined statistical distribution.

This simple vertically loaded pipeline problem is investigated with reliability based methods to determine the probability of pipeline penetration to a given z/D ratio for a defined V load case. The probability of exceeding a given embedment depth was treated as the probability of failure (P_F), in a similar way to over-penetration of a foundation can be viewed as failure.

This problem definition is similar to what might be relevant to design practice for an offshore project and provides an example of the application of reliability based techniques to this type of problem. However, as this problem definition is limited to a single set of variables, pipeline diameter, soil shear strength and vertical load, it lacks generality and provides limited information on the nature of the problem. The rest of the problem definitions discussed here consider more general cases providing greater insight into these aspects of pipe-soil interaction on a clay seabed.

Having undertaken analysis for a simple case of V loading analysis was extended to investigate V_{max} within a stochastic framework. A range of pipeline embedment depths up to 1.0D were considered. The probability of exceeding a given depth of embedment was analysed, with this defined in terms of the probability of failure (P_F) for a given V load i.e. probability of $V>V_{max}$. V load, soil shear strength and pipeline diameter were expressed in general terms by using the dimensionless load group $V/s_{u\mu}.D$, extending applicability.

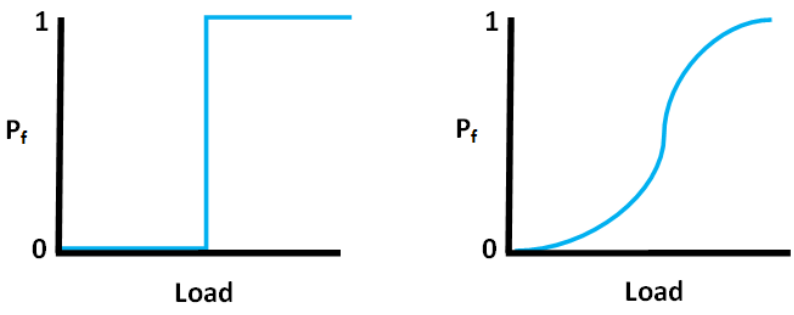

Figure 3.12 *- Problem definition - System fragility.*

Analysis of this more general case for V loading enables investigations into the overall system behaviour within a reliability framework. A useful concept for considering system behaviour is the concept of fragility, for example as

discussed by Schultz et al. (2010). Figure 3.12 shows a representation of fragility. The sketch on the left shows a deterministic system, a system with no fragility, and the sketch on the right shows a higher fragility system. Fragility considers the probability of failure relative to an applied load, for example V loading on a pipeline. A well understood system, which would have a trend very similar to deterministic system shown on the left of Figure 3.12, has low fragility, brittleness and a well understood behaviour. For a low fragility system the difference between a negligible chance of failure (i.e. close to P_F=0) and a near certain chance of failure (i.e. close P_F=1) is a very small increment of load. A high fragility system is less well understood, possibly more complex and extends over a wider load range. For this high fragility system there is a general trend of increasing chance of failure with increasing load. Additionally, over a wide load increment there is a potentially non-trivial chance of failure. To quantify fragility the concept of a Fragility Index (I_F) was developed as part of this study. I_F quantifies the dimensionless load increment (e.g. $V/s_{u\mu}.D$ or $H/s_{u\mu}.D$) over which the P_F goes from a defined low P_F to a defined high P_F. See Section 6.3 for a full definition and the approach used to derive I_F.

An important variable for a pipeline subjected to V-H loading is H_{max}. Prior to considering full V-H loading stability envelopes within a reliability framework, H_{max} was analysed using a similar methodology to that used for considering V_{max}. Investigating P_F in terms of the probability of $H>H_{max}$. The dimensionless load group $H/s_{u\mu}.D$ was used. Fragility and I_F were also investigated, providing an opportunity to compare and contrast fragility and I_F for V_{max} and H_{max}.

As part of this study a methodology was developed to produce reliability based V-H pipeline stability envelopes. For increased generality these envelopes were plotted within a $V/s_{u\mu}.D$ against $H/s_{u\mu}.D$ load space. A deterministic V-H stability envelope is a surface within V-H load space. Within this surface the pipeline is stable and viewed as not moving, although there may be small movements associated with confined plastic flow and/or elastic soil behaviour. When a load case exceeds the stability envelope for a given set of conditions the pipeline moves. This pipeline displacement may result in an increase in the size of the stability envelope and the pipeline may become stable again, or alternatively the stability envelope may stay the same size, or contract, and the pipeline will continue to displace. A reliability based stability envelope essentially follow the same principle. For a given set of conditions a range of stability envelopes can be produced. These stability envelopes are essentially contours of P_F in load space and can be presented for a range of P_F of interest. When a load case is

within a reliability based stability envelope of a given P_F the chance of failure/movement is less than this P_F, or equal to it if the load case touches the envelope. Stability envelopes were defined using a series of reliability based probes in load space. The V-H load ratio for these probes was fixed. This is equivalent to these probes being undertaken along a fixed angle in load space, δ_{LS}.

3.3 Numerical Analysis Methodology

3.3.1 Introduction

Numerical analysis within this study was undertaken using the commercial 2D explicit finite difference code FLAC (Fast Lagrangian Analysis of Continua). Some early problem familiarisation was undertaken with version 5.0 of this code (Itasca, 2005). However, all analysis reported in this thesis uses FLAC version 6.0 (Itasca, 2008c).

Analysis was largely undertaken on a desk top computer with a 2.4 GHz Intel dual core processor, 2 GB of memory and operating with Microsoft Windows XP. Some post-analysis processing and a limited amount of short duration analysis was undertaken on various laptop computers. As can be expected a desk top computer was better suited to longer duration analysis. By monitoring computer system processes it was noted that FLAC analysis was processor driven with minimal memory usage. The FLAC licence dongle allowed for up to two analysis windows to run at one time. When two analysis were running simultaneously each analysis was assigned to one of the processor cores. However, when a single analysis was being undertaken only one core was used. There was therefore no benefit in considering multi-processor or larger multi-core systems with this version of the FLAC. A slightly faster processor would have been of benefit in speeding up analysis times. However, with longer analysis running overnight and through weekends only very significant decreases in analyses time would have been of appreciable benefit with respect to analysis scheduling.

Analysis time for this software and hardware configuration varied significantly with the problem being considered, in particular with mesh dimensions and density. A small strain analysis of vertical penetration with a relatively coarse mesh would typically take less than 1-2 minutes. At the other extreme, for a fine mesh V-H analysis at deep embedment each displacement probe might take 24 to 60 hours. With each V-H envelope made up of multiple probes defining the full

envelope could take 1-2 weeks of analysis time. Another time consuming analysis was consideration of soil unit weight on a sloping seabed. This case required displacement probes through 360° to capture up slope and down slope effects, adding to the total analysis time.

As noted in Section 3.1, the use of a well established commercial numerical analysis code had advantages from a validation standpoint. There was also significant advantages in being able to focus on the problem being considered rather than having to divert time to software development and validation. FLAC provided both small strain and large strain analysis options, although the large strain analysis still required some user intervention at very large displacement to implement a manual re-mesh when mesh deformation issues arose. The graphical user interface (GUI) used by FLAC simplified the process of configuring analysis, although this still required a familiarity with FISH programming (Itasca, 2008a), FLAC's built in programming language. After initial familiarisation, the use of FISH and the direct access to the analysis configuration file provided within FLAC became a significant advantage. Editing of this analysis configuration file within a text editor allowed for large batches of analysis and parametric studies to be automated. For example, with a V-H stability envelope the analysis for the various displacement vectors were run automatically from the analysis configuration file. Each analysis case was calculated, save files created and data output as text files prior to stepping onto the next analysis in the configuration file. Output of the results of a FISH program as text file was also very useful for additional post processing and interpretation of analysis data. In general FLAC was considered a good choice of software for this study.

3.3.2 General Aspects of Numerical Analysis

There are a number of aspects in common for all the numerical analyses undertaken using FLAC for this study. The general approach to analysis and these common aspects will be discussed in this section. Later sections will address problem specific elements of analysis e.g. Section 3.3.3 addresses V loading and Section 3.3.4 describes aspects of analysis of V-H loading.

Configuration of analysis can be subdivided into several broad categories, as follows;

- Simplification of geometry and exploitation of symmetry
- Problem boundary location and properties

- Definition of pipeline and soil surface geometry
- Mesh density and refinement
- Assign material properties
- Assign interface conditions
- Displacement or load application
- Commence analysis with recording of results

An important consideration early in the analysis process is simplification of the analysis geometry. This may include exploitation of symmetry within the problem. The choices made early in this process have significant implications for analysis "cost" and how much can be achieved in a given period of time. Unnecessary complication can also hinder interpretation. Early in this study, in conjunction with numerical analysis software selection, it was decided to simplify analysis to a two dimensional plane strain case for all the problems considered here.

Exploitation of symmetry within an analysis problem is also an important consideration. For example, for V loading analysis times can be approximately halved by undertaking analysis of half a pipeline cross section around a central line of symmetry. Forces are then simply multiplied by two to produce an identical result to a full pipeline cross section. For V-H loading on a flat seabed, while a full pipeline cross section has been analysed, displacement vectors can be limited to 180°. Analysis results are identical when displacing a pipeline in a right hand or left hand direction. A full 360° envelope can then be developed by exploiting the symmetry of this envelope in V-H load space.

Having defined the problem geometry, definition of the analysis field in the calculation has to be addressed by defining the boundary locations. The properties of these boundaries also have to be assigned. In defining the boundary locations the competing objectives are to reduce the size of the finite difference mesh to improve analysis efficiency, while still having the mesh extend a suitable distance so that the boundary locations are not influencing the analysis results.

During the problem familiarisation phase of this study experience was gained in assessing boundary location with test analysis undertaken to gain understanding of these requirements. Figure 3.13 shows a plot of analysis results for a

vertically displaced pipeline. Analysis has been progressed to peak vertical capacity, V_{max}. This figure shows two ways of presenting analysis result to assist in assessing suitable boundary locations, with these plots presented side by side for comparison. Note this is a single analysis of a half pipeline cross section, the two approaches to presenting these results are mirrored using image processing techniques to allow a side by side comparison. The left hand side of Figure 3.13 is a state plot, where a colour coding is used to show the calculation of the plastic state of a mesh element. Three states are shown elastic, plastic and those elements that have been plastic at an earlier stage of the calculation. The right hand side of Figure 3.13 shows the calculated displacements at V_{max}, presented as a vector plot. Understanding the extent of the zone of plastic failure and the zone of large displacement can be used to position the base and side boundary at a conservative distance from these zones. A number of analyses were undertaken with different boundary locations to confirm the validity of this approach. When the boundaries are sufficient distance away two sets of analysis with different boundary locations will give identical results, demonstrating the results are independent of boundary effects. Displacement vector plots are available for many of the problems considered in this study, see Chapter 4 and chapter 5. These vector plots can be used as guidance for likely analysis field requirements.

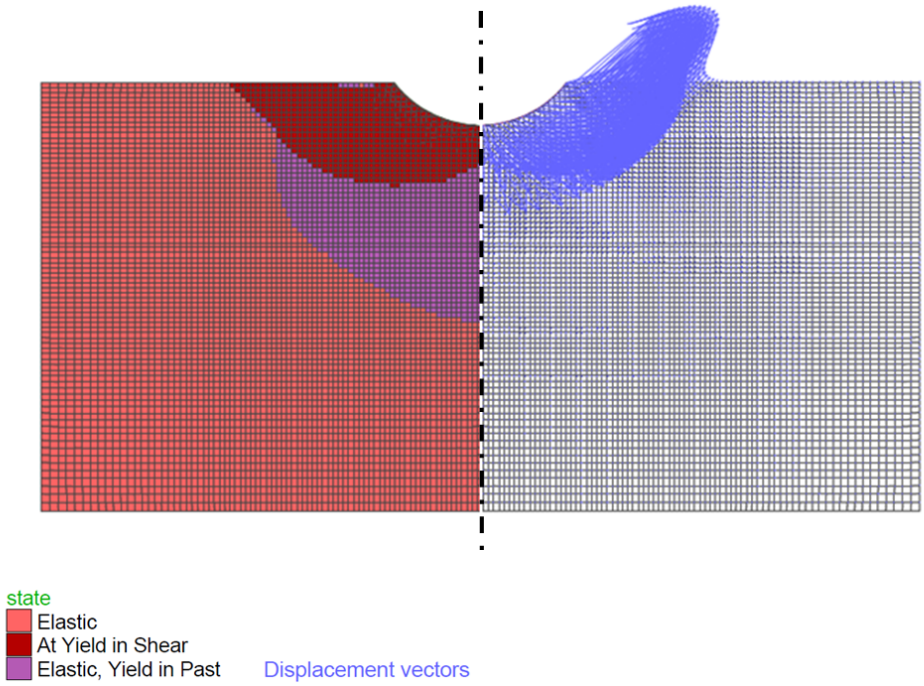

Figure 3.13 *- Example plots to aid assessment of appropriate boundary locations.*

Standard boundary properties for analysis was to fix the base of the analysis field in both the x and y plane. For models that used a line of symmetry it was important that this line of symmetry was only fixed in the x plane with free movement in the y direction, ensuring that this boundary did not affect the analysis results. The outer vertical boundary needed to be fixed in the x direction and was also typically free to move in the y direction. The precise nature of the outer vertical boundary was less important for most analysis, with this boundary being a sufficient distance away not to have an influence on analysis results. The exception was where unit weight was considered. For this case all vertical boundaries needed to be free in the y direction to allow uniform elastic compression of the soil when gravity was applied at the start of the calculation process.

With the boundary location set the final part of defining the analysis geometry is to delineate the soil surface and the pipeline shape. To aid interpretation the soil surface, mudline, was defined as zero in the y direction within FLAC's coordinate system, with a distance below mudline as a negative distance and a distance above a positive distance. As in Figure 3.13 the soil surface is a horizontal line. However, with the use of a wished in place methodology for small strain analysis, an area of seabed also needs to be removed to allow the pipeline to be wished in place to the target embedment depth. The pipeline was formed from an area of mesh above the seabed level prior to deletion of mesh in this area when the seabed surface was defined. The pipeline mesh is then relocated to the required position, either the wished in place embedment depth or, for the large strain analysis, touching the soil surface. Results in this study are typically normalised by the pipeline diameter, therefore the actual pipeline diameter used is not especially important. However, a credible pipeline diameter was still used. All analysis in this study considers a pipeline with an outside diameter of 0.3 m.

The next consideration in analysis configuration was the determination of the mesh density, the level of mesh refinement. Similar to defining the boundary locations, the conflicting requirements were to have sufficient mesh refinement to produce an appropriately accurate solution while still maintaining analysis efficiency. With this being an academic study a degree of conservatism was adopted with a bias towards a finer mesh than may be required in design practice.

An understanding of mesh density requirements was gained during the problem familiarisation stage of this study. Further, additional formal checks were also

incorporated into the analysis schedule. V loading (V_{max}) analyses and H loading (H_{max}) analyses were undertaken at a range of mesh densities in order to incorporate a mesh convergence study into the analysis of these problems. These mesh convergence studies were used to confirm adequate mesh refinement by noting the change in the value of V_{max} and H_{max} with increasing mesh density. An example of the effect of mesh density dependence is shown in Figure 3.14. Mesh density is measured in terms of the mesh zone size (Δ_z) in the zone of plastic failure. This could also be expressed in dimensionless form by normalising by the diameter of the pipeline D, i.e. Δ_z/D. Maximum resistance to vertical loading V_{max} in this example is shown in Newtons. However, this could also be expressed in dimensionless form e.g. $V/s_u.D$.

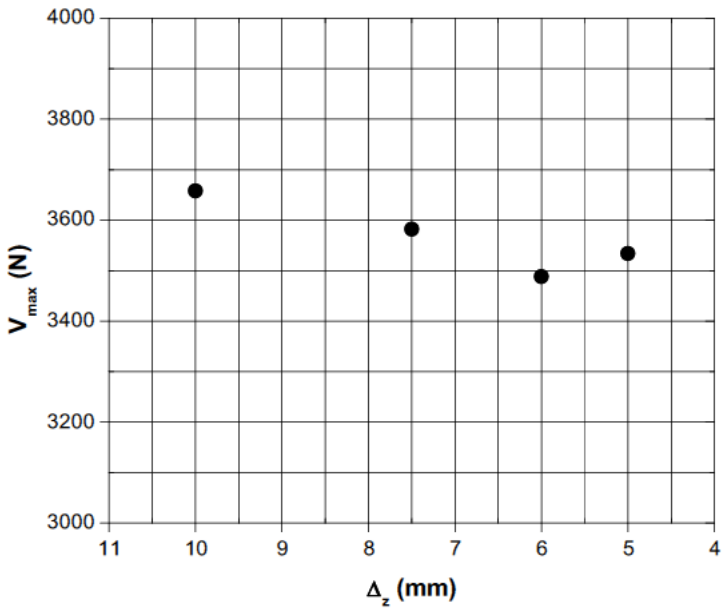

Figure 3.14 *- Example mesh convergence for V loading at z= 0.05D with a rough interface 0.3m diameter pipeline.*

Figure 3.14 shows a relatively low sensitivity to mesh density with a change of around 5% in V_{max} when approximately doubling the mesh density. However, the range of mesh density considered in this figure was selected following the problem familiarisation phase of this study. A larger change in V_{max} can be expected over a greater range of mesh densities and inclusion of some coarser mesh. These coarser meshes are also affected by issues such as loss of circular shape for the pipeline and inaccuracy arising from a limited number of pipeline mesh nodes where load can be analysed. With these effects there is limited

value in extending these convergence studies to include coarse meshes, other than to be aware that these coarser mesh will give inaccurate results. For further details of the analysis variables used, including mesh density, see analysis summaries in Appendix A and Appendix B. For further discussion also see Chapter 4 for V loading and Chapter 5 for H and V-H loading.

The next aspect in configuring analysis for this study is assigning material properties for the seabed soils and the pipeline. Further background information on the occurrence of clay seabed soils is provided in Section 2.5. Within analysis the seabed soil is modelled as a linear elastic perfectly plastic material with a Tresca yield criteria, see Figure 3.15 and 3.16.

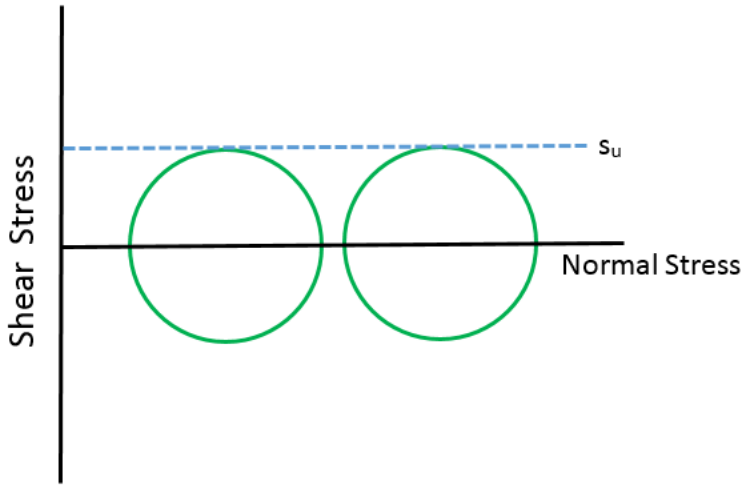

Figure 3.15 *– A 2D representation of a Tresca yield criteria, plotted in terms of shear stress and normal stress. Modified from Das (1997)*

Figure 3.15 shows a 2D representation of the Tresca yield criteria plotted in terms of shear stress and compressive normal stress. In this figure two Mohr circles are plotted with a dashed line representing the soil undrained shear strength (s_u). It can be seen that the shear strength is independent of normal stress. This contrasts with a Mohr Columb yield criteria, where an increase in normal stress results in an increase in shear strength. The Tresca criteria can also be presented in 3D stress space, see Figure 3.16. This representation shows the same properties as the 2D representation, with the Tresca criteria shown as a hexagon symmetric around the hydrostatic axis. This hexagon remains a constant distance around the hydrostatic axis, contrasting with a Mohr Columb

criteria which would splay outwards from the hydrostatic axis in conjunction with an increase in stress. Within the analysis reported in this thesis tensile capacity is taken as equal to the compressive strength i.e. isotropic rather than anisotropic shear strength. In Figure 3.16 this can be seen with the hexagon shaped Tresca yield criteria extending beyond the origin into a region of negative stress space, representative of tensile rather than compressive stress. In Figure 3.15 tensile stress is simply a mirror image of the compressive stress representation, extending into the tensile stress space.

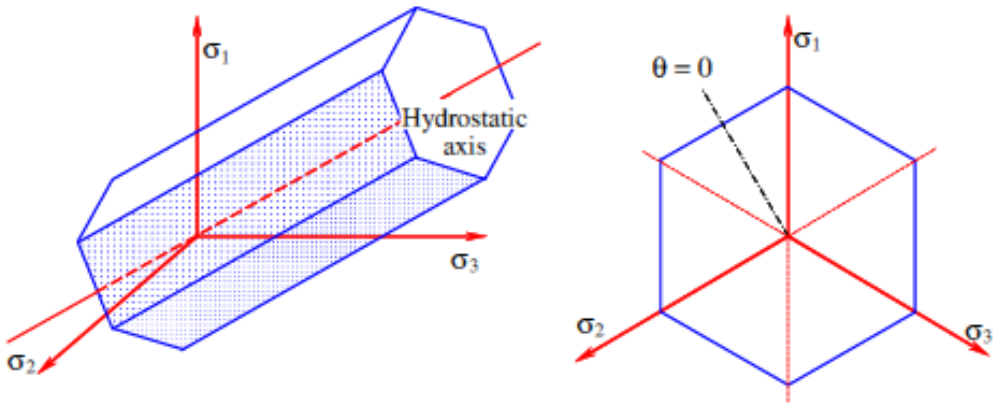

Figure 3.16 *– A 3D representation of a Tresca yield criteria, plotted in terms of major (σ_1) minor (σ_3) and intermediate stress (σ_2). Extracted from Taiebat & Carter (2008).*

Analysis within this study is typically expressed in dimensionless form e.g. $V/s_u.D$ for V loading. Therefore the specific choice of undrained shear strength is not especially important. A very soft clay strength of 5 kPa was generally adopted as a nominal undrained shear strength (s_u) in analyses, unless otherwise stated. One variation on this case was when a slightly lower shear strength was used for a limited number of analysis in order to achieve a target $s_u/\gamma'.D$ for investigation into the effect of soil unit weight.

The elastic properties for this constitutive model were determined using a multiple of the shear strength to determine Young's modulus. As much of the analysis in this study is focused on maximum capacity associated with unconfined plastic flow, e.g. V_{max}, in most cases the actual value of the elastic parameters selected is not especially important. Although it can be noted that this will have some influence at the very shallowest pipeline embedment depths and therefore may be more important for high strength clays, where penetration

is less, and, or for very light pipeline. With no significant impact on analysis time, or similar detrimental impact, and within in this context, there is some benefit in progressing analysis with credible parameters. On this basis Young's Modulus (E) is set at 200 times soil undrained shear strength (s_u). This is reasonable for a high plasticity low over consolidation ratio clay, for example as discussed by Padfield and Sharrock (1983). A higher E to s_u ratio reduces the influence of E, for even extreme cases of pipeline weight and higher s_u, with plastic flow occurring at smaller pipeline displacements. Lower values of E to s_u ratio would most likely be unrealistic and would moderately increase the pipeline displacement before plastic flow occurs for the shallowest pipeline embedment depths.

Materials that exhibit an undrained response have no volume change and a Poisson's ratio (υ) of 0.5 is appropriate. A Poisson's ratio of exactly 0.5 can lead to numerical instability during finite difference and finite element analysis. Therefore a value of 0.49 is adopted as a reasonable approximation of undrained behaviour while still maintaining stability within the analysis. Within FLAC's calculation process Young's modulus and Poisson's ratio are used to obtain Bulk Modulus and Shear Modulus using Equations [3.1] and [3.2] following the widely used relationship between these parameters (Itasca, 2008c).

[3.1] $$K = \frac{E}{3(1-2\nu)}$$

[3.2] $$G = \frac{E}{2(1+\nu)}$$

In addition to soil shear strength and elastic soil parameters some analysis investigates the influence of soil unit weight, hence the requirement to assign an effective soil unit weight (γ') during the analysis configuration. As with previous geotechnical parameters, the use of a dimensionless interpretation framework reduced the importance of the particular value adopted. Within FLAC the soil unit weight is based on a soil density and the application of gravity within the calculation, in this case standard earth gravity. Gravity is applied vertically except for analysis related to a sloping seabed, see Section 3.3.5 for further details. As this study addresses subsea pipelines the seabed soils are submerged in seawater, therefore the effective unit weight is equivalent to the submerged soil unit weight. This can be addressed by applying a density equivalent to the submerged density, which is significantly simpler than trying to model the presence of seawater buoyancy effects in analysis. Soil density was set to a

value that resulted in an arbitrary effective unit weight of 10 kN/m^3, except in a few cases when it was adjusted to obtain a particular $s_u/\gamma'.D$ ratio.

The pipeline is treated as a rigid body for all analysis within this study. This was primarily facilitated by assigning a uniform displacement velocity around the complete boundary of the pipeline, effectively translating the pipeline as a rigid object. Using this approach the pipeline properties no longer have an influence on the geotechnical analysis results. However, assigning appropriate properties for the pipeline may also contribute to analysis numerical stability, with inappropriate properties such as a very large stiffness contrast within the finite difference mesh potentially slowing analysis times (Itasca, 2008b). The pipeline was also assigned a constitutive model with a Tresca failure criteria, for simplicity, with nominal plastic and elastic parameters one hundred times that of the seabed soil.

Within the calculation configuration interface conditions are assigned as described in the problem definition, for example a rough or smooth interface condition. Intermediate conditions were also be assigned in some calculations, expressed in terms of a ratio of the interface properties to that of the seabed soils e.g. an interface shear strength set to 50% of the shear strength of the seabed soil $s_{ui}/s_u = 0.50$.

A number of interface options were available for calculations in FLAC. A rough interface could be established by either using a "glued" interface or a bonded interface with plastic and elastic parameters equivalent to the seabed soils i.e. $s_{ui}/s_u = 1.0$. Intermediate interface properties could be produced using a bonded interface with reduced plastic and elastic parameter e.g. $s_{ui}/s_u = 0.5$. Smooth interface conditions were produced using an unbonded interface with a zero interface shear stiffness (k_s) assigned. The normal interface stiffness (k_n) in FLAC is a parameter that does not have a specific physical analogy for the problems being considered. As k_n controls the transfer of normal forces across the interface it is important to assign an appropriate value. A large stiffness for k_n will ensure load transfer across the interface without any erroneous effects in displacement, consistent with the pipeline behaving as a rigid body. However, care is needed not to assign an overly large stiffness which would impact analysis time due to the large stiffness contrast within the finite difference mesh. The guidance provided in Itasca (2008b) was followed, with the normal interface stiffness set to ten times the equivalent stiffness of the adjacent soil mass. This guidance is show in Equation [3.3]. This approach was checked during problem

familiarisation and found to be suitable i.e. displacements either side of the interface were the same for the range of analysis parameters being considered.

[3.3] $$k_n \geq 10\left[\frac{(K+(4/3.G)}{\Delta_z}\right]$$

Where;

k_n = Interface normal stiffness
K = Bulk Modulus
G = Shear Modulus
Δ_z = Minimum soil finite difference zone dimension at the interface

As previously noted a displacement controlled analysis approach has been used for this study. Consideration was given to load controlled analysis during problem definition. However, it was concluded that there would be significant disadvantages when compared to displacement controlled analysis. Load controlled analysis approaches reviewed included a FISH program that would incrementally apply load and the automatic safety factor calculation method built into FLAC.

The first of these load controlled analysis approaches was thought to be overly complicated to implement, possibly with a feedback loop required in the FISH program linked to the numerical stability of the analysis i.e. analogous to choosing an appropriate displacement velocity. The second of these load controlled analyses approaches was overly time consuming with a number of individual analysis required to initially bracket the result and then further analysis cases to refine the accuracy of the result.

Displacement controlled analysis also had some additional advantages. The displacement probe method adopted in this study not only provided information on peak capacity, or plastic collapse load, but also provided information on post failure behaviour by allowing the plastic potentials to be plotted for the various cases analysed. Additionally by applying the displacement uniformly around the pipeline shape a rigid body can be maintained.

To undertake a displacement probe a boundary condition with a fixed displacement velocity is applied in FLAC. Both an x displacement component (u) and a y displacement component (v) are applied. For vertical displacement the x velocity is set to zero to increase analysis stability, this is particularly important when only half a pipeline section is considered.

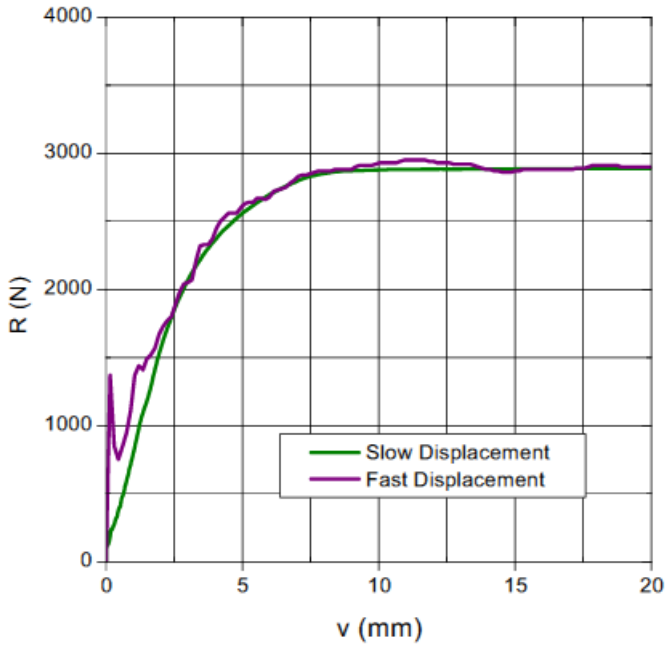

Figure 3.17 *- The effect of displacement velocity on calculated resistance.*

When configuring analysis the displacement velocity ($\bar{\upsilon}$) needed to be slow enough to ensure numerical stability in the analysis process. There is an interaction between the displacement velocity, the mesh density, mesh stiffness and the mechanical damping algorithm used within FLAC (Itasca, 2008b). An example of the effect of two different displacement velocities is shown in Figure 3.17. Resistance (R) is plotted against displacement (v) for two different displacement velocities, a "fast" displacement velocity of 3E-6 m/s and a "slow" displacement velocity of 5E-7 m/s. Note; the selection of a slow and fast displacement velocity for this example is somewhat arbitrary and based on the appearance of the data produced. Further details of velocity requirements, including how these vary with analysis conditions, can be seen later in the thesis. They are also summarised in the analysis data summary reported in Appendix A and Appendix B. From Figure 3.17 the noise arising from numerical instability and inertial forces can be seen in the faster displacement. Figure 3.18 shows a similar effect, plotting the unbalanced forces in the finite difference mesh. Which can be viewed as an analogue of numerical stability. The fast displacement described here can be viewed as too fast for most applications where as the slow velocity is an appropriate basis to progress analysis.

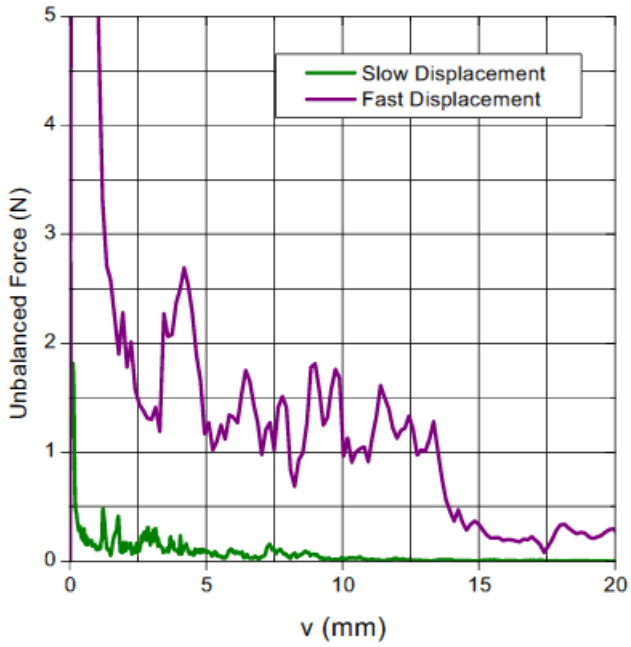

Figure 3.18 *- Unbalanced forces in the finite difference mesh for two different displacement velocities.*

Having set all the calculation parameters described in this section, analysis can be started. Small strain or large stain analysis is mode is selected with a configuration command and FLAC analysis is commenced with a number of analysis steps defined. These analysis steps are related to a small increment of displacement derived from the displacement velocity. Each analysis typically comprised tens or hundreds of thousands of steps, with experience of the required number of steps gained during problem familiarisation. Analysis was progressed until a constant resistance was reached, either in V or combined V and H. This typically was interpreted conservatively from a load displacement plot in FLAC, with final checks within Excel as part of data post-processing. It was also relatively easy to add additional steps to analyses that had not progressed sufficiently to provide the required results. During the analysis a wide range of parameters are calculated. FISH scripts were written as part of the analysis configuration file to record results for pipeline displacement and the sum of V and H components of load at nodes around the pipeline circumference. These parameters could then be exported for further post-analysis processing and interpretation, see Section 3.4. Other parameters such as soil displacement, or the plastic or elastic state of mesh elements could also be exported from FLAC as a range of plots.

3.3.3 Vertical Loading

Configuration of analysis to investigate V loading followed the same general pattern outlined in the previous section. As described in Section 3.2.1 a range of problems were analysed including shallow embedment, deeper embedment to 1.0D, large strain effects, pipe-soil interface conditions, the effect of soil unit weight and various non-uniform shear strength distributions. An example finite difference mesh for a V loading analysis is shown in Figure 3.19.

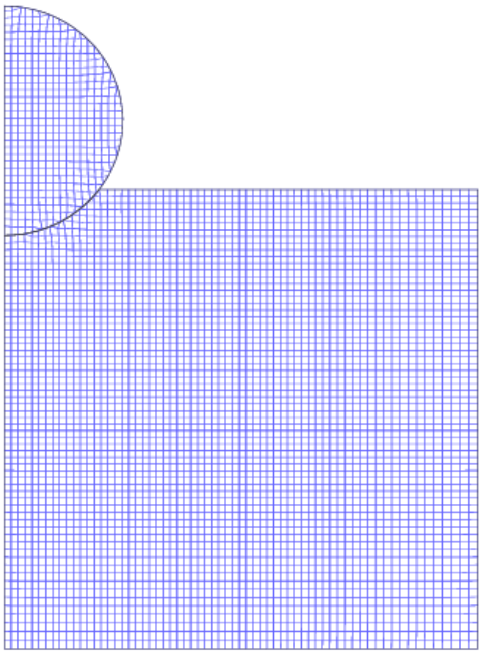

Figure 3.19 *- Example mesh for a pipeline wished in place to an embedment depth z/D= 0.3 and subjected to vertical displacement,* D =0.30m, Δ_z=0.01m.

A slight grading to a coarser mesh can be noted towards the boundaries of the example mesh. In early analysis this approach was investigated as a strategy to speed up analysis times. The slightly coarser mesh is out with the area of plastic flow and large displacement; it therefore does not affect the analysis results. The coarsening in the mesh reduces the number of elements within the analysis field, reducing calculation time. However, as these mesh adjustments are relatively minor the speed up in analysis time is limited. In later analysis a uniform mesh was adopted as it was decided the additional effort in configuring analysis with a non-uniform mesh was not worth minor reductions in analysis time.

As per the steps to analysis configuration, the symmetry in the problem has been exploited in Figure 3.19 to cut the mesh size in half. The base of the mesh

is fixed in the x and y direction, whereas the right hand boundary and the boundary on the line of symmetry are fixed in the x direction with free movement in the y direction. In this example a half pipeline cross section has been formed and the soil surface defined. An area of the mesh has been removed and the pipeline wished in place to a depth of z=0.3D. For small strain analysis at a pipeline embedment of greater than 0.5D the mesh was similar to this example. However, a vertically sided slot is used when wishing the pipeline in place below 0.5D, see this problem definition in Figure 3.2. For large strain analysis the mesh was also similar to this example, but no soil was removed and the pipeline was in contact with a flat seabed prior to displacement, rather than being wished in place.

A range of mesh densities were investigated for these problems including convergence studies for V_{max}. Material properties and interface conditions were defined for the problem being considered. Displacement controlled boundaries were then applied to the half pipeline cross section, displacing the pipeline vertically. Analysis was progressed with analysis results recorded for subsequent post-processing and interpretation.

3.3.4 Combined Vertical and Horizontal Loading

Analysis for the combined V-H loading problem definitions also followed the basic analysis steps previously outlined. However, unlike for V loading, for the VH case a full pipeline cross section had to be analysed. An example mesh is shown in Figure 3.20.

The mesh shown in Figure 3.20 also includes some minor grading towards the boundaries. However, as with V loading, in later analysis a uniform mesh was used as the advantages in reduced analysis time were outweighed by the extra time in analysis configuration. In this example the base of the mesh is fixed in x and y direction, with the two outer boundaries fixed in x direction only. The pipeline shape is formed, the soil surface defined, and an area of soil removed to wish the pipeline in place to the defined embedment depth.

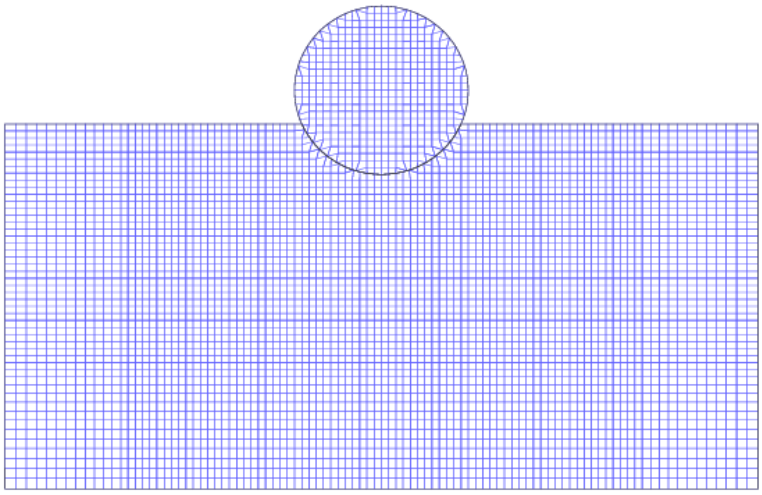

Figure 3.20 *- Example V-H analysis mesh with a pipeline embedment depth of z/D= 0.3.*

A range of mesh densities were investigated as part of analysis of H_{max}. For V-H loading mesh density was based on the H_{max} convergence study and the convergence study previously undertaken for V_{max}. When a pipeline embedment greater than 0.5D was required a vertically sided slot is used. For large strain analysis the mesh is similar to the example shown with the exception that the pipeline is not wished in place.

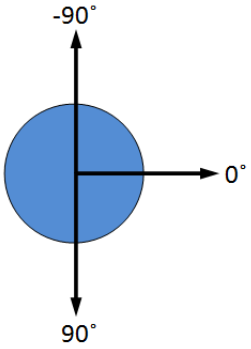

Figure 3.21 *- Displacement angle conventions.*

Material properties and interface conditions were then assigned based on the problem being considered. Displacements were applied to the pipeline shape using a combination of vertical (v) and horizontal (u) displacements to achieve the desired displacement angle (δ). The convention for defining δ is shown in Figure 3.21. Vertical displacement into the seabed is defined as 90˚ and

horizontal displacement as 0°. Displacement angles with an uplift component, above horizontal, are negative up to -90° which is the pipeline being pull out vertically out of the seabed. Displacement angles below horizontal are positive. With symmetry in V-H load space δ only needs to be defined through 180°.

3.3.5 Pipelines on Sloping Seabed

Analysis of a pipeline subjected to V-H loading on a sloping seabed follows similar principles to those outlined for the flat seabed case. However, due to the presence of the slope it is no longer possible to define a V-H stability envelope from displacement probes through 180°. Instead a full 360°needs to be investigated in order to capture up-slope and down-slope effects. The displacement angle convention used for this 360° analysis is shown in Figure 3.22.

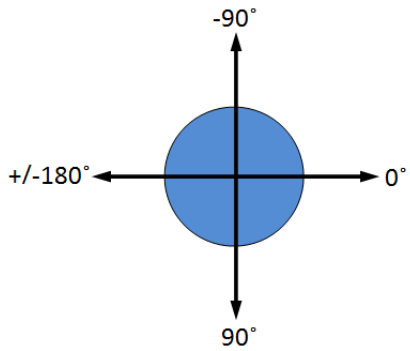

Figure 3.22 *- Displacement angle conventions for sloping seabed analysis.*

Analysis can be undertaken for a wide range of slope angles by creating a slope within the finite difference mesh in FLAC. However, this is time consuming and very inefficient. Reviewing the problem of a pipeline subjected to V-H loading on sloping weightless clay seabed, it can be noted that the geometry of the stability envelope will remain the same, rotating through load space in response to the slope angle. This enables an analysis methodology to be developed that can produce V-H stability envelopes for any slope angle from the flat seabed case.

Figure 3.23 shows the concepts needed to produce a sloping seabed V-H stability envelope from the flat seabed case. This figure shows both a conventional global reference system and a new local reference system. Within the global reference system V-H loading arises from a pipeline, at a given embedment depth, being

displaced at an angle δ, where δ is relative to a horizontal plane. This pipeline displacement occurs on a slope of angle ψ.

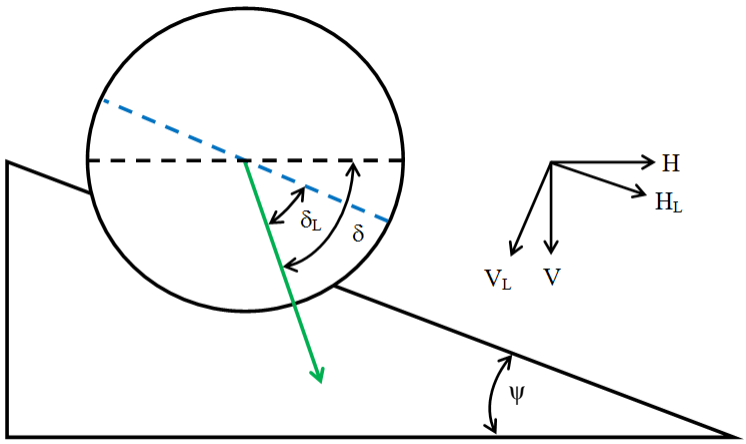

Figure 3.23 *- Local and global reference system for a sloping seabed.*

The new local reference system is defined relative to a plane parallel to the seabed slope. Pipeline displacement is relative to this plane and assigned the notation δ_L. H_L is parallel to the seabed slope and V_L perpendicular to this slope. For a weightless seabed the V-H stability envelope within this local reference system is identical to the flat seabed case. Additionally, as the local coordinate system rotates round with slope angle, this stability envelope is independent of slope angle. Conversion between these two reference systems provides a method to derive a stability envelope for any slope angle.

Conversion from the local coordinate systems (H_L,V_L) to the global coordinate system (H,V) is undertaken by resolving the force components as shown in Equations [3.4] and [3.5].

[3.4] $$H = [H_L.cos(\psi)] - [V_L.sin(\psi)]$$

[3.5] $$V = [V_L.cos(\psi)] + [H_L.sin(\psi)]$$

Where;

H = Horizontal load (global reference system)
V = Vertical load (global reference system)
H_L = Horizontal load (local reference system)
V_L = Vertical load (local reference system)
ψ = Slope angle

When the seabed soil has weight the effect of slope will not be fully represented by the local to global reference system conversion alone. Although, these concepts are still relevant for this case. The approach used in this study to consider unit weight on a sloping seabed was similar to the approach used for a flat seabed. The difference was that the vector of gravity forces is varied to model the slope effect i.e. vertical in the global reference system and changing with slope angle relative to the local reference. A parametric study can readily be run for various slope angles using the same finite difference mesh and a different vector of gravitational forces. However, with a full 360° envelope required for each slope angle, this remains computationally intensive. Different unit weight to shear strength ratios can also be investigated using this approach e.g. $s_u/\gamma.D$.

3.4 Interpretation Framework and Correlation Methodology

The various stages of the analysis process have been described in this chapter, up to the point when the calculation results are available. These results can then be processed further within FLAC or exported for processing, interpretation and presentation in other software packages. Initial analysis data sampling is incorporated into the FISH scripts that derive analysis results, such as displacement or load. These FISH scripts record various calculation parameters at a defined step interval e.g. load recorded every 10, 50 or 100 analysis steps. The interval for recording analysis results was selected based on the displacement velocity and the amount of displacement expected to analysis completion. It was beneficial to avoid large data files associated with oversampling of analysis results. However, the methods used to review and further process analysis data were robust and the step size for analysis results could be selected conservatively.

The text files exported from FLAC using the FISH scripts were imported into Microsoft Excel for further processing. Post processing of parameters such as calculated displacement was undertaken within FLAC, with vector plots exported in a pdf format. Presentation of graphs within this thesis was undertaken within the graphing package Origin.

One of the simplest examples of further processing of analysis results in Excel is in interpretation of peak load, for example V_{max} for a pipeline under vertical displacement. Load against displacement results were imported into Excel and the maximum value easily found, either visually or using an Excel formula. If the analysis included some numerical noise then Excel could be used to find an average value over an appropriate range. Throughout this study, where possible,

results are presented in a general dimensionless format, for example V and H load as $V/s_u.D$ and $H/s_u.D$. Calculation of these dimensionless groups was undertaken in Excel.

Various plots throughout this thesis include curves fitted to the analysis results. This assists in data interpretation and increases the usefulness of these plots. The fitting equation and associated fitting coefficients used for these plots are also reported, allowing the data fit to be reproduced and potentially used as a design tool.

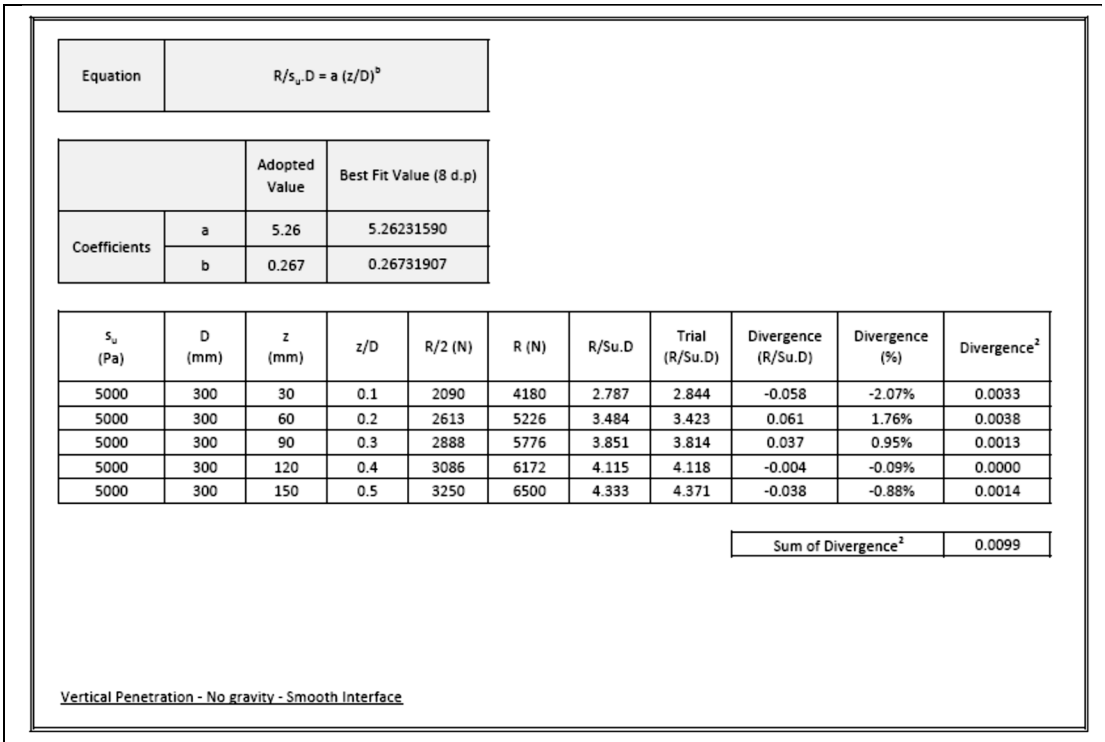

Equation	$R/s_u.D = a\,(z/D)^b$

		Adopted Value	Best Fit Value (8 d.p)
Coefficients	a	5.26	5.26231590
	b	0.267	0.26731907

s_u (Pa)	D (mm)	z (mm)	z/D	R/2 (N)	R (N)	R/Su.D	Trial (R/Su.D)	Divergence (R/Su.D)	Divergence (%)	Divergence^2
5000	300	30	0.1	2090	4180	2.787	2.844	-0.058	-2.07%	0.0033
5000	300	60	0.2	2613	5226	3.484	3.423	0.061	1.76%	0.0038
5000	300	90	0.3	2888	5776	3.851	3.814	0.037	0.95%	0.0013
5000	300	120	0.4	3086	6172	4.115	4.118	-0.004	-0.09%	0.0000
5000	300	150	0.5	3250	6500	4.333	4.371	-0.038	-0.88%	0.0014

Sum of Divergence^2	0.0099

Vertical Penetration - No gravity - Smooth Interface

Figure 3.24 *- Example data fitting Excel sheet.*

The methodology to fit equations to the analysis data was implemented in Microsoft Excel. These spreadsheets were formulated in terms of an optimisation problem, where the objective is to adjust the fitting coefficients to minimise the divergence between the fitting equation and the analysis data. The fitting coefficients were adjusted iteratively using Excel's Solver function to produce an optimal fit. The use of Excel's Solver function is described by Bourg (2006). Figure 3.24 shows an example of this approach.

The example shown in Figure 3.24 is for a V_{max} relationship, see Chapter 4 for further details. The fitting equation for this problem, is shown in Equation [3.6], a power law equation which produces resistance, V_{max}, for a given pipeline

diameter, embedment depth and soil shear strength. Two fitting coefficients *a* and *b* are used. The fitting spreadsheet initially assesses the difference between the analysis results and a trial value of resistance produced by the fitting equation. Random values of the coefficients *a* and *b* were initially assigned. This divergence from the trial equation is calculated as a percentage to avoid bias towards deeper depths where resistance will be higher. The sum of the square of the divergence is used as the parameter that is minimised in this optimisation problem. The results of Excel solver are initially reported to eight decimal places in this spreadsheet before being rounded to an appropriate level of precision.

[3.6] $$V_{max} = a \left(\frac{z}{D}\right)^{b} s_u D$$

Where;

V_{max} = Maximum resistance to vertical loading
s_u = Soil undrained shear strength
D = Pipeline diameter
z = Pipeline embedment depth
a, *b*, = Fitting coefficients

Various fitting equations are used throughout this study including a more complex parabolic equation for V-H loading. However, the same general methodology is used in fitting these equations to the data with an Excel spreadsheet sheet formulated as an optimisation problem using Excel Solver.

3.5 Reliability Based Design Methods

3.5.1 General

Following on from the deterministic analysis described earlier in this chapter reliability based analysis was applied to a range of problems, see Section 3.2.4 for a summary of these problems. Reliability based analysis in this case provides an approach to address uncertainty in input parameters, such as soil shear strength, as well as offering an approach to consider appropriate safety factors for a design problem. Two complementary methodologies were adopted in undertaking this reliability based analysis. The first approach was a simplified analysis methodology where the probability of failure (P_F), e.g. $V > V_{max}$, is determined analytically within an Excel spreadsheet. This approach had significant advantages in speed and efficiency. However, in selecting this analysis method it was not clear that it would always give accurate results,

either in general or for all of the specific problems being considered. This simplified methodology is described in Section 3.5.2.

The second reliability based analysis methodology adopted in this study is Monte Carlo analysis. This was also implemented in Excel. Monte Carlo analysis represents a more rigorous approach then the simplified methodology. However, it is also computationally more intensive requiring large numbers of simulations to be undertaken, especially for lower P_F. The Monte Carlo methodology used in this study is described in Section 3.5.3.

As there are no previously published studies into the application of reliability methods to the problems being considered here, the use of two different methods is beneficial in demonstrating two different approaches to these problems. If, in the future, further work was undertaken for multi-variant problems the use of two methods would also provide additional validation of the analysis results. Within this context the two methods selected complement each other well. The simplified analytical method could be used to rapidly progress parametric studies and define the likely nature of a problem. The estimated probability of failure from the simplified method could also be used to assist in defining the approximate number of simulations that would be required for subsequent Monte Carlo analysis.

3.5.2 Simplified Methodology

As part of this study a simplified reliability based analysis methodology for pipe-soil interaction on a clay seabed was adapted from the principles outlined in Phoon (2004). This method is applicable to cases with a single stochastic variable having a normal distribution (in this case, of s_u). For further details of the rationale for selecting a normal distribution see Section 2.6. Care was needed in formulating the risk premise when using this simplified method, as it does not incorporate the ability to interact with complex stochastic failure surfaces. Particular care was needed for considering V-H loading, which was addressed by considering failure along a fixed V-H load ratio, reducing the dimensions in the problem. While Phoon (2004) generally describes the results of reliability analysis in terms of a reliability index (β_R) it is relatively simple to convert from β to probability of failure (P_F). P_F was considered a more readily understood concept within the context of this study. Reliability analysis was implemented within a series of Excel spreadsheets.

An example of the simplified methodology used in this study is presented in Equation [3.7] and [3.8]. Conversion from β to P_F is shown in Equation [3.9].

[3.7] $$\beta_R = \frac{F_{S\mu}-1}{F_{S\mu}.CoV_{Vmax}}$$

[3.8] $$CoV_{Vmax} = \frac{\sigma_{Vmax}}{\mu_{Vmax}}$$

[3.9] $$P_F = 1 - \Phi(\beta_R)$$

Where;

β_R = Reliability Index
$F_{S\mu}$ = Mean Factor of safety e.g. V/V_{max}
CoV_{Vmax} = Coefficient of variation for V_{max}
σ_{Vmax} = Standard deviation of V_{max}
μ_{Vmax} = Mean V_{max}
P_F = Probability of failure i.e. $V_{max}<V$
Φ = Standard normal cumulative function

The example outlined in Equation [3.7] and [3.8] has been formulated in terms of V_{max} i.e. a pipeline under vertical loading. The mean factor of safety for V_{max} can be obtained from the V load being considered and the V_{max} data fitting equations for the problem being analysed. The reference shear strength for the fitting equation is the mean soil undrained shear strength ($s_{u\mu}$). A problem can be considered for a range of coefficient of variation in capacity, e.g. CoV_{Vmax}, which is analogous to a coefficient of variation in s_u. While this study uses coefficient of variation, alternatively with some minor changes to the methodology standard deviation could be used to consider variation in s_u, if preferred. For further discussion values of s_u CoV in the literature see Section 2.6.

The reliability based analysis example outlined in this section can easily be formulated in terms of the other design problems considered in this study. For example analysis of H_{max} can be undertaken by substituting H_{max} terms for V_{max} in Equations [3.7] and [3.8].

The simplified reliability analysis method for V-H analysis follows the same general approach outlined in the presented example. In this case CoV is a general variation in capacity. The safety factor term for V-H loading is relative to a reliability probe at a fixed V-H ratio across V-H load space. The reference deterministic failure load in this safety factor calculation is the point where the fixed V-H ratio probe intercepts the V-H stability envelope for the case being

considered. The deterministic V-H envelope can be derived from any of the V-H fitting equations reported in this thesis.

The Excel spreadsheets used to apply this simplified methodology to various design problems were typically formulated to calculate P_F for a given combination of parameters and a specific dimensionless load term e.g. $V/s_{u\mu}.D$ or $H/s_{u\mu}.D$. However, as Excel and an analytical approach was used it was also possible to use Excel Solver to find iteratively the dimensionless load for a target P_F. In some cases this was a more convenient approach.

3.5.3 Monte Carlo Methods

A traditional Monte Carlo (MC) analysis method was implemented as part of this study, for example as described by Fenton and Griffiths (2008) and Ching (2011). The additional mathematical complexity of importance sampling and similar methodologies was avoided. For a traditional MC analysis methodology a large number of simulations are undertaken using the fitting equations obtained in other sections of this study, e.g. for V_{max}, the s_u input to these equations is treated as a random parameter with a defined statistical distribution. A normal distribution of s_u was used in this study and a range of different CoV were investigated in parallel to the simplified reliability methodology. For further discussion of the basis for selecting a normal distribution see Section 2.6.

A large number of simulations are undertaken as part of a MC analysis with the probability of failure calculated using the simple formulae shown in Equation [3.10].

[3.10] $$P_F = \frac{N_F}{N}$$

Where;

P_F = Probability of failure i.e. $V_{max}<V$
N_F = Number of simulations that result in failure
N = Number of simulations

For a MC analysis with a small number of simulations the P_F is very volatile, especially for analyses that will have a low P_F. As the number of simulations increases the MC analysis converges towards a solution. There are a range of methods to estimate the number of analyses required for a given MC analysis ranging from simple guidance such as $N=10/P_F$ to more mathematically complex methods e.g. as described by Fenton and Griffiths (2008). An understanding of typical number of simulations was gained during problem familiarisation and the

results from the simple analysis methodology could be used with simple guidance. However, the most useful approach was to review various analysis parameters for convergence. For higher probabilities of failure the mean value of capacity, e.g. V_{max}, could be reviewed with increasing number of simulations. More useful and more sensitive for lower P_F the value of P_F could be reviewed directly with increasing simulations. Initial volatility could be noted in all analysis parameters. When these parameters started to converge to a constant value this was considered an acceptable number of simulations. This was typically greater than $N=P_F/10$. For high P_F it was trivial to undertake ~10,000-20,000 simulations rather than trying to optimise the N, with this number of simulations only taking 10-20 seconds.

During initial investigation of reliability based analysis an Excel spreadsheet and associated macro was developed to undertake MC analysis. However, commercial Excel add on risk Analyzer was used for all the analysis reported in this study. The primary advantage of the commercial add on was in productivity, with analysis easier to configure using graphical user interfaces and automatic graphs and statistics. MC analysis using Excel was limited to 1 million simulations, the maximum size of excel spreadsheet. For large analysis multiple simulations runs were undertaken, say 500,000 each. These smaller simulation runs could then be combined into a text file. Text editors have significantly larger constraints on number of data rows, primarily related to file size and computer system resources such as memory. These large text files could be sorted and filtered in the text editor. Analysis results could be determined directly in the text file, although typically it was simpler to extract the relevant portion of the text file and import into excel for interpretation.

The problem definitions described earlier in this chapter have been investigated using the methodologies outlined here, with results of these investigations reported in the following chapters. Chapter 4 considers the problem definitions where a pipeline is subjected to V loading. Chapter 5 considers V-H loading and the results obtained using reliability based analysis techniques are reported in Chapter 6.

4 Pipelines Subjected to Vertical Loading

4.1 Introduction

This chapter presents the results of analyses undertaken to investigate pipelines subjected to Vertical (V) loading. This includes investigation of the general case of maximum vertical capacity under vertical loading (V_{max}) for a range of pipeline embedment depths. Initial analyses reported in Section 4.2 consider the case of a homogenous shear strength weightless clay seabed. There are similar analyses for this problem undertaken by previous researchers and reported in the literature, allowing comparisons between this study and previous research to be made, see Section 4.2.3.

Following on from the idealised case of a homogenous shear strength weightless seabed, and going beyond the work of previous researchers, a range of other factors are investigated using numerical analysis techniques. This includes large strain up to a pipeline embedment of 1.0D (Section 4.3), the effect of interface conditions (Section 4.4) and the effect of soil unit weight to 1.0D (Section 4.5). The effect of a variable shear strength gradient is investigated (Section 4.6) with analysis results reported for both linear increasing shear strength gradients and shear strength crusts. Section 4.7 summarises the findings of the analyses reported in this chapter.

4.2 Homogenous Shear Strength Weightless Clay

4.2.1 Analysis Results - Small Strain Analysis at Shallow Embedment

Using the methodology described in Chapter 3 a suite of analyses was undertaken for a pipeline subjected to vertical loading within a small strain analysis framework. A 0.3 m diameter pipeline was adopted in analyses. This pipeline was wished in place at embedment depths of 0.05 the pipeline diameter (D), 0.1D, 0.2D, 0.3D, 0.4D and 0.5D. A homogenous undrained shear strength (s_u) of 5 kPa was used for the soil with elastic behaviour based on a Poisson's ratio (υ) of 0.49 and a Young's modulus (E) of $E = s_u \times 200$. Analyses used weightless soil with no gravity forces applied in the calculations.

Further information on analysis parameters, as well as analysis results, is summarised in Table 1-1 and 1-2 in Appendix A. This includes details of

parameters that were adjusted with embedment depth such as displacement velocity and mesh refinement, as described by the mesh zone dimension (Δ_z). It should be noted that while analysis was based on half a pipeline cross section to exploit the symmetry of the problem, for clarity all results presented in this chapter have been multiplied by two and are equivalent to the behaviour of a full pipeline cross section.

Following initial problem familiarisation a total 22 analyses were undertaken for a smooth interface condition and 25 analyses for the rough interface condition. These analyses included a range of mesh densities to ensure adequate mesh refinement for the embedment depth being considered. Adequate mesh density was typically confirmed in 3 to 4 analyses at a given embedment depth. However, in some instances up to 5 analyses were required. The final two analysis at a given embedment depth either gave the same value of peak load, V_{max}, or a small increase in V_{max} was noted in the final analysis. The penultimate analysis represented the convergence state i.e. adequate mesh refinement.

In general mesh density requirements, as measured by mesh zone dimension (Δ_z) adjacent to the pipeline, were coarser for the smooth interface condition then the rough interface condition. For both interface conditions a fine mesh was required for the shallowest embedment depth of 0.05D. Both these trends can be explained by the geometry and dimensions of the problem. At a shallow depth, e.g. 0.05D, the pipe-soil contact width and the number of interface elements is small. It is therefore reasonable that there should be a particular sensitivity to the level of refinement in this zone. As embedment depth increases the contact width increases rapidly reducing the sensitivity to this aspect of the analysis. Embedment in itself is also likely to be beneficial in assisting load transfer to a larger body of soil. The differences between mesh requirements for a rough and smooth interface conditions can also be explained. A smooth interface does not transfer shear forces to the adjacent mesh and hence can be viewed as having no thickness. In contrast a rough interface effectively attaches the pipeline to the soil mass. Therefore the thickness of the elements immediately adjacent to the pipeline need to be fine enough to not unduly influence the geometry of the problem. A rough interface, contrasted with a smooth interface, can also be expected to result in larger strain and strain localisation close to the pipeline, which will also require a more refined mesh to accurately calculate resistance.

The velocity of the vertical displacement (v) was selected to reduce numerical instability and produce higher quality data. This ranged from 1E-6 m/s to 7.5E-8 m/s. As noted in Chapter 3, displacement velocity requirements are entirely related to the numerical analysis methodology with no relationship to actual pipeline behaviour e.g. all analysis considered undrained soil behaviour. Therefore no parametric study into analysis displacement velocity requirements is undertaken. However, despite this, some general trends could still be noted. Typically a slower velocity was required for a finer mesh, with a requirement to reduce displacement velocity as mesh density was increased as part of a convergence study. There was also a requirement to reduce displacement velocity with greater embedment depth for the range 0.05D to 0.5D. There appeared to be no clear trend in displacement velocity requirements with interface condition, other than the effects related to the requirement for a finer mesh for a rough interface condition.

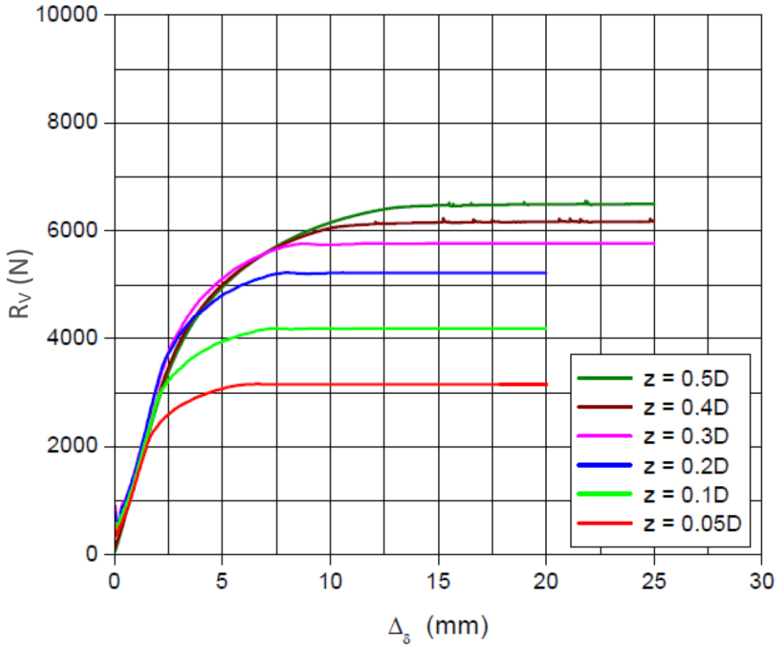

Figure 4.1 *- Load-displacement behaviour for a pipeline subjected to vertical loading, 0.05D to 0.5D. Smooth interface condition, homogenous shear strength weightless soil.*

During the calculations undertaken with FLAC, FISH scripts were written to record load/resistance (R_V) and pipeline displacement (Δ_δ). This data was then exported as text files. Having determined adequate mesh refinement this data can be plotted to investigate load-displacement behaviour. Figure 4.1 shows the

load-displacement behaviour for a smooth interface condition. Results for the rough interface case are shown in Figure 4.2. Note, displacement (Δ_δ) is relative to the initial wished in place depth.

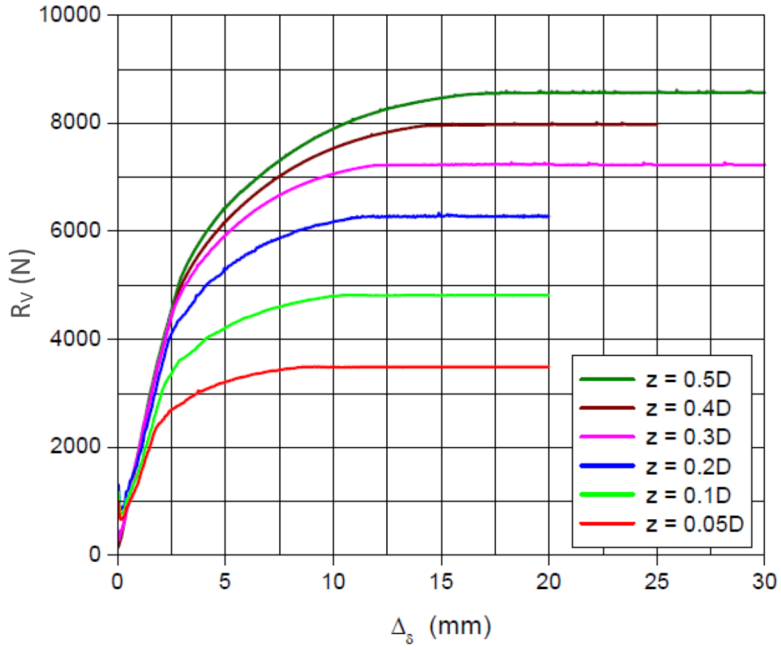

Figure 4.2 *- Load-displacement behaviour for a pipeline subjected to vertical loading, 0.05D to 0.5D. Rough interface condition, homogenous shear strength weightless soil.*

The data presented in Figures 4.1 and 4.2 shows the same general trend in the load-displacement relationship. Initially resistance increases relatively rapidly with pipeline displacement, following a linear trend. This stage can be attributed to elastic soil behaviour (also see example in Figure 4.3a).

Following initial linear behaviour the load-displacement relationship starts to curve and there is a reduction in the rate of increase, or gradient of increase, in resistance for a given increment of displacement. This can be attributed to the onset of plastic flow within the soil continuum (also see example in Figure 4.3b). In Figure 4.3b plastic flow can be observed extending from pipe embedment depth to a limited distance down the central axis. This can be characterised as confined plastic flow, being constrained within an otherwise elastic soil mass. The zone of plastic soil behaviour does not interact with the seabed surface.

At larger displacements the load-displacement behaviour continues to curve until a constant peak load, V_{max}, is reached. Analysis was progressed further to ensure a constant value and an accurate assessment of V_{max}. Review of state plots, for example see Figure 4.3c, and vector plot of soil displacement (Figure 4.4 a to f) show V_{max} is associated with unconfined plastic flow and full development of a failure mechanism within the soil.

It can be noted that the constant value of peak load, V_{max}, that occurs at larger displacements such as shown in Figure 4.1, Figure 4.2 and Figure 4.3, is attributable to the small strain analysis methodology and the constitutive model used to represent plastic behaviour in this analysis.

Close observation of Figures 4.1 and 4.2 will show that the load-displacement relationship does not start at exactly zero load. Some small spikes in load can be noted on initial pipeline displacement. These spikes in load arise from numerical instability within the calculations due to inertial forces arising in the calculation process. FLAC uses a damping algorithm to remove these inertial forces within a pseudo static calculation (Itasca, 2008b). The efficiency of this damping algorithm depends on the choice of algorithm, its configuration and most importantly the ratio of analysis steps to displacement increment, as determined by the displacement velocity. In undertaking analysis variables have been controlled to produce good quality data in the area of plastic failure, consistent with the objectives of this study. If the initial segment of elastic behaviour was of particular interest then further steps could be undertaken to improve the data quality in this zone.

Further to the load displacement relationships shown in Figure 4.1 and 4.2, additional insight can be gained into this problem by reviewing the calculated soil displacement at failure, when constant peak resistance is reached, V_{max}. This displacement field is shown as a vector plot in Figure 4.4 a to f. Rough and smooth interface conditions are shown, which for ease of comparison have been mirrored around the central axis of symmetry using image processing techniques. The smooth interface condition is on the left of the page and rough interface on the right.

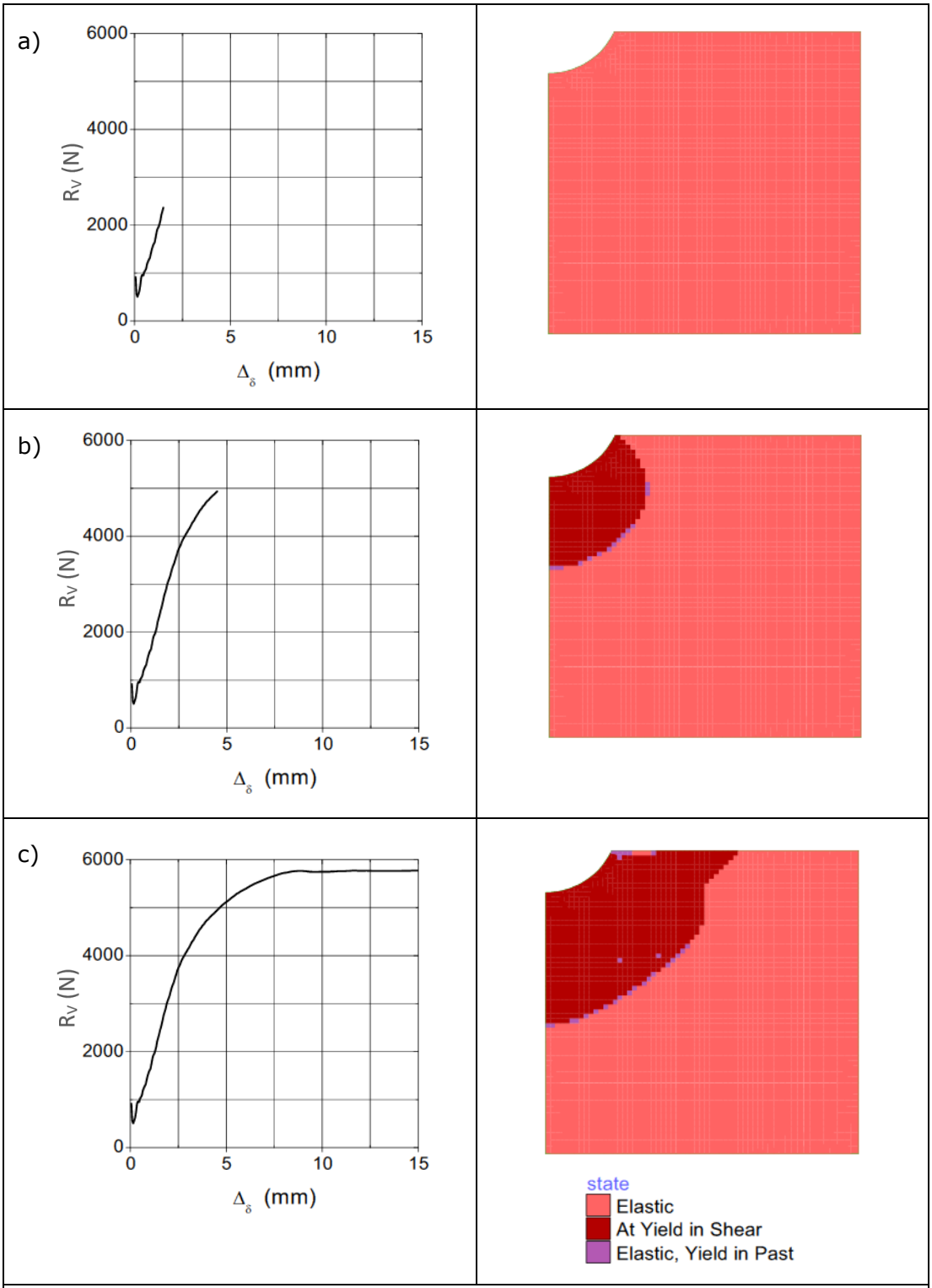

Figure 4.3 a,b,c *- An example comparison between load-displacement relationship and state plots (elastic or plastic state). Example is a 0.3D embedment with a smooth interface. a) shows elastic behaviour (1.5 mm), b) show confined plastic flow (4.5mm), c) shows unconfined plastic flow (15mm).*

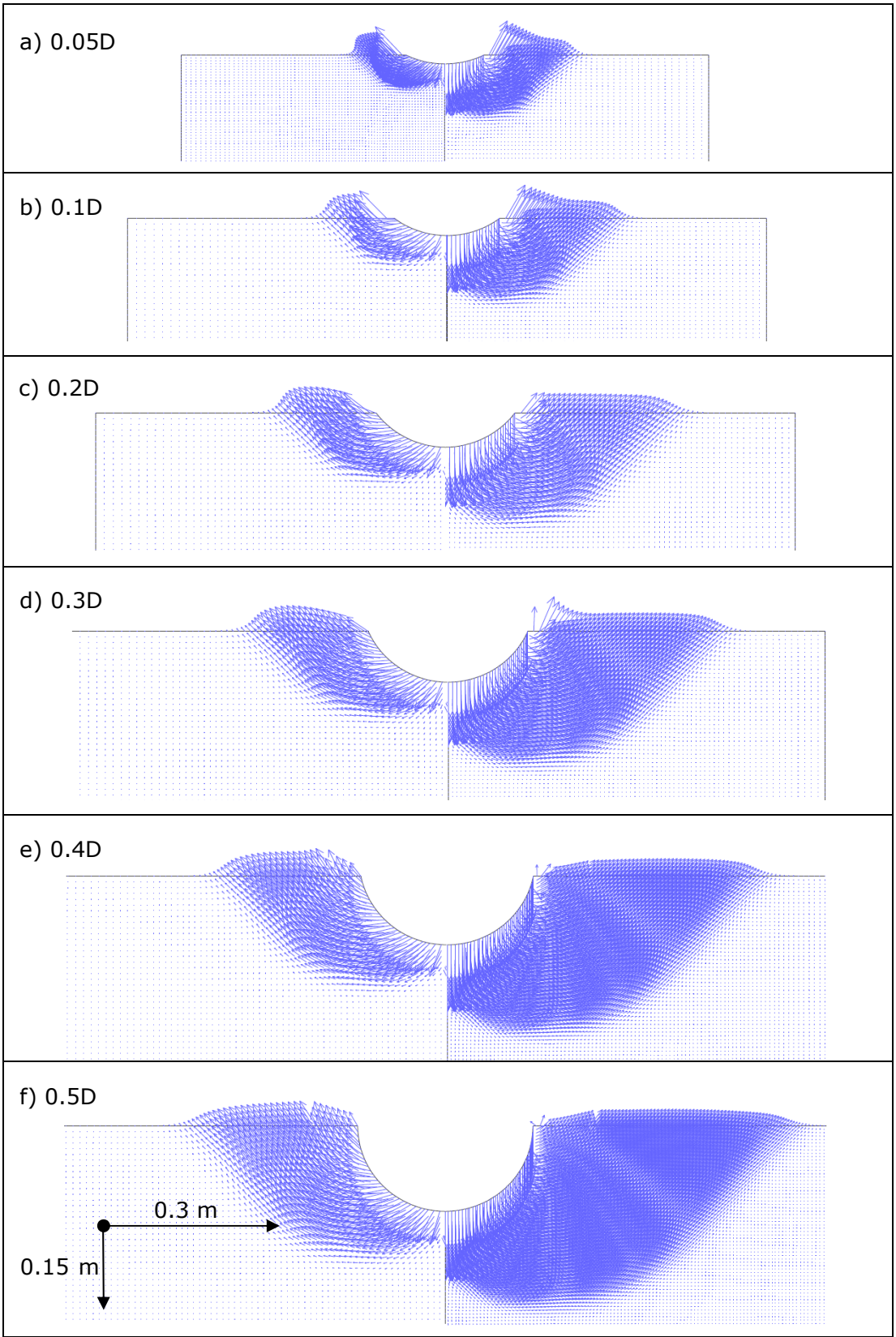

Figure 4.4 a,b,c,d,e,f - *Vector plots of soil displacement at peak load, $V_{max,}$ 0.05D to 0.5D for a 0.3m diameter pipeline. Uniform shear strength weightless soil. The left hand image is a smooth interface condition and the right hand image the rough interface case.*

In addition to the observations on the general form of the load-displacement relationship noted previously in this section, a number of further trends can be seen in Figures 4.1 and 4.2. These trends relate to rate of increase in resistance, for a given displacement, and maximum resistance, V_{max}. The nature of these trends changes with pipeline embedment depth and interface properties. After the initial linear phase, resistance to displacement can be seen to increase with embedment depth for both interface conditions, including an increase in the value of V_{max}. The displacement distance to reach V_{max} can also be seen to increase with embedment depth. It can be noted that the displacement distance to reach V_{max} is greater for a rough interface condition compared to a smooth interface and that a greater resistance is mobilised by these rough interface conditions. The reason for these trends are not easily determined purely from the data presented in Figures 4.1 and 4.2. However, this becomes clearer when reviewed in conjunction with Figures 4.4a to 4.4f.

From Figure 4.4 the geometry of the failure mechanism at peak load, V_{max}, can be observed. Two easily identified observations from these failure mechanisms are that; a rough interface produces a larger failure mechanism then a smooth interface at the same embedment depth and that the size of the failure mechanism increases with depth for both interface conditions.

The observations on failure mechanism size can be used to explain the trends in load-displacement behaviour seen in Figures 4.1 and 4.2. Within an elasto-plastic soil model a larger failure mechanism will be associated with shearing a larger amount of soil and, or, compressing a larger volume of soil elastically. The failure mechanisms that can be seen in Figure 4.4 are consistent with an increase in V_{max} with increasing depth, i.e. an increase in size of mechanism with depth. Additionally the higher values of V_{max} for a rough interface condition compared to a smooth interface are also consistent with the larger failure mechanisms noted for the rough interface case. A larger failure mechanism also provides an explanation for the larger displacements required to mobilise V_{max}, with a larger soil volume or length of shear plane needed to be mobilised to reach peak resistance.

Although a trend of increasing peak resistance with embedment depth and the differing peak resistance between rough and smooth interface conditions can be identified in Figures 4.1 and 4.2, a more appropriate format to review these trends is to plot peak resistance against embedment depth, see Figure 4.5. In Figure 4.5 V_{max} has been plotted against the wished in place embedment depth.

In both cases embedment depth and V_{max} are expressed in dimensionless format. The data presented in Figure 4.1 and Figure 4.2 is specific to the conditions adopted in analysis e.g. pipeline diameter, soil shear strength, etc. As such this data lacks generality and is of limited value as a design tool. An alternative method of presenting this data is in terms of two dimensionless groups for embedment depth and resistance. This follows the procedure used by previous researchers e.g. Aubeny et al. (2005) Merifield et al. (2008). Peak resistance, V_{max}, is expressed in the dimensionless group $V_{max}/s_u.D$ where V_{max} is normalised by the soil shear strength (s_u) and pipeline diameter (D). This $V_{max}/s_u.D$ term is analogous to a cohesive soil bearing capacity factor N_c, such as used by BSI (2003). Embedment depth (z) is normalised by the pipeline diameter (D). The dimensionless form used in Figure 4.5 also lends itself to comparison with the work of other researchers, which is undertaken later in this chapter, see Section 4.7.

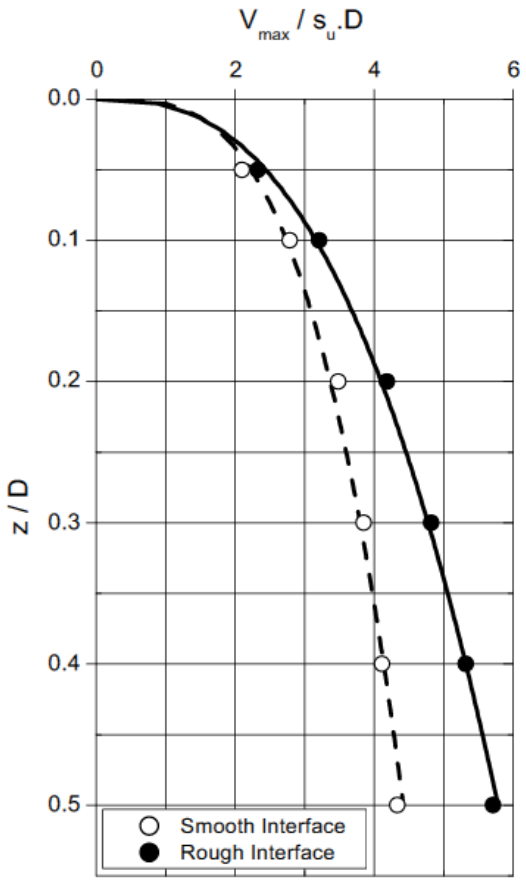

Figure 4.5 *- Peak resistance to vertical loading (V_{max}) by embedment depth in dimensionless form, 0.05D to 0.5D. Rough and smooth interface conditions, homogenous strength weightless soil.*

From Figure 4.5 a clear trend of increasing resistances with depth can be seen, as noted in previous studies, e.g. Aubeny et al. (2005) Merifield et al. (2008), and consistent with the failure mechanisms discussed earlier in this section. It can be seen in Figure 4.5 that a rough interface condition resulted in a higher resistance then a smooth interface condition at a given embedment depth. This difference increased in relative terms, with an 11% increase in resistance between smooth and rough interfaces at 0.05D, rising to 32% at 0.5D.

In a dimensionless format a general equation can also be fitted to the analysis data. This equation can then be used to determine behaviour with different pipeline diameters, different soil strength, etc, provided interpolation and extrapolation from the original numerical analysis is appropriate. Curves produced by this fitting equation are also shown on Figure 4.5, with a solid line representing a fit to the analysis of the rough interface conditions and a dashed line for the smooth interface condition. The numerical analysis data from this study is shown as hollow and solid points, representing smooth and rough interface conditions respectively. A power law equation was used for the fitting equations in the form shown in Equation [4.1], which can also readily be expressed in terms of resistance with depth by multiplying each side of the equation by $s_u.D$.

[4.1] $$\frac{V_{max}}{s_u D} = a \left(\frac{z}{D}\right)^b$$

Where;

V_{max} = Maximum capacity under vertical loading
s_u = Soil undrained shear strength
D = Pipeline diameter
z = Pipeline embedment depth
a, *b*, = Fitting coefficients

The coefficients *a* and *b* were used to fit Equation 4.1 to the numerical analysis data within an excel spreadsheet, for further details on the methodology used see Section 3.4. Table 4.1 shows the results of this assessment, as used in the curves previously plotted in Figure 4.5.

Interface Conditions	Coefficient	
	a	*b*
Smooth	5.43	0.297
Rough	7.50	0.375

***Table 4.1**: Correlation coefficients for Equation [4.1], as obtained from this study.*

The values of coefficients *a* and *b* derived from this study show good agreement with those produced by earlier researchers, see Section 4.2.3 for additional details.

In this study coefficient *b* is quoted to 3 decimal places instead of the two decimal places used by previous researchers. An example of the effect of this selection would be a rough pipeline, D= 0.3m, s_u= 5kPa, z= 0.3D, where the difference between b=0.375 and b=0.37 is 43 N, ~0.6%. Using 3 decimal places for *b* produces a typical precision of <0.1% in this range of design parameters. The objective was to ensure that the precision of the proposed correlations was greater than the anticipated accuracy, with this additional decimal place for *b* providing a pragmatic and conservative way to satisfy this objective. In general this is expected to result in a correlation precision approximately one order of magnitude greater than the accuracy of the analysis methods used, or slightly more in some cases. While this increased precision may be unwarranted for many applications, for example when input parameters such as soil shear strength are uncertain and within the context of the assumptions and accuracy of the analysis method used, it is preferable for the correlations to have a precision a margin greater than is likely to be required.

The fit of the proposed equations to the numerical analysis data from this study is relatively good over the depth range 0.1D to 0.5D. It can be noted that the precision of the fit is poorer at the shallowest depth considered, 0.05D. From 0.1D to 0.5D the equation fits to within 3.4% of the analysis data for a smooth interface and 2.0% for a rough interface. At 0.05D the equation is within 6.2% of the analysis data for a smooth interface and 4.9% for a rough interface, with the fitting equations over predicting resistance.

This poorer fit at shallow depth may be linked to change in the geometry of the problem e.g. at shallow embedment the pipeline shape has less of an effect and the contact geometry approaches that of a strip footing. Previously Aubeny et al.

(2005) had issues making a single power law equation fit to an embedment range less than 0.5D and embedment greater than 0.5D. This will be discussed further in Section 4.2, however this is an example when a change in the geometry of the problem (i.e. beyond 0.5D the contact width no longer increases but remains constant at 1D) raises an issue with fitting a correlation equation to analysis data. Also, while the fit is poorer as a percentage or in relative terms, due to the reduced resistance at shallow depths in absolute terms the difference is relatively small. In this case it is likely to be acceptable for most applications, although if very shallow depths are of interest further work could be undertaken using an alternative fitting relationship in conjunction with further analysis.

Equation [4.1] provides a useful way of relating pipeline penetration resistance to embedment depth. However, as a design tool it may be more useful to relate depth of penetration into the seabed to a vertical load or pipeline weight(s). White and Randolph (2007) suggested an equation for this relationship, see Equation [4.2]. This equation used alternative fitting coefficients, shown as *A* and *B* in this study to differentiate from *a* and *b* used in Equation [4.1]. However, the derivation of *A* and *B* was not fully detailed by White and Randolph (2007) and it is relatively cumbersome, and could introduce errors, to use different fitting coefficients without a clear interrelationship.

Equation [4.3] reproduces Equation [4.2] in terms of *a* and *b*, as summarised in Table 4.1 for this study, or in Aubeny et al. (2005) Merifield et al. (2008) for previous studies. Alternatively *A* and *B* can be derived separately as suggested by Dean (2009). Although it is noted this reference contains a mathematical or typographic error in the derivation of *A*, a corrected version is shown in Equation [4.3].

[4.2] $$\frac{z}{D} = A\left(\frac{V}{Ds_u}\right)^B$$

[4.3] $$z = D\left[\frac{1}{a^{\frac{1}{b}}}\left(\frac{V}{s_u D}\right)^{\frac{1}{b}}\right]$$

Where;

z = Depth of embedment

D = Pipeline diameter

V = Vertical load

s_u = Soil undrained shear strength

A, B, = Alternative coefficients

a, b, = Fitting coefficients

If Equation [4.2] is used directly the coefficients A and B can be obtained from Table 4.2, which is equivalent to the values of *a* and *b* in Table 4.1. Coefficient *A* is quoted to 5 decimal places and *B* to 3 decimal places, which is consistent with the previous discussion on precision of coefficients *a* and *b*. Using similar design examples to that previously discussed (e.g. D=0.3m, su=5kpa, z/D=0.3) the sensitivity of quoting *A* to 4 decimal places is ~ 1mm and 5 decimal places in <0.1mm. Sensitivity to *B* is similar at 2 and 3 decimal places.

Interface Conditions	Coefficient	
	A	*B*
Smooth	0.00336	3.367
Rough	0.00464	2.667

Table 4.2*: Correlation coefficients for Equation [4.2], as obtained from this study.*

4.2.2 Analysis Results - Small Strain Analysis at Deeper Embedment

Analysis was undertaken to extend this study to pipeline embedment depths greater than 0.5D up to a pipeline embedment of 1.0D. Limiting analysis to depths of less than 0.5D, e.g. Merifield et al. (2008), seems to have some logic as an arbitrary value when shallower embedment is the principal area of interest. However, as 0.5D is also the depth at which there is no longer an increase in contact width with further penetration, some aspects of the problem could be obscured by this choice. Additionally, these greater embedment depths may be relevant to heavier pipelines in lower strength soil conditions and, or, pipelines that experience an increase in vertical load during installation, as discussed by Cathie et al. (2005).

A 0.3 m diameter pipeline was used in analysis. This pipeline was wished in place at an embedment depth of 0.75D and 1D, with a vertical sided trench adopted above the pipeline shoulder i.e. depths >0.5D. As with analyses summarised in the previous section of this thesis a homogenous undrained shear strength (s_u) of 5 kPa was used for the soil with elastic behaviour characterised by a Poisson's ratio (υ) of 0.49 and a Young's modulus (E) of $E = s_u \times 200$. Analyses considered the case of a weightless soil. As with previous analysis, results were obtained for half a pipeline cross section. However, for clarity they have been multiplied by two and the results reported within this section are equivalent to a full pipeline.

Once initial problem familiarisation was addressed, 7 analyses were undertaken for the smooth interface condition and 11 analyses for the rough interface condition. Further information on analysis parameters, as well as analysis results, is provided in Table 1-3 and 1-4, Appendix A. This includes details of depth specific variables, such as displacement velocity (v) and mesh refinement as characterised by the mesh zone dimension (Δ_z).

A range of mesh densities were analysed to determine adequate refinement for the smooth and rough interface conditions, accounting for any variation in this requirement with embedment depth. In contrast with the shallower embedment depths, determination of adequate mesh refinement was slightly more subtle. At shallow depths adequate refinement could be determined when two mesh densities had the same value of V_{max}, to the nearest Newton, or when an increase in mesh density actually lead to a small increase in V_{max}, i.e. the minimum value of V_{max} had been determined in the penultimate analysis. For these deeper depths there was a more subtle trend, in that a series of relatively large increases in mesh refinement lead to a very small decrease in V_{max} i.e. V_{max} from the final analysis is extremely close to the minimum value of V_{max}. For the smooth interface condition a series of analyses were undertaken, with the level of mesh refinement consistent with the shallow embedment analyses. The final analysis of this series resulted in <0.2% decrease in V_{max} for a relatively large increase in mesh density.

The same approach used for the smooth interface was adopted for a rough interface condition, albeit higher levels of mesh refinement were required then for a smooth interface. The rough interface condition had a slower decrease in V_{max} for a given increase in mesh refinement, both compared to a shallower embedment depth and in comparison to the smooth interface case. For the rough interface condition convergence was taken as a <0.9% decrease in V_{max}, although 0.75D analysis produced a <0.25% decrease for the final analysis.

Mesh refinement requirements for a smooth and rough interface case were generally consistent with those at shallower depths, with a similar requirement for a finer mesh for a rough interface condition compared to the smooth interface. A smooth interface condition at an embedment of 0.75D was slightly anomalous in requiring a relatively fine mesh. Although there was no clear reason for this requirement and it may well be an artefact of some aspect of these specific calculations, such as mesh geometry, rather than a true effect related to the problem being considered. Displacement velocity requirements

were similar to those at shallower embedment depths for both interface conditions, although the analysis did seem slightly more numerically stable and it was possible to use slightly faster displacement speeds. This may be attributable to the larger displacement distance to reach V_{max} and the larger body of soil mobilised at V_{max}.

FISH scripts recorded the load/resistance (R) against displacement (Δ_δ) behaviour, where displacement is measured from the wished in place depth. This relationship is shown in Figure 4.6 and 4.7 for the smooth and rough interface conditions respectively.

The data for deeper embedment depths, shown in Figure 4.6 and 4.7, exhibits the same general trend in the load-displacement relationship noted for an embedment of 0.5D and shallower. Following an initial linear phase associated with elastic behaviour the relationship curves with the onset of confined plastic flow. The trend of a curving in the load-displacement relationship continues until a constant value of peak load, V_{max}, is reached. V_{max} is associated with unconfined plastic flow and full development of the failure mechanism.

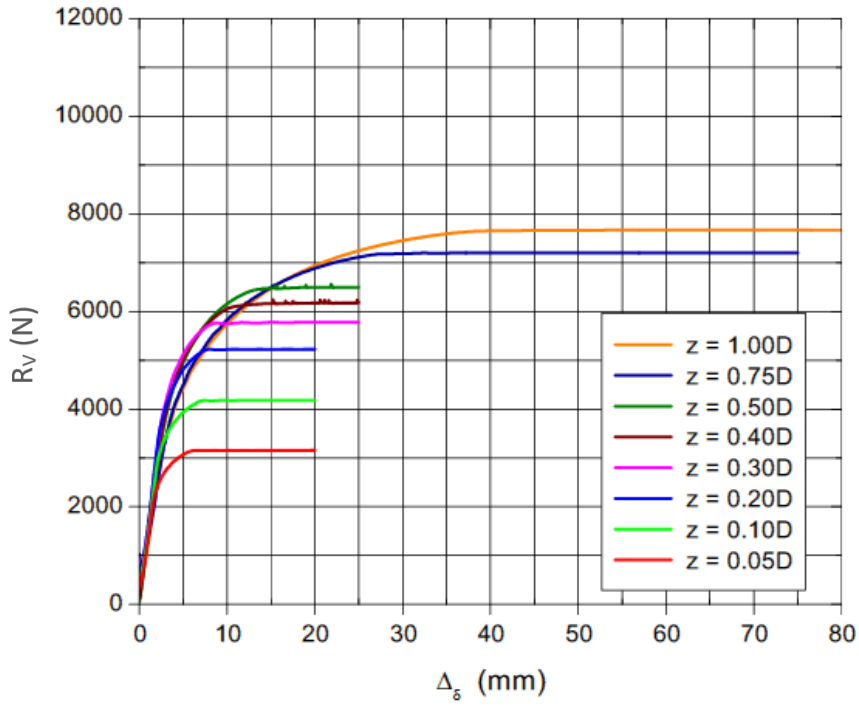

Figure 4.6 *- Load-displacement behaviour for a pipeline subjected to vertical loading, 0.05D to 1D. Smooth interface condition, homogenous strength weightless soil.*

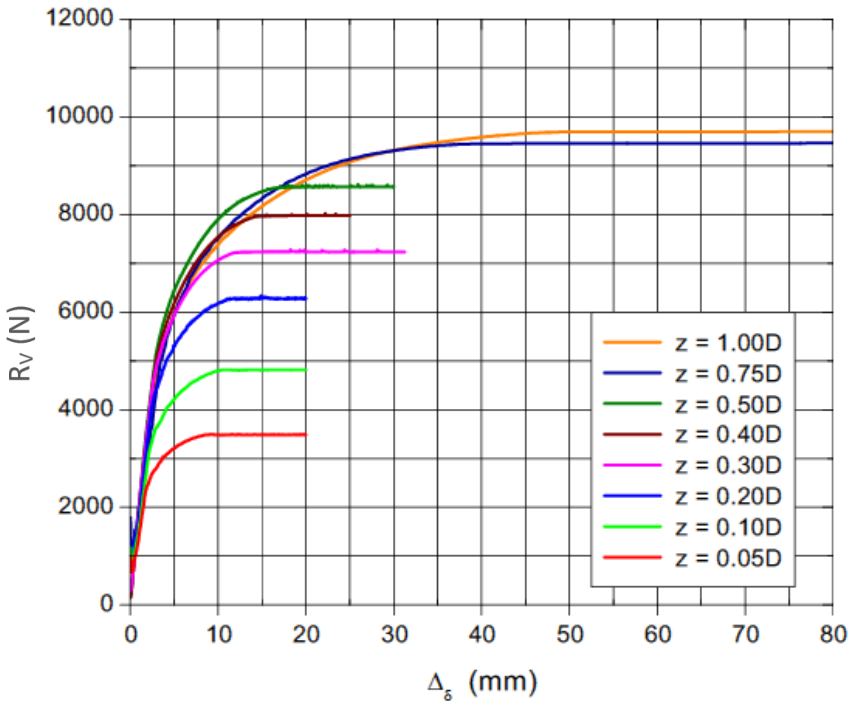

Figure 4.7 *- Load-displacement behaviour for a pipeline subjected to vertical loading, 0.05D to 1D. Rough interface condition, homogenous strength weightless soil.*

From Figure 4.6 and 4.7 it can be seen that a larger displacement is required to reach V_{max} for a rough interface compared to a smooth interface. This trend has been previously noted at shallower embedment depths and can be seen to continue over this deeper embedment range.

At a pipeline embedment depth shallower then 0.5D the general form of the load displacement relationship resulted in a similar resistance at smaller displacement. With increasing embedment depth the linear elastic and the curved load displacement relationship associated with confined plastic flow extended over a larger displacement range, resulting in a higher value of V_{max} at a larger displacement. The similarities in the load displacement relationship noted over the depth range 0.05D to 0.5D can be attributed to a similar failure mechanism.

The similarity between the load displacement relationship at shallower depths can also be contrasted with load displacement relationship for the analysis undertaken at 0.75D and 1.0D, which is not so similar to these shallower depth analysis. The load displacement relationship for 0.75D and 1.0D are similar to each other and follow the general trend of the shallow analyses at smaller displacement. At larger displacement they undercut shallower analyses results

e.g. 0.5D and 0.4D showing lower resistance at a given displacement. The larger values of V_{max} for these deeper embedment depths is associated with a larger displacement. This pattern is particularly marked for the smooth interface condition (Figure 4.6). This difference in load displacement behaviour between the two depth ranges can be attributed to different failure mechanisms. As previously noted for shallow embedment analyses, insight can be gained into these trends by reviewing the soil displacement at failure, V_{max}. This is presented as vector plots in Figure 4.8 a and b.

As with shallower embedment depths, the failure mechanisms that can be seen in the vector plots (Figure 4.8) support interpretation of the trends noted in the load-displacement behaviour (Figure 4.6 and 4.7). The differences between the smooth and rough interface conditions noted in the load displacement plots are reflected in soil displacement at failure. These vector plots can also be reviewed with respect to the form of the failure mechanism, as compared to those previously presented for the shallower depth range in Section 4.2.1.

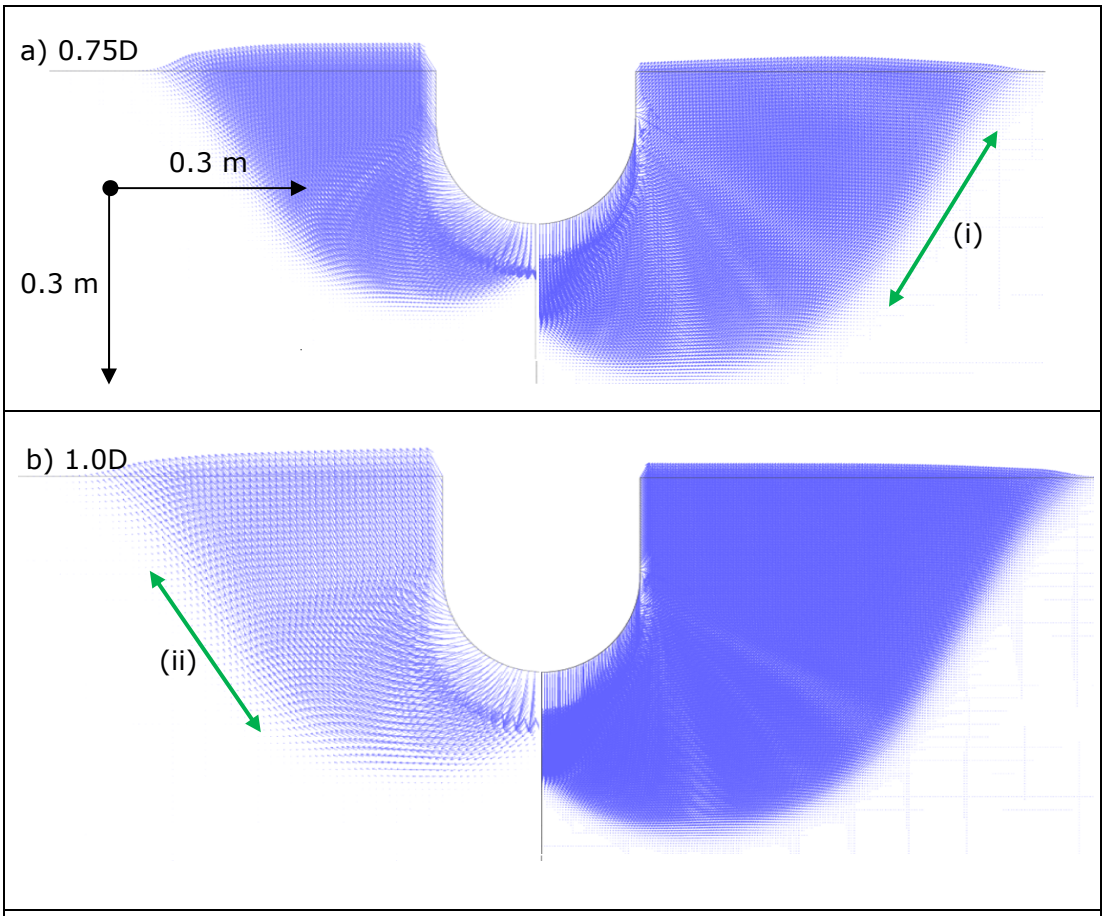

Figure 4.8 a, b *- Vector plots of soil displacement at peak load, V_{max}, 0.75D and 1.0D for a 0.3 m diameter pipeline. Uniform shear strength weightless soil. The left side is a smooth interface the right side rough interface case.*

The vector plots in Figure 4.8 can be likened to those for shallower pipeline embedment depths presented in Figure 4.4, although it can be seen that the increase in depth has resulted in some subtle changes in geometry, particularly at 1D. This can be seen in a steepening in the sides of the failure mechanism, for example contrast the areas marked at (i) and (ii) in Figure 4.8 with the same areas at shallow embedment depths in Figure 4.4. This trend is as can be expected and should become more marked over a larger depth range, in association with a transition from shallow failure mechanism to a flow around mechanism at a large embedment depth.

As previously, the difference between smooth and rough interface conditions are clear within the vector plots and the larger failure mechanisms for the rough interface can be used to explain both the greater V_{max} and the larger displacements required to mobilise V_{max}. The differences in failure mechanism with depth can also be seen in Figure 4.8, consistent with the increase in V_{max} with embedment depth. The largest increase in V_{max} with depth is for the smooth interface condition, which also shows a clear and significant change in the size of mechanism from 0.75D to 1D. The change in the failure mechanism for the rough interface condition is less marked, which is also consistent with the smaller change in V_{max} over this depth range for this interface conditions.

It has been noted that the deeper depths considered in this section require a markedly larger mobilisation distance to V_{max}, compared to the form of the load-displacement behaviour observed at 0.5D and shallower. In addition to the increase in mechanism size, which has already been linked to an increase in mobilisation distance, the steepening and the increase of the vertical extent of the mechanism is expected to be a factor that is influencing this mobilisation distance. The vertical sided trench and the void above the pipeline shoulder is also a difference in the geometry of the problem and may have an influence on the displacement distance to V_{max}.

The analyses results reported in this section can also be plotted in dimensionless form, see Figure 4.9. For comparison purposes Figure 4.9 includes the correlation previously proposed for an embedment depth of 0.5D and shallower (see Figure 4.5).

It can be seen in Figure 4.9 that the correlations derived from analysis of embedment depths of 0.5D and shallower deviate from the data for deeper depths, especially for the rough interface condition. At 1.0D the analysis results for the rough interface condition are 16.0% less than the shallow embedment

correlation and 6.2% for the smooth interface condition. However, this is perhaps not unsurprising. In addition to the observations on failure mechanisms, correlations to shallow embedment analysis implicitly include for an increase in contact width with depth. When this no longer occurs from 0.5D an increasing error can be expected if these correlations are extrapolated to a greater depth.

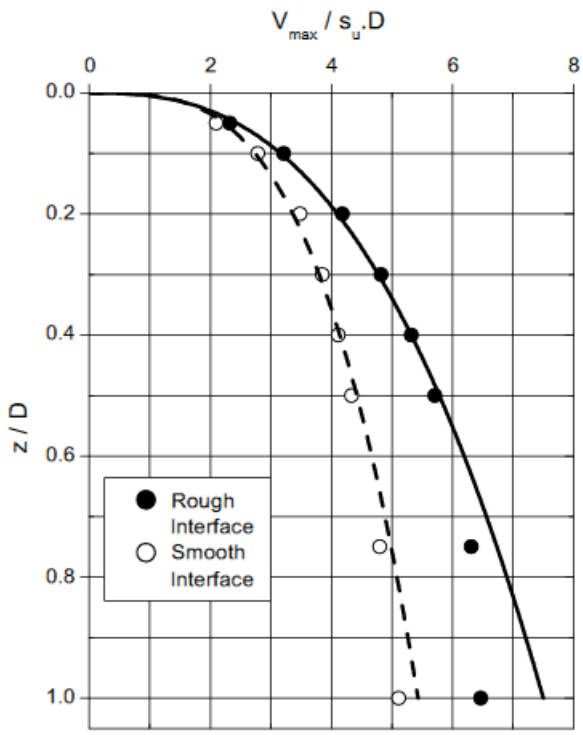

Figure 4.9 *- Peak resistance to vertical loading (V_{max}) against embedment depth in dimensionless form, 0.05D to 1.0D. Rough and smooth interface conditions, homogenous strength weightless soil.*

Two options are available to improve correlations for the depth range 0.5D to 1.0D. The first option is to derive a fitting equation using only the deeper analysis (0.5D to 1D), the second option is to derive a fitting equation for all the data (0.05D to 1.0D). Both these options are presented in Figure 4.10.

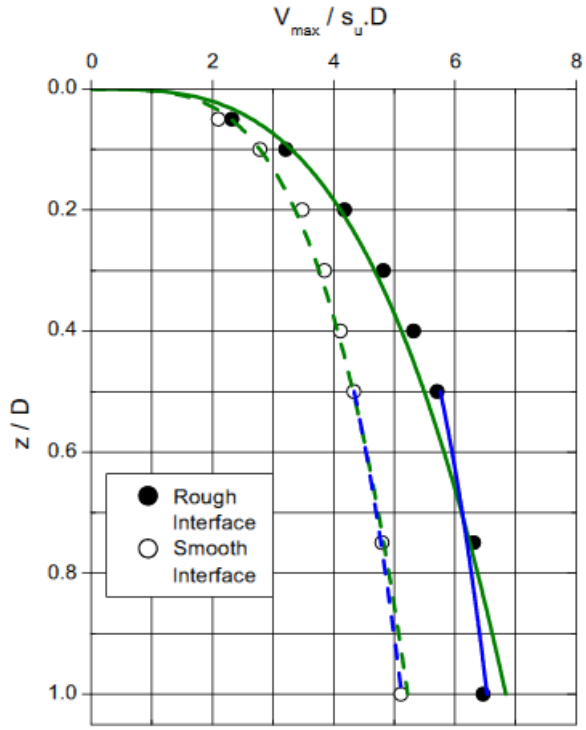

Figure 4.10 *- Peak resistance to vertical loading (V_{max}) against embedment depth in dimensionless form, 0.05D to 1.0D. Rough and smooth interface conditions, homogenous strength weightless soil. New correlations as per Table 4.2 and 4.3. Green lines are for all data correlations and blue lines for deep data only correlations.*

The process for deriving these two sets of fitting equations was the same as outlined in the previous section, where excel solver was used to iteratively derive fitting coefficients. The fitting equation used is shown in Equation [4.4]. The fitting coefficients derived from this analysis are presented in Table 4.3 and 4.4.

[4.4] $$V_{max} = a \left(\frac{z}{D}\right)^{b} s_u D$$

Where;

V_{max} = Maximum capacity under vertical loading
s_u = Soil undrained shear strength
D = Pipeline diameter
z = Pipeline embedment depth
a, *b*, = Fitting coefficients

Interface Conditions	Coefficient	
	a	*b*
Smooth	5.22	0.273
Rough	6.84	0.316

***Table 4.3**: Correlation coefficients, Equation [4.4], z=0.05D to 1D.*

Interface Conditions	Coefficient	
	a	*b*
Smooth	5.12	0.239
Rough	6.53	0.181

***Table 4.4**: Correlation coefficients, Equation [4.4], z= 0.5D to 1D.*

The alternative approach of providing equations that can be used to obtain pipeline penetration from a given vertical load, e.g. pipeline weight, is also presented here. The fitting equation used is shown in Equation [4.5] and the associated coefficients in Table 4.5 and Table 4.6.

[4.5] $$\frac{z}{D} = A\left(\frac{V}{Ds_u}\right)^B$$

Where;

z = Depth of embedment
D = Pipeline diameter
V = Vertical load
s_u = Soil undrained shear strength
A, B, = Alternative coefficients

Interface Conditions	Coefficient	
	A	*B*
Smooth	0.00235	3.663
Rough	0.00228	3.165

***Table 4.5** - Correlation coefficients, Equation [4.5], z= 0.05D to 1D.*

Interface Conditions	Coefficient	
	A	*B*
Smooth	0.00108	4.184
Rough	0.00003	5.525

Table 4.6 *- Correlation coefficients, Equation [4.5], z= 0.5D to 1D.*

4.2.3 Comparisons with Previous Research

As noted in Chapter 2, the analysis results presented for the case of a pipeline on a homogenous strength weightless seabed is similar to previous analyses undertaken by Aubeny et al. (2005) and Merifield et al. (2008). The analysis fitting equations proposed by Merifield et al. (2008) were limited to <0.5D, those proposed by Aubeny et al. (2005) extended to 1.0D and beyond. Comparisons between these earlier studies and this study are shown in Figure 4.11 for a smooth interface conditions and Figure 4.12 for a rough interface.

For the case of a smooth interface at shallow depth (<0.5D) the fitting equations proposed in this study are nearly identical to those proposed by Aubeny et al., (2005) and Merifield et al. (2008). There is also very good agreement between this study and Aubeny et al. (2005) at depth from 0.5D to 1.0D.

For rough interface at shallow depth (<0.5D) there is very good agreement between the fitting equation produced from this study and that proposed by Aubeny et al. (2005). There is also good agreement with the relationship proposed by Merifield et al. (2008), which slightly underlies this study and Aubeny et al. (2005). At greater depth (0.5D to 1.0D) there is reasonable agreement between this study and Aubeny et al. (2005).

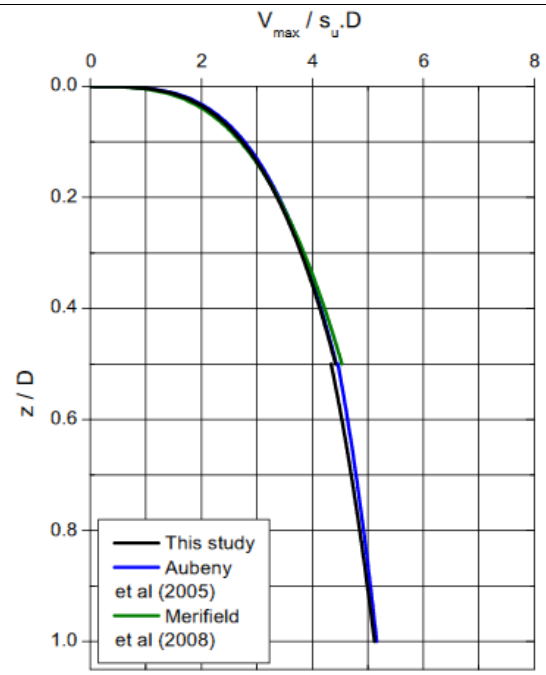

Figure 4.11 - *Comparison between this study,* Aubeny et al. (2005) *and* Merifield et al. (2008) - smooth interface.

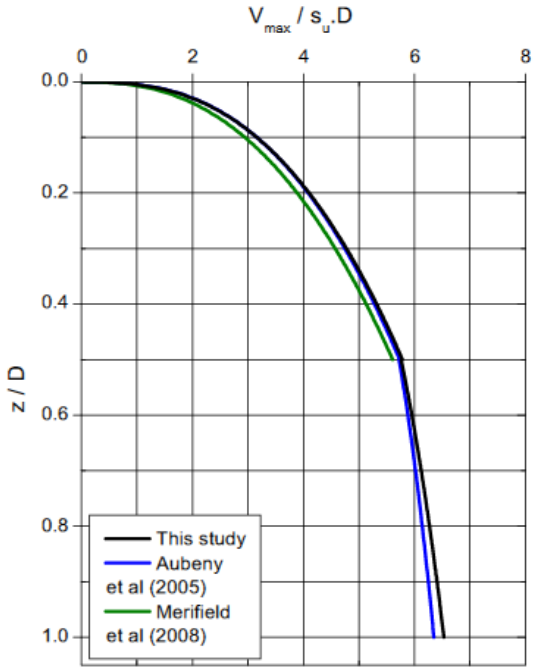

Figure 4.12 - *Comparison between this study,* Aubeny et al. (2005) *and* Merifield et al. (2008) - rough interface.

The agreement between this study and the work of previous researcher has acted as initial validation of the methods used in this study. In addition to undertaking analysis for similar cases to Aubeny et al. (2005) and Merifield et al. (2008), a minor extension has been included, with an analysis case a pipeline at an embedment of 0.05D. An alternative design equation has also been presented that links pipeline penetration to parameters such as pipeline diameter and soil shear strength. For some design tasks this may be a more convenient formulation than equations that produce V_{max} against depth profiles.

4.3 The Influence of Large Strain Effects

A large strain problem definition for a pipeline subjected to vertical loading was described in Chapter 3. Analysis of this problem definition has been undertaken with results reported in this section. A 0.3m diameter pipeline was displaced from seabed level (z=0) to an embedment of z=1.0D with calculation of resistance to displacement. A homogenous soil shear strength of 5 kPa was adopted. However, all results in this section are reported in terms of dimensionless factors i.e. $V_{max}/s_u.D$ and z/D. The seabed soils were treated as being weightless for these analyses. Elastic behaviour was based on a Poisson's ratio (υ) of 0.49 and a Young's modulus (E) of $E = s_u \times 200$. Both smooth and rough interface conditions were investigated.

Mesh refinement requirements were based on earlier small strain analysis as were the displacement velocities. It was noted that the smooth interface was especially sensitive to displacement velocity on initial penetration into the seabed. This can be attributed to the lack of constraints on soil movement for initial contact of a smooth interface. This was addressed by using a slower penetration velocity for this initial phase of penetration. Details of analysis parameters are provided in Appendix A, Tables 1-11 and 1-12.

Figure 4.13 shows the results of analyses undertaken into the smooth interface case with analyses results for the rough interface case shown in Figure 4.14. Analyses for each of these interface conditions represents a continuous V_{max} profile. After the initial penetration into the seabed subsequent analyses follow on from a series of re-meshes of the analysis field. Initial load following re-mesh starts from zero load until plastic flow fully develops again, at which point the load displacement data starts to follow the same trend as the previous analysis

step, providing data to a greater depth. Re-mesh steps were planned to provide continuous or near continuous data across the depth range being investigated.

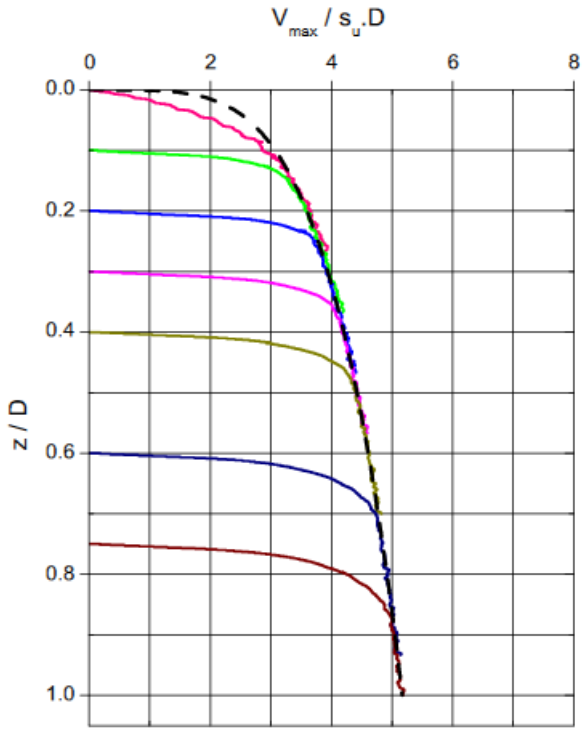

Figure 4.13 *- Large strain analysis of V loading, smooth interface.*

In Figure 4.13 and Figure 4.14 a fitting relationship to the large strain analysis data is included, shown as a dashed black line. The individual analysis phases are differentiated by assigning different colours to the data from each phase. The reloading following a new analysis phase can be seen at the start of the data from each phase. It was preferable to allow for some data overlap from each analysis phase. However, in all cases analysis phases were planned to provide sufficient data to ensure the overall trend in V_{max} could be determined. The data fitting follows the same methodology described and used in previous sections. Although instead of fitting to discreet analysis points, as with small strain data, there was the requirement to fit to a larger amount of data. Data associated with initial displacement after a re-mesh was filtered out prior to establishing coefficients. These fitting relationships to the large strain analysis results use Equation [4.4], with the fitting coefficients presented in Table 4.7.

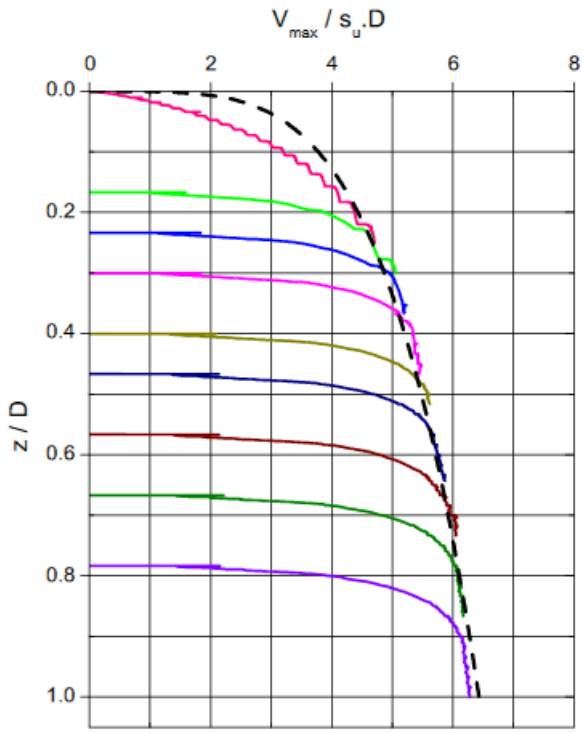

Figure 4.14 *- Large strain analysis of V loading, rough interface.*

Interface Conditions	Coefficient	
	a	*b*
Smooth	5.17	0.266
Rough	6.43	0.231

Table 4.7*: Large strain V loading correlation coefficients, Equation [4.4].*

Unlike the small strain problem there was no requirement for two sets of correlations for the shallow (<0.5D) and deep behaviour (>0.5D to 1.0D) with one correlation providing a reasonable fit to the data, although it does appear that the rough interface relationship may be showing the first signs of over predicting resistance towards 1.0D. A second fitting relationship may be required at a deeper embedment depth if the scope of these analyses was extended.

One feature that can be noted for both the smooth and rough interface fitting relationships is the tendency to over predict V_{max} at very shallow embedment depths e.g. <0.1D. This trend is more marked for the rough interface. It has already been noted that the power law relationship did not fit especially well to

the small strain analysis data at 0.05D. The large strain analysis show a continuous profile of resistance in this depth range, emphasising this observation. It is believed that this observation is representative of something more fundamental than quality of data fitting alone and that there are implications for pipeline behaviour in the field.

It was noted during large strain analysis that initial penetration into the seabed reflected a similar process to that shown in Figure 4.3 for small strain analysis. There was an elastic compression of the seabed, followed by confined plastic flow, followed by development of a full failure mechanism and unconfined plastic flow. At greater depth the analysis results are governed by unconfined plastic flow. However, at these shallowest pipeline embedment depths the resistance to displacement may also be influenced by factors such as elastic behaviour and confined plastic flow. This is manifested in the difficulties in finding a fitting relationship that also encompasses these shallowest depths. More fundamentally this suggests that if very shallow pipeline penetration depth is of interest, for example very light pipes on higher shear strength soils, there will be some additional complexities. For example the elastic soil parameters may become more important to behaviour. This may need to be investigated further if the shallowest embedment depths are of particular interest.

This explanation for the trend in pipeline resistance at shallow depth is also consistent with the differences that can be noted between the rough and smooth interface analysis. The rough interface results in a large failure mechanism, as with the small strain analysis. This large mechanism for the rough interface will require a larger displacement distance to mobilise and hence the observed trend can be expected over a larger depth range then for the smooth interface. A larger mechanism would also be expected to be influenced to a larger extent by these factors, such as elastic behaviour, and hence the more marked effect for the rough interface conditions.

Figure 4.10 previously presented a series of correlations for small strain analysis. This consisted of a general fitting relationship for the full depth range 0.05D to 1.0D and a deep only relationship for the depth range 0.5D to 1.0D. One way to compare large strain and small strain analysis from this study is to compare these small strain fitting relationships with the large strain fitting relationships presented in Figure 4.13 and 4.14. This has been done in Figure 4.15.

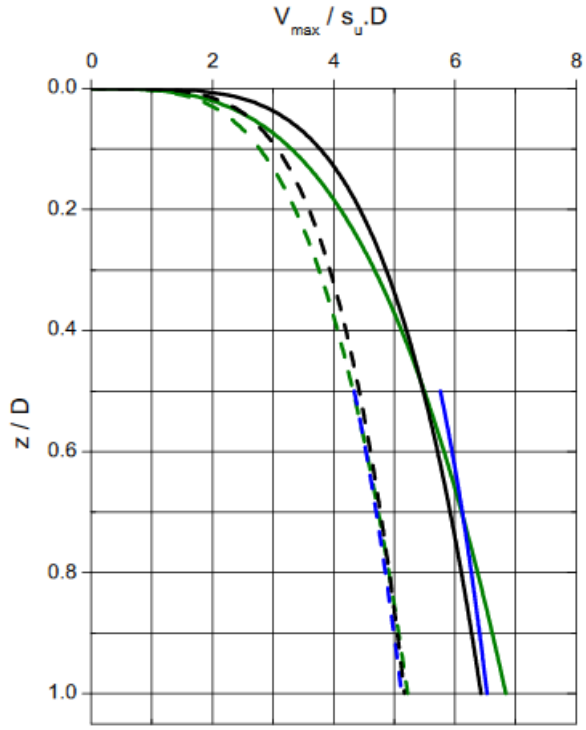

Figure 4.15 *- Correlations for smooth and rough interfaces dashed and solid lines respectively, small strain analysis (in green and blue) and large strain analysis (in black).*

The main observation that can be made from Figure 4.15 is that the large strain analysis fitting relationship gives a slightly higher resistance than the small strain relationships at shallow depth. This difference becomes negligible at approximately z=0.4D and disappears at z=0.5D. This can be attributed to the geometry of the problem. Within a large strain problem definition soil heave brings soil up into contact with an area of the pipeline still above the seabed level. This produces a larger effective contact width, essentially producing a resistance to V loading equivalent to a slightly greater embedment depth. This effect reduces with embedment depth. For example at 0.4D most of the pipeline is in contact with soil including a small area above seabed level, at 0.5D the maximum width of the pipeline is mobilised and large strain effects appear to no longer influence the problem for this problem definition.

For the smooth interface small strain and large strain analysis correlations match extremely well following the phase of shallower penetration and the associated

soil heave effects at <0.5D. For the rough interface the large strain correlation slightly underlies the small strain correlations. There is some scatter in analysis for these cases and the minor differences could relate to this scatter. However, it's also possible that this is attributable to some slight differences in the failure mechanism, with penetration from the surface producing a slightly more efficient mechanism then the wished in place case with a vertical sided trench.

Although the principal large strain effect of interest is soil heave coming in contact with the pipeline during penetration, and the associated change in V_{max}, more general features of soil heave can also be reviewed, see Figure 4.16 for soil heave profiles for smooth interface and Figure 4.17 for a rough interface.

At a very shallow pipeline embedment depth, e.g. 0.05D, there is no soil heave and no berm can be seen. This can attributed to largely elastic soil behaviour at these smaller pipeline displacements. As pipeline embedment depth increases, first a very subtle and flat soil berm can be seen. At larger pipeline displacement the volume of soil displaced by the pipeline becomes relatively large and the associated berms are more prominent.

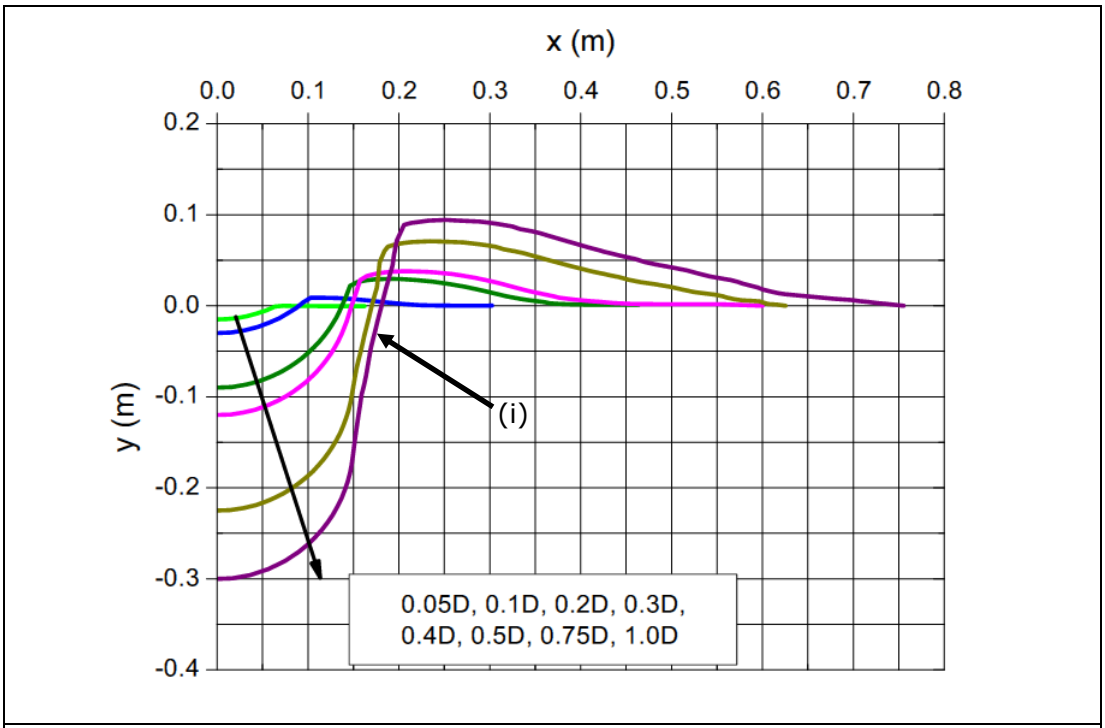

Figure 4.16 *- Soil heave profiles, smooth pipe-soil interface.*

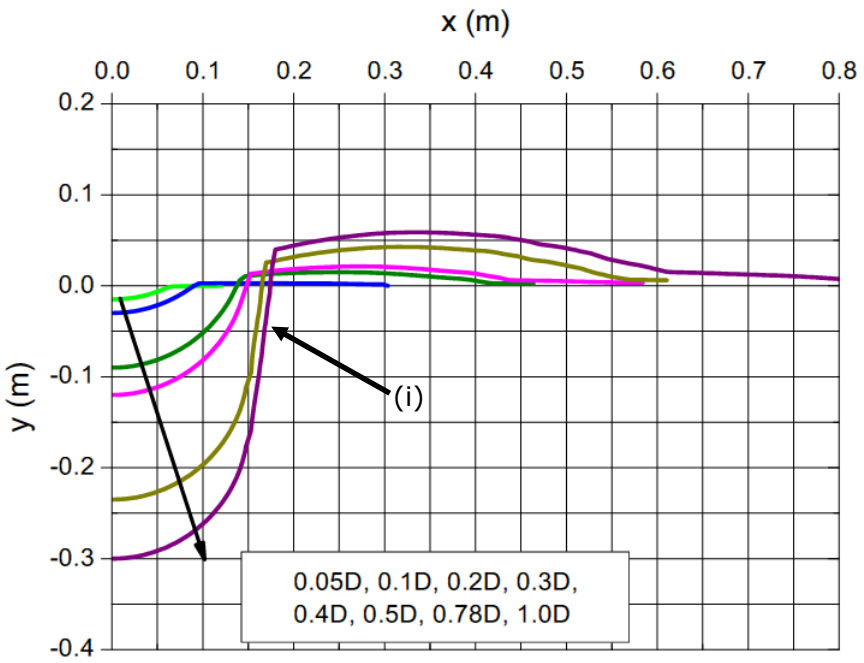

Figure 4.17 *- Soil heave profiles, rough pipe-soil interface.*

It can be seen from Figure 4.16 and Figure 4.17 that there is a marked difference in the geometry of the soil berms formed by the smooth and rough interface pipelines. For the smooth pipeline interface conditions the berms tend to higher and with more soil closer to the pipeline, whereas for the rough interface the berm tends to be lower height and spread over a wider area away from the pipeline. For both interface cases berm volume was reviewed and found to be consistent with the pipe trench volume i.e. conservation of volume, although it can be noted that for the rough interface this volume redistribution is more diffuse and over a larger area of seabed.

In addition to the geometry of the berm, below a pipeline embedment of 0.5D some subtle differences in the trench wall geometry can also be noted between the two interface conditions, see area marked as (i) in Figure 4.16 and Figure 4.17. The trench wall for the rough interface is steeper than for the smooth interface conditions. In both case the trench wall is sub vertical rather than vertical. However, this does not seem to have significantly impacted the similarity between these large strain analyses and the small strain analyses wished in place with a vertical sided trench.

Analysis using large strain analysis techniques has shown the impact of soil heave on V_{max}. Some interesting observations on berm geometry have also been

noted. However, these do not appear to significantly impact resistance to V loading within this problem definition. The results of these analyses will be discussed further alongside other factors that impact pipeline behaviour under V loading in Section 4.7.

4.4 The Effect of Interface Conditions

Previous analysis has considered pipe-soil interface conditions as either a perfectly smooth interface or a rough interface, bounding the range of possible interface behaviour for the problem of a pipeline subjected to vertical loading. While there is no substantive data to relate pipeline properties in the field, or even in model tests, to these theoretical bounds, it would seem unlikely that any pipeline behaves exactly as either of these two extremes. It is therefore of interest to investigate how interface conditions between these bounds influences the problem being considered.

Within an undrained material model the behaviour of an interface can be considered in terms of the resistance that can be mobilised in shear at this interface. This is conveniently expressed as a ratio, or percentage, between the interface undrained shear strength (s_{ui}) and the undrained shear strength of the adjacent seabed soil (s_u). Within this framework, perfectly smooth interface conditions are represented by $s_{ui}/s_u = 0$ and a rough interface condition is represented by $s_{ui}/s_u = 1$. An example of an interface that is half way between rough and smooth condition would be an interface that mobilises 2.5 kPa in shear within a seabed soil of 5 kPa i.e. $s_{ui}/s_u = 0.5$.

Using the methodology outlined in Chapter 3 analysis was undertaken to investigate the effect of interface conditions on a pipeline subjected to vertical loading. A small strain analysis framework was adopted. A total of 25 analyses were undertaken over 5 embedment depths, 0.1D, 0.3D, 0.5D, 0.75D and 1D. At each depth 5 interface conditions were considered $s_{ui}/s_u = 0$, 0.25, 0.50, 0.75 and 1.00. Mesh refinement for these analyses was based on previous convergence studies, as described in Section 4.2. Where, for a particular pipeline embedment depth, the mesh refinement requirements varied between the previously considered rough and smooth interface conditions then the finest mesh was used for all cases within this suite of analyses. Displacement velocities were based on those used in previous analyses, which were also found to be satisfactory in this application. Further details of analysis parameters and a summary of the results is provided in Table 1-6, Appendix A.

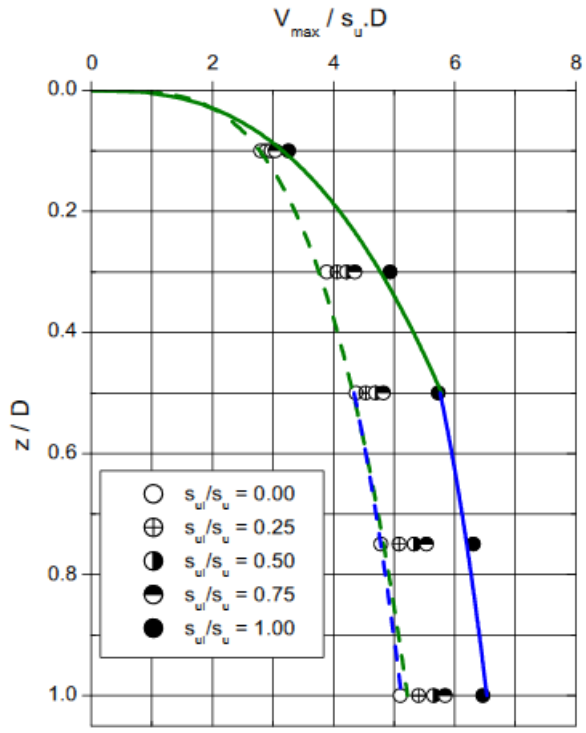

Figure 4.18 *- Peak resistance to vertical loading (V_{max}) against embedment depth in dimensionless form. For comparison purposes the correlations for a rough and smooth interface conditions included from Section 4.2.2.*

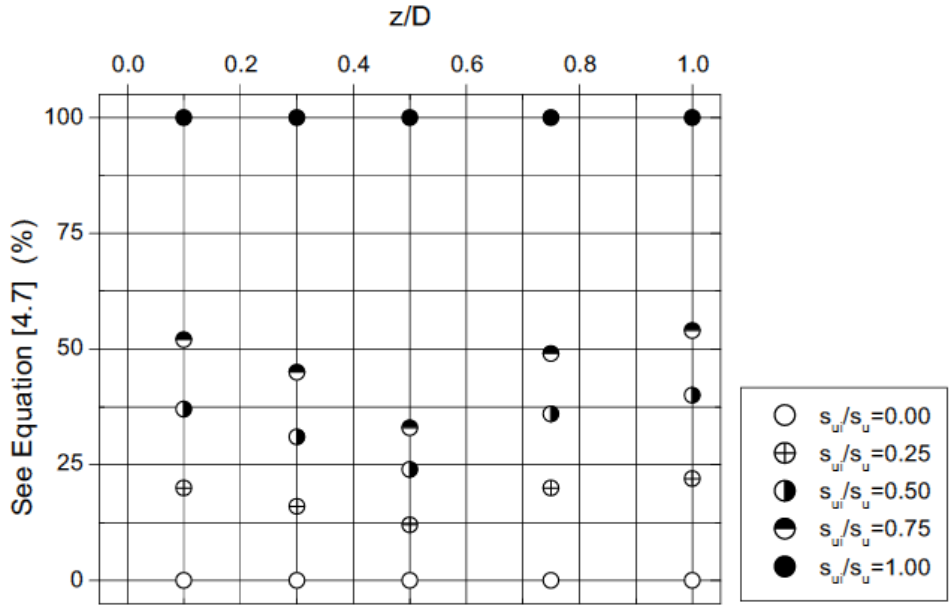

Figure 4.19 *- Analysis of the effect of interface effects presented as a percentage of the difference in V_{max} between the bounding conditions of a smooth and rough interface.*

Due to minor changes in the analysis configuration checks were undertaken between the results for a rough and smooth interface condition analysed in this area of study and the results previously provided in Section 4.2.1 and 4.2.2. As can be seen from Appendix A Table 1-6, and a comparison with Tables 1-1 to 1-4, the smooth interface analysis was found to be within 1% of previous analysis and the rough interface analysis within 2%, This was considered acceptable. Results for all the interface conditions analysed were plotted against depth as shown in Figure 4.18. For comparison purposes the correlations provided in Section 4.2.2 are included.

For all embedment depths Figure 4.18 shows an increase in resistance to penetration under vertical load when there is an increase in interface strength i.e. higher values s_{ui}/s_u ratio. This is as can be expected from previous results, and is consistent with a progression in resistance from a smooth interface condition to the higher resistance for a rough interface. It can however be noted that although a increase in s_{ui}/s_u leads to an increase in V_{max}, this increase does not appear to be proportional to the increase in interface strength. In other words a 50% increase in the interface strength, the halfway point between a rough and smooth interface, does not appear to produce a resistance exactly half way between the values obtained for the rough and smooth cases. There also appears to some changes in the degree of proportionality across the embedment depth range considered. There are difficulties in identifying trends in the data presented in Figure 4.18, primarily due to the relative closeness in the resistances obtained for a variation in interface condition, especially at shallow embedment. Figure 4.19 presents the data in an alternative format to assist in interpretation.

[4.6] $$\frac{V_{max} - V_{\max\_smooth}}{V_{\max\_rough} - V_{\max\_smooth}} \times 100$$

Figure 4.19 presents V_{max} for a given interface condition in terms of Equation [4.6]. This expresses V_{max} relative to the vales of V_{max} for a smooth and rough interface condition, expressed as a percentage. Within this framework a smooth interface is 0% and a rough interface is 100%. An interface of s_{ui}/s_u =0.5 could be analysed and might produce a value of 50%, if resistance was proportional to interface conditions, alternatively if s_{ui}/s_u =0.5 produced a different value this

could be easily identified as could the relationships for other s_{ui}/s_u ratio and any changes with embedment depth.

Data is plotted for the interface conditions and embedment depths previously presented in Figure 4.18. The trends noted in Figure 4.18 can be seen clearly in this format. Additionally, not only is resistance not directly proportional to the s_{ui}/s_u ratio, e.g. s_{ui}/s_u =0.50 does not equal 50 %, this relationship also changes with depth. From 0.1D to 0.5D the influence on resistance of the s_{ui}/s_u ratios 0.25, 0.50 and 0.75 decreases in a broadly linear trend. Deeper than 0.5D there is a counter trend, were the influence on resistance increases.

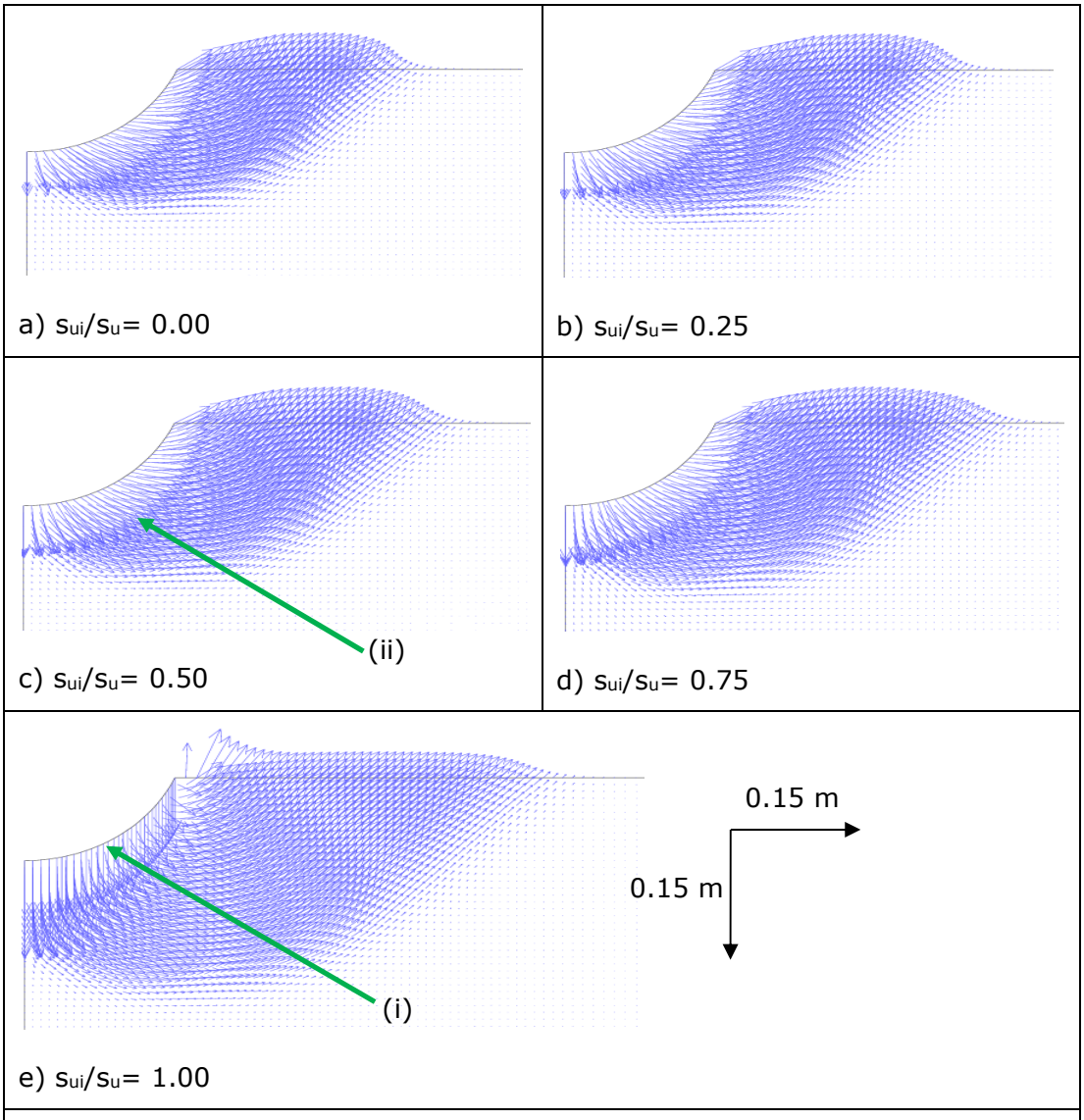

Fig 4.20 a,b,c,d,e *- Example of the effect of interface conditions on vector plots for a 0.3 m diameter pipeline under vertical loading at an embedment depth of 0.3D. Interface conditions s_{ui}/s_u = 0.00, 0.25, 0.50, 0.75, 1.00.*

To provide additional information on the trends noted in V_{max} with changes in interface properties it is beneficial to investigate the associated failure mechanisms as show in the calculated displacement fields at V_{max}. This displacement has been presented as a vector plot and is shown in Figure 4.20.

Figure 4.20 provides example vector plots for a pipeline embedment of 0.3D and s_{ui}/s_u = 0.00, 0.25, 0.50, 0.75, 1.00. For the case of a smooth and a rough interface (s_{ui}/s_u =0 and s_{ui}/s_u =1) it can be seen that the failure mechanism generated from vertical loading is the same as previously shown in earlier sections. Variation in mechanism can be noted as the interface strength increases or decreases. These changes are relatively subtle at lower s_{ui}/s_u ratio, with the most obvious variation being between s_{ui}/s_u = 0.75 and s_{ui}/s_u = 1.00. This is consistent with the analysis results and the values for V_{max} presented in Figures 4.18 and 4.19. The more marked difference between s_{ui}/s_u = 0.75 and s_{ui}/s_u = 1.00 plots is associated with the most significant change in V_{max} with these vector plot also showing the biggest variation in mechanism. The minor changes in V_{max} for lower s_{ui}/s_u ratio are associated with minor variation in the mechanism.

From Figure 4.20 some observations can also be made with respect to the displacement of the soil directly adjacent to the pipe-soil interface. The rough interface acts as a substantial constraint with the soil immediately adjacent to the pipeline displaced in the same direction as the pipeline i.e. vertically (see area marked as (i)). For all other interface conditions the interface does not fully constrain the soil adjacent to the interface, which instead displaces at an angle approximately perpendicular to the interface (see area marked as (ii)). This implies that for all the cases considered, except the fully rough interface, the shear forces exceed the strength of the interface, allowing the soil directly adjacent to the interface to slide relative to it and adopt a more efficient displacement vector.

Perhaps the most important observation from the analysis reported in this section is that the effect of interface strength variation is not proportional to the interface strength, as described by the s_{ui}/s_u ratio, and that this effect varies with depth. The interface conditions act as a kinematic constraint to the failure mechanism associated with vertical loading of a pipeline, which can be used to explain the associated change in resistance to vertical loading. The vector plots of soil displacement provide some insight into the nature of this constraint which, with the exception of the rough interface, does not fully constrain the soil

adjacent to the interface. Instead shear displacement occurs at this interface. Where the interface has strength this shearing will be associated with plastic work as well as influencing the geometry of the failure mechanism within the soil. Both these factors contribute to changes on the resistance to vertical loading, as well as providing an explanation on why this effect should vary with depth.

It can be seen from a review of the previous displacement vector plots (see Figure 4.4 in Section 4.2.1, and Figure 4.8 in Section 4.2.2) that the influence of the interface as a kinematic constraint will vary with embedment depth. This is both due to surface area of the interface in contact with the soil and the geometry of the problem, in particular the geometry of the soil failure mechanism at V_{max}. For example if the interface represents a relative large contact area for a small failure mechanism in the soil, e.g. 0.1D, the effect of interface strength would be greater. An alternative example is a pipeline at an embedment of 0.5D, where the failure mechanism is relatively large and distant from the interface. This is consistent with the trend noted in Figure 4.19, where by the influence of the interface properties reduces across the depth range 0.1D to 0.5D.

In reviewing the counter trend in the influence of the interface properties over the depth range 0.5D to 1.0D, see Figure 4.19, it has already been noted in Section 4.2.2 that beyond 0.5D there is a marked change in behaviour under vertical load. The increase in V_{max} for a given increase in embedment reduces and the failure mechanism develops steeper sides. There is also a reduction in the variation in failure mechanism size and geometry with increasing embedment. The contact area of the pipe-soil interface becomes constant from 0.5D within the idealisation of a vertical sided trench with no collapse. Therefore the contribution from plastic work at the interface is not expected to change with deeper embedment and is therefore not expected to be the primary factor producing this trend noted in Figure 4.19.

A link between the effect of interface properties, the overall failure mechanism and the associated capacity is credible and can explain the trend after 0.5D, the point at which the maximum pipe-soil contact area is reached. The increase in capacity with depth beyond 0.5D has already been noted, including the change in the trend of capacity from shallower depths. This larger capacity is associated with a larger mechanism, which the interface properties influence by increasing the relative size of the mechanism even though the contact area remains

constant. The influence of the interface strength is expected to trend towards a steady value as embedment increases beyond 1.0D. At deeper embedment a trend towards a depth independent influence of interface properties can also be expected.

4.5 The Effect of Soil Unit Weight

Previous sections of this chapter have reported analysis cases where the seabed soil is considered as weightless. This approach to the calculations simplified the analysis process as well as allowing the soil shear strength component of resistance to be presented separately from other components of resistance, such as unit weight. Following analysis for weightless soil the effect of soil unit weight was investigated to an embedment depth of 1.0D within a small strain analysis framework. The results of this investigation are reported here.

A pipeline of 0.3 m diameter (D) was wished in place at an embedment depth of 0.1D, 0.3D, 0.5D, 0.75D, and 1.0D. A vertical sided trench was used for an embedment depth deeper than 0.5D. A homogenous undrained shear strength was used with the shear strength adjusted to ensure a low $s_u/\gamma'.D$ ratio. A low $s_u/\gamma'.D$ ratio helped to increase the magnitude of the soil unit weight effect improving the accuracy of the calculations. Soil shear strength was typically 1.5 kPa, although this was adjusted to 5 kPa for 1.0D embedment. As in previous analysis elastic properties were governed by a Young's modulus (E) of $E = s_u \times 200$ and a Poisson's ratio (υ) of 0.49. As these analyses consider a pipeline in a subsea setting, i.e. submerged in sea water, effective unit weight (γ') was applicable to this problem. A γ' of 10 kN/m^3 was used in all analysis by assigning an appropriate submerged soil density (ρ_S) and applying vertical gravity forces of 9.81 m/s^2 in analysis. Analysis results were adjusted to provide equivalence to a full pipeline cross section i.e. multiplied by two. Reporting of results was in dimensionless format e.g. $V_{max}/s_u.D$.

Mesh refinement requirements and displacement velocity was based on the results of previous analyses within this study, as described in earlier sections. However, minor changes were required to the mesh geometry and the calculation sequence to allow for the application of gravity forces to the model prior to vertical displacement of the pipeline. To ensure the effects of these changes were negligible a weightless soil analysis and a soil with weight analysis was undertaken for each embedment depth. The weightless soil analysis could then be compared to the results presented in previous sections. Following

problem familiarisation a total of 10 analyses were undertaken, all with smooth interface conditions. Further details of these analysis parameters and a summary of the analysis results are provided in Table 1-5, Appendix A.

In addition to the use of numerical analysis to investigate the effect of soil unit weight, there is also an analytical solution for a small strain analysis framework and at embedment depth of <0.5D, as noted by Merifield et al. (2009). This solution is based on calculating the volume of soil (V_s) that is replaced by the pipeline due to its embedment, see example illustrated in Figure 4.21, and multiplying this volume by γ'. This is analogous to Archimedes principle. Merifield et al. (2009) provided an approach where a dimensionless group, a soil weight bearing capacity term (N_{swV}), is calculated directly. This is reproduced in Equation [4.7]. However, it is also beneficial be able to calculate the volume of soil replaced by the wished in place pipeline. Equation [4.10] can then be used to calculate N_{swV} from the soil volume.

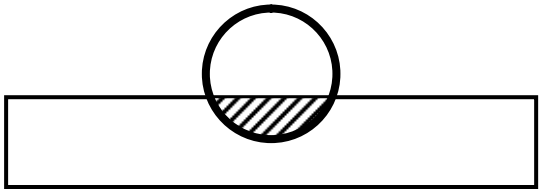

Figure 4.21 *- Illustration of the replaced volume of soil (shaded area) in a small strain and plane strain analysis framework.*

[4.7] $$N_{swV} = \frac{1}{4\widehat{w}} \left[sin^{-1}\left(\sqrt{4\widehat{w}\,(1-\widehat{w})}\right) - 2(1-2\widehat{w})\sqrt{\widehat{w}(1-\widehat{w})} \right]$$

[4.8] $$V_S = \frac{D^2}{8}\,(\Gamma_r - \sin(\Gamma))1m$$

[4.9] $$\Gamma = acos\left(1 - \frac{2z}{D}\right)2$$

[4.10] $$N_{swV} = \frac{V_S.\gamma'}{(D.z.\gamma')}$$

Where;

N_{swV} = Soil unit weight vertical bearing capacity term
$\hat{w}$ = z/D
z = Pipeline embedment depth
D = Pipeline diameter
V_S = Volume of soil replaced for a given pipeline embedment
Γ_r = angle of sector of a circle in radians
Γ = angle of sector of a circle in degrees
m = metre, the equation is multiplied by 1m to give a volume
γ' = Effective soil unit weight i.e. submerged unit weight

Geometrically Equation [4.8] is the calculation for the area of a segment of a circle, which is then used to produce a volume for a one metre length of pipeline. This segment is based on the sector of a circle where the radius is equivalent to that of the pipeline and the arc length is equivalent to the soil-pipeline contact area, for a given embedment. Solutions to this geometry problem are widely presented e.g. Gieck and Gieck (1997). Equation [4.9] is used in conjunction with Equation [4.8] to calculate the angle of the segment of the circle for a given embedment depth.

As noted soil unit weight effects for a pipeline embedment >0.5D have not been considered by previous researchers e.g. Merifield et al. (2009). As part of this study analytical solutions have been postulated for a deeper embedment then 0.5D, which can then be compared to the numerical analysis results. Two analytical solutions are proposed, see Figure 4.22. The basic solution (black and white shading) is similar to the solution for an embedment <0.5D. A rectangular soil volume is allowed for above the pipeline shoulder when an embedment of >0.5D occurs. This is described in Equation [4.11]. The extended solution includes for an additional soil volume (shaded in green) consisting of triangular zones extending from the pipeline shoulder into the adjacent soil mass. The angle of these triangular zones (δ) can be varied to fit the numerical analysis data, if required. This additional soil volume can be calculated using Equation [4.12]. Equation [4.13] provides a method to calculate N_{swV} from this analytical solution.

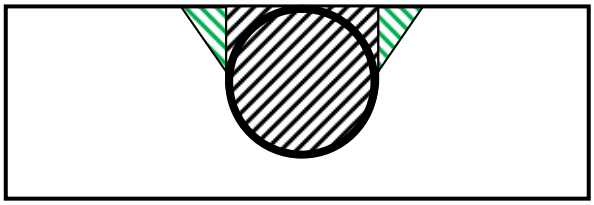

Figure 4.22 *- Illustration of a basic (black and white shaded) and extended analytical (green shaded) solution of N_{SW} for an embedment of >0.5D.*

[4.11] $$V_S = \frac{\pi D^2}{8} + [D(z - 0.5D)].1m$$

[4.12] $$V_{S\_add} = (z - 0.5D).[(z - 0.5D).\tan(\delta_{SW})].1m$$

[4.13] $$N_{swV} = \frac{V_{S\_tot}.\gamma'}{(D.z.\gamma')}$$

Where;

V_S = Volume of soil replaced for a given pipeline embedment
V_{S_add} = Additional soil volume of soil from extended solution
V_{S_tot} = Total soil volume of soil i.e. sum of Equation [4.11] and [4.12]
π = Pi
D = Pipeline diameter
m = metre, the equation is multiplied by 1m to give a volume
z = Pipeline embedment depth
δ_{SW} = Angle of triangle for extended solution
γ' = Effective soil unit weight e.g. submerged unit weight
N_{swV} = Soil unit weight vertical bearing capacity term

Comparison between the weightless analysis undertaken in this section and the analysis reported in previous sections indicated only negligible effects due to changes in the analysis configuration, with a difference of <0.05%. The analyses where soil unit weight was included for in calculations showed an appreciable increase in soil resistance over the weightless soil case. Unit weight effects increased with embedment depth, as predicted by the analytical solutions. The magnitude of the increase due to soil unit weight is specific to the analysis

parameters adopted, however greater insight can be gained by expressing this in terms of a range of dimensionless groups.

The increase in resistance attributable to soil unit weight can be expressed as a dimensionless group $R_{sw}/(D.z.\gamma')$, where R_{sw} is the resistance due to soil weight, D is the pipeline diameter, z is the pipeline embedment and γ' is the effective soil unit weight. This provides a useful format for comparison between numerical analysis and analytical solutions, as well as comparison with the work of pervious researchers. The dimensionless group $R_{sw}/(D.z.\gamma')$ is also analogous to N_{swV}, a soil unit weight bearing capacity term for vertical loaded pipelines. N_{swV} can be used in a generalised bearing capacity calculation alongside a soil shear strength bearing capacity term i.e. N_{cV}.

The results of the numerical analysis into soil unit weight effects undertaken as part of this study are presented in Figure 4.23. Depth of embedment is also represented in dimensionless form, in terms z/D, where z is the depth of pipeline embedment and D is the pipeline diameter.

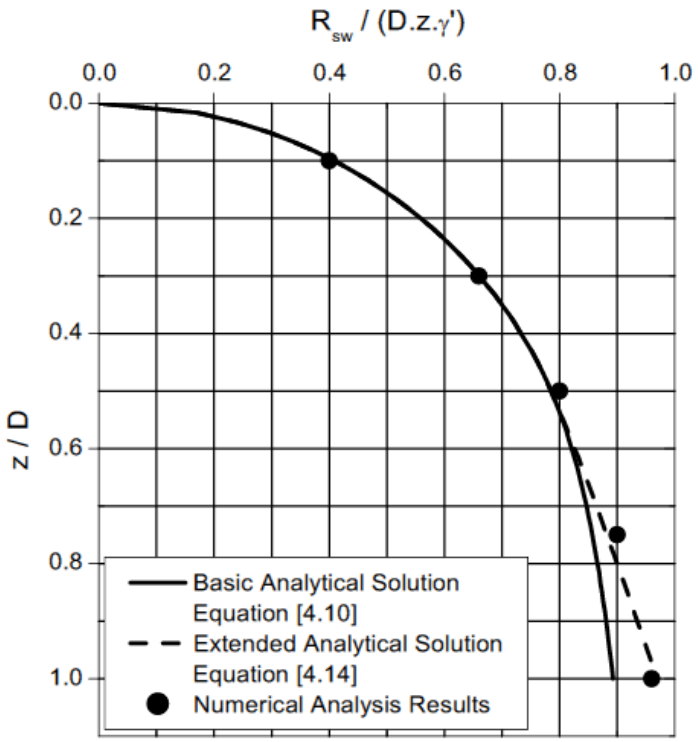

Figure 4.23 *- Numerical analysis results showing the effect of soil unit weight on pipeline resistance to penetration under vertical loading. A basic and extended analytical solution are provided for comparison purposes.*

In Figure 4.23 it can be seen that there is good agreement between the numerical analysis results and the basic analytical solution down to a pipeline embedment depth of 0.5D, as previously noted by Merifield et al. (2009) in their study. Deeper than 0.5D, e.g. 0.75D and 1D, the basic analytical solution does not fit the data as well as at shallower depth. There also appears to be a trend that the basic solution will be less suitable as embedment depth increases. Within this context the extended solution was fitted to the numerical analysis, with an angle (δ) of 17° providing a good fit to the numerical analysis data. This extended analytical solution can be used as a method for deriving N_{swV}. This fit is valid to 1.0D. However, given the nature of this relationship there may be changes to this angle beyond this depth. An additional interesting observation can be made by reviewing the pipe trench wall angle in the soil displacement plots previously provided for large strain analysis e.g. Figure 4.16 and Figure 4.17. Given the difference between analysis methodologies and the analysis basis a detailed comparison is unlikely to be directly relevant. However, it can be noted that the trench wall adopts a sub-vertical slope and that angle of this slope is similar to δ, albeit slightly less.

The influence of soil unit weight on a pipeline subjected to vertical loading, both in absolute terms and relative to the soil shear strength component, depends on a number of factors. For example, soil unit weight, soil shear strength and pipeline diameter. The influence also changes with embedment depth as the penetration into the seabed soil by the pipeline increases.

Given the range of variables that influence the soil unit weight component of resistance for a vertically loaded pipeline a range of dimensionless groups are needed to present a generalised illustration of this effect. Total resistance to penetration under vertical loading can be presented in terms of $V_{max}/s_u.D$, as previously used, where V_{max} is the maximum capacity under vertical loading, s_u is soil shear strength and D is pipeline diameter. Increasing influence of soil unit weight will raise $V_{max}/s_u.D$ relative to a weightless soil analysis. Embedment depth can be presented in terms of z/D, where z is the pipeline embedment and D the pipeline diameter. The effect of soil unit weight will vary in terms of another dimensionless group $s_u/\gamma'.D$, which includes soil effective unit weight (γ') in addition to the shear strength and diameter terms. As $V_{max}/s_u.D$ varies with interface condition the effect of unit weight can be illustrated both smooth and rough interface condition, although the absolute effect of unit weight is not affected by interface conditions, only the relative effect. Using the relationships

and correlations presented early in this section see Figure 4.24 for the smooth interface condition and Figure 4.25 for the rough interface.

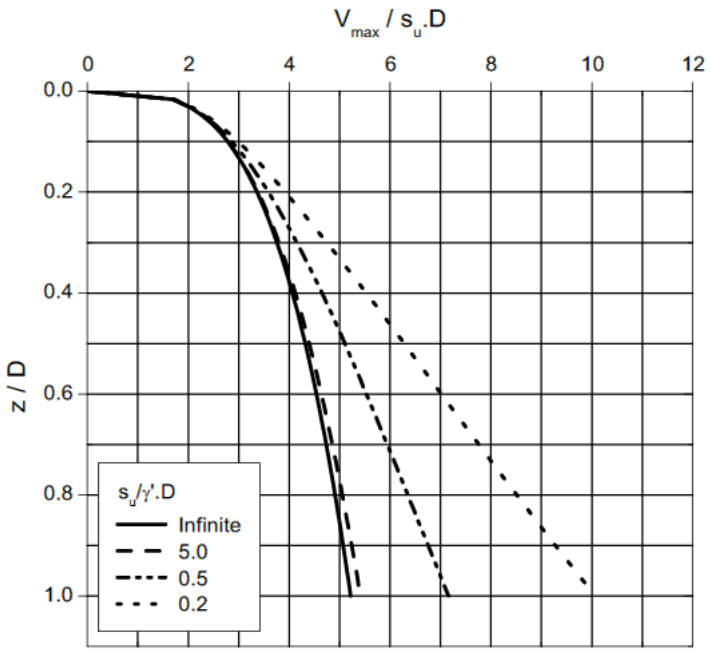

Figure 4.24 *- The influence of effective soil unit weight on resistance to vertical loading by embedment depth, smooth interface conditions.*

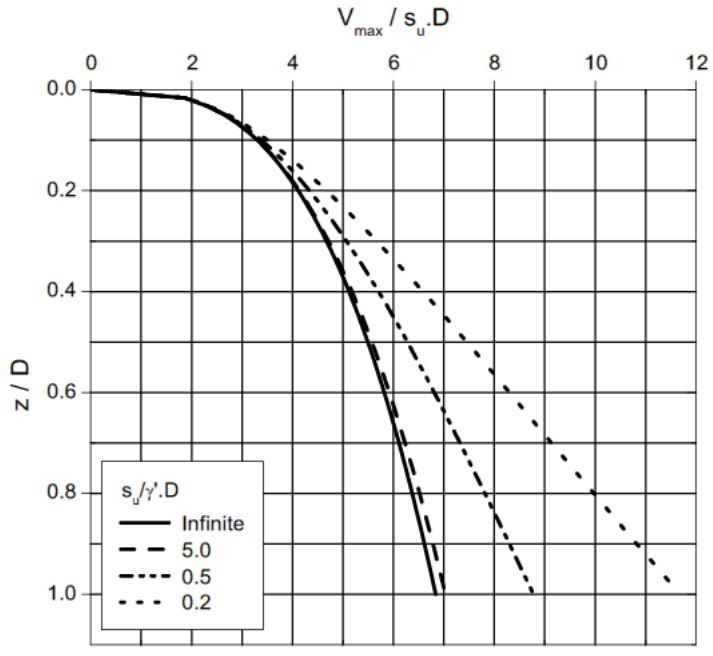

Figure 4.25 *- The influence of effective soil unit weight on resistance to vertical loading by embedment depth, rough interface conditions.*

An infinite $s_u/\gamma'.D$ is equivalent to the weightless soil case. A large value of $s_u/\gamma'.D$ is when the effect of soil unit weight is limited, for example a small diameter pipeline on a higher shear strength clay seabed. For low values of $s_u/\gamma'.D$ the effect of soil unit weight is the most significant especially at deeper embedment. An example would be a lower shear strength seabed, where the shear strength component is smaller, and a larger diameter pipeline at a deeper pipeline embedment, where a larger amount of soil has been replaced. Heavier soil also lowers $s_u/\gamma'.D$, where unsurprisingly a heavier soil increases the influence of the unit weight effect.

From Figure 4.24 and 4.25 it can be seen that at a $s_u/\gamma'.D= 5$ the effect of soil unit weight is limited. For this case soil unit weight leads to an increase in resistance of less than 4%, <3% for a rough interface, even at a depth of 1.0D. At shallow embedment the effect is even less at a <1.5% increase at an embedment of <0.4D.

The effect of soil unit weight at lower $s_u/\gamma'.D$ ratios is more discernible in Figure 4.24 and 4.25, e.g. $s_u/\gamma'.D= 0.5$ and $s_u/\gamma'.D= 0.2$. However, is strongly dependent on embedment depth. For example at depth of <0.2D the increase due to soil unit weight is <10% for both interface conditions and both $s_u/\gamma'.D$ ratio. As depth increases the influence of soil unit weight becomes more important, in terms of the increase in resistance. For example up to a 23 % increase in resistance at 0.5D for a smooth interface with $s_u/\gamma'.D= 0.2$. Rising further to an increase of 41% for the extreme case of a smooth interface at $s_u/\gamma'.D= 0.2$ and 1.0D.

For a summary of the effects of unit weight on a pipeline subjected to vertical loading, along with further discussion within the context of other factors effecting a vertically loading pipeline, see Section 4.7.

4.6 The Effect of a Variation in Shear Strength

4.6.1 Analysis Results - Linear Increasing Shear Strength Gradient

A uniform undrained shear strength, as used for previous analyses in this chapter, can be a reasonable representation of seabed soils. However, there may be cases when a more complex model of shear strength distribution will be more appropriate. Based on the methodology described in Chapter 3 a series of analyses were undertaken to investigate the influence of a linear increasing shear strength gradient on a pipeline subjected to vertical loading. A small strain

analysis methodology was adopted. The results reported here have also been reported in (Morrow and Bransby, 2010).

A total of 70 analyses were undertaken, 35 for a smooth interface condition and 35 for a rough interface condition. Analysis was undertaken for 7 embedment depths 0.1D, 0.2D, 0.3D, 0.4D, 0.5D, 0.75D, and 1D. The frame work used in this study for describing shear strength gradient is based on the ratio of undrained shear strength of the seabed soils at mudline (s_{u0}) and the shear strength of the soil at the base of pipeline (s_{uzp}) i.e. the pipeline embedment depth. For example a pipeline embedded in a soil with a linear increasing shear strength gradient which results in a shear strength of 5 kPa at the pipeline embedment depth and 2.5 kPa at mudline can be described by the a ratio s_{u0}/s_{uzp} = 0.5. Further discussion of this method of describing shear strength including illustrations is provided in Section 3.2.1. At each pipeline embedment depth 5 shear strength distributions were considered including a uniform distribution, s_{u0}/s_{uzp} = 0, 0.25, 0.50, 0.75, 1.00.

Mesh refinement requirements were based on previous convergence studies, e.g. Section 4.2. Displacement velocity was initially based on previous analysis however during problem familiarisation it was found that for the lower s_{u0}/s_{uzp} ratio a minor reduction in velocity was beneficial in increasing numerical stability and associated data quality. For example for a rough interface at 0.2D embedment vertical displacement (v) was reduced from v = 5E-7 m/s to v = 2.5E-7 m/s. This effect can be attributed to the influence of very low near surface strength and the steep strength gradients on the ability of the damping algorithm within FLAC to remove unbalanced inertial forces within the calculation process. Once an appropriate velocity was determined for the lower s_{u0}/s_{uzp} ratio it was then simpler to use this velocity for all s_{u0}/s_{uzp} ratio, with exception of the constant strength case. Although some analysis could have been progressed with the faster displacement velocities the benefit in data quality were considered to outweigh the minor inconvenience of longer analysis times. Further details of analysis parameters and a summary of the analysis results is provided in Appendix A, Tables 1-7 and 1-8.

A uniform shear strength case was first analysed as part of this analysis suite in order to confirm that minor changes in analysis configuration had not had an unwanted influence or detrimental effect on data quality. Comparisons were made between this analysis and that detailed in Section 4.2.1 and 4.2.2. As can be seen from Table 1-7, for the smooth interface conditions analyses were within

<1% of the previous analyses. For the rough interface conditions analyses reported in this section was within < 3% (see Table 1-8). For both interface conditions this were considered acceptable.

With the smooth interface condition results for a range of shear strength gradients, as described by a s_{u0}/s_{uzp} ratio, were plotted against embedment depth, see Figure 4.26. For comparison purposes correlations previously detailed in Section 4.2.1 and 4.2.2 are also included. A readily identifiable trend can be seen in this data. At shallower depths, approximately less than 0.2D, the presence of a shear strength gradient results in an increase in resistance to vertical load. There is a transitional behaviour around 0.3D to 0.4D, where the steeper shear strength gradients, lower s_{u0}/s_{uzp}, and a lower shear strength at mudline (s_{u0}), results in a slight reduction in resistance compared to the constant strength case. With increasing depth, beyond 0.3D to 0.4D, the presence of any shear strength gradient results in a reduction in resistance compared to the uniform shear strength case. This trend extends to the limit of the analysis considered in this study, 1.0D.

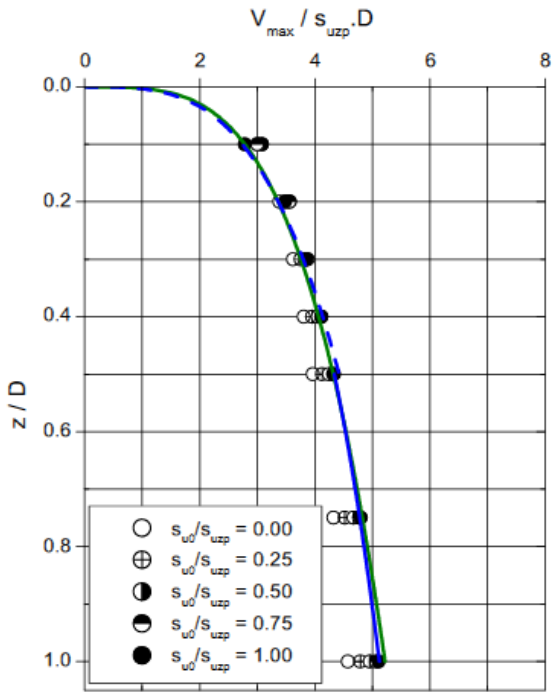

Figure 4.26 *- The effect of shear strength gradient on peak resistance to vertical loading (V_{max}), smooth interface conditions. For comparison purposes the correlations from Section 4.2.1 and 4.2.2 are included.*

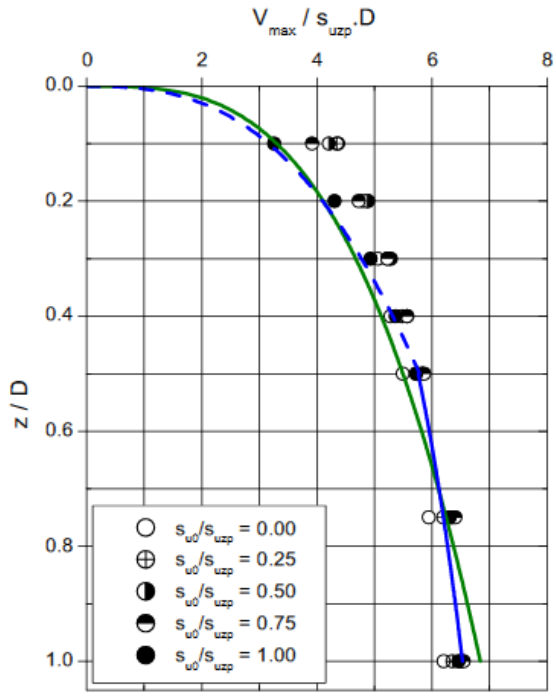

Figure 4.27 *- The effect of shear strength gradient on peak resistance to vertical loading (V_{max}), rough interface conditions. For comparison purposes the correlations from Section 4.2.1 and 4.2.2 are included.*

As with the smooth interface condition the results were also plotted for the rough interface, see Figure 4.27. Again the influence of a shear strength gradient can be seen, with a more marked effect then for a smooth interface. A similar depth related trend can also be noted, albeit over a different depth range. At shallow depth the presence of any shear strength gradient results in an increase in resistance. This effect is most pronounced at the shallowest depth considered, i.e. 0.1D, and with increasing depth this effect becomes less marked. A transitional behaviour can be observed around 0.75d and 1.0D, where lower s_{u0}/s_{uzp} ratio result in a slight decrease in resistance compared to the uniform s_u case. The trend where by all shear strength gradients result in a decrease in resistance, as seen for the smooth interface condition, is also expected to occur for a rough interface. However, this would occur at depth greater than 1.0D and beyond the depth range analysed in this study. For both interface conditions it is expected that the effect of a shear strength gradient will trend towards a constant value, related to the effect on a deep flow around mechanism. This can be expected to be at embedment depths deeper than considered in this study.

The displacement vector plots at V_{max} can also be reviewed. For some cases the effect of a shear strength gradient on the geometry of the failure mechanism is particularly marked, for example see Figure 4.28 and 4.29. In Figure 4.28 the rapid increase in shear strength below the pipeline embedment depth for $s_{u0}/s_{uzp}=0$ results in a smaller and shallower mechanism, compared to the uniform s_u case. However, even though the mechanism is smaller, as can be noted from Figure 4.26, it also produces a higher value of V_{max} with higher shear strength soil below the pipeline embedment depth mobilised within the mechanism. Figure 4.29 shows a similar effect. However, in this case the presence of a rough interface has led to this effect occurring at a deeper embedment in association with larger failure mechanisms.

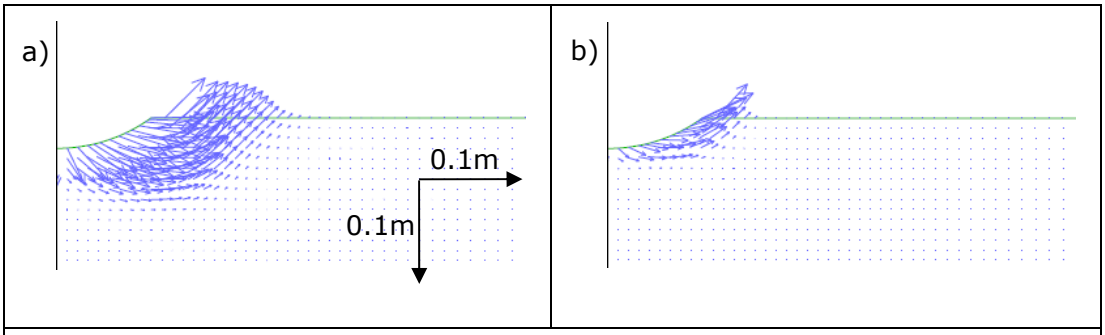

Figure 4.28 a,b *- A pipeline at an embedment depth of z=0.1D and a smooth interface condition. a) Uniform shear strength b) $s_{u0}/s_{uzp}=0$.*

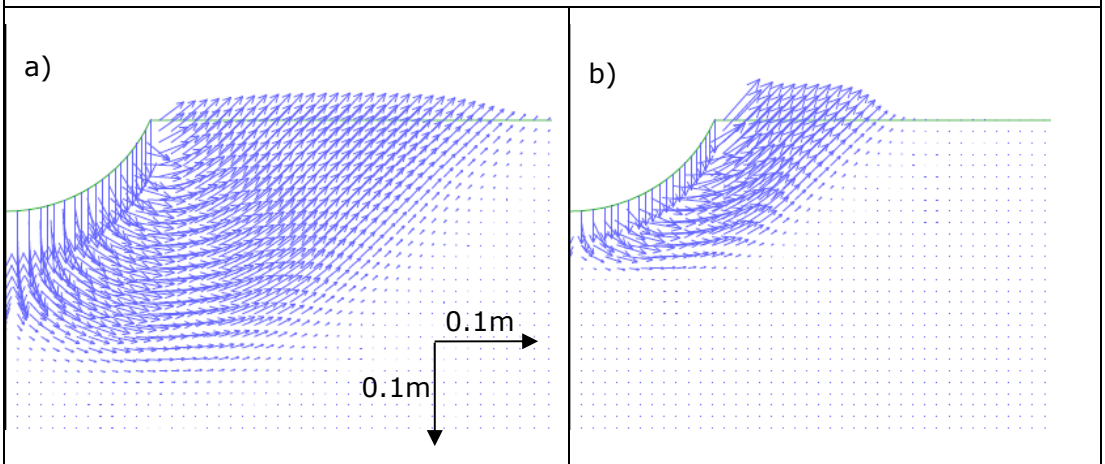

Figure 4.29 a,b *- A pipeline at an embedment depth of z=0.3D and a rough interface condition. a) Uniform shear strength b) $s_{u0}/s_{uzp}=0$.*

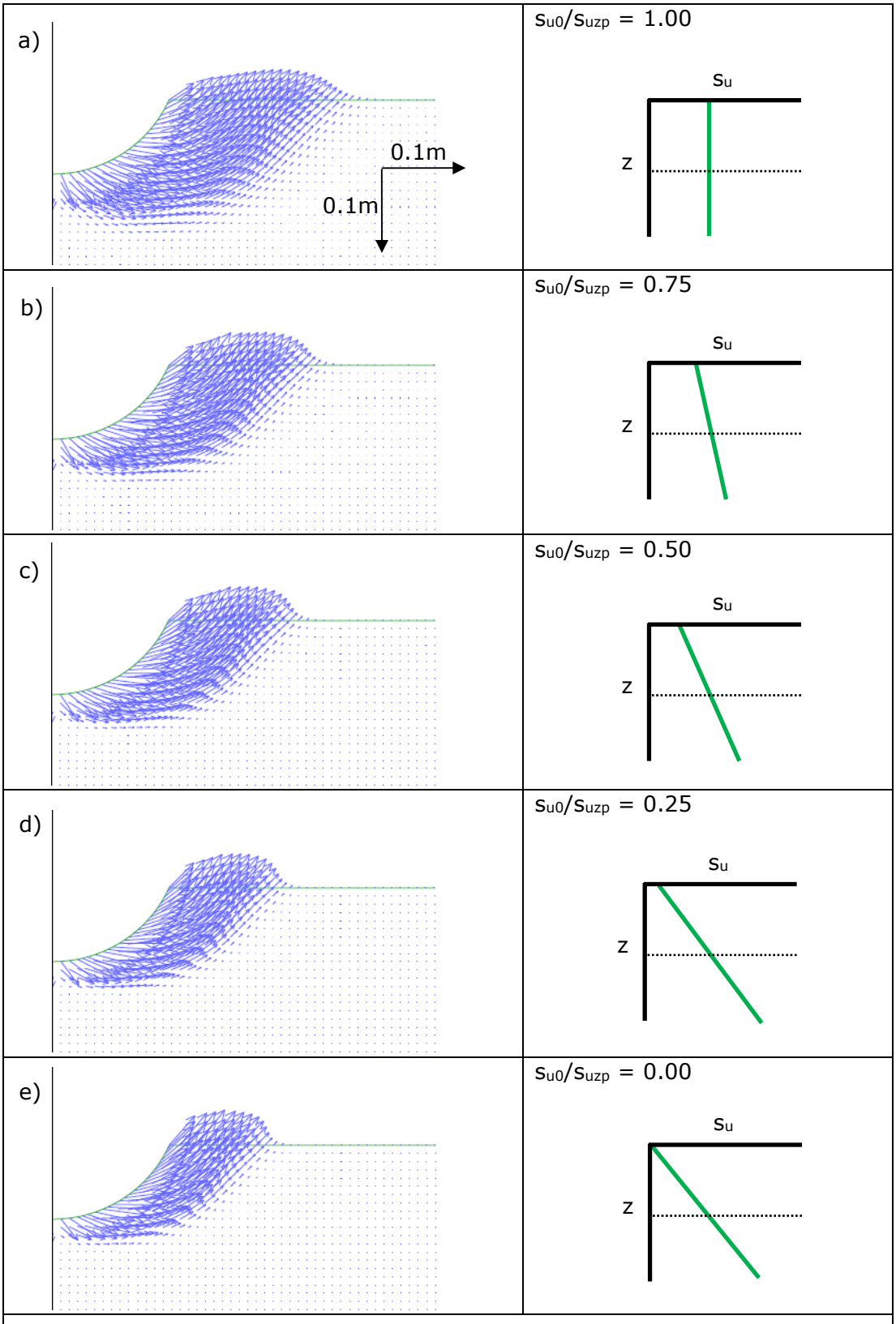

Figure 4.30 a,b,c,d,e *- Example displacement vector plots for an embedment depth of z = 0.3D and a smooth interface condition.*

Figure 4.30 shows example displacement vector plots for the full range of shear strength gradients at a pipeline embedment of 0.3D. For these cases the changes in mechanism are less dramatic than noted previously in Figures 4.28 and 4.29. Figure 4.30 also presents a graphical aid to help visualise that in addition to the change in mechanism a change in shear strength gradient also effects the strength of the soil sheared by this mechanism.

In Figure 4.26 and 4.27 there are some difficulties in identifying the detail of the trends in data beyond those noted, it is therefore beneficial to re-plot this data in an alternative format, see Figure 4.31 for a smooth interface and Figure 4.32 for the rough interface. In this format V_{max}, for a given embedment depth and shear strength gradient, is expressed as a ratio of V_{max} for the uniform shear strength case. Note, as can be seen from Table 1-7, Appendix A, in some instances (e.g. at 0.1D) some shear strength gradients produce near identical values of V_{max} and hence only one point may be visible in the plot.

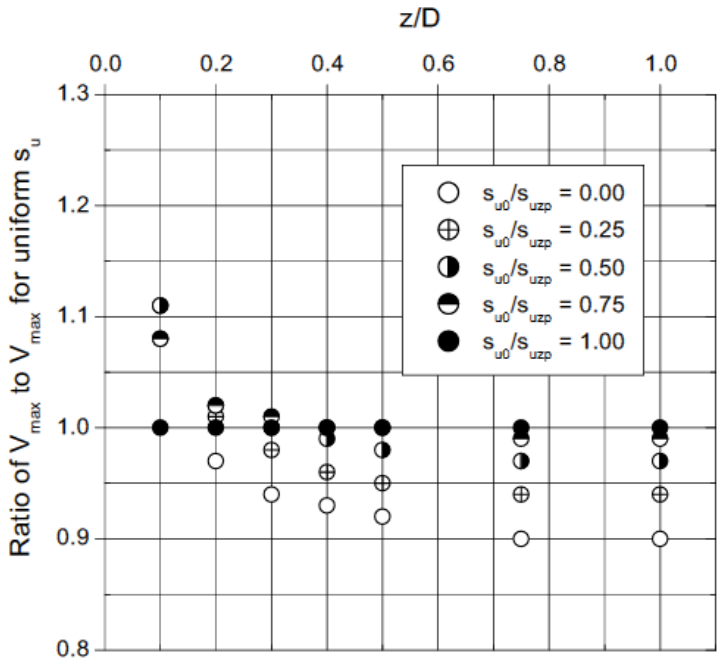

Figure 4.31 *- V_{max} for a given shear strength gradient expressed as a proportion of V_{max} for the uniform strength case. Smooth interface.*

For the smooth interface conditions it has already been noted that at shallow depth (~0.1D) all shear strength gradients lead to an increase in V_{max}, followed by a transitional behaviour at ~0.2D, and then trending towards a decrease in resistance at a depth of 0.3D to 0.4D and greater. In Figure 4.31 it can be seen

that from 0.4D the relative resistance decreases in the order of s_{u0}/s_{uzp} ratio with the constant s_u case having the greatest resistance s_{u0}/s_{uzp} = 0 the lowest. In the shallow part of this depth range it should be noted that the s_{u0}/s_{uzp}=0.75 values are very close to the constant shear strength case and the data point cannot always be seen as a separate point. These trends suggest that at a depth of 0.3D to 0.4D, and greater, the behaviour of a pipeline with a smooth interface is strongly influenced by the shear strength of the soil above the pipeline embedment depth, soil that will be weaker with the steeper shear strength gradients. At a shallower depth, ~0.1D, the alternative behaviour can be explained by this being dominated by the strength of the soil below the pipeline embedment depth. The transitional behaviour is also consistent with this interpretation. At 0.2D the failure mechanism is generally governed by the shear strength of the soil below the embedment depth, as is the case for the shallower depths. However, in this transition a very low shear strength above the pipeline embedment depth, e.g. as for s_{u0}/s_{uzp}=0, can influence the problem, reducing V_{max} to less than the uniform strength case.

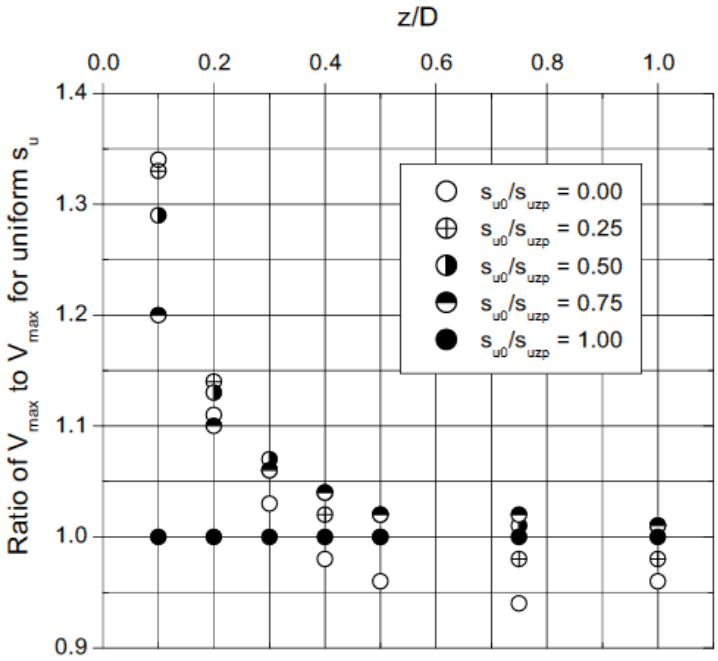

Figure 4.32 *- V_{max} for a given shear strength gradient expressed as a proportion of V_{max} for the uniform strength case. Rough interface.*

An interpretation of the analysis results for the rough interface condition could initially appear more difficult than the smooth interface condition. However,

when considered within the same framework used for the smooth interface condition, interpretation of the observed behaviour can be readily explained.

The smooth interface conditions shows the full range of behaviour from the influence of soils below the pipeline embedment depth at shallow embedment, to a transitional behaviour, through to behaviour influenced by the soils above embedment depth. It has already been seen from the results reported earlier in this chapter (e.g. Sections 4.2.1 and 4.2.2) that rough interface failure mechanism influences a larger body of soil. This observation in conjunction with the interpretation used for the smooth interface can be used to explain the behaviour of a pipe with rough interface in the presence of a linear increasing shear strength gradient.

The rough interface conditions exhibits the shallow behaviour for much of the depth range analysed. At pipeline embedment depths less than 0.4D the behaviour is governed by soils deeper than the pipeline embedment depth. From around 0.4D the transitional behaviour governs, where the behaviour is either governed by the soil below or above pipeline embedment depth depending on the steepness of the shear strength gradient. The steeper shear strength gradients results in behaviour being governed by soil above the pipe embedment depth. For the rough interface the transitional behaviour occurs at a deeper embedment and extends over a larger range of embedment depths. The deep behaviour, where all shear strength gradients are influenced by soil above pipeline embedment depth, does not occur with the depth range considered in this study, but it can be expected to occur at a depth greater than 1.0D.

As previously undertaken for the uniform shear strength case the analyses results presented in this section can be used to provide equations that describe the influence of shear strength gradient on a pipeline subjected to vertical loading. Equation [4.1] was previously fitted to results. This equation can be formulated in terms of the shear strength at the pipeline embedment depth (s_{uzp}), as show in Equations [4.14] and [4.15]

[4.14] $$V_{max} = a \left(\frac{z}{D}\right)^{b} s_{uzp} D$$

[4.15] $$s_{uzp} = s_{u0} + (k.z_p)$$

Where;

V_{max} = Maximum capacity under vertical loading

a, b, = Fitting coefficients

s_{uzp} = Soil undrained shear strength at pipeline embedment depth

D = Pipeline diameter

z_p = Pipeline embedment depth

s_{u0} = Shear strength at mudline

k = Shear strength gradient

Fitting coefficients *a* and *b* are specific to the shear strength gradient s_{u0}/s_{uzp}. Table 4.8 provides fitting coefficients for a shallow depth range (0.1D to 0.5D). For this depth range the fitting equation falls within 1% of the analysis data for both the smooth and rough interfaces.

Interface Conditions	s_{u0}/s_{uzp}	Coefficient	
		a	*b*
Smooth	0.00	4.46	0.171
	0.25	4.67	0.180
	0.50	4.87	0.197
	0.75	5.06	0.223
Rough	0.00	6.03	0.141
	0.25	6.43	0.170
	0.50	6.71	0.200
	0.75	6.99	0.248

Table 4.8*: Correlation coefficients, Equation [4.14], shallow (0.1D to 0.5D).*

Table 4.9 provides fitting coefficients for a deep embedment range (0.5D to 1.0D). For this depth range and a smooth interface condition this equation falls within 0.5% of the analysis data and within 1.5% for the rough interface.

A correlation for an "all data" correlation can also be undertaken with a slight reduction in precision. This correlation is within 1% of the data for the smooth interface condition. For the rough interface the correlation is generally within 1.5 % but up to 3.5% for the deepest and shallowest analysis at s_{u0}/s_{uzp}=0.75. The correlation presented in Table 4.10 are plotted against the analysis data in Figure 4.33 and Figure 4.34. Even for this reduced quality fit the closeness between the analysis results and the proposed correlations can be seen.

Interface Conditions	s_{u0}/s_{uzp}	Coefficient	
		a	*b*
Smooth	0.00	4.58	0.206
	0.25	4.80	0.216
	0.50	4.97	0.224
	0.75	5.08	0.230
Rough	0.00	6.22	0.176
	0.25	6.39	0.149
	0.50	6.56	0.162
	0.75	6.61	0.161

Table 4.9*: Correlation coefficients, Equation [4.14] deep (0.5D to 1.0D).*

Interface Conditions	s_{u0}/s_{uzp}	Coefficient	
		a	*b*
Smooth	0.00	4.55	0.184
	0.25	4.76	0.193
	0.50	4.94	0.207
	0.75	5.07	0.225
Rough	0.00	6.17	0.156
	0.25	6.42	0.168
	0.50	6.62	0.191
	0.75	6.73	0.220

Table 4.10*: Correlation coefficients, Equation [4.14], all data (0.1D to 1.0D).*

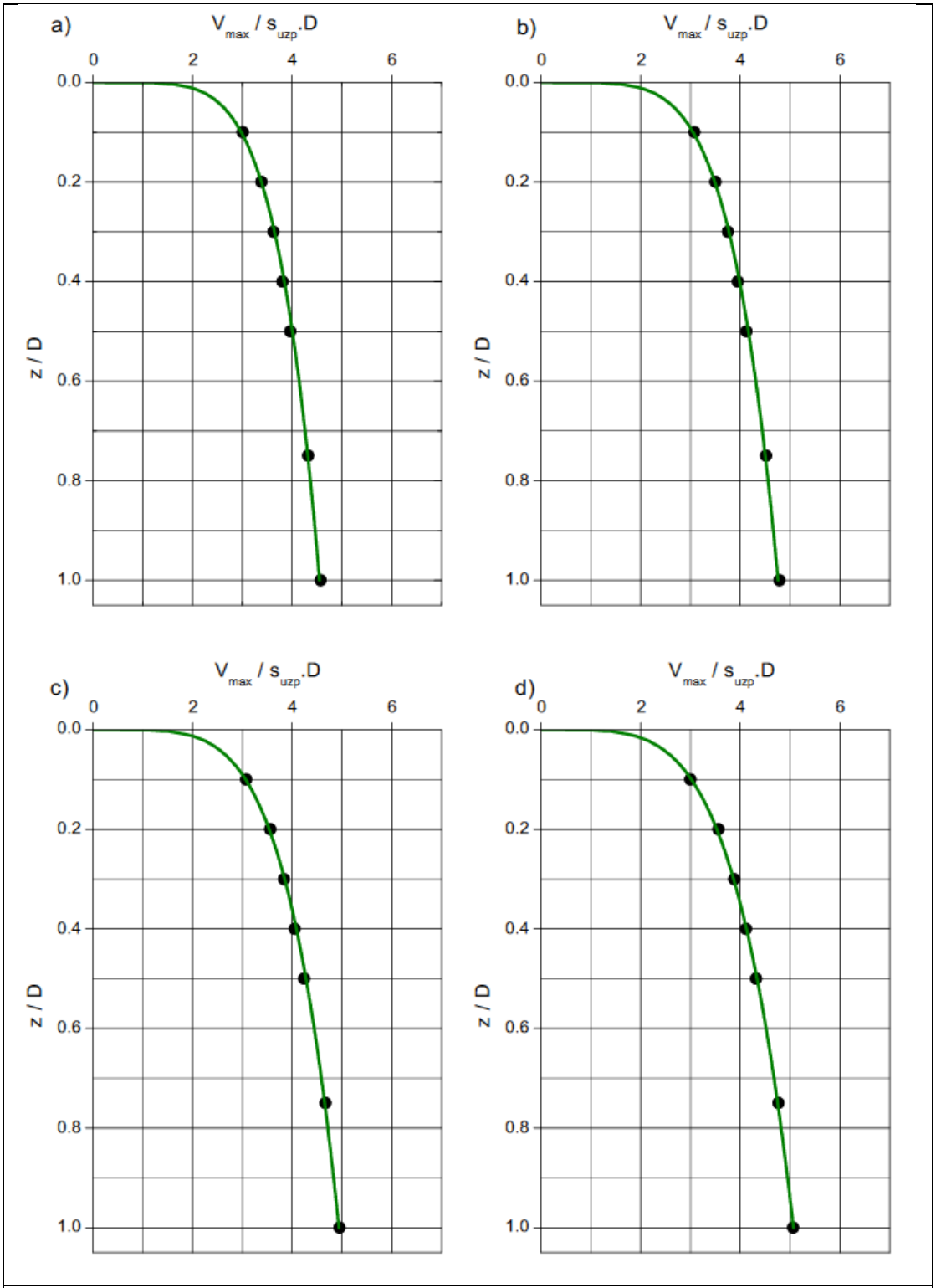

Figure 4.33 *- All data correlations (0.1D to 1.0D, Table 4.10) against data for a smooth interface s_{u0}/s_{uzp} = a)0, b)0.25, c)0.5, d)0.75.*

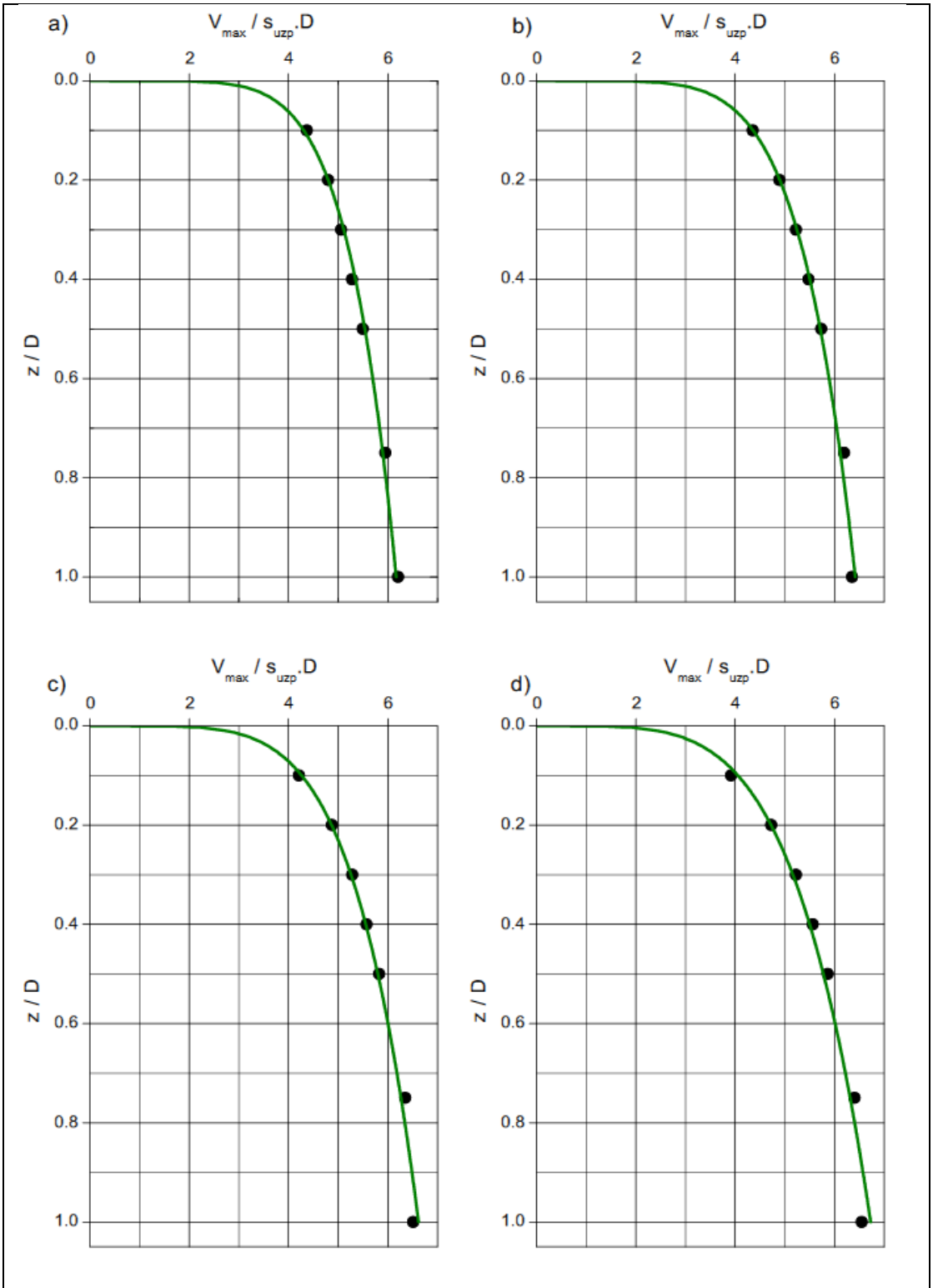

Figure 4.34 *- All data correlations (0.1D to 1.0D, Table 4.10) against data for a rough interface s_{u0}/s_{uzp} = a)0, b)0.25, c)0.5, d)0.75.*

As Equation [4.14] is in general form it can be applied to a wide range of conditions. However, while this provides useful information for pipeline design this may cumbersome for some design problems. For example, as previously discussed in Section 4.2.1 it may be convenient to have an alternative formulation of these equations which presents embedment depth from a specific pipeline weight and diameter. While this was undertaken previously in Equation [4.1] an equation equivalent to Equation [4.1] cannot readily be produced for the linear increasing shear strength case due to the dependence of shear strength on depth. This equation can however be solved iteratively or graphically, such as in a spreadsheet, removing this issue and providing a design method.

An additional issue with application of an equation similar to Equation [4.1] for design in the presence of a linear increasing strength gradient is the dependence of the correlation coefficients *a* and *b* on the s_{u0}/s_{uzp} ratio. In most site specific applications it is envisaged analysis will be undertaken for a single, or a small number of shear strength gradients. In this case penetration of the pipeline will alter the s_{u0}/s_{uzp} ratio for this fixed shear strength gradient, as s_{uzp} increases with depth.

This issues can be solved by deriving correlations for the change in *a* and *b* with s_{u0}/s_{uzp} ratio, allowing these to be incorporated into Equation [4.2], or similar. A review of Table 4.8, Table 4.9 and Table 4.10 suggests a linear correlation would provide a good fit to these coefficients, such as in the form of Equation [4.16] and [4.17].

[4.16] $$a = E_a \left(\frac{s_{u0}}{s_{uzp}}\right) + F_a$$

[4.17] $$b = E_b \left(\frac{s_{u0}}{s_{uzp}}\right) + F_b$$

Where;

a, *b*, = Fitting coefficients
s_{u0} = Shear strength at mudline
s_{uzp} = Soil undrained shear strength at pipeline embedment depth
E_a, E_b, = gradient term for the linear relationship
F_a, F_b, = y intercept term for the linear relationship

Values for the coefficients to derive *a* and *b* from Equation [4.16] and [4.17] are shown in Table 4.11. Plots of the correlations for *a* and *b* against the values obtained are shown in Figure 4.35 and Figure 4.36.

The use of an additional correlations within a design method has the potential to introduce an additional, and cumulative, source of error. In this context error is defined as the difference between the equation based fitting relationship and the data it is based upon. For the equation that represents smooth interface conditions from 0.1D to 1.0D, including the derivation of *a* and *b* with s_{u0}/s_{uzp} ratio, generally results in an error of <3% and a maximum error of <4%. The narrow depth range equations show a slight improvement, in particular the deep equation 0.5D to 1.0D. For 0.1D to 0.5D relationship the comparison with the analysis data was generally within 3 % and always within <3.5%. For 0.5D to 1.0D this comparison was always with <2%. In all cases this is a small and reasonable error that is likely to be acceptable for most applications.

Interface Conditions	z/D range	Linear Fitting Coefficient			
		E_a	F_a	E_b	F_b
Smooth	0.1 - 0.5	0.932	4.432	0.118	0.1546
	0.5 - 1.0	0.544	4.638	0.032	0.2070
	0.1 - 1.0	0.660	4.578	0.084	0.1744
Rough	0.1 - 0.5	1.400	6.032	0.218	0.1410
	0.5 - 1.0	0.336	6.294	0.009	0.1614
	0.1 - 1.0	0.660	6.226	0.149	0.1358

Table 4.11*: Correlation coefficients for Equation [4.16] and Equation [4.17].*

A similar exercise was undertaken for the rough interface condition. The difference between the wide depth range correlation, 0.1D to 1.0D, was generally good. However, it did not fit especially well with the constant shear strength case $s_{u0}/s_{uzp} = 1$. In most cases this correlation was within <5 % of the analysis data, often better. However, although unlikely to be used in design practice a departure of up to 9.6% was noted for deeper depths of the constant shear strength case. Narrower depth range correlations were generally better for the rough interface conditions, generally within <4 % and always within <5% for 0.1D to 0.5D and within 3% for the 0.5D to 1.0D correlation. It is not

recommended that the wide depth range correlation method is used for a rough interface constant shear strength case, for all other cases the error is relatively small and is likely to be acceptable for most applications.

For further discussion of the results outlined in this section see Section 4.7.

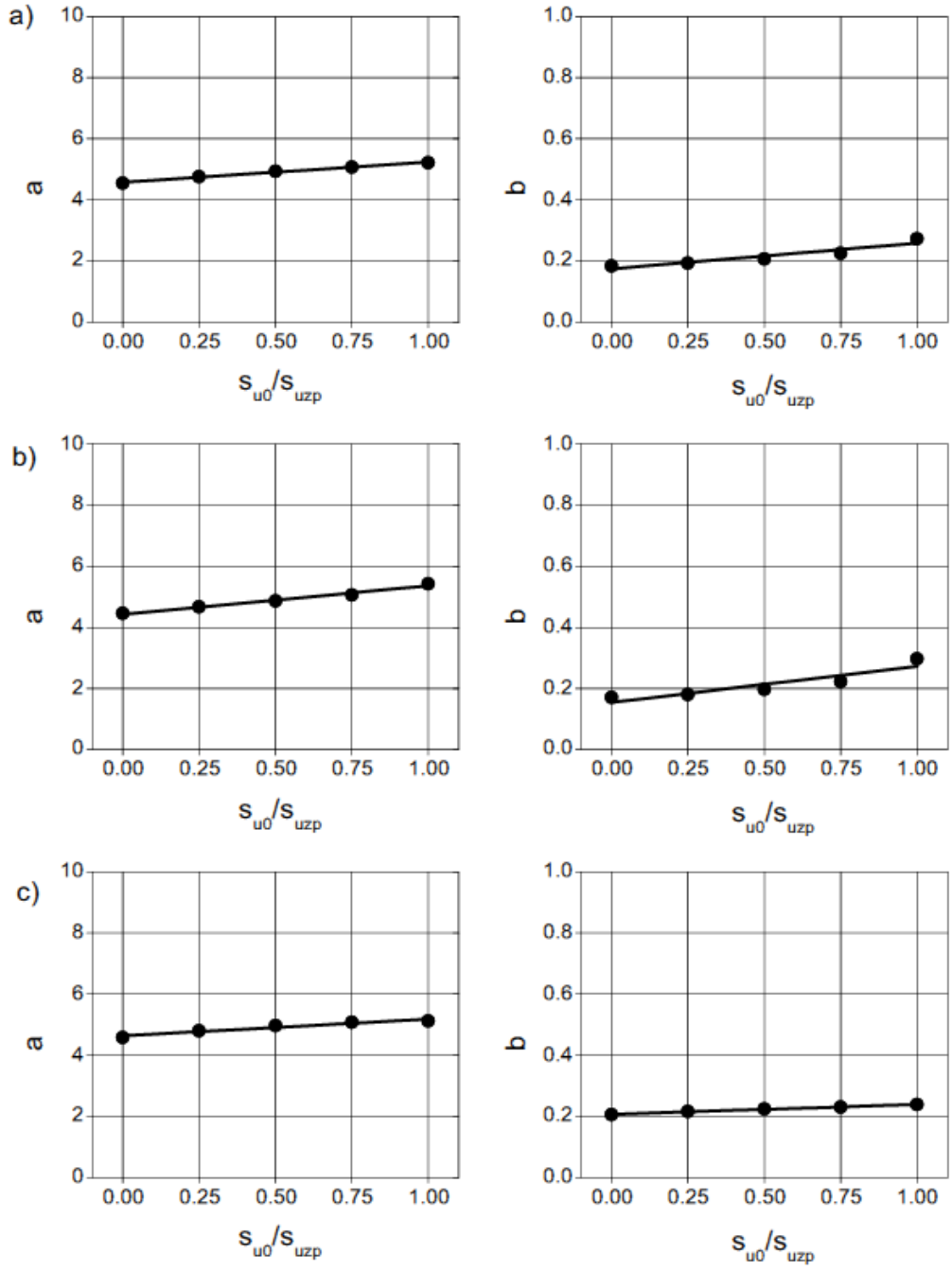

Figure 4.35 a,b,c *- Values for the correlation coefficient a and b against changes in s_{u0}/s_{uzp} ratio and the linear correlations, smooth interface. a) 0.1-1.0 D correlation b) 0.1-0.5 D correlation c) 0.5D-1.0D correlation.*

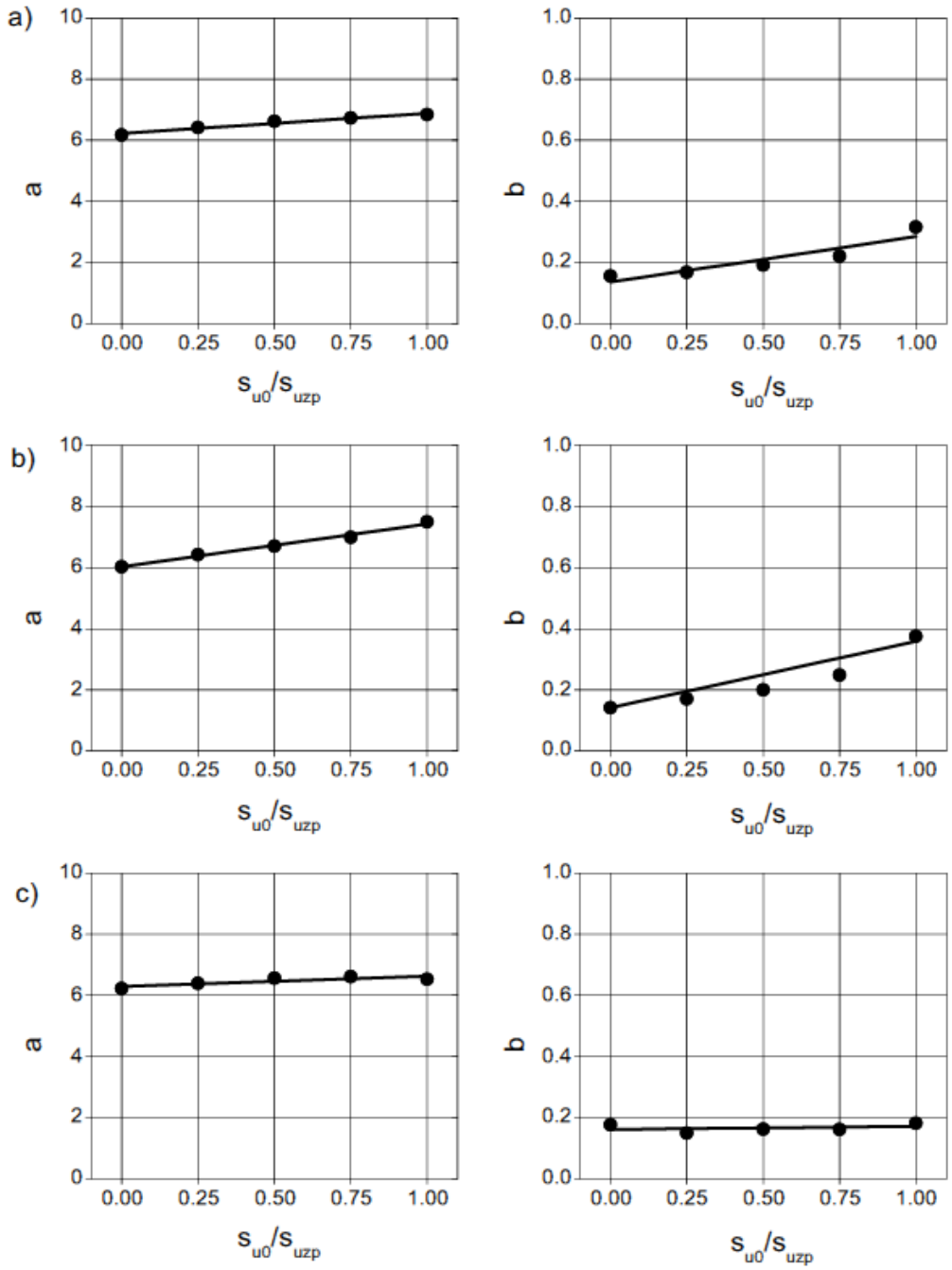

Figure 4.36 a,b,c *- Values for the correlation coefficient a and b against changes in s_{u0}/s_{uzp} ratio and the linear correlations, smooth interface. a) 0.1-1.0 D correlation b) 0.1-0.5 D correlation c) 0.5D-1.0D correlation.*

4.6.2 Analysis Results - Shear Strength Crusts

Following the methodology previously outlined in Chapter 3 a suite of analyses were undertaken to investigate the effect of a shear strength crust, for example as described by Ehlers et al. (2005) and Kuo et al. (2010), on a pipeline subjected to vertical loading. The results shown here have also been reported in Morrow and Bransby (2010). In these analyses shear strength crusts were represented as a series of linear shear strength gradients with either a positive or negative gradient. For clarity and ease of reference this representation and the accompanying notation, as previously presented in Chapter 3, is reproduced below in Figure 4.37. As the problem lacks generality with a significant number of variables, even within this linear gradient model, the focus of this section will be a small number of examples that will provide some insight into this problem.

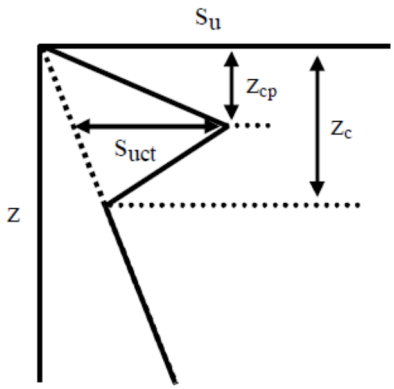

Figure 4.37 *- Model of a shear strength crust together with associated notation.*

Analysis cases are based on a shear strength crust that represented a departure from an underlying linearly increasing shear strength gradient, shown as the dotted line in Figure 4.37. This underlying shear strength gradient is taken as having a zero strength intercept at mudline. The geometry of the shear strength crust within this model can then be defined by three variables, the peak shear strength of the crust (s_{uct}), the depth of the crust peak below mudline (z_{cp}) and the depth the shear strength rejoins the underlying shear strength gradient (z_c). The crusts considered here all follow the rule $z_c = z_{cp}x2$, and therefore can be fully defined by z_{cp} and s_{uct} alone.

The peak strength of the crust (s_{uct}), at z_{cp}, was considered as a multiple of the strength of the underlying shear strength gradient with x10 and x5 cases analysed. A range of z_{cp} were considered, for a smooth interface condition $z_{cp}/D=$

1.00, 0.433, 0.30, 0.20 and for a rough interface z_{cp}/D = 1.00, 0.50, 0.30, 0.20. The value of z_{cp}/D = 0.433 for the smooth interface condition is based on a review of previous vector plots and is selected to place the smaller smooth interface failure mechanism a similar distance from the crust peak as the rough interface case at z_{cp}/D = 0.50. Pipeline embedment (z_p) is fixed for all analyses at z_p=0.3D. To check analysis configuration both a uniform shear strength case and the case of a linear increasing shear strength with a zero strength intercept were analysed. These analysis cases together with the variations in crust peak depth and interface conditions gave a total of 20 analyses. Details of analysis parameters and a summary of the results are provided in Table 1-9 and 1-10, Appendix A.

Mesh refinement requirements for the analysis of shear strength crusts was based on the findings of analyses previously discussed in this chapter. However, due to the way shear strength gradients are defined in FLAC, relative to mesh nodes, there were advantages in using the same mesh density for both the smooth and rough interface analysis. The mesh requirements for a smooth interface case, at a mesh size (Δ_z) of 10 mm for a 300 mm pipe, also had advantages in definition of shear strength gradients in that the geometry coincided well with the mesh density. This mesh dimension is a little coarser than optimal for the rough interface condition and can be expected to result in a slight over prediction of capacity for this case. For example, as can be seen from Table 1-9, Appendix A, the uniform shear strength case was 3.7% greater than analysis earlier in this chapter, and the linear increasing shear strength case 4.2% greater. This was considered acceptable, with the focus of this section on gaining a high level understanding into the potential influence of shear strength crusts rather than a detailed parametric study to develop specific design guidance. Displacement velocity for analyses are also summarised in Table 1-9 and 1-10. This velocity was generally consistent with previous analysis. However, it was possible to use a slightly faster displacement velocity for some of the crusts, while still maintaining data quality. This can be attributed to the larger displacement distances and larger failure mechanisms for these cases.

Figure 4.38 plots the peak resistance to vertical displacement of a pipeline in the presence of a shear strength crust. V_{max} is expressed in the dimensionless form $V_{max}/s_{uzp}.D$. Note the use of s_{uzp}, normalising by the shear strength at the pipeline embedment depth z_p. The resistance for the underlying linear increasing shear strength gradient is presented as a dashed and dotted line, for a rough and smooth interface condition respectively. This provides a useful comparison

for subsequent analysis. The key variables of crust geometry are represented in this figure with the crust peak depth (z_{cp}) plotted in dimensionless form relative to the pipeline diameter, z_{cp}/D. The depth of embedment is fixed at z_p=0.3D, so the distance of the crust peak to the pipeline is entirely controlled by the z_{cp}/D parameter. Strength of the crust, either x5 or x10, is shown by a different symbol on this graph, as is interface conditions.

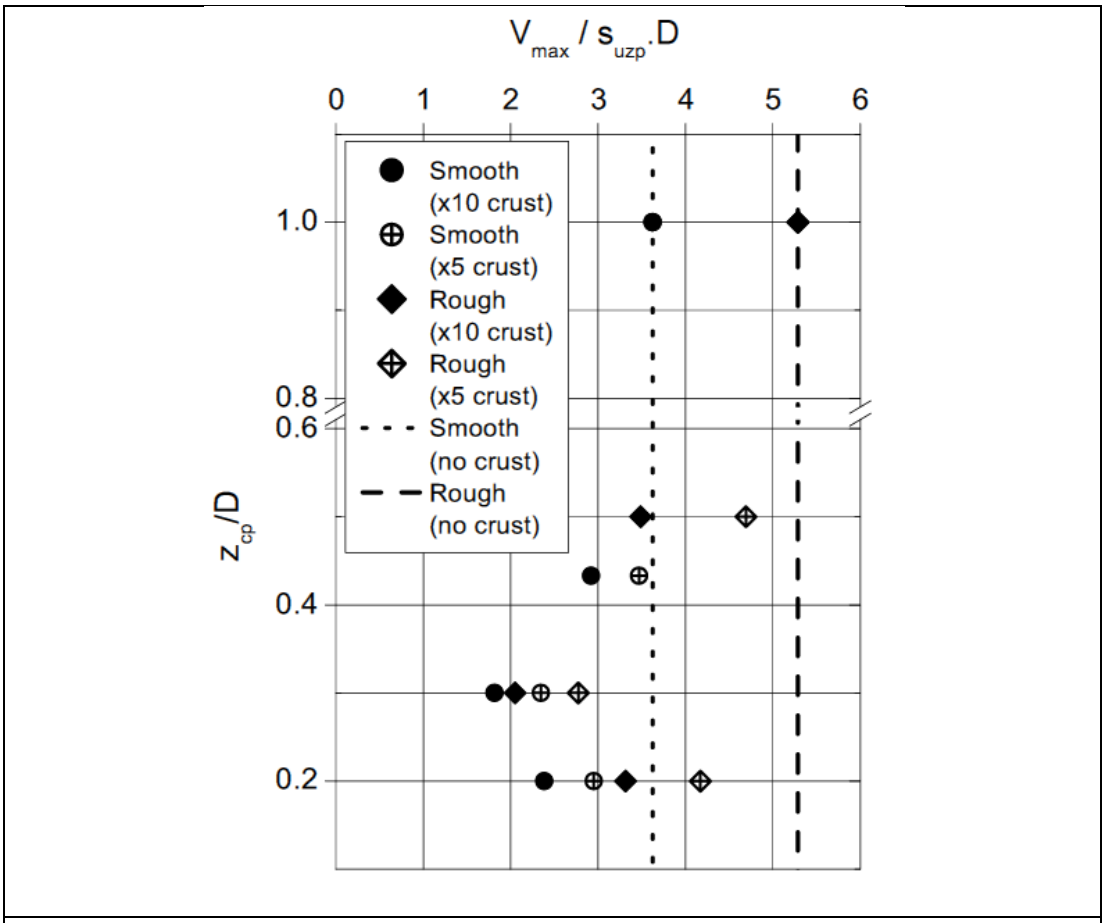

Figure 4.38 *- Analysis of a pipeline subjected to vertical loading in the presence of a shear strength crust, z_p=0.3D for all analysis.*

When the crust has a geometry described by z_{cp}/D=1.0 the resistance calculated for all the analysis variables are identical, both to each other and to the value associated with underlying linear shear strength gradient. This can be explained by reference to the failure mechanism in the presence of a linear increasing shear strength gradient, for example see Figure 4.30 previously presented in Section 4.5.1. With a crust peak at z_{cp}/D=1.0 this mechanism will be contained entirely within the upper portion of the shear strength crust, marked as the z_{cp} depth range in Figure 4.37. The crust peak will be located significantly lower than the zone of influence of the failure mechanism. In this case the pipeline

does not "see" the crust and the behaviour is governed entirely by the linear gradient that forms the upper part of the crust. Although the shear strength at z_p=0.3D will be greater, due to the steeper shear strength gradient associated with the crust, values of V_{max} /s_{uzp}.D will be identical. With resistance normalised by s_{uzp}, as previously described in Section 4.5.1, this produces a unique relationship that describes all shear strength gradients with the same intercept at mudline, in this case a zero strength intercept at mudline.

With no influence from crust geometry when the crust peak is relatively deep analyses then considered cases when the failure mechanism, under vertical loading, could be expected to intersect with the region of the crust peak. This was varied for the rough and smooth interface, where the larger failure mechanism associated with a rough interface was analysed with a slightly deeper value of z_{cp}/D. For both interface conditions the peak resistance to vertical loading is reduced. In most cases this reduction is relatively small. The exception is a rough interface condition with a x10 crust peak strength, where reduction is resistance is approximately 30%. For these cases (z_{cp}/D = 0.4 and 0.5) the failure mechanism is starting to interact with, and expand into, the lower shear strength below the crust peak. For the stronger crust and rough interface the dramatic reduction in resistance is associated with a punch through type failure mechanism and a significant interaction with the lower shear strength zone.

Having seen the start of a punch through mechanism and a large reduction in resistance for one case at z_{cp}/D = 0.4 and 0.5, it also was noted that z_{cp}/D=0.3 results in a dramatic reduction in resistance for all cases. Figure 4.39 shows an example displacement vector plot of the punch through type failure mechanism that can develop. This can be contrasted with the significantly smaller failure mechanism shown for a linear increasing shear strength gradient, for example Figure 4.30 in Section 4.5.1. The x10 crust is a more extreme geometry compared to the x5 case and analysis shows the x10 case results in a greater reduction in resistance. It should be noted while much of the discussion of larger failure mechanisms so far in this study has been in terms of an increase in V_{max}, a punch through mechanism is an example when the larger mechanism mobilises lower strength soil and leads to a reduction in V_{max}.

The final case analysed was a z_{cp}/D=0.2. For this case there is also a reduction in resistance to vertical loading, although this reduction is less than for z_{cp}/D=0.3. There is also a large failure mechanism for this case. However, for this geometry the mechanism is now starting to interact with the linear

increasing shear strength gradient below the crust, mobilising some stronger soil as part of the mechanism.

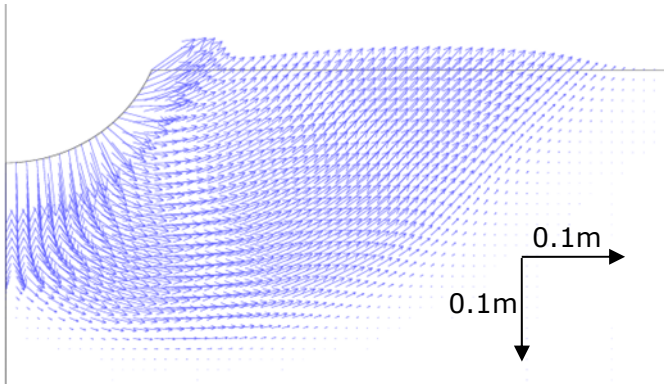

Figure 4.39 *- Vector plot showing a large punch through type mechanism for a smooth interface z_p=0.3D, crust strength x10 and z_{cp}/D=0.3.*

Large numbers of variables in geometry of shear strength crust could exist and the geometry of the problem will also be influenced by the pipeline diameter and the depth of embedment. However, this section has provided a framework for investigating this problem in dimensionless form and analysis results for a number of examples have been presented. The kinematics of how the failure mechanism of a pipeline under vertical loading interacts with the geometry of the shear strength crust governs this problem and a dramatic reduction in resistance can be experienced in conjunction with a punch through type failure mechanism. The analysis in this section has shown that the presence of a shear strength crust could have a significant effect on a pipelines behaviour under vertical loading. For further discussion see Section 4.7.

4.7 Summary and Discussion

This chapter has reported the results of investigations into a pipeline subjected to vertical loading undertaken as part of this study. The following areas have been considered;

- Homogenous strength seabed weightless seabed
- Large strain effects
- The effect of interface conditions
- The effect of soil unit weight
- The effect of variation in soil shear strength

It was noted that the analysis results for the case of a pipeline on a homogenous strength weightless seabed is similar to previous analyses undertaken by Aubeny et al. (2005) and Merifield et al. (2008). Comparisons between the fitting relationships developed as part of this study and those from this previous research are presented in Section 4.2.3. These comparisons show good agreement between this and these previous studies, both at shallow pipeline embedment depths (<0.5D) and for a deeper embedment (0.5D to 1.0D). This has acted as initial validation of the methods used in this study.

In general this study has been able to provide more detailed interpretation, compared to previous studies, for the case of a pipeline embedment of <1.0D on a homogenous shear strength weightless seabed. Soil displacement vector plots and state plots have been used to describe a basis for the form of the load displacement relationship as well as more detailed information on soil displacement at V_{max}, i.e. failure mechanism, including how this changes with interface conditions and pipeline embedment depth. An alternative design equation was also presented that linked pipeline penetration to parameters such as pipeline diameter and soil shear strength.

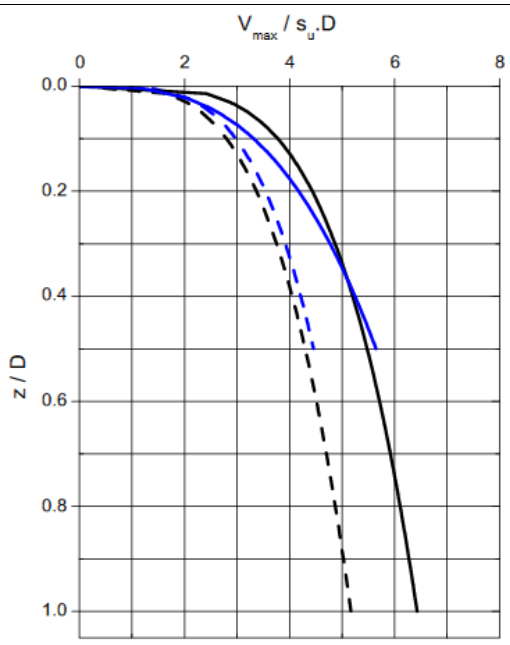

Figure 4.40 *- Comparison between this study and Merifield et al. (2009) large strain analysis of a V loaded pipeline. Dashed lines smooth interface, solid lines rough interface, blue lines Merifield et al. (2009) black lines this study.*

Larger strain analysis for a vertically loaded pipeline has previously been undertaken for depths <0.5D by Merifield et al. (2009). This study undertook

similar analysis and extended the scope to a depth of 1.0D. A comparison between this study and Merifield et al. (2009) is presented in Figure 4.40. This figure also shows the trend in V_{max} with increasing pipeline embedment

For smooth interface condition there is reasonable agreement between this study and the fitting relationship proposed by Merifield et al. (2009). The relationship proposed from the analysis undertaken in this study slightly underlies that of Merifield et al. (2009). The relationship provided in this study extends to 1.0D. A comparison between the fitting relationships for the rough interface conditions, as shown in Figure 4.40, show reasonable agreement although this is poorer quality at shallow depth e.g. <0.2D. In Section 4.3 it has been noted that the fitting relationship proposed in this study are less accurate below 0.1D. This has been attributed to elastic behaviour at very shallow pipeline penetrations into the seabed, an issue that may be more significant for lighter pipelines on higher strength seabeds.

There is no information in Merifield et al. (2009) on the equation fitting process used. However, it seems likely that with a smaller depth range 0-0.5D their equation has been skewed to fit the data at shallower depths, perhaps using a manual rather than mathematical fit. This reduces the quality of the data fit at deeper depths and prevents extrapolation beyond 0.5D. Additionally, in skewing towards the shallowest data this relationship would have a bias to the elastic parameters adopted in analysis, reducing generality. The rough interface proposed in this study fits well to the analysis data associated with plastic soil behaviour (see Section 4.3), with a slightly reduced quality of fit to the shallowest soil behaviour. The quality of this fit at the shallowest depth can also be expected to vary depending on elastic soil properties. It can be noted that pipeline behaviour at the shallowest depth has been identified as an area that could benefit from further study, see Chapter 7 for further details.

Previous numerical analysis based research has been limited to a fully rough and perfectly smooth interface conditions. This study has presented the results of investigations into a range of intermediate conditions. An important observation from this analysis was that behaviour between the rough and smooth conditions was not directly proportional to the interface strength and that behaviour varied with pipeline embedment depth.

Merifield et al. (2009) has previously presented research into unit weight effects for a pipeline embedment depth of <0.5D. This study reproduced this work before extending analysis to a pipeline embedment depth of 1.0D. There was

very good agreement between numerical analysis and the analytical solution for a pipeline embedment of less than <0.5D. However, below 0.5D and to 1.0D a basic analytical solution did not fit analysis well. As part of this study a modified analytical solution was proposed and fitted to the analysis data.

An extensive parametric study was undertaken to investigate behaviour of pipelines subjected to vertical loading in the presence of a linear increasing shear strength gradient. Fitting equations were proposed, which can be used as design tools. There are some challenges in implementing design methods for a linearly increasing gradient due to the change in strength with penetration and change in the steepness of shear strength gradient relative to a reference point at the depth of pipeline penetration. This can be solved iteratively in a spread sheet program. Additional correlations were presented to assist in this implementation i.e. change in correlation coefficient *a* and *b* with change in shear strength gradient.

In addition to investigating linear increasing shear strength gradients analysis was also undertaken to investigate various geometries of shear strength crust. Pipeline behaviour in the presence of these crusts is an area not addressed by previous researchers, although their presence is noted in a number of deepwater areas. Results of analysis into shear strength crusts varies from cases where the shear strength crust has no influence, with behaviour dominated by a linear increasing shear strength gradient, to the dramatic reduction in V_{max} associated with a punch through failure.

This chapter has presented the results of analysis to investigate a wide range of aspects of pipelines subjected to vertical loading. Comparisons have been made with analysis undertaken by other researchers with good to reasonable agreement between their research and this study. Investigations have extended the cases considered by previous researchers as well as investigating topics not addressed previously. Analysis undertaken as part of this study provides insight into pipeline behaviour under vertical loading. Additionally various relationships have been investigated further, with fitting equations presented. These fitting equations can be used as a design tool in place of undertaking full numerical analysis. Application of this study to design practice is discussed in Chapter 7. Conclusions for this study are also presented in Chapter 7, including discussion of potential areas for future research.

5 Pipelines Subjected to Combined V-H Loading

5.1 Introduction

A pipeline may be subjected to more complex loading then the Vertical (V) load problem definitions considered in Chapter 4. This chapter addresses pipelines subjected to combined Vertical and Horizontal loading (V-H). Section 5.2 considers the maximum capacity under Horizontal loading (H_{max}) and V-H stability envelopes for the case of a homogenous shear strength weightless clay. This allows comparisons with previous research, which is discussed in Section 5.6. Section 5.2 also presents results for analyses of V-H loading at deeper embedment depths then considered by previous researchers, extending analysis from a pipeline embedment depth of half a pipeline diameter (0.5D) to one pipeline diameter (1.0D).

In addition to the case of homogenous shear strength weightless seabed, analyses investigating a range of other factors is reported in this chapter. The effect of various linear increasing shear strength gradients on H_{max} and V-H stability envelopes is investigated (Section 5.3). Pipelines subjected to V-H loading on a sloping seabed are discussed in (Section 5.4) along with large displacement behaviour under V-H loading (Section 5.5). Section 5.6 summaries the findings of the analyses reported in this chapter.

The analysis reported in this chapter uses a perfectly smooth pipe-soil interface condition with no tensile capacity. This is a more clearly defined case then a rough interface, which for V-H loading could also have a range of tensile behaviour. This could range from no tensile capacity to tensile capacity equivalent to soil undrained shear strength. As noted in the previous chapter a smooth interface also underlies the rough interface in terms of capacity. It therefore may be of more use to a pipeline designer, i.e. conservative, perhaps used prior to adding additional site or pipeline specific elements to the analysis. As in the previous chapter the seabed soils are treated as weightless, unless unit weight is the factor specifically being investigated, allowing the impact of factors such as shear strength gradient to be investigated individually.

5.2 Homogenous Shear Strength Weightless Clay

5.2.1 Maximum Horizontal Capacity (H_{max})

When considering the behaviour of a pipeline subjected to V-H loading on a clay seabed two important characteristics of this behaviour are the maximum capacity when subjected to Vertical loading (V_{max}) and the maximum capacity when subjected to Horizontal loading (H_{max}). For a displacement controlled analysis this relates a pipeline displacement angle (δ) of $\delta=90^{\circ}$ and $\delta=0^{\circ}$ for V_{max} and H_{max} respectively. V_{max} has already been discussed in Chapter 4. H_{max} will be addressed in this section, with full V-H stability envelopes discussed in the next section, Section 5.2.2.

Following the methodology outlined in Chapter 3 analyses were undertaken to investigate H_{max} for a pipeline embedded at various depths within a clay seabed. A small strain analysis methodology was adopted with 7 wished in place embedment depths, 0.1D, 0.2D, 0.3D, 0.4D, 0.5D, 0.75D, and 1.0D. A total of 18 analysis were undertaken, which included checks on mesh refinement requirements. A smooth interface condition and a homogenous strength weightless seabed was used in all analyses.

Initial problem familiarisation suggested that mesh refinement requirements for investigating H loading were coarser then those required for analysis of V_{max}. This would suggest that mesh refinement requirements for V-H loading would be driven by those previously established for analysis of V_{max}. This premise was investigated with a convergence study for a horizontal displaced/loaded pipeline. When undertaking the analysis of H_{max} multiple analyses with different mesh sizes (Δ_z) were undertaken for pipeline embedment depths of 0.1D, 0.2D. 0.3D, 0.5D, and 1.0D. In all these cases analysis converged at mesh dimensions coarser or equal to those previously indicated in the convergence studies investigating V_{max} e.g. see Section 4.2 and associated data summaries in Appendix A. Following the results of this investigation the mesh requirements for the intermediate embedment depths, 0.4D and 0.75D, were based on the more stringent V_{max} mesh requirements. Further details of analysis variables, including mesh requirements, are summarised in Table 2-1, Appendix B.

The horizontal displacement velocity adopted in analysis varied between 5.0E-6 m/s at the shallowest embedment depths and 5.0E-7 m/s for the deeper embedment depths. At the shallowest depth this was faster than could be undertaken for analysis of V_{max}. However, in general, displacement velocity

requirements were similar to those for analysis of V_{max}. For an analysis results summary and additional details of analysis parameters see Table 2-1, Appendix B.

Analysis of H_{max} was interpreted within a dimensionless framework, increasing the generality of any correlations and aiding in comparison to other research. Analysis results are plotted in Figure 5.1 with H_{max} expressed in terms of the dimensionless group $H_{max}/s_u.D$ at a range of embedment depths z/D.

Figure 5.1 initially suggests two broadly linear trends in H_{max} with embedment depth, one trend over the depth range 0.1D to 0.5D and a second trend over a deeper depth range, 0.5D to 1.0D. However, a more detailed review reveals a slight curvature in these relationships. A linear relationship would also result a small non-zero intercept at mudline. A power law relationship similar to that used for V_{max} can better accommodate this slight curvature in the relationship, providing a better fit to the data and allowing for zero resistance at mudline.

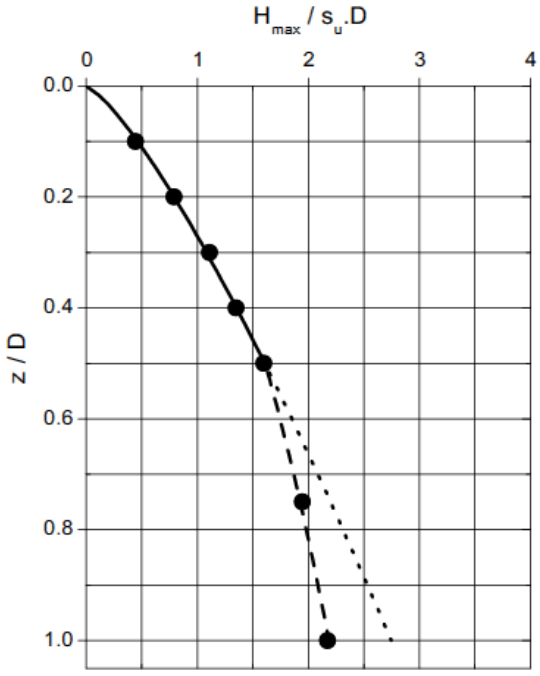

Figure 5.1 *- Comparison between H_{max} analysis data and the proposed fitting equations.*

When providing a fitting equation for the relationship between H_{max} and embedment depth there are two principal choices in the form of the power law equation used. The first choice is to establish an equation that treats H_{max} as

being independent of other aspects of resistance to displacement e.g. not related directly to V_{max}, for example the approach used by (Merifield et al., 2009). The second approach is to relate H_{max} directly to V_{max} e.g. by expressing H_{max} as a ratio of V_{max} such as undertaken by (Merifield et al., 2008). For this study the latter approach has been adopted.

In reviewing both approaches to a H_{max} depth relationship no clear advantages can be seen in providing a relationship where H_{max} is treated independently of V_{max}. Indeed this approach can be viewed as being somewhat artificial as an embedment depth will always be required in this relationship, which will arise from the V load history and the associated V_{max} depth relationship. Additionally in most instances there will be some V loading present, such as pipeline self weight. Expressing H_{max} as a proportion of V_{max} is also consistent with the approach required for considering a V-H stability envelope, as addressed in Section 5.2.2, with advantages in maintaining a consistent approach with later sections of this study. Equation [5.1] shows the relationship adopted. This equation can also be rearranged in terms of H_{max} by multiplying both sides of the equation by V_{max}.

[5.1] $$\frac{H_{max}}{V_{max}} = c\left(\frac{z}{D}\right)^{d}$$

Where;

H_{max} = Maximum resistance to horizontal pipeline displacement
V_{max} = Maximum resistance to vertical pipeline displacement e.g. see Equation [4.1]
s_u = Soil undrained shear strength
D = Pipeline diameter
z = Pipeline embedment depth
c, *d*, = Fitting coefficients, see Table 5.1

Depth Range	Coefficient	
	c	*d*
0.1D to 0.5D	0.506	0.4763
0.5D to 1.0D	0.427	0.2022

***Table 5.1**: Fitting coefficients for Equation [5.1].*

The relationships obtained from Equation [5.1] can be plotted against the analysis data from this study, also shown in Figure 5.1. The solid line shows the relationship over the depth range to 0.5D, with a dashed line showing the deeper relationship, from 0.5D to 1.0D. A finer dashed line shows the extension of the shallow depth relationship, emphasising the change in trend and the requirement for an alternative relationship at a pipeline embedment depth greater than 0.5D.

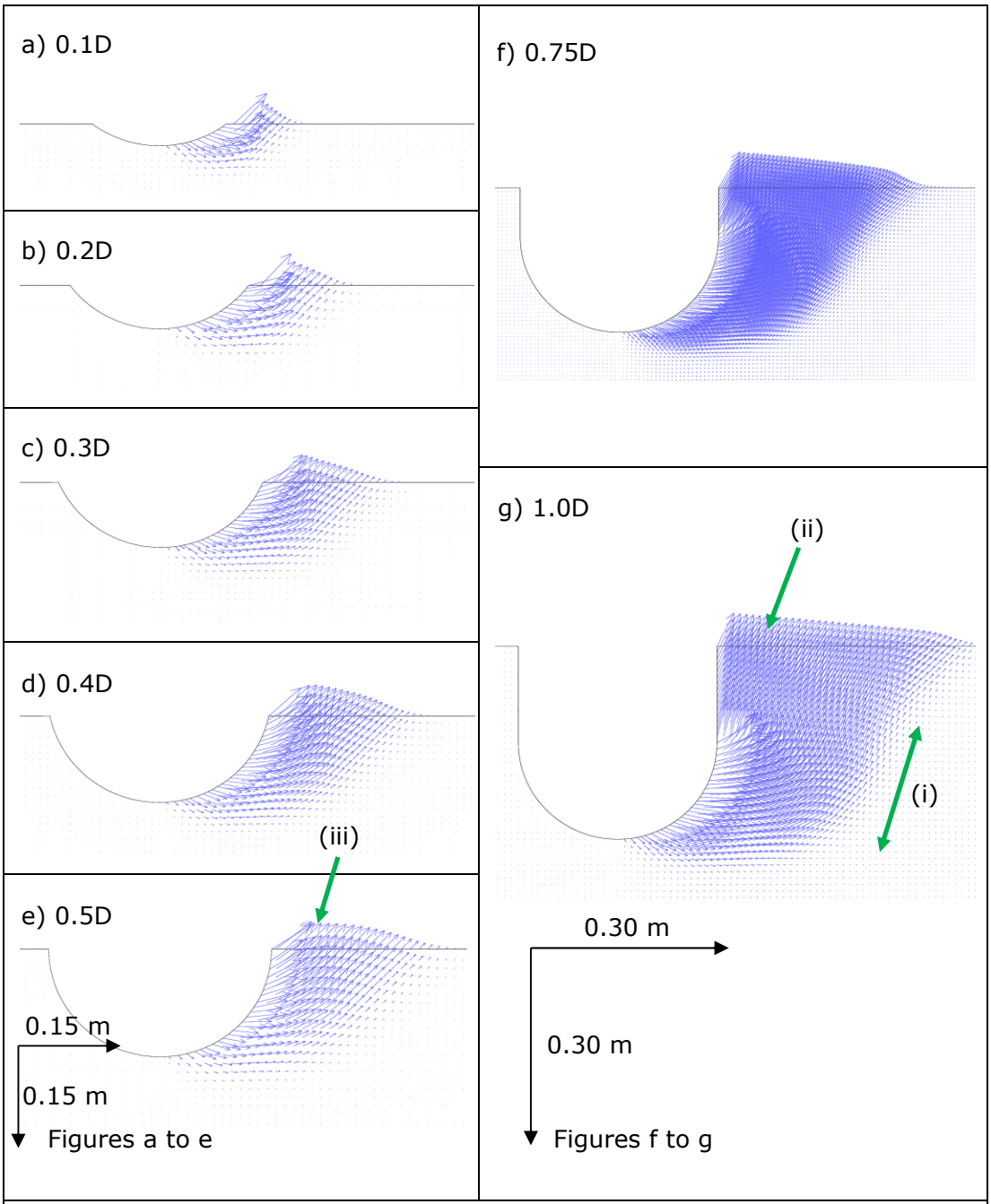

Figure 5.2 a,b,c,d,e,f,g, *- Vector plots of soil displacement at H_{max}, 0.1D to 1.0D.*

As can be seen in Figure 5.1 the proposed equations and associated fitting coefficients provide a good fit to the data. For the depth range 0.1D to 0.5D the equations are generally within 2.5% of the data with the exception of 0.1D which is within 4.2% of the data. H_{max} at this shallow depth is very low, and although this represents the largest deviation in percentage terms, it is very small in absolute terms. Over the depth range 0.5D to 1.0D the alternative fitting coefficients produce a relationship within 1.1% of the analysis data.

As with previous analysis of V_{max}, consideration of the soil displacement at H_{max} can provide some additional information with respect to relationships and trends seen in the analysis data. Vector plots of the calculated displacement field at H_{max} are shown in Figure 5.2.

Figures 5.2 a to e relate to the shallow depth correlation from 0.1D to 0.5D. Figure 5.2 f and g are for an embedment depth of 0.75D and 1.0D respectively. The 0.1D to 0.5D vector plots show a similar failure mechanism geometry across this depth range, consistent with the observed trends in the data at shallow depth. It can be seen that the low values of H_{max} at very shallow depth, e.g. 0.1D, are associated with a small failure mechanism and mobilisation of a small volume of soil. As embedment depth increases the sizes of mechanism grows in association with an increase in H_{max}, while still maintaining a similar geometry.

Perhaps the most interesting insights from the vector plots are observations related to the change in the rate of increase in H_{max} for depths greater than 0.5D i.e. change in the gradient of the H_{max} correlation. Some variation at this depth can reasonably be expected in a small strain analysis framework, with the projected height of the pipeline in contact with the soil remaining constant from 0.5D despite the increase in embedment depth. The vector plots, in particular the coarser mesh in Figure 5.2g, show a change in mechanism below 0.5D. This deeper mechanism has a steeper side extending to mudline, e.g. see area annotated as (i), shearing less soil proportional to the embedment depth when compared to the more circular geometry of the shallower mechanisms. Additionally from the pipeline shoulder, at 0.5D, the displacement vectors are more vertical in orientation, for example contrast the area annotated as (ii) at 1.0D to the area marked as (iii) at a shallower embedment depth. These steeper displacement vectors at greater depth can be linked to the steeper less circular failure mechanism. The trend in H_{max} below 0.5D can be expected to continue beyond 1.0D until a deep seated flow around mechanism develops and no interaction with the soil surface.

This section has provided details of analyses into H_{max} for a pipeline embedment range of 0.1D to 1.0D and a uniform shear strength weightless seabed. The correlations produced from these analyses will be used in the following section, Section 5.2.2, to produce V-H stability envelopes in conjunction with V_{max} correlations from Chapter 4 and further analyses at a range of displacement vectors. Further discussion and comparison with the work of previous researchers will be presented in Section 5.6.

5.2.2 V-H Loading

In addition to a pure horizontal displacement ($\delta=0^{\circ}$) to define H_{max} other pipeline displacement vectors can be investigated using numerical analysis. A range of displacement vectors over an appropriate angle range, and at suitably close intervals, can be used to define the full pipeline stability envelope in V-H load-space. This envelope would be specific to the embedment depth selected. However, a range of embedment depths can be considered as has previously been undertaken for V_{max} in Chapter 4 and H_{max} in the previous section. The results reported in this section address the case of a homogenous shear strength, flat, weightless seabed and a pipeline with smooth interface condition. As part of the smooth interface configuration, in addition to no shear capacity at the interface, the tensile capacity was also set to zero. Further problem definitions have been investigated and are reported later in this chapter. For clarity the pipeline displacement angle convention previously presented in the methodology (Chapter 3, Figure 3.21) is reproduced in Figure 5.3.

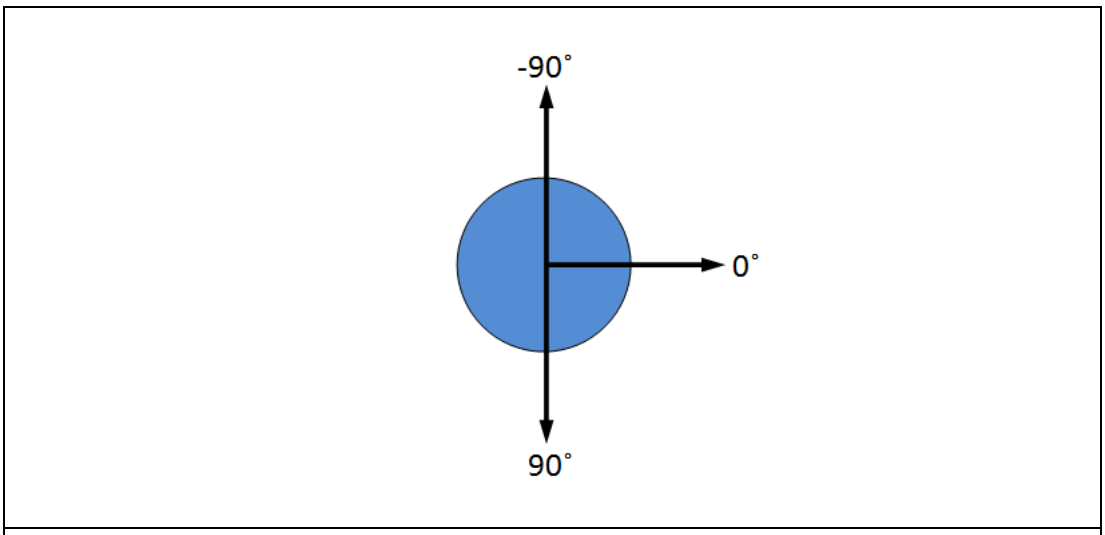

Figure 5.3 *- Angle notation convention for pipeline displacement angle (δ)*

The range of pipeline displacement angles (δ) required to define a V-H stability envelope is dependent on embedment depth. For example a deeper embedment depth can be expected to result in a larger V-H stability envelope, both in terms of capacity and the range of δ that produces a significant resistance. In addition to having to address the wider range of δ a greater number of analysis points are required for a larger envelope so that the spacing of these analysis points provides a reasonable definition of the stability envelope. For the case of a flat seabed there is symmetry in the problem limiting displacement angle requirements to a maximum of 180° i.e. displacing a pipeline to the right hand side is identical to displacing the pipeline to the left. For a smooth interface condition there is no tensile capacity in vertical uplift (δ=-90°) therefore the stability envelope intersects zero H and zero V load at δ=-90°, with no analysis required for this case. At a shallow embedment depth displacement angles close to δ=-90° produce negligible V-H capacity and do not need to be investigated to adequately define the stability envelope. Minimum displacement angle requirements were investigated with the objective of producing a termination point on the stability envelope close enough to zero V-H load to adequately define the upper part of the envelope. At an embedment depth (z) of z=0.1D this minimum displacement angle was δ=-30° decreasing to δ=-70° at z=1.0D. Further details of the displacement angles selected for analysis are summarised in Table 2-2, Appendix B.

Pipeline embedment depths of z=0.1D, 0.2D, 0.3D, 0.4D, 0.5D, 0.75D and 1.0D were investigated in this study. Points on the V-H stability envelope for a given embedment depth were known for δ=-90° (uplift), δ=90° (V_{max}) and δ=0° (H_{max}) and the minimum displacement angle had been determined e.g. -30° for z=0.1D. The objective was then to undertake analyses for a range of displacement vectors to produce results distributed around the V-H envelope between these known points. The required displacement vectors were not known *a priori*, and would not necessarily be evenly distributed for a uniform change in angle, so a relatively close spacing was adopted. Particular attention was given to areas of high envelope curvature when selecting displacement vectors.

As previously suggested the number of analysis required to adequately define the V-H stability envelope varied with embedment depth. At z=0.1D this was 12 analyses, including analysis of H_{max} and V_{max}. With increasing embedment the number of displacement vectors analysed was incrementally increased, with 17 displacement vectors used to investigate an embedment of z=1.0D. A total of 101 analyses were undertaken for the embedment depths reported in this

section. V_{max} was known from previous analysis in this study (Section 4.1.1 and 4.1.2). However, because of changes in analysis configuration V_{max} analysis was repeated as part of this V-H analysis suite. In almost all cases this was within <0.5% of previous analyses and in all cases <1.2% of previous analyses. A summary of all analysis results along with analysis parameters, such as displacement angle, are presented in Table 2-2, Appendix B.

For V-H analysis mesh requirements were based on those previously used for considering V_{max}, see Chapter 4. The displacement velocity ($\bar{v}$), resulting from the x (u) and y (v) displacement components, were set to the same velocity as used to investigate H_{max}. A slower velocity was required for vertical displacement (δ=90°) as previously found in Chapter 4. In general the adopted displacement velocities using this approach produced good quality data. However, at shallow depth, e.g. 0.2D, a small number of displacement probes close to δ=90° produced data with a moderate amount of noise attributable to numerical instability. These displacement probes benefited from a slower displacement velocity closer to that required to investigate V_{max}. Details of mesh dimensions and displacement velocity is also presented in Table 2-2, Appendix B, along with a summary of the analysis results.

Figure 5.4 shows the example of a series of V-H analyses for an embedment depth of z=0.2D with a pipeline diameter of 0.3 m. In this example conditions comprised a flat seabed with a uniform undrained shear strength of 5 kPa and a pipeline with a smooth pipe-soil interface condition. For each of the displacement probes V and H load components were calculated, with the load path plotted in Figure 5.4. Displacement probes track across V-H load space until a constant value of V-H is reached, marked as a termination point. These termination points define the pipeline stability envelope for this embedment depth and the adopted analysis conditions. The plastic potential for each pipeline displacement angle (δ) is also plotted Figure 5.4. These plastic potentials were calculated using the approach described by Bransby and Randolph (1998) for foundations and adopted for pipelines by Morrow and Bransby (2009). At the termination point, where plastic failure within the soil is full established, the ratio of plastic displacement increments (dv^p/du^p) is equal to the vertical and horizontal displacement ratio (v/u), where $\delta = \tan^{-1}(v/u)$.

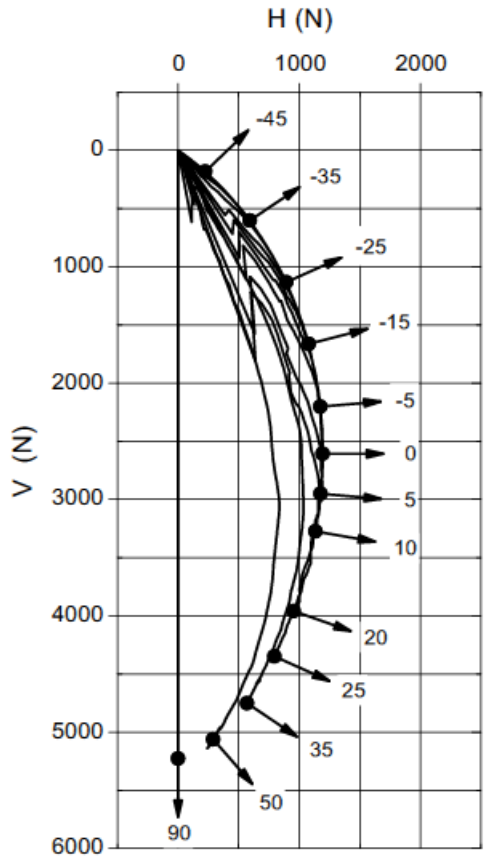

Figure 5.4 *- Example V-H analyses for an embedment depth of 0.2D. Smooth interface.*

In Figure 5.4 δ=90° can be seen to have no horizontal load component, with the remaining displacement probes producing some horizontal resistance and a reduction in vertical resistance. For a number of shallower angle displacement probes e.g. less than δ=20° through to δ=-45°, the final part of the load path tends to behave similar to a swipe test, e.g. as discussed by (Bransby and Randolph, 1998), tracking the edge of the pipeline stability envelope. While this is interesting the termination points alone are sufficient to define the stability envelope and this effect does not need to be relied upon.

It can be noted for the z=0.2D example, particularly the upper part of the stability envelope at lower values of V, that the load path is somewhat "spiky" with a rapid change in the load path. This change in the load path can be associated with transition from elastic to plastic soil behaviour with the onset of plastic flow. A similar phenonmenon was previously discussed in Chapter 4 for V loading, although in the case of Figure 5.4 there are both V and H components to

this spike in data. The plastic flow is a transient state where initially a small area of soil is experiencing plastic flow. This area then expands with further pipeline displacement, while still remaining a confined plastic flow within an otherwise elastic soil mass. The expansion in plastic flow can continue until it intersects with the soil surface (mudline) to become unconfined plastic flow. It is believed that the sudden change in load path is attributable to a large area of plastic flow significantly changing the soils stiffness response along the displacement path, with plastic soil having a lower apparent stiffness then its previous elastic state; a redistribution of forces would then occur within the soil mass. This redistribution in forces, and potentially some numerical noise associated with this rapid change, is expected to be the cause of the spike in the load path. It is noted there is some impact on the magnitude of this load reversal with pipeline displacement speed, which relates to the numerical noise element of this phenomenon. As the focus of analyses was to determine the maximum load for a given displacement vector and the termination point on the stability envelope this effect did not influence the results obtained and therefore the transition from elastic to plastic behaviour has not been investigated in detail in this study.

Vector plots of soil displacement at failure, peak load, were produced for a selection of points around the z=0.2D pipeline V-H stability envelope, see Figure 5.5 a to e. Each of these vector plots is representative of a termination point and plastic potential in Figure 5.4, providing additional information on soil behaviour at these points on the stability envelope.

Figure 5.5a shows the case of pure vertical displacement, i.e. $\delta=90^{\circ}$. This displacement probe is associated with maximum vertical capacity, V_{max}, and does not result in any horizontal component of resistance, as can be seen in the load path presented in Figure 5.4. The geometry of soil displacement shown in this vector plot is the same as previously reported in Chapter 4. However, in this case the full displacement mechanism is shown symmetrically around a central vertical line of symmetry.

At a displacement of $\delta=50^{\circ}$ a small change in the geometry of the displacement mechanism can be seen, Figure 5.5b, with the mechanism no longer symmetric. It can be noted that a slightly larger body of soil is being displaced on the right hand side of the pipeline. This asymmetry explains the small H component of resistance shown in Figure 5.4.

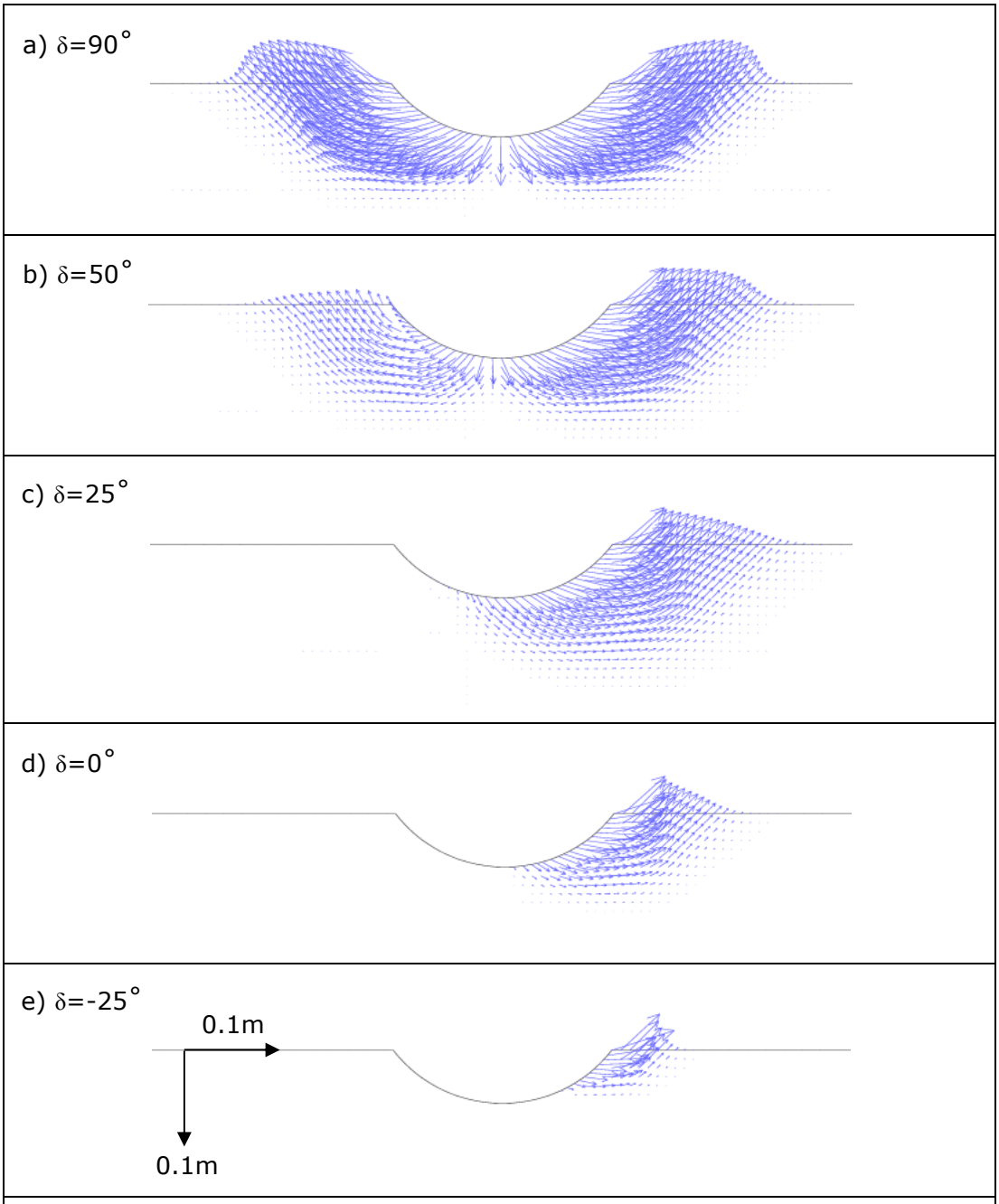

Figure 5.5 a,b,c,d,e *- Vector plots for an embedment depth of 0.2D*

The vector plot for the δ=25° displacement probe shows a relatively dramatic change in the geometry of the soil displacement mechanism when compared to Figures 5.5a and 5.5b. For this probe there is a significant asymmetry in soil displacement with a failure mechanism that is largely confined to the right hand side of the pipeline, with this portion of the mechanism intersecting with the seabed. Soil displacement on the left hand side of the pipeline is negligible and does not intersect with the seabed. This asymmetry explains the increase in the H component of resistance. The mechanism can also be seen to mobilise less soil

explaining the reduction in total resistance compared to steeper displacement probes e.g. δ=90° and δ=50°.

For the horizontal displacement probe, δ=0°, soil displacement is entirely on the right hand side of the pipeline. This is associated with the maximum horizontal resistance H_{max}. The amount of soil being displaced has also reduced further from the previous vector plot. Although the H component of resistance has increased with the extreme of asymmetry in the soil displacement the total resistance has reduced further in association with a large reduction in the V component of resistance.

The final vector plot in Figure 5.5 is associated with δ=-25°, a displacement vector above horizontal. The uplift angle in this displacement probe can be seen to significantly reduce the amount of soil being displaced, reducing the total resistance as well as the V component of resistance. As with the previous vector plot (δ=0°), soil displacement is confined entirely to the right hand side of the pipeline with the H component of resistance forming a relatively large proportion of total resistance.

In addition to the example presented for z=0.2D analysis was progressed for the embedment depths z=0.1D, 0.3D, 0.4D, 0.5D, 0.75D and z=1.0D. As noted earlier in this study it is beneficial to present this data in a dimensionless form, for example V_{max} was expressed in terms of V_{max} /s_u.D in Chapter 4. Figure 5.6 provides a summary of analysis undertaken for these cases, presenting the V-H stability envelope termination points in terms of the dimensionless V and H groups V/s_u.D and H/s_u.D. Here V and H components of resistance are normalised by the undrained shear strength of the soil (s_u) and the pipeline diameter (D). This increases the generality of the results and represents a more robust format then in Figure 5.4, where the results are reported in Newton's and are specific to a particular soil shear strength and pipeline diameter.

Figure 5.6 shows the expansion of the stability envelope in conjunction with increasing embedment depth and the associated increase in V_{max} and H_{max}. Some changes in geometry can be also be noted. However, in addition to simply plotting termination points there are advantages in providing an envelope fitted to this data. Plotting the plastic potentials, as previously done in Figure 5.4, is also of interest.

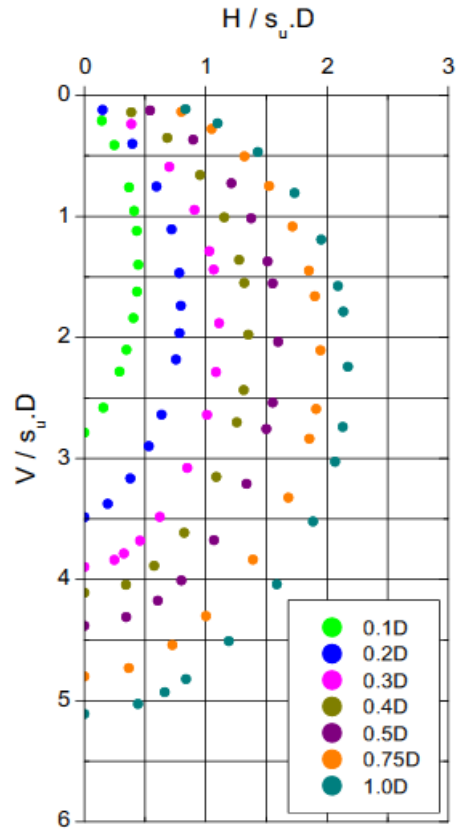

Figure 5.6 *- Summary plot of all V-H stability envelope termination points.*

The parabolic equation previously used by (Merifield et al., 2008) was fitted to the analysis data summarised in Figure 5.6, providing V-H stability envelopes for these pipeline embedment depths. Various choices on the form of this equation were available. An approach was selected that expressed H as a ratio of H_{max} for a range of V/V_{max} ratios as shown in Equation [5.2]. V_{max} and H_{max} can be obtained from the equations provided in previous sections of this study. For example Equation [4.1] with the fitting coefficients in Table 4.1 can be used for obtaining V_{max} for the shallow embedment (0.05D to 0.5D) of a smooth interface pipeline in a uniform shear strength seabed. Equation [5.4] and Equation [5.5], along with the coefficients in Table 5.2, can be used to obtain the skew parameters β_1 and β_2.

[5.2] $$\frac{H}{H_{max}} = \beta \left(\frac{V}{V_{max}}\right)^{\beta_1} \left(1 - \frac{V}{V_{max}}\right)^{\beta_2}$$

Where;

H = Horizontal load/resistance

H_{max} = Maximum horizontal load
V = Vertical load/resistance
V_{max} = Maximum vertical load
β_1 , β_2 = Parabolic skew parameters
β = See Equation [5.3]

[5.3] $$\beta = \frac{(\beta_1+\beta_2)^{(\beta_1+\beta_2)}}{{\beta_1}^{\beta_1}{\beta_2}^{\beta_2}}$$

Having previously obtained V_{max} and H_{max} relationships for various cases the only additional requirement in developing a V-H Stability envelope is to fit the parabolic skew parameters to the analysis data. Spread sheets to fit β_1 and β_2 to the analysis data were developed following the general data fitting methodology outlined in Section 3.4. The values of β_1 and β_2 obtained from these spreadsheets are plotted in Figure 5.7. While the value of these skew parameters for each embedment depth are optimal for that specific depth, for use as a design tool it is beneficial to develop a relationship to describe changes in β_1 and β_2 with depth. (Merifield et al., 2008) has previously proposed a linear relationship for the changes in skew parameters with embedment depth, although from this paper it is unclear how well their data fitted this linear relationship. The Merifield et al. (2008) relationship is plotted in Figure 5.7.

A logarithmic relationship was found to provide a better fit to the data from this study. This may be partly due to the larger depth range considered here compared to (Merifield et al., 2008). However, even over the depth range 0.1D to 0.5D a logarithmic relationship would seem more appropriate then a linear fit. See Equations [5.4] and [5.5] along with the fitting coefficients in Table 5.2. These relationships have also been plotted in Figure 5.7.

[5.4] $$\beta_1 = f\left[ln\left(\frac{z}{D}\right)\right] + h$$

[5.5] $$\beta_2 = f\left[ln\left(\frac{z}{D}\right)\right] + h$$

Where;

β_1, β_2 = Parabolic skew parameters
f,h = Fitting coefficients

ln = Natural logarithm

z = Pipeline embedment depth

s_u = Soil undrained shear strength

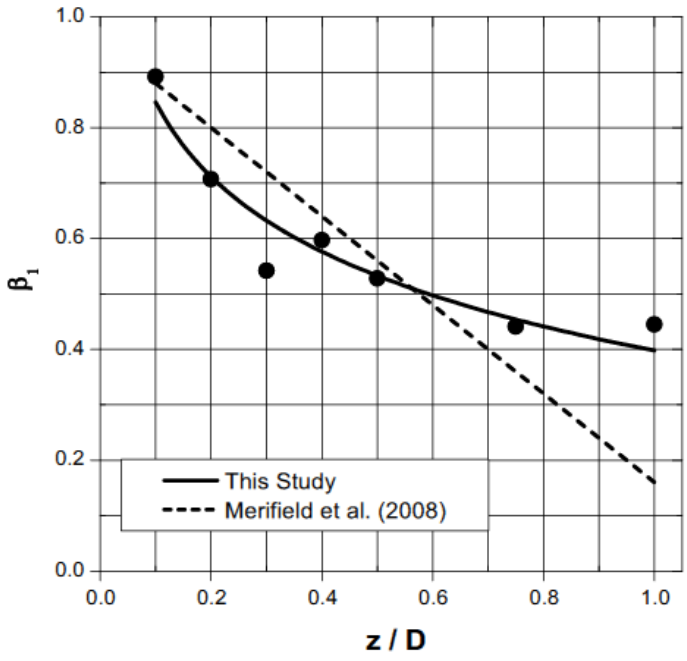

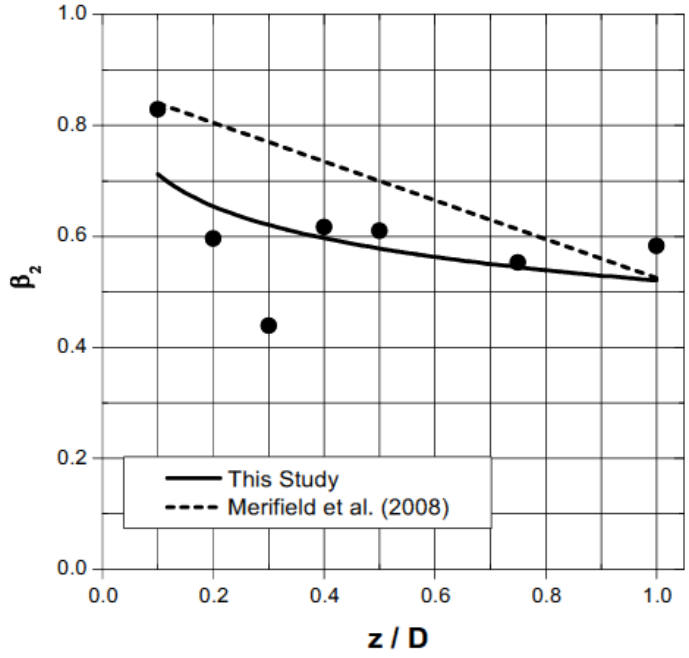

Figure 5.7 *- Changes in the parabolic skew parameters β_1 β_2 with pipeline embedment depth and the fitting equation developed to describe this relationship. Relationship from Merifield et al. (2008) also included.*

	f	*h*
β_1	-0.1948	0.3979
β_2	-0.0830	0.5206

***Table 5.2**: Fitting coefficients for Equation [5.4] and [5.5].*

From Figure 5.7 it can be seen that the proposed relationships provide a reasonable fit to β_1, fitting the trend of the data with some minor scatter. The fit to β_2 exhibits more scatter, in particular the point for z=0.3D, although the relationship still appears to track a general trend. However, while review of Figure 5.7 is of interest the principal criteria for the suitability of these relationships is a comparison between the pipeline stability envelopes and the analysis data. This will be addressed in the remainder of this section.

The stability envelopes produced by Equation [5.2] using skew parameters from Equation [5.4] and Equation [5.5] can be plotted directly in terms of the dimensionless groups V/V_{max} and H/H_{max}, see Figure 5.8. This is a useful format for an initial review of the form of this equation and direct comparison of the geometry of envelopes over a wide depth range. There are some disadvantages with this format for comparison with analysis data and use as a design tool and an alternative format in terms of $V/s_u.D$ and $H/s_u.D$ is presented later in this section.

In reviewing Figure 5.8, and later figures in this section, it is useful to consider during interpretation that β_1 relates to the upper part of the stability envelope from δ=-90° to δ=0° and that β_2 relates to the lower part of the envelope from δ=0° to δ=90°. In Figure 5.8 it can be seen that the lower part of the stability envelope remains a similar shape over the depth range considered, with only relatively small changes approaching H_{max} at δ=0°. This implies that vertical, and close to vertical, pipeline displacement results in a similar failure mechanism over the depth range considered. This also appears to be reflected in the relatively shallow gradient for β_2 in Figure 5.7, the skew parameter relevant to the lower part of the stability envelope.

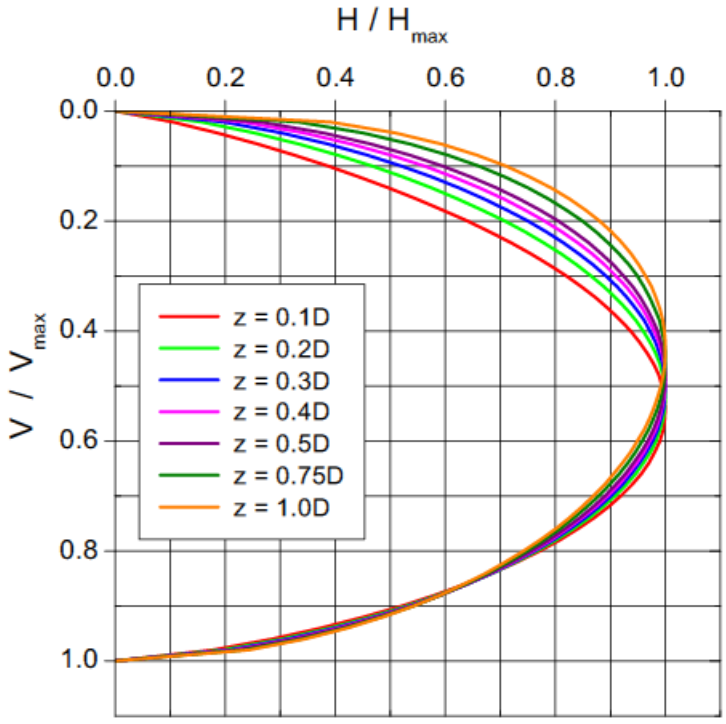

Figure 5.8 *- Results from Equation [5.2] for a range of pipeline embedment depths*

In contrast to the trend in β_2 the skew parameter associated with the upper part of the envelope, β_1, has a steeper gradient and a greater degree of change can be noted in this portion of the stability envelopes. This suggests a significant change in failure mechanism, with increasing embedment, for a pipeline displacement with a degree of uplift i.e. in the range δ=0° to δ=-90°. It can also be noted that the degree of change in the envelope reduces with increasing depth, keeping in mind the change in embedment depth increment from z=0.5D to z=0.75D and z=1.0D. This is also consistent with an effect relating failure mechanism and the soil mobilised for displacement vectors with an uplift angle, as relevant to this area of the stability envelope.

Using the alternative dimensionless groups $V/s_u.D$ and $H/s_u.D$ plots have been prepared for z=0.1D, 0.2D, 0.3D, 0.4D, see Figure 5.9 a to d. The deeper embedment depths of z=0.5D and z=0.75D are shown in Figure 5.10 a to b and z=1.0D in Figure 5.11. Again the proposed relationships for β_1 and β_2 were used.

Reviewing Figure 5.9 shows the proposed stability envelopes provides a good fit to the analysis data in particular for z=0.1D and z=0.4D. Some minor differences can be noted in the lower part of the stability envelopes for z=0.2D

and z=0.3D. This can be attributed to scatter in the V_{max} relationship, as previously noted and discussed earlier in Chapter 4. The value for V_{max} represents a fixed point at δ=90°, where any scatter between the analysis data and the V_{max} fitting relationship will impact the lower part of the stability envelope. The influence of the V_{max} correlation reduces as the envelope trends towards H_{max} at δ=0°. Scatter in the H_{max} relationship was less which is also reflected in the data fit. δ=-90°can be viewed as a fixed point.

The influence of V_{max}, H_{max} and δ=-90° on the stability envelope can also explain some of the effects noted in the plots of the skew parameters β_1 β_2 in Figure 5.7. When a depth specific fit is undertaken then this is based on these three predefined points. The skew parameters then fit the envelope to the analysis data between these fixed points. However, when one or more of these fixed points, such as V_{max} for z=0.3D, diverges from the data there is a tendency for a fit to the skew parameters to be influenced as they try and accommodate offsets near these fixed points. This explains some of the scatter in Figure 5.7. Additionally β_2 relates to the bottom half of the stability envelope and β_1 the upper part of the envelope, explaining the greater scatter in β_2 due to the influence of V_{max}. Despite this effect the objective of developing a fitting relationship that captures the general trend in β_1 β_2 has been achieved. In addition, and more importantly, the objective to produce a good fit to the analysis data across the depth range considered has been achieved, see the Figures 5.9 to 5.11 to review this fit.

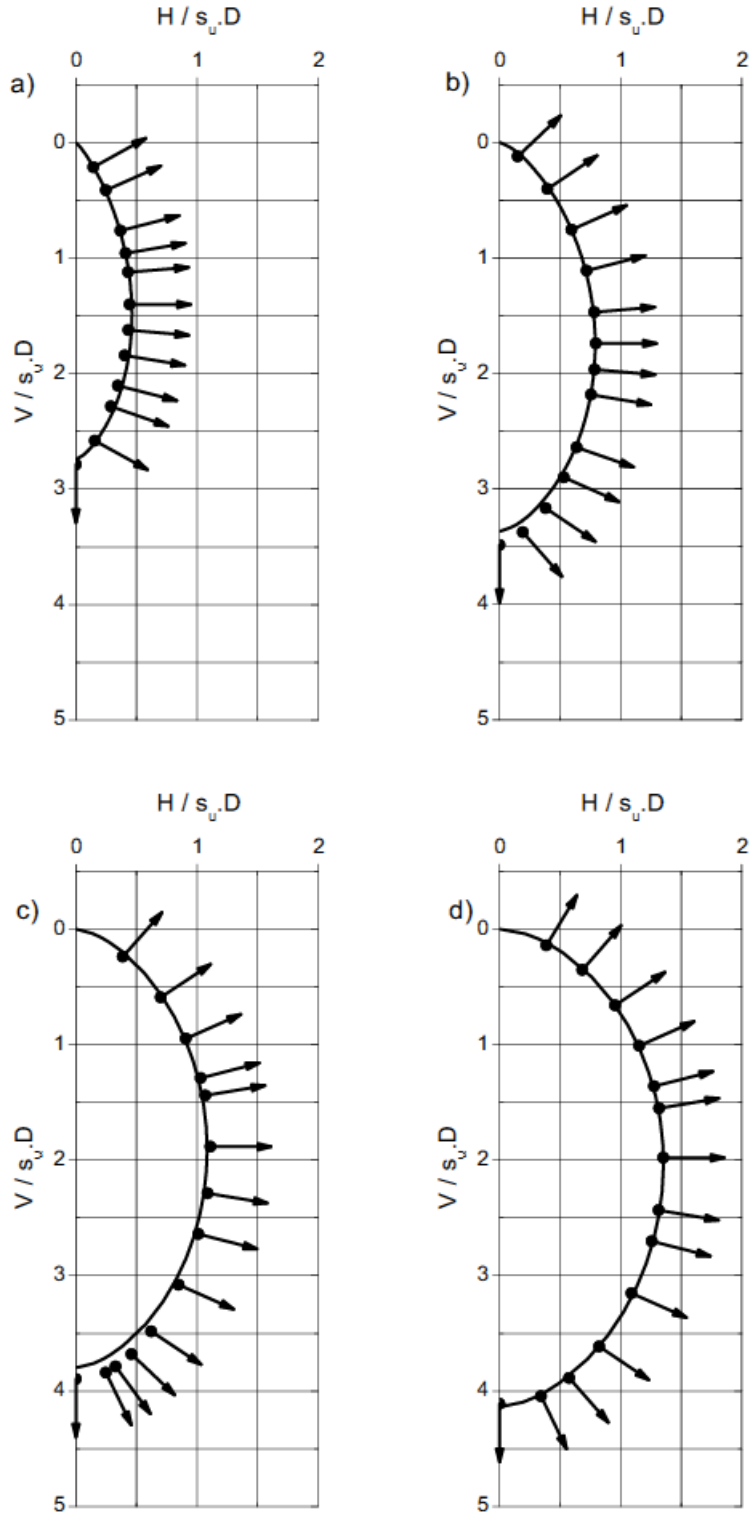

Figure 5.9 a,b,c,d *- V-H pipeline stability envelopes a) z= 0.1D, b) z=0.2D, c) z=0.3D, d) z=0.4D.*

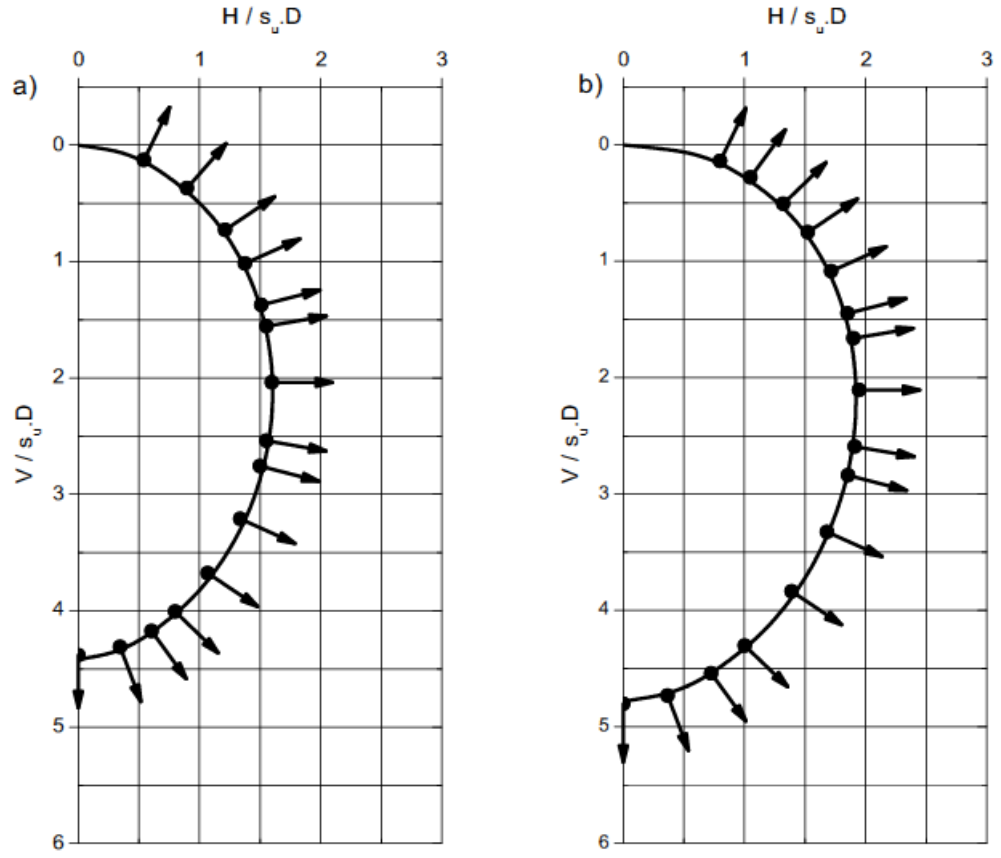

Figure 5.10 a,b *- V-H pipeline stability envelopes a) z=0.5D and b) z=0.75D*

The proposed fitting relationships provide stability envelopes that provide a good fit to the analysis data, with only minor scatter in the areas near V_{max} for some depths, as previously discussed. Comparing the stability envelopes in Figure 5.9 and Figure 5.10a, covering the pipeline embedment depth z=0.1D to z=0.5D, the shape of the envelopes are very similar. There is a gradual increase in the size of the envelope associate with an increase in V_{max} and H_{max}. H_{max} is found at around 50% of V_{max} with the envelope approximately symmetric above and below H_{max}. This in conjunction with the plotted plastic potentials has implications for large displacement behaviour, e.g. ride in and ride out behaviour. For further discussion see Section 5.5.

For depths greater then z= 0.5D, in particular z=1.0D there is gradual change in the shape of the envelope. The upper part of the envelope becomes more bulbous compared to the lower part, with some loss of symmetry in the envelope around H_{max}. This change can be attributed to the effect of soil above the pipeline shoulder below 0.5D. This trend can be expected to continue with

increasing embedment beyond z=1.0D, becoming more marked as the depth of soil above the pipeline shoulder increases. Although there are some changes in shape H_{max} is found at around 45% of V_{max}, only a slight change from the shallower envelopes.

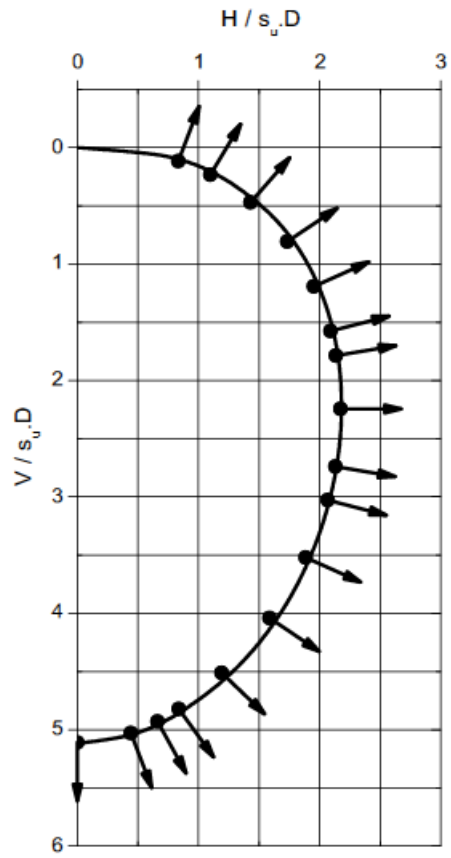

Figure 5.11 *- V-H pipeline stability envelopes for z=1.0D*

A review of the calculated plastic potentials and pipeline stability envelopes in Figure 5.9, Figure 5.10 and Figure 5.11 can be used to confirm the plastic flow rule for these pipeline stability envelopes. From this review the plastic potentials appear to be normal to the stability envelope, i.e. associative flow as assumed in the Tresca soil model, even when there is a slight offset between the analysis data and the fitted stability envelope. A normal flow rule can be used with these stability envelopes and is consistent with the numerical analysis configuration that the stability envelopes are based on.

In addition to the observations of normality a further observation can be made in reviewing the relationship between the stability envelopes and the plastic potentials. Close to $\delta=90^{\circ}$, i.e. pure vertical displacement into the seabed, the

stability envelopes for shallower embedment depths are particularly pointed. This implies that a minor H load component, for example arising from a slight variation in soil strength or a small seabed slope, could result in a relatively large change in the angle of the plastic potential. This suggests that in field conditions some lateral movement may occur during shallow pipeline penetration. At deeper pipeline embedment the stability envelope becomes more rounded and this potential effect reduces.

The analyses reported in this section address some of the analysis cases previously considered by (Merifield et al., 2008). Comparison between this study and (Merifield et al., 2008) will be discussed in Section 5.7. Correlations to produce stability envelopes have been produced, both for the depth range to 0.5D considered by previous researchers and an extension to this range to 1.0D. Plastic potentials were not considered by previous researchers, this has been addressed in this study. Plastic potentials for stability envelope to a pipeline embedment depth of 1.0D have been considered in this section. These plastic potentials have implications for large displacement behaviour, see Section 5.5 for further details. For further discussion of results reported in this section see Section 5.7.

5.2.3 Comparisons with Previous Research

It has previously been noted in Chapter 2 that investigations into H_{max} for a homogenous strength weightless seabed are similar to a study undertaken by Merifield et al. (2008). The scope of this earlier analysis addressed cases up to a pipeline embedment depth of 0.5D. The study reported in this thesis analysed these cases as well extending this type of analysis to a depth of 1.0D, capturing the effects associated with these deeper penetration depth. There was good agreement between analysis results from this study and this earlier work. At shallower pipeline embedment depths the H_{max} fitting equations from this study produce results within <3% of the equations presented by Merifield et al. (2008). From 0.3D to 0.5D results are even closer with a <2% difference. Beyond 0.5D this study showed a change in the gradient of the H_{max} to embedment depth relationship. Fitting equations are provided for this relationship with interpretation supported by vector plots of soil displacement at H_{max}.

As with the H_{max} design problem Merifield et al. (2008) also presented some analysis results and fitting equations for V-H loading of a pipeline on a homogenous strength weightless seabed. Analysis from this study was compared

to this earlier research up to a pipeline embedment depth of 0.5D. This study then extended analysis up to a depth of 1.0D. As with H_{max} good agreement was found between this study and the previous research, an example comparison for a pipeline embedment depth of 0.1D is shown in Figure 5.12. This study showed the evolution of a pipeline V-H stability envelope with depth and provided a new fitting relationship for the β skew parameters.

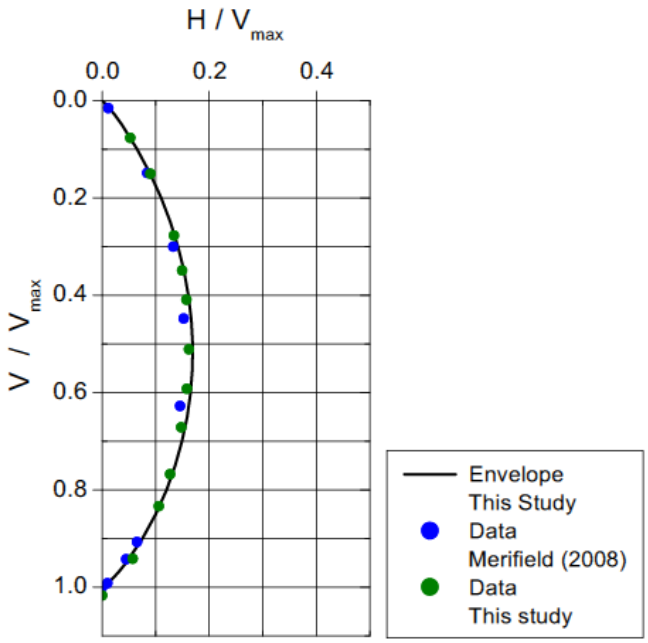

Figure 5.12 *- Example comparison between this study and Merifield et al., (2008), smooth interface pipeline on a homogenous strength weightless seabed at a wished in place pipeline embedment depth of 0.1D.*

5.3 The Effect of a Variable Shear Strength Profile

5.3.1 Maximum Horizontal Capacity (H_{max})

This study has already shown that the behaviour of a pipeline subjected to vertical loading can be in influenced by the presence of seabed soils with a non-uniform shear strength profile in place of a homogenous seabed, see Chapter 4. In addition to the effect on V_{max} previously investigated a linearly increasing shear strength gradient can also be expected to influence the behaviour of a pipeline under V-H loading. This section considers maximum capacity under horizontal loading (H_{max}) in the presence of some linear increasing shear

strength gradients. The next section, Section 5.3.2, considers the effect of a linear increasing shear strength gradient on the full V-H stability envelope.

In this study a linearly increasing shear strength gradient is described by the ratio of the soil undrained shear strength at mudline (s_{u0}) and the shear strength at the pipeline embedment depth (s_{uzp}). Analysis was undertaken for two shear strength gradients, s_{u0}/s_{uzp}=0.5 and s_{u0}/s_{uzp}=0, with the constant shear strength case s_{u0}/s_{uzp}=1.0 also available for comparison purpose, as previously reported in Section 5.2.1. As some information is already available from the constant shear strength case, for example a fitting relationship, a reduced number of embedment depths were considered. These consisted of z=0.1D, 0.3D, 0.5D and z=1.0D. A total of 8 analyses were undertaken with analysis results summarised in Appendix B, Table 2-3.

Analysis considered a pipeline with a perfectly smooth interface condition. Calculations were configured with the same displacement velocities previously used to investigate H_{max} for the constant shear strength case. This was found to be acceptable and produce good quality data, therefore there was no requirements to reduce displacement velocities for this change in shear strength profile. Mesh refinement, as control by the mesh zone dimension (Δ_z), was set to the same as previously used for investigating H_{max}, see section 5.2.1 for further discussion. Details of analysis parameters are summarised in Appendix B, Table 2-3.

In Figure 5.13 analysis results have been plotted in dimensionless form in terms of $H_{max}/s_{uzp}.D$, s_{uzp} is the soil undrained shear strength at the pipeline embedment depth and D is the pipeline diameter. This data is plotted against a dimensionless depth term z/D, where z is the pipeline embedment depth and D the pipeline diameter. Correlations have also been included in Figure 5.13 using the same approach adopted for the constant shear strength case.

The analysis data for these two linear increasing shear strength gradients were fitted to the same relationship previously used for the constant shear strength case, Equation [5.1], reproduced for clarity as Equation [5.6]. Fitting coefficients are shown in Table 5.3.

[5.6] $$H_{max} = c \left(\frac{z}{D}\right)^d V_{max}$$

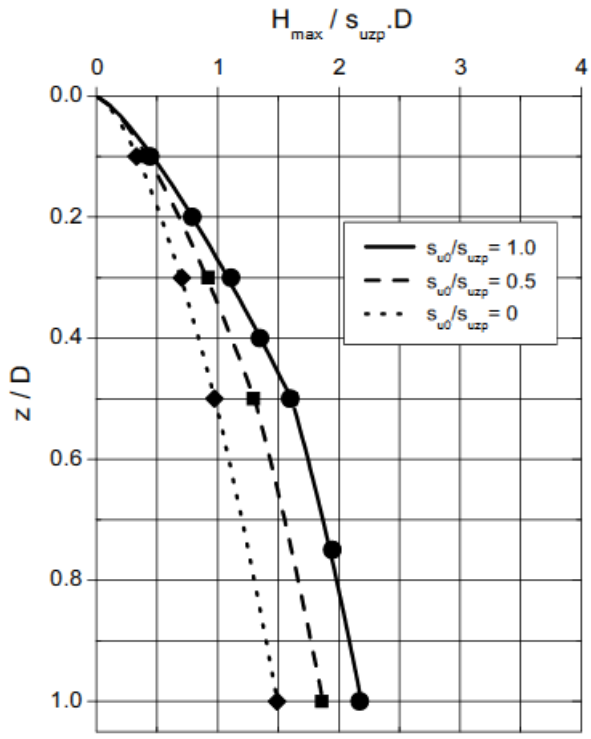

Figure 5.13 *- H_{max} in terms of H_{max} /s_{uzp}.D at a range of embedment depths, z/D, for two linear increasing shear strength gradients and the constant shear strength case.*

Depth Range	Coefficients s_{u0}/s_{uzp}=0.5		Coefficients s_{u0}/s_{uzp}=0	
	c	*d*	*c*	*d*
0.1D to 0.5D	0.437	0.5102	0.347	0.4936
0.5D to 1.0D	0.376	0.2955	0.326	0.4061

Table 5.3*: Fitting coefficients for Equation [5.6].*

With the relatively wide spacing in embedment depths considered here there is the option to undertake further analysis. However, the fitting relationships developed for the two shear strength gradients show the same general trend as the constant shear strength case and the data exhibits minimal scatter around these relationships. On this basis these relationships appear representative without additional analysis. Similarly, while further shear strength gradients could be considered, e.g. s_{u0}/s_{uzp}=0.25, s_{u0}/s_{uzp}=0.75, the cases presented are considered to define the bounds of the problem. The differences between cases,

especially at shallow depth, is also such that additional cases would not add significant refinement to the definition of the problem

For the deeper depth range from z=0.5D to z=1.0D the limited analysis cases presented a potential challenge. Based on the relationships at depth following the same general form as the constant shear strength case some nominal fictitious data points were developed at z=0.75D within the fitting spreadsheet. These data points were not based on actual analysis, but took an average of the offset between data points at 0.5D and 1.0D, forming a similar curvature as the constant shear strength case. It is not expected that this approach has introduced a significant error, however this could be investigated further if this was an area of particular interest.

In contrast with V_{max} the presence of a shear strength gradient always results in a reduction in H_{max}, even at the shallowest depths considered here. A horizontal displacement at $\delta=0^{\circ}$ would appear to always be influenced by the presence of lower shear strength soils above pipeline embedment depth, as associated with a linear increasing shear strength profile. This contrasts with $\delta=90^{\circ}$ where for some case a higher shear strength soil below the pipeline embedment depth can have an influence on the problem, as previously discussed in Chapter 4.

At z=0.1D the small values for H_{max} make a pattern difficult to discern in Figure 5.13. However, both $s_{u0}/s_{uzp}=0$ and $s_{u0}/s_{uzp}=0.5$ produce a lower resistance then $s_{u0}/s_{uzp}=1$. The lowest resistance is for the $s_{u0}/s_{uzp}=0$ case, which at 26% less the constant shear strength case at this depth. With increasing embedment depth $s_{u0}/s_{uzp}=0$ continues to produce the lowest value of H_{max}, with $s_{u0}/s_{uzp}=0.5$ representing an intermediate case. The influence of shear strength gradient appears to increase across the depth range z=0.1D to z=0.5D resulting in both a larger absolute effect, as well as proportionally larger effect. Over the depth range z=0.5D to z=1.0D the influence of the shear strength profile appears to be almost constant, becoming a smaller proportion of resistance as absolute resistance continues to increase with depth. As with many aspects of this study it would appear that there is a change behaviour at depths greater then z=0.5D.

In addition to the analysis results presented in Figure 5.13 the calculated soil displacement at H_{max} was also reviewed. Vector plots have been produced from these calculations with these shown in Figure 5.14 for z=0.3D, Figure 5.15 for z=0.5D and Figure 5.16 for z=1.0D. No vector plot is presented for z=0.1D. At z=0.1D the differences in displacement mechanisms were difficult to discern, in

conjunction with low values of H_{max}, a plot for this embedment depth therefore contributes little to the understanding of the problem.

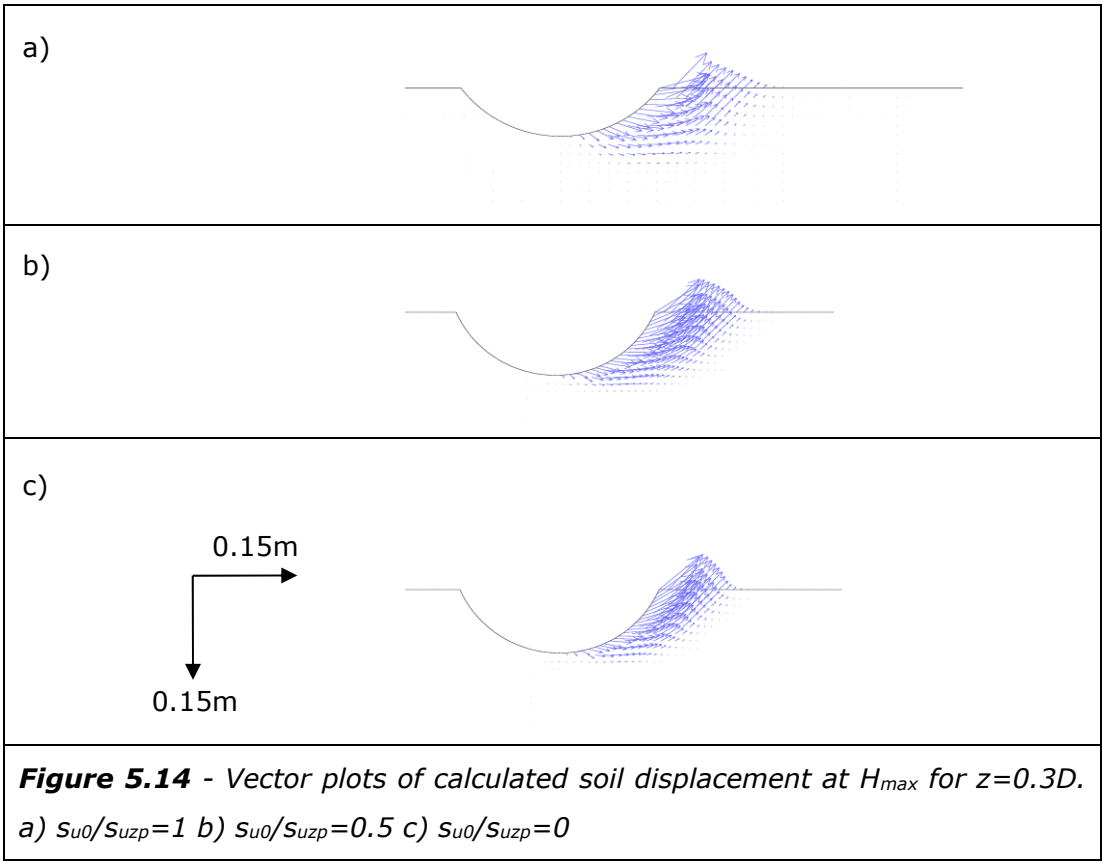

Figure 5.14 *- Vector plots of calculated soil displacement at H_{max} for z=0.3D. a) s_{u0}/s_{uzp}=1 b) s_{u0}/s_{uzp}=0.5 c) s_{u0}/s_{uzp}=0*

Figure 5.14 shows the effect of the two linear increasing shear strength gradients at an embedment depth of z=0.3D. The most marked contrast is between s_{u0}/s_{uzp}=0 and s_{u0}/s_{uzp}=1. Unsurprisingly these two cases also differ the most in the value of H_{max} obtained in analysis. For s_{u0}/s_{uzp}=1 it can be seen that a relatively circular displacement mechanism has developed, extending below the pipeline embedment level. For the s_{u0}/s_{uzp}=0 case the soil below the pipeline embedment depth has a higher shear strength, which has had the effect of truncating the displacement mechanism. The overall width of the mechanism is also reduced slightly for this case. The combination of a smaller mechanism which is also concentrated towards lower shear strength soil above the pipeline embedment depth is consistent with the lower value of H_{max} calculated for this case. s_{u0}/s_{uzp}=0.5 is an intermediate case in resistance with the displacement mechanism also showing intermediate behaviour between the observations for the s_{u0}/s_{uzp}=1 and s_{u0}/s_{uzp}=0 cases.

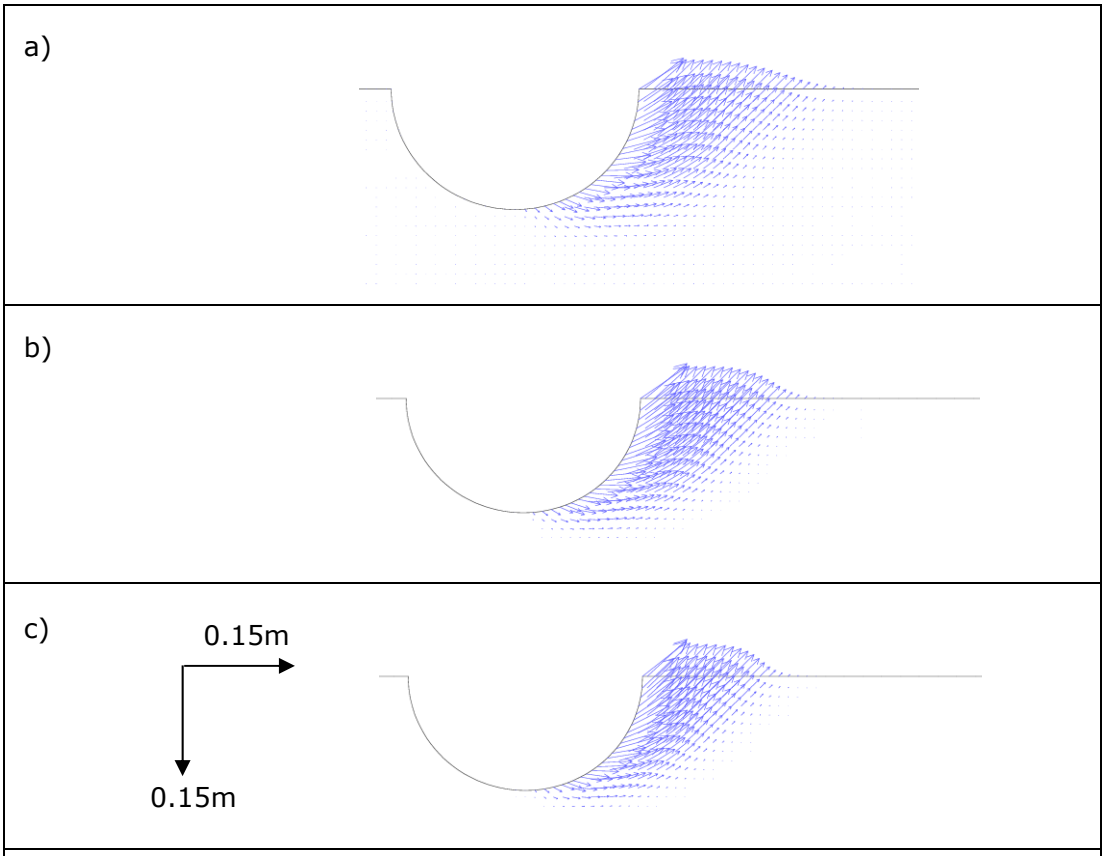

Figure 5.15 *- Vector plots of calculated soil displacement at H_{max} for z=0.5D. a) s_{u0}/s_{uzp}=1 b) s_{u0}/s_{uzp}=0.5 c) s_{u0}/s_{uzp}=0*

Figure 5.15 shows the effect of an increase in embedment depth to z=0.5D. As for Figure 5.14 the biggest difference is between s_{u0}/s_{uzp}=0 and s_{u0}/s_{uzp}=1. However, the truncation of the displacement mechanism below the pipeline embedment depth for s_{u0}/s_{uzp}=0 is less marked then at shallower depth. This can be attributed to the shear strength gradient being shallower as pipeline embedment depth increases. The effect on the width of the mechanism is now more marked then at shallower depth, and it can be noted that a progressively smaller mechanism occurs for s_{u0}/s_{uzp}=0.5 and s_{u0}/s_{uzp}=0, when compared to s_{u0}/s_{uzp}=1. Additionally the smaller mechanisms are also located within lower shear strength soil above the pipeline embedment depth.

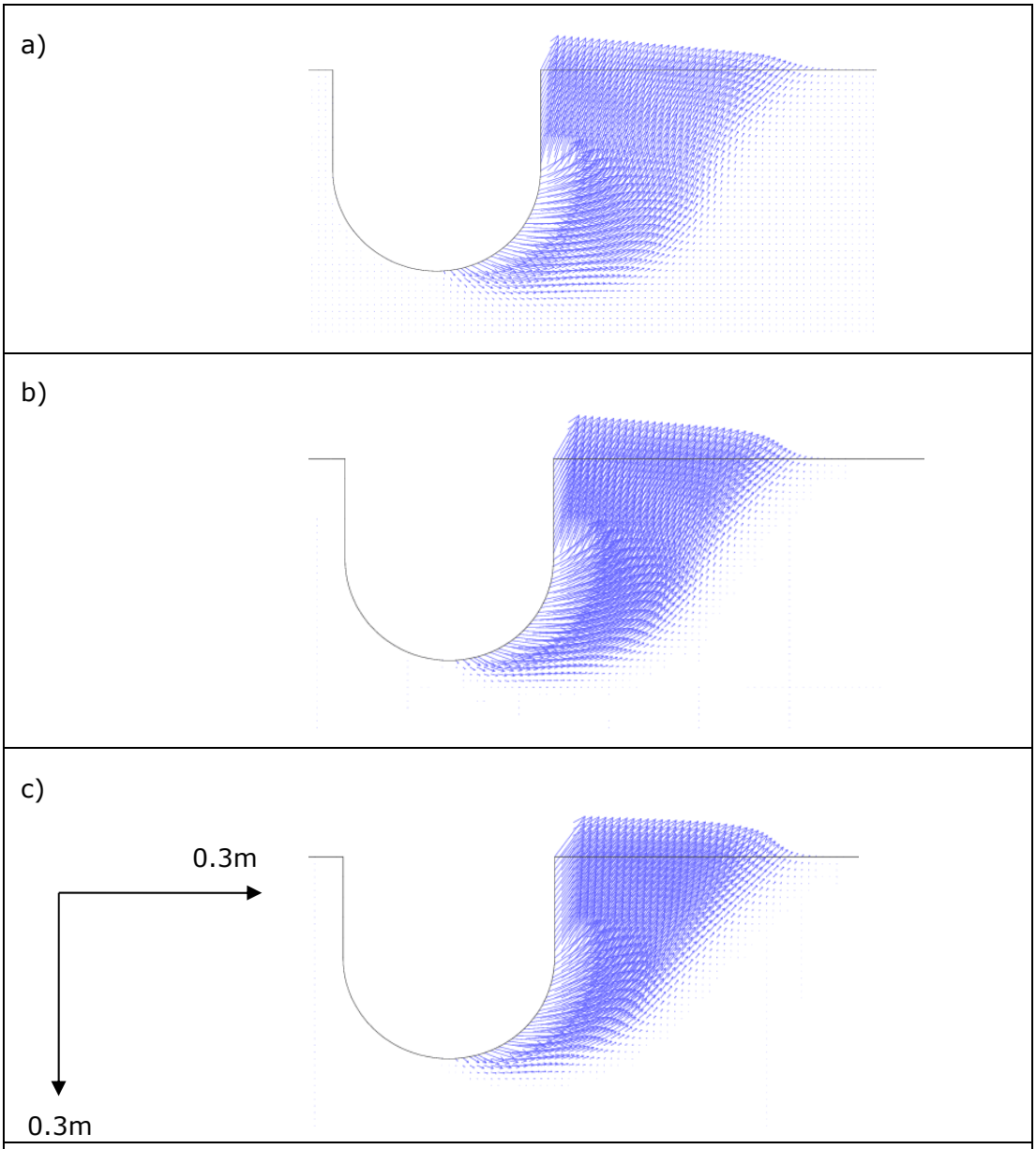

Figure 5.16 *- Vector plots of calculated soil displacement at H_{max} for z=1.0D. a) s_{u0}/s_{uzp}=1 b) s_{u0}/s_{uzp}=0.5 c) s_{u0}/s_{uzp}=0*

Figure 5.16 considers soil displacement at z=1.0D, the deepest depth in this analysis. At this embedment depth truncation towards the base of the displacement mechanism appears to be minimal, even for s_{u0}/s_{uzp}=0. The principal effect of the shear strength gradient is on the width and geometry of the displacement mechanism. It can be seen that the displacement mechanism for s_{u0}/s_{uzp}=0 is narrower than for s_{u0}/s_{uzp}=0.5, and markedly less than for s_{u0}/s_{uzp}=1. This thinning is largely concentrated towards the bottom of the mechanism. Associated with this observation, it can be seen that the mechanism for s_{u0}/s_{uzp}=0 is more circular in geometry with similarities to displacement

mechanisms at a shallower pipeline embedment depth. This is likely to be attributable to the lower shear strength material being sheared for this case.

5.3.2 V-H Loading

A suite of analyses was undertaken to extend investigations into the effect of a linearly increasing soil shear strength gradient from a pipeline subject to vertical (δ=90°) or horizontal loading (δ=0°) to a full V-H stability envelope. Pipeline embedment depths of z=0.1, 0.3, 0.5, 1.0 were analysed for two shear strength gradients, s_{u0}/s_{uzp}=0 and s_{u0}/s_{uzp}=0.5. The constant shear strength case, s_{u0}/s_{uzp}=1, was also available for comparison purposes, as previously reported in Section 5.2.2. A total of 116 analyses were undertaken, the results of which are summarised in Table 2-4, Appendix B.

As with the previous V-H analysis, Section 5.2.2, the objective was to calculate a series of termination points and plastic potentials around the pipeline stability envelope in V-H load space. Analysis progressed on the basis of the same pipeline displacement angles used for the uniform shear strength case. The minimum displacement angle previously used for the uniform shear strength cases were found to adequately define the upper part of the stability envelope, ranging from δ=-30° at z=0.1D to δ=-70° at z=1.0D. The location of the termination points for a given displacement angle changed from the uniform shear strength case and between the two shear strength gradients. However, the displacement angles previously used still produced adequate definition of the V-H envelope and there was no requirement for adjustment or additional cases to be analysed. The mesh dimensions used in this analysis were the same as used for the uniform shear strength case. The same displacement velocities were also used, which was found to produce acceptable data. A summary of analysis parameters is also provided in Table 2-4, Appendix B.

The V-H analysis suite reported in this section included analysis of V_{max} at δ=90°. The effect of changes in analysis configuration were checked by comparing these results to the analyses previously presented in Chapter 4. Typically these two sets of analysis were within <1.0% of each other and in all cases within <1.5%. This was considered acceptable.

Following the approach previously used in Section 5.2.2 for the constant shear strength case, Equation [5.2] was fitted to the analysis data for each pipeline embedment depth and s_{u0}/s_{uzp} ratio. Skew parameters β_1, β_2, were obtained for

each case. These skew parameters are plotted in Figure 5.17 for $s_{u0}/s_{uzp}=0$ and Figure 5.18 for $s_{u0}/s_{uzp}=0.5$. Equation [5.4] and Equation [5.5] were used to provide a fit against embedment depth to the skew parameters, with this fit also show in Figure 5.17 and Figure 5.18. The fitting coefficients for Equation [5.4] and Equation [5.5] are provided in Table 5.4.

	$s_{u0}/s_{uzp}=0$		$s_{u0}/s_{uzp}=0.5$	
	f	*h*	*f*	*h*
β_1	-0.1431	0.4718	-0.1696	0.4181
β_2	-0.1174	0.5068	-0.1250	0.4840

Table 5.4*: Fitting coefficients for use with Equation [5.4] and [5.5].*

Reviewing Figure 5.17 and Figure 5.18 it can be seen that the proposed logarithmic relationships provide a similar quality fit to the skew parameters as previously obtained for the uniform shear strength case. In both cases, $s_{u0}/s_{uzp}=0$ and $s_{u0}/s_{uzp}=0.5$, the fit to β_1 is good with little scatter and a close tracking of the trend in β_1. β_1 relates to the skew of the upper half of the V-H stability envelope from $\delta=0^\circ$ to $\delta=-90^\circ$. As previously the skew for the lower half of the envelope $\delta=0^\circ$ to $\delta=90^\circ$, described by the parameter β_2, exhibits a greater degree of scatter. It is expected this relates to the skew parameters trying to accommodate variation in the fit to V_{max} correlation in the area of the stability envelope closer to $\delta=90^\circ$. This will be considered further when comparing the fit the proposed envelopes provide to the analysis data, later in this section.

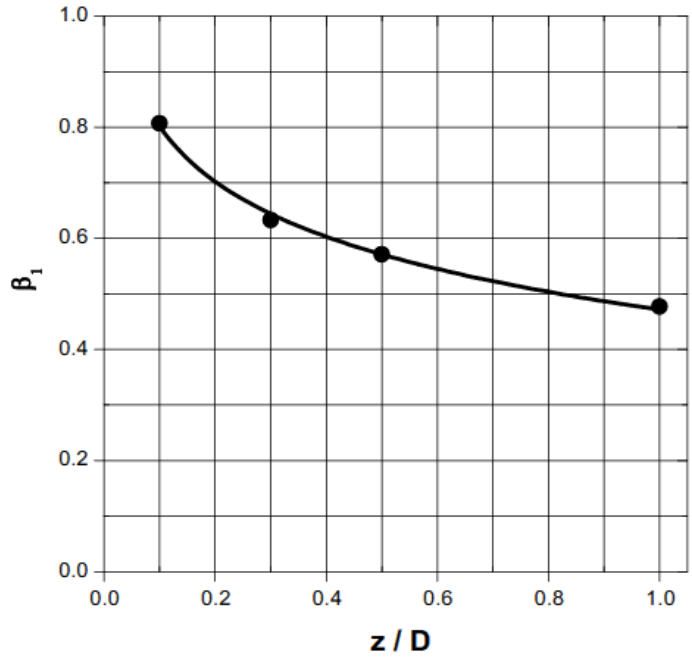

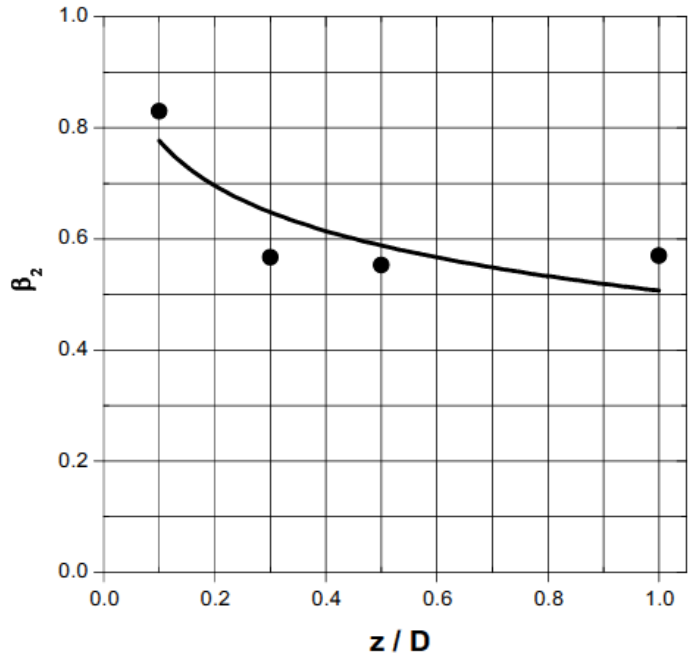

Figure 5.17 *- Parabolic skew parameters β_1 β_2 and fitting relationships for $s_{u0}/s_{uzp}=0$.*

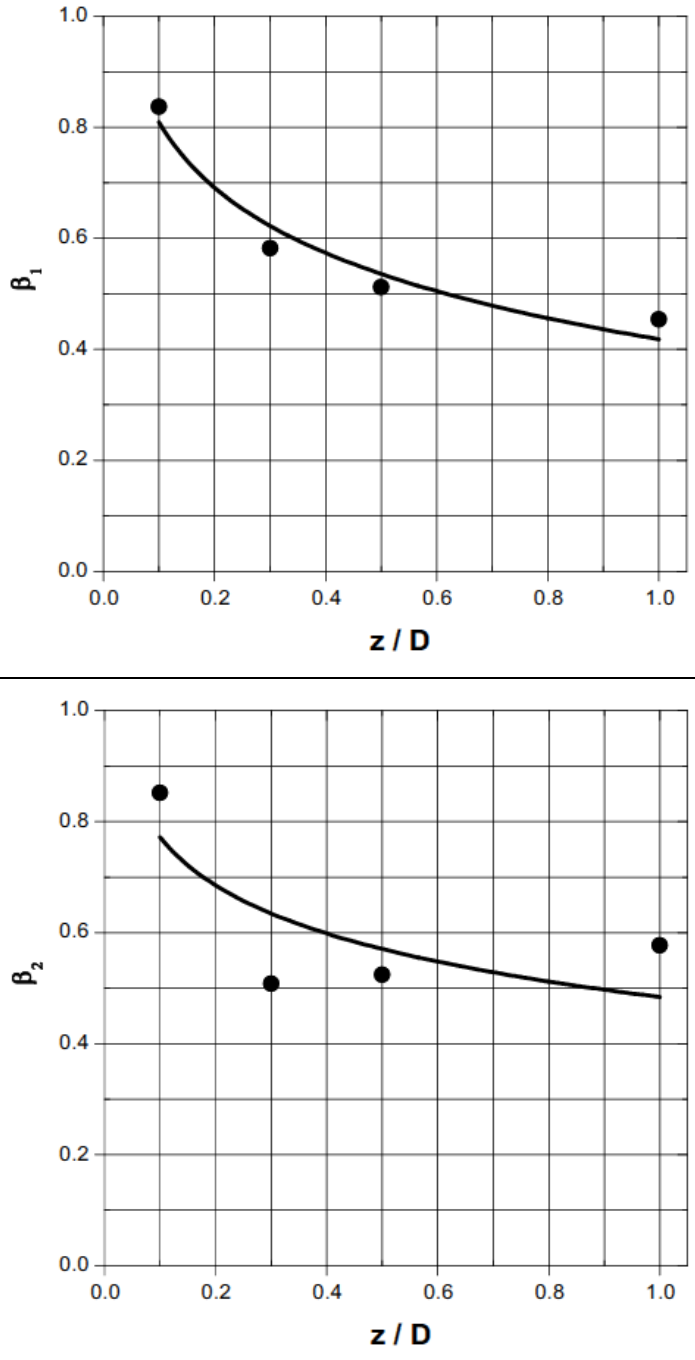

Figure 5.18 *- Parabolic skew parameters β_1 β_2 and fitting relationships for $s_{u0}/s_{uzp}=0.5$.*

The fit to the skew parameters in Figure 5.17 and Figure 5.18 look very similar, as well looking similar to those previously presented for the constant shear strength case. A closer comparison between these cases is of interest, as having previously considered the effect on V_{max} and H_{max} changes completes the question; does the presence of a linear increasing shear strength gradient

change the shape of a pipeline V-H stability envelope. These comparisons are plotted in Figure 5.19.

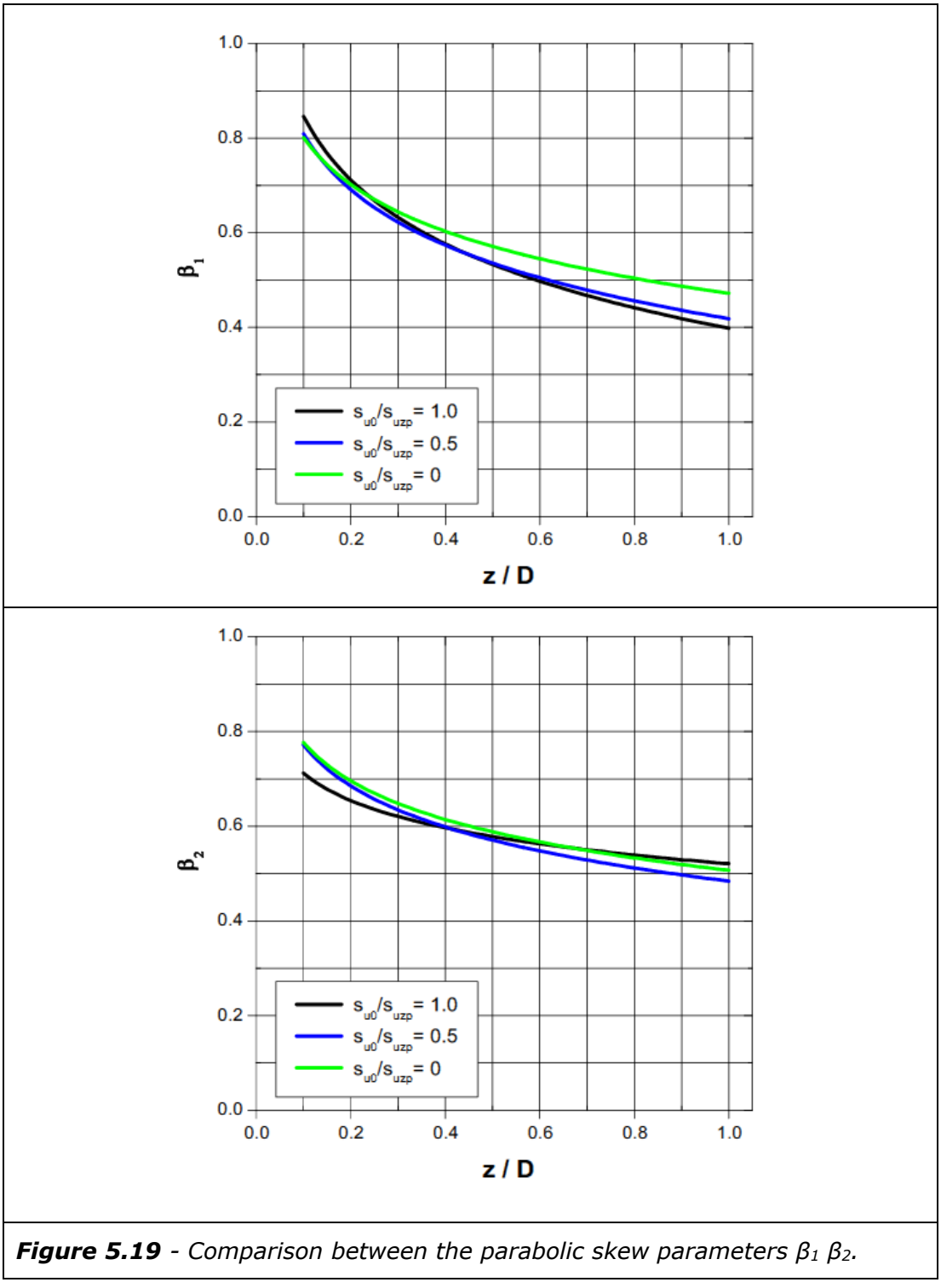

Figure 5.19 *- Comparison between the parabolic skew parameters β_1 β_2.*

Figure 5.19 shows that β_1 for the case of s_{u0}/s_{uzp}=1.0 and s_{u0}/s_{uzp}=0.5 are very similar, similar enough for the variation to be attributed to the analysis and fitting methodology rather than a physical effect. The constant shear strength

case, $s_{u0}/s_{uzp}=1.0$, and a shear strength gradient of $s_{u0}/s_{uzp}=0.5$ do not have an influence on the skew of the upper part of the stability envelope. The presence of the most extreme shear strength gradient, $s_{u0}/s_{uzp}=0$ does appear to have a small influence on the skew of the upper part of the V-H stability envelope. However, only at deeper embedment depth. It is likely this is related to some of the pipeline displacement vectors with a large uplift component interacting with very low shear strength soil associated with a zero strength intercept at mudline.

Having, previously noted the scatter in the β_2 parameter less weight should be attached to variation in the fit to this parameter. However, even with this scatter the similarity over the full range of shear strength variation considered is high. The β_2 parameter relates to the shape of the bottom half of the pipeline V-H stability envelope and from this data it can be seen that the presence of a linear increasing shear strength gradient has only a minor effect on the skew of the lower portion of the pipeline V-H stability envelope. A minor effect can be noted at shallow embedment depth, approximately less then z=0.3D, where the two linear shear strength gradients differ slightly from the constant shear strength case. This would appear to be related to the effect of the very high shear strength soil that occurs below the pipeline embedment depth within the shear strength gradient description framework of a s_{u0}/s_{uzp} ratio. However, even at these extremes the effect is minor.

Given the similarities in β_1 and β_2 over a very wide range of shear strength gradients a fit to all the skew parameter data may be of interest. This fit to all the data was undertaken, with the relevant coefficients presented in Table 5.5. However, for increase accuracy in particular for the purposes of comparison with analysis data the shear strength gradient specific fits previously presented in Table 5.4, will be used later in this section.

	f	*h*
β_1	-0.1718	0.4252
β_2	-0.1063	0.5046

***Table 5.5**: Fitting coefficients for Equation [5.4] and [5.5].*

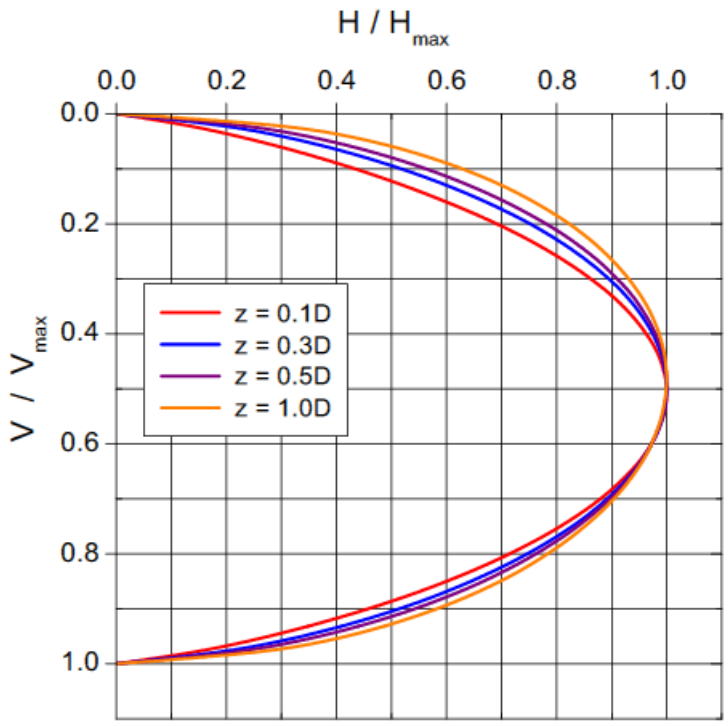

Figure 5.20 *- V-H stability envelopes for $s_{u0}/s_{uzp}=0$*

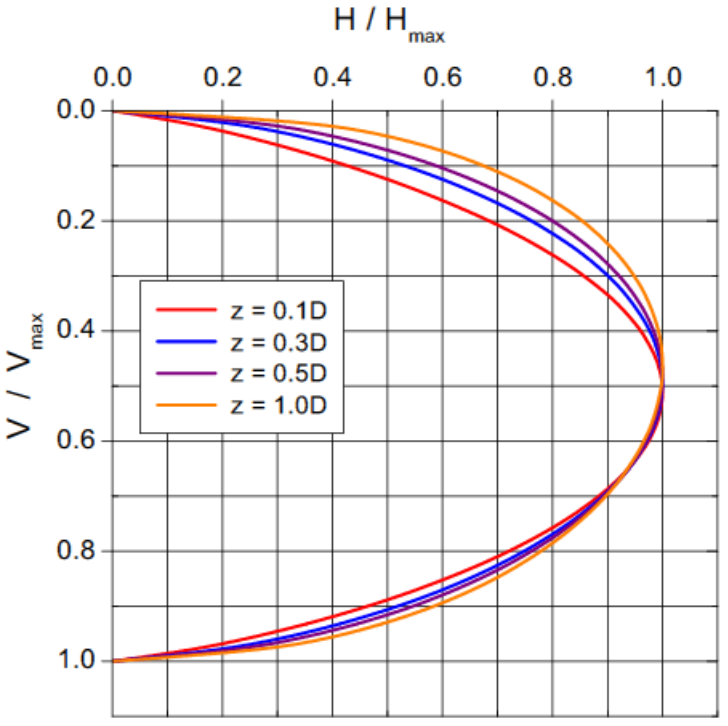

Figure 5.21 *- V-H stability envelopes for $s_{u0}/s_{uzp}=0.5$*

V-H stability envelopes were produced using the V_{max} and H_{max} correlations from previous sections and the skew parameter correlation coefficients detailed in Table 5.4. These stability envelopes have been presented in two formats. The first approach is in terms of the V/V_{max} and H/H_{max}, see Figure 5.20 and Figure 5.21 for $s_{u0}/s_{uzp}=0$ and $s_{u0}/s_{uzp}=0.5$ respectively. The second format adopted was to present the stability envelopes and analysis data in terms of $V/s_u.D$ and $H/s_u.D$ See Figure 5.22, Figure 5.23 and Figure 5.24.

Figure 5.20 and Figure 5.21 can be compared with Figure 5.8 in Section 5.2.2, which represents the uniform shear strength case. The most obvious difference that can noted in the presence of a linear increasing shear strength gradient is that a change in pipeline embedment depth leads to a change in the shape of both the upper and lower half of the V-H stability envelope. Whereas for a uniform shear strength seabed soil the changes in the envelope with depth were largely confined to the upper portion of the stability envelope, close to $\delta=0^{\circ}$ and through towards $\delta=-90^{\circ}$. For the constant shear strength case this change was attributed to the change in soil depth alongside the pipeline and the differences in the amount of soil mobilised for a given displacement vector in this range. For the linear increasing the shear strength cases the strength of the soil also changes below the pipeline, which appears to effect the shape of the lower portion V-H stability envelope. The change in the upper part of the envelope is still present for the linear increasing shear strength cases, being slightly more marked then the lower portion of the envelope. This can be attributed to a combination of a change in soil depth to the side of the pipeline and the influence of the shear strength gradient on the strength of this soil.

Comparing the stability envelopes for the $s_{u0}/s_{uzp}=0$ and $s_{u0}/s_{uzp}=0.5$ shear strength gradients with each other shows less difference then when these two cases are compared to the constant shear strength case of $s_{u0}/s_{uzp}=1.0$. The lower part of the stability envelope, in particular, is very similar for both cases. There is a significant difference in shear strength gradient steepness between a $s_{u0}/s_{uzp}=0$ and $s_{u0}/s_{uzp}=0.5$. However, the similarities between the stability envelopes for these two cases suggest that it is a variation in shear strength below pipeline embedment level that results in a change in envelope shape rather than a specific effect related to a specific shear strength gradient, or a progressive effect that changes in magnitude with changing gradient.

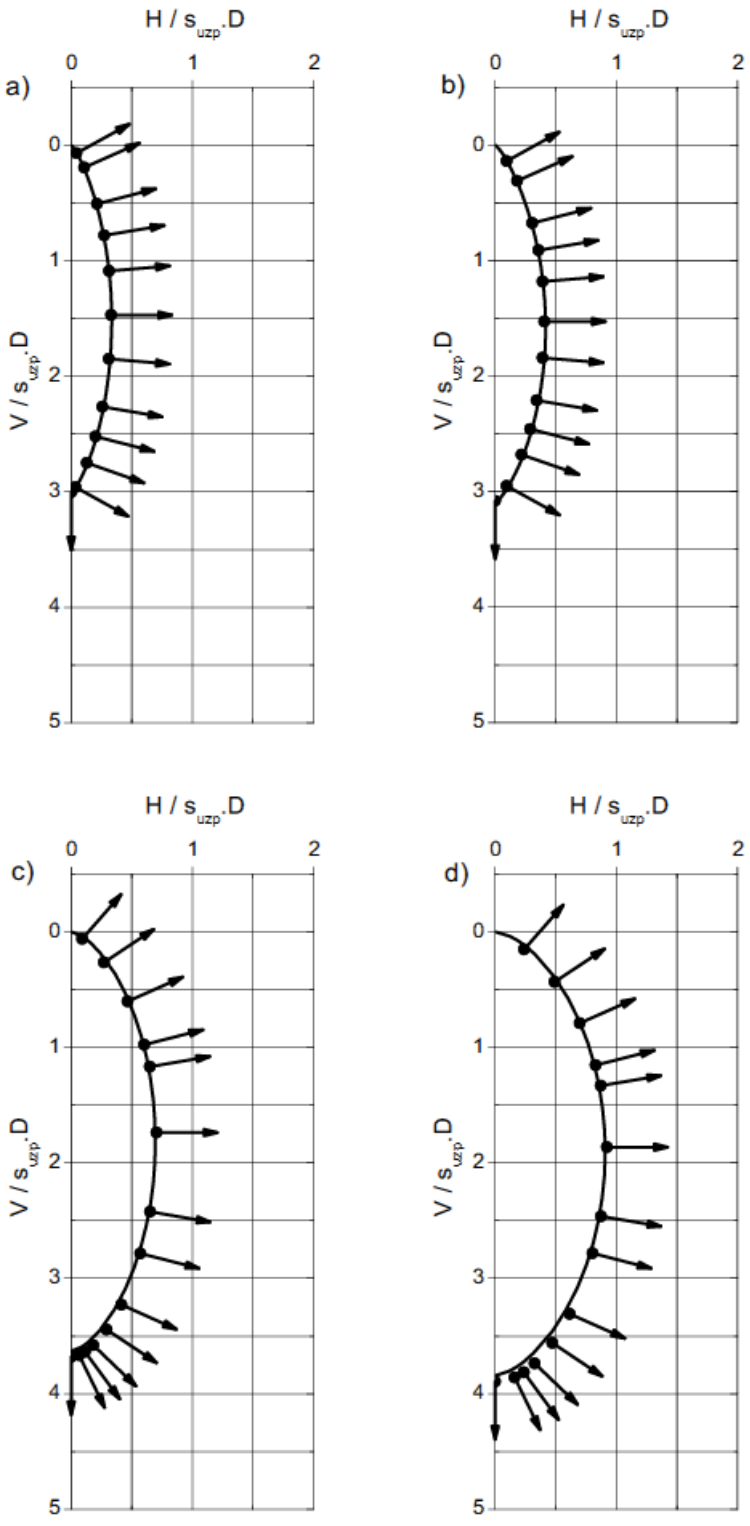

Figure 5.22 a,b,c,d *- V-H pipeline stability envelopes a)0.1D s_{u0}/s_{uzp}=0, b)0.1D s_{u0}/s_{uzp}=0.5, c)0.3D s_{u0}/s_{uzp}=0, d)0.3D s_{u0}/s_{uzp}=0.5*

As for the constant shear strength case, stability envelopes presented in terms of the dimensionless groups $V/s_u.D$ and $H/s_u.D$ represent a more robust format for application to design practice as well as providing a useful means of comparing the proposed stability envelopes with analysis data. Figure 5.22, Figure 5.23 and Figure 5.24 show stability envelopes for the case of $s_{u0}/s_{uzp}=0$ and $s_{u0}/s_{uzp}=0.5$ at an embedment depth of z=0.1D, 0.3D, 0.5D and z=1.0D.

Figure 5.22 shows good agreement between the proposed stability envelopes and analysis data. As with the uniform shear strength case a small amount of scatter can be noted between analysis and the stability envelopes towards V_{max} e.g. z=0.3D with $s_{u0}/s_{uzp}=0.5$. As previously this relates to scatter in the V_{max} relationship and is considered negligible. Calculated plastic potentials show that associated plastic flow is also reasonable for the stability envelopes produced for these linear increasing shear strength gradient cases.

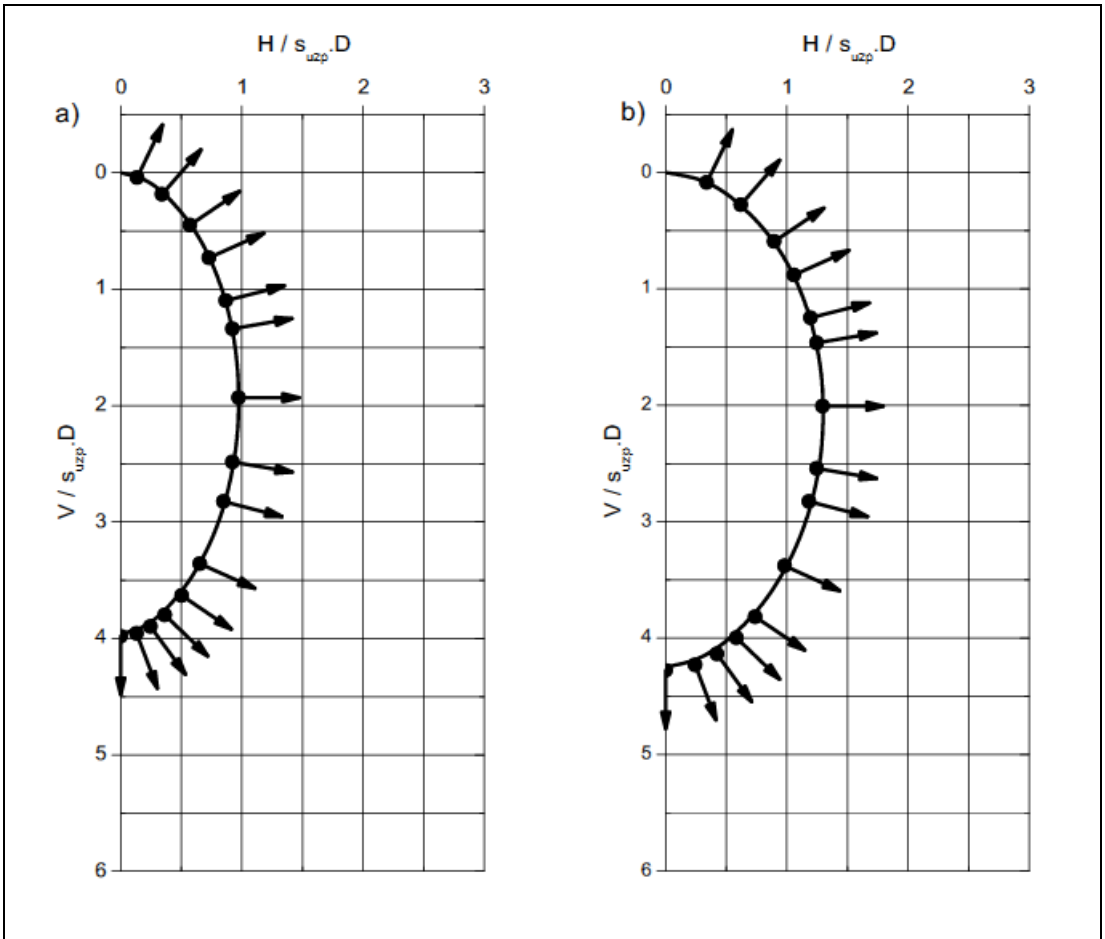

Figure 5.23 a,b *- V-H pipeline stability envelopes z=0.5D a) $s_{u0}/s_{uzp}=0$ b) $s_{u0}/s_{uzp}=0.5$*

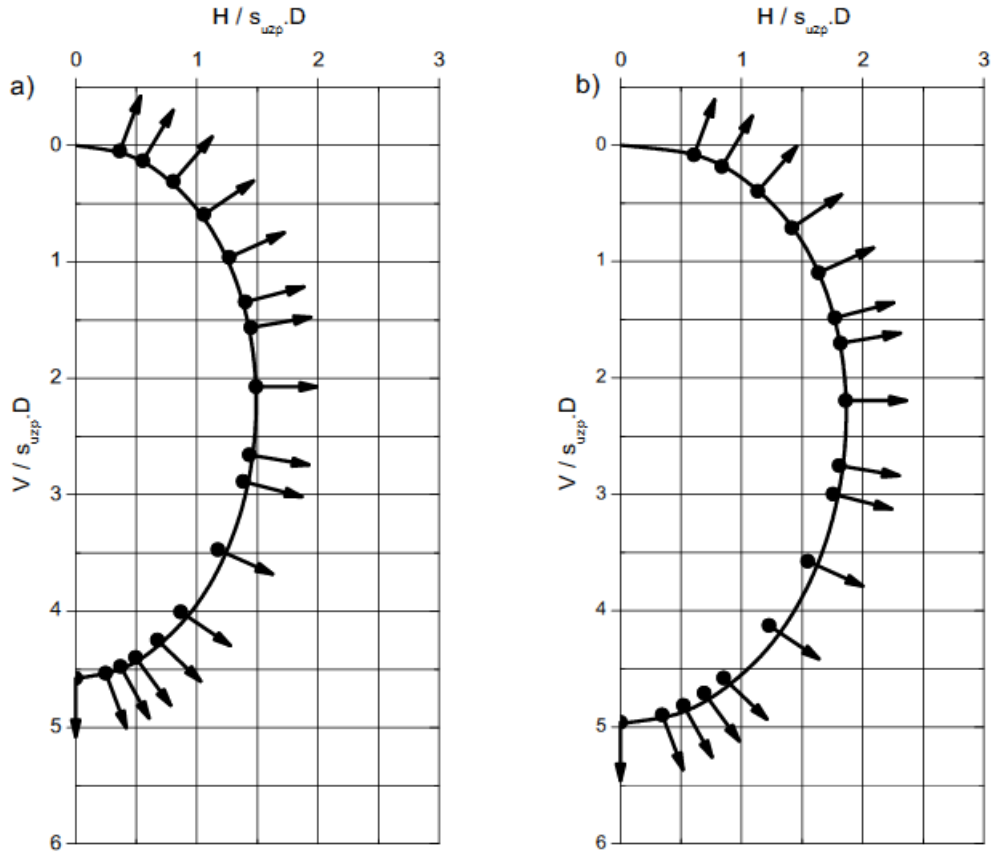

Figure 5.24 a,b *- V-H pipeline stability envelopes z=1.0D a) s_{u0}/s_{uzp}=0 b) s_{u0}/s_{uzp}=0.5*

Figure 5.23 and Figure 5.24 show the deeper pipeline embedment depths. These plots also show reasonable agreement between the analysis data and the proposed stability envelopes. Scatter around V_{max} would appear to be less, although at the z=1.0D there is scatter between data and the stability envelope in the lower part of the envelope. This does not relate to the V_{max} relationship, but to the β_2 fitting relationship, the amount of skew in the lower part of the stability envelope. This scatter, as with that previously noted for V_{max}, is also negligible. However, if analyses are extended beyond 1.0D this may need to be considered further. As with the shallow depth plots the plastic potentials indicate associated flow provides a good representation of post failure behaviour across different shear strength cases, consistent with the with the material flow rule used in the analyses these stability envelopes are derived from.

Having established good agreement between the proposed stability envelopes and the analysis data, the effect of a linear increasing shear strength gradient

can also be investigated by comparing the stability envelopes for different gradients and the uniform shear strength case. This has been done in Figure 5.25 and Figure 5.26.

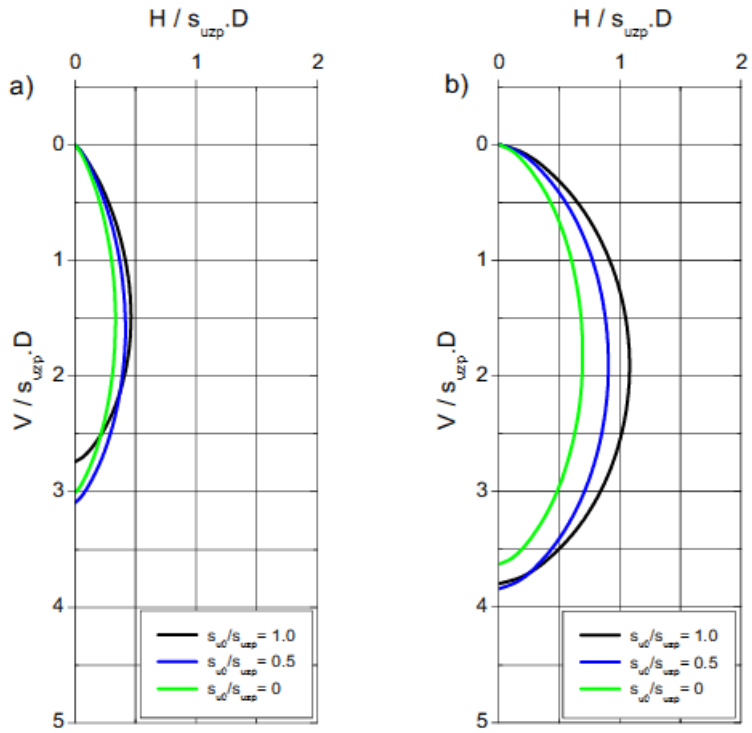

Figure 5.25 a,b *- V-H pipeline stability envelopes a) z=0.1D and b) z=0.3D*

Figure 5.25a shows the shallowest pipeline embedment depth. This is a relatively cluttered plot with small overlapping stability envelopes impacted by the relatively complex pattern in V_{max} previously noted, whereby a shear strength gradient can increase V_{max} elongating the envelope. With increasing depth, Figure 5.25b and Figure 5.26, the simpler V_{max} relationship results a simpler relationship between envelopes. From Figure 5.25b the presence of a linear increasing shear strength gradient reduces the size of the envelope compared to the uniform shear strength case, also reflecting the trends in H_{max}. All envelopes increase in size with embedment depth, with the shear strength gradient effecting the degree to which this occurs. The uniform shear strength envelope at 1.0D is the largest envelope

An additional observation that can be made with respect to the stability envelope shape relates to the value of V at which H_{max} occurs. For the constant shear strength this was noted to occur at approximately 50% of V_{max} for a shallow pipeline depth, with some asymmetry in the envelope developing as H_{max}

trended towards approximately 45% of V_{max} at deepest depths considered in this study. This same trend can also be noted in the stability envelopes presented in this section, with no significant differences between linear increasing shear strength gradients and the constant strength case.

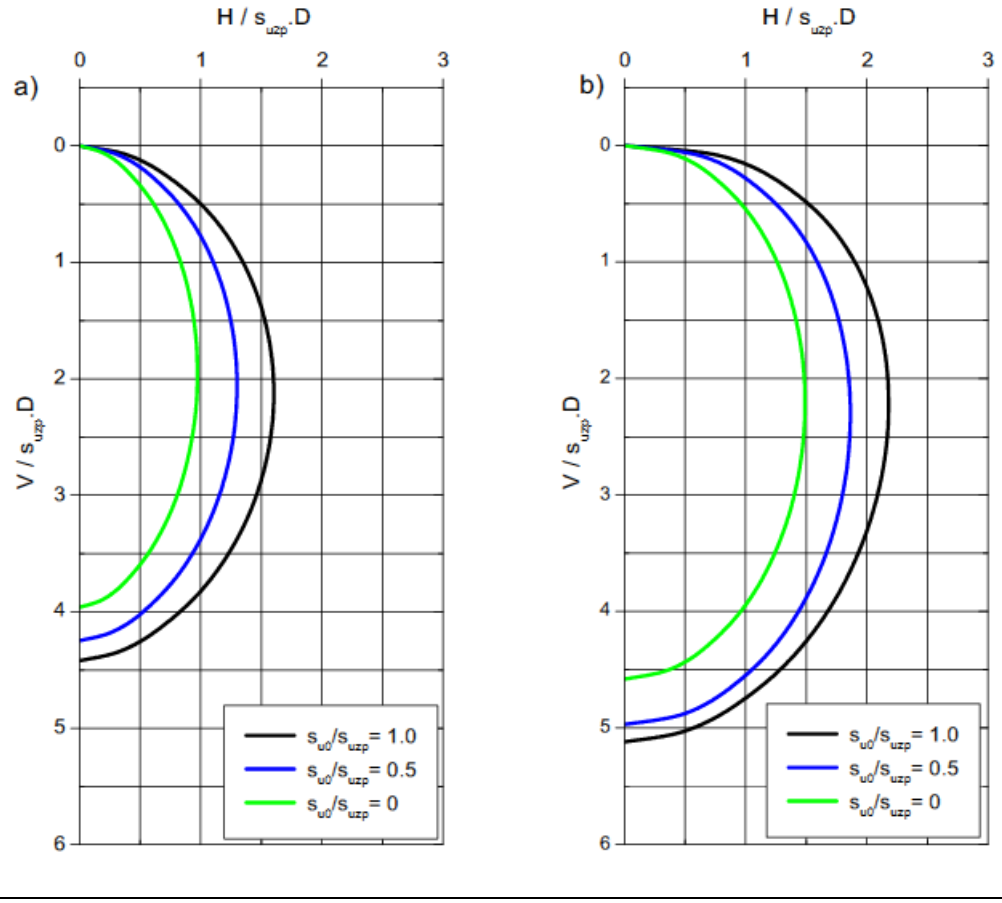

Figure 5.26 a,b *- V-H pipeline stability envelopes a) z=0.5D and b) z=1.0D*

For further discussion of the findings presented in this section see Section 5.6

5.4 Pipelines Subjected to V-H Loading on a Sloping Seabed

In Chapter 3 a problem definition was given for a pipeline subjected to combined Vertical (V) and Horizontal (H) loading on a sloping seabed. An analysis methodology for investigating this problem was described, both a general method for a weightless seabed and an approach to investigate soil unit weight effects. The analysis results summarised in this section have previously been reported in Morrow and Bransby (2009).

For a weightless seabed case the concept of a local coordinate system parallel to the seabed slope is used, see Section 3.3.5 for further details. The conversion from this local coordinate system to a more conventional global coordinate system provides a method for rapidly assessing the effect of seabed slope for this weightless seabed. The conversion of the H coordinate of a point on the V-H stability envelope is undertaken using Equation 3.4 and the V coordinate conversion uses Equation 3.5. The coordinates of the calculated plastic potentials can also be updated for seabed slope. Figure 5.27 presents an example of the results produced with this technique showing the effect of in plane seabed slopes of 5°, 10° and 15° degrees on pipeline stability when subject to V-H loading.

The effect of soil unit weight on a pipeline subjected to V-H loading on a sloping seabed lacks generality and analysis is computationally intensive. Unlike the weightless soil cases there is not a general solution where slope effects can be accounted for with modification of a stability envelope derived from a single suite of numerical analysis. Instead a suite of numerical analysis is required for every slope angle and unit weight. However, some limited investigations can provide some interesting insights into the problem as well as demonstrating the techniques that could be used for a site specific series of analyses. The effect of soil unit weight will be governed by the dimensionless group $s_u/\gamma.D$, as previously used to describe the effect of soil unit weight on a vertically loaded pipeline in Chapter 4. A weightless seabed is equivalent to $s_u/\gamma.D=\infty$ and three other cases were investigated $s_u/\gamma.D$= 3.50, 2.27 and 0.45. These $s_u/\gamma.D$ ratio were based on credible ranges of soil parameters, as well as the finding of initial problem familiarisation where the approximate sensitivity to changes in this ratio were noted. With the requirement for analyses to address pipeline displacement through a full 360° a total of 22 displacement probes were undertaken for each case. Analysis was limited to one embedment depth z= 0.1D on a 10° slope. A smooth interface condition was used in analyses.

The analyses reported in this section were undertaken during the problem familiarisation section of this study, out of sequence with and, prior to completion of all the V-H work presented earlier in this chapter. As investigation into V-H loading was limited at this stage mesh density was configured conservatively with a density twice that used earlier in Section 5.2 and 5.3 for a smooth pipeline of z= 0.1D. With a greater mesh density slightly slower displacement velocities were required. For a details of analysis variables and a summary of results see Table 2-5, Appendix B.

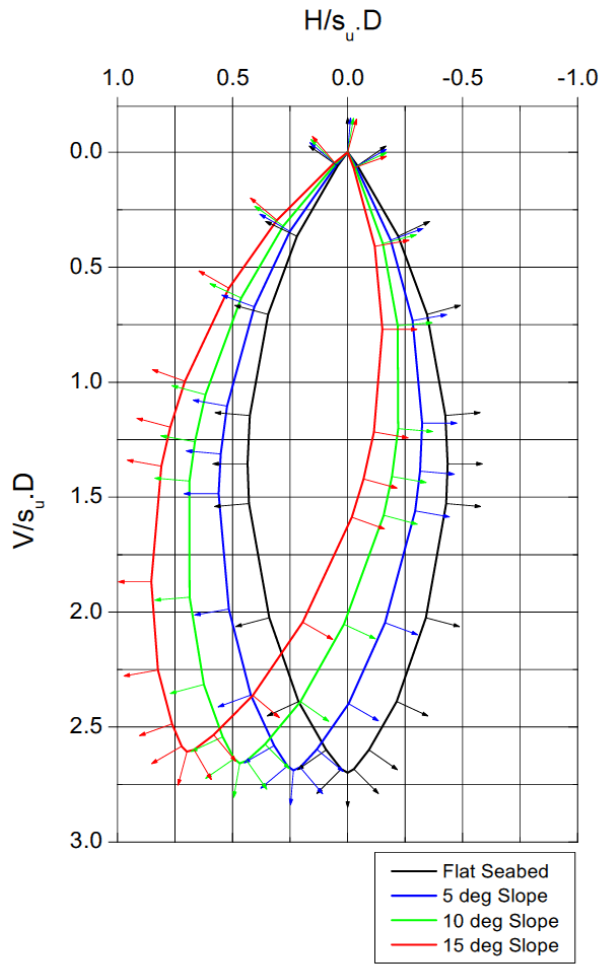

Figure 5.27 *- The effect of a seabed slope, z=0.1D, smooth interface conditions with a weightless seabed.*

In Figure 5.27 the significant effect of a seabed slope on the V-H stability envelope, and associated plastic potentials, can be seen with a rotation in the up slope direction, to the left. Unsurprisingly, the resistance to displace a pipeline in the upslope direction is greater than the flat slope case, further increasing with increasing slope angle. Similarly the resistance in the down slope direction decreases with the associated increase in slope. In both cases the degree of change appears to be approximately proportional to the change in slope angle. Rotating the stability envelopes and associated plastic potentials by the slope angle would appear to provide a simple design method to account for the effect of an in plain seabed slope.

The effect of a seabed slope change of 5° is significant. This can be visualised by reviewing the size of the stability envelope either side of the zero H load axis. The down slope portion of the envelope decreases dramatically in size until with

15° slope it is extremely small with limited capacity to accommodate V-H loading. The upslope portion has a similar increase in size. Another interesting observation can be noted by following the zero horizontal axis. Where this axis intersects the stability envelope is the point at which the pipeline will become unstable under V loading. Reviewing the plastic potentials in this region indicates that the instability will result in a down slope rather than pure vertical displacement.

The down slope area of the stability envelope will be of interest for pipeline stability on a sloping seabed. However, the upslope area may also be of interest. For example it could be used to quantify the increased resistance provided by placing the pipeline in an open (not backfilled) ploughed v-shaped trench. The example provided here is for a pipeline embedment depth of z=0.1D. However, this method can be applied to other embedment depths, as required. Although it should be noted that beyond z=0.5D there may be inaccuracy introduced depending on the assumptions with respect to the geometry of the slot shaped trench associated with deeper penetration i.e. the trench geometry may remain constant rather than rotating with the slope angle.

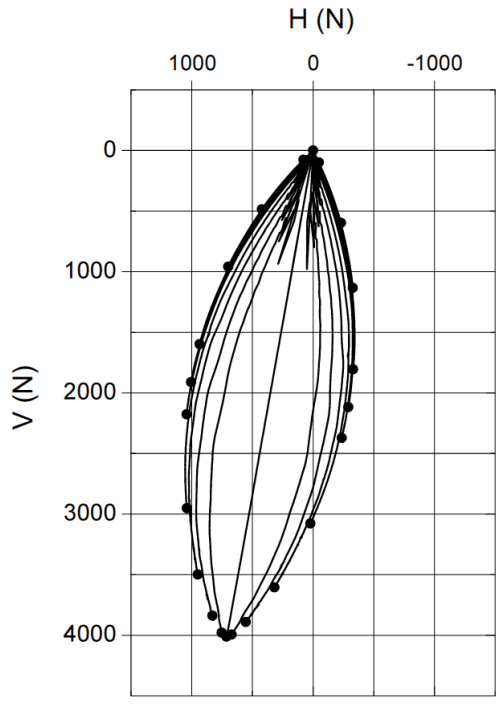

Figure 5.28 *- Example analyses of a pipeline on subjected to V-H loading on a sloping seabed. Seabed slope (ψ) =10°. $s_u/\gamma.D$= 2.27.*

The method outlined here is applicable to weightless soil with a range of cases derived from a single flat seabed analysis suite. For unit weight effects to be analysed a specific analysis needs to be undertaken for each case, including each slope angle. An example of this type of analyses is given in Figure 5.28. This example suite of analyses shows the same upslope rotation noted for the weightless analyses. However, the unit weight effects are very subtle and difficult to assess in this plot. Figure 5.29 allows a direct comparison between different $s_u/\gamma.D$ ratio which is also of interest as well as helping to emphasise the magnitude of the unit weight effect. Note following completion of analyses it was found that $s_u/\gamma.D$= 3.50 was so similar to the weightless case that it could not be seen in this plot, it was therefore removed. The results for $s_u/\gamma.D$= 3.50 are however still presented in Table 2-5, Appendix B.

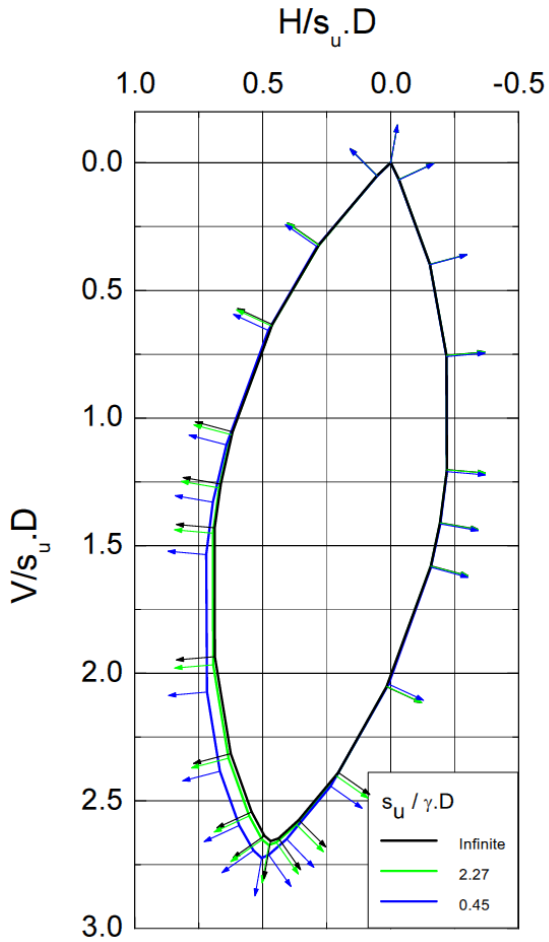

Figure 5.29 *- Comparison between different $s_u/\gamma.D$, z= 0.1D, smooth interface, seabed slope (ψ) =10°.*

Figure 5.28 shows a series of termination points around the V-H stability envelope. Load paths for each displacement vector are similar to those reported earlier in this chapter for flat seabed cases. The equivalent to a vertical load case is δ=+100°, where the pipeline is displaced at an angle perpendicular to the 10° sloping seabed. This load path can be seen in the centre of the V-H stability envelope. The load paths are somewhat spiky, or noisy, at the start of displacement. As with the flat seabed case this can be attributed to the transition from elastic to plastic soil behaviour and initial expansion of the zone of confined plastic flow. Many of the load paths, especially those towards the upper part of the envelope, track the bounds of the stability envelope prior to reaching the termination point.

From a review of Figure 5.29 the most obvious observations are that the effect of unit weight is small and that this effect is confined to specific sections of the V-H stability envelope. To aid interpretation Figure 5.30 shows the portion of the V-H stability envelope impacted by unit weight effects a in a larger format.

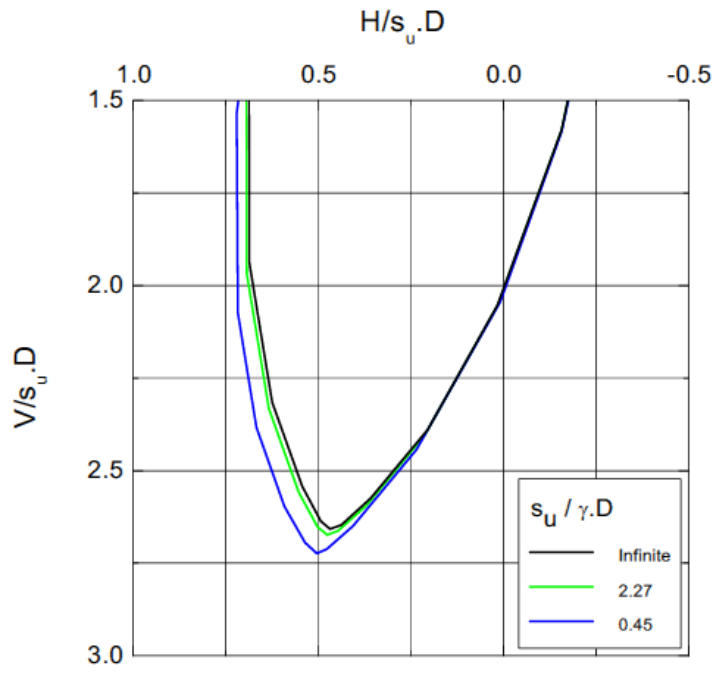

Figure 5.30 *- Enlarged lower portion of V-H stability envelope, a comparison between different* $s_u/\gamma.D$, *z= 0.1D, smooth interface, seabed slope (*ψ*) =10°.*

The effect of soil unit weight on a pipeline V-H stability envelope is confined to the lower tip of the envelope extending to the upslope portion of the envelope. At the tip of the envelope the change is confined to displacement close to

δ=+100° (perpendicular into the slope) on the upslope portion the effect diminishes with increasing uplift angle with no effect once there is uplift greater than the slope angle. It has already been noted that the case of $s_u/\gamma.D$= 3.50 was so similar to the weightless case that it could not be sensibly plotted. The case of $s_u/\gamma.D$= 2.27 shows negligible effect and it is only at a relatively extreme $s_u/\gamma.D$ of 0.45 that the effect becomes clear. This explains the difficulties in seeing a trend in Figure 5.28. For the depth and conditions considered the effect of submerged unit weight is minimal even for a low $s_u/\gamma.D$ and the impact is also limited to a specific portion of the stability envelope.

As for a number of previous problems a review of the calculated displacement field as a vector plot can provide some insights into observations on the resistance to a given load case or displacement vector, see Figure 5.31.

Figure 5.31 shows several cases that are relevant to the observations made with respect to unit weight effects. Figure 5.31 a and b shows a pipeline displaced at δ=+100° with the first of these plots for a weightless soil and the second for a $s_u/\gamma.D$ of 0.46. For the weightless soil the displacement mechanism at failure is symmetric with no effect from the presence of the slope. This mechanism is also the same as previously shown in Chapter 4 for a flat seabed. With the introduction of soil unit weight in Figure 5.31b the mechanism is no longer symmetric. The upslope portion of the displacement mechanism decreases in size with an associated increase in the down slope side. With the soil having weight, displacing soil upslope requires a larger force then for the down slope side with the optimal displacement mechanism is an asymmetric mechanism. It can also be seen that δ=+100° results in a rotational mechanism that requires uplift of soil, uplift which will require a greater force if the soil has weight explaining the impact of unit weight at, and close to, δ=+100°.

Figure 5.31 c and d is relevant to the observation that the soil weight effect impacts up slope displacements but not down slope displacement. δ=-5° in Figure 5.31 c is a displacement vector with a down slope displacement. The very small mechanism is consistent with the small resistance to down slope displacement for this slope angle. It also explains the non-discernible impact of soil weight for this case. Not only is the mechanism small, mobilising a small soil volume and small weight of soil, but most of the soil displacement is horizontal or down slope and therefore not impacted by soil weight. The upslope displacement vector, δ=+175°, shows a markedly different mechanism which is

consistent with the impact of soil weight. Not only is the mechanism larger but it also involves upward displacement of soil.

a)

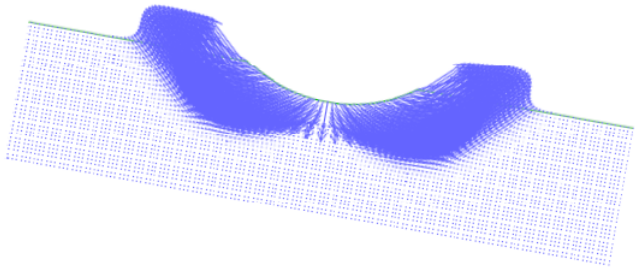

b)

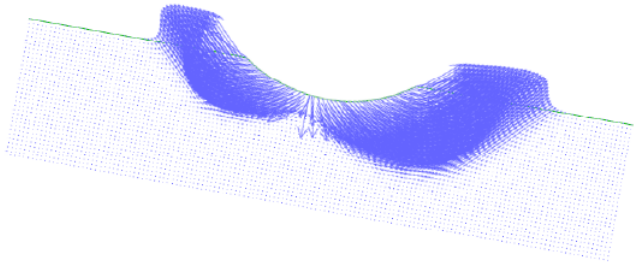

c)

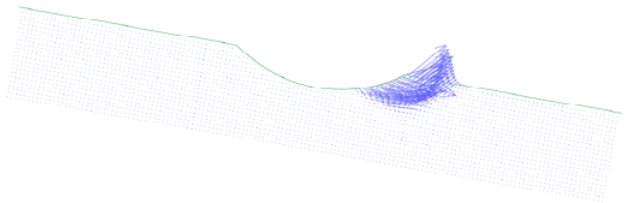

d)

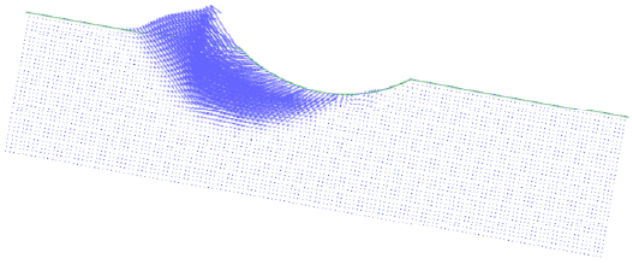

Figure 5.31 a,b,c,d *- Calculated displacement field presented as vector plots for a pipeline subject to V-H loading on a 10° seabed slope a) δ=+100° weightless soil b) δ=+100° $s_u/\gamma.D$=0.46 c) δ=-5° $s_u/\gamma.D$=0.46 d) δ=+175° $s_u/\gamma.D$=0.46.*

This section has summarised a method for rapidly assessing the impact of seabed slope by adopting the assumption of a weightless soil. The effect of soil unit weight has also been investigated, albeit these investigation were limited in scope. The investigations into soil unit weight not only demonstrated a methodology, but also indicated this effect would be limited at higher $s_u/\gamma.D$ and

for lower $s_u/\gamma.D$ it will be limited to certain portion of the V-H stability envelope. The impact of soil unit weight was explained by investigating soil displacement mechanisms, which were consistent with observation with respect to V-H stability envelope geometry. For further discussion see Section 5.6, the implication to design practice are also discussed in Chapter 7.

5.5 V-H Loading - Large Displacement Behaviour

In Chapter 4, Section 4.3, the influence of a large strain problem definition on a vertically loaded pipeline was investigated. For this case soil berms formed during vertical pipeline penetration with an associated increase in resistance as the berms contacted the pipeline at a level above the seabed level. It was noted this effect was relatively small and became negligible at pipeline embedment depths beyond 0.5D. For a pipeline subjected to V-H loading the presence of a berm following an initial pipeline penetration into the seabed can also be expected to have an effect on resistance to horizontal displacement as suggested by Merifield et al. (2009).

The study undertaken by Merifield et al. (2009) was relatively limited in scope presumably due to the lack of generality in this problem and that the calculations are computationally intensive. For example Merifield et al. (2009) only considered a constrained horizontal displacement, i.e. H_{max}. Load history and vertical load during displacement were neglected and the full V-H stability envelope was not investigated, instead it was postulated that a large strain envelope may be the same shape as those derived for a small strain problem definition. It should also be noted that H_{max} does not necessarily describe the resistance to horizontal displacement, only the maximum resistance at one specific vertical load case. Additionally, although not explicitly stated, the large strain H_{max} figures presented by Merifield et al. (2009) do not consider larger displacement behaviour or assess how resistance may change with displacement. The limitations in this earlier study potentially obscure important aspects of this problem.

Throughout this study there has been an emphasis on plotting the plastic potentials, this had not been undertaken within previous numerical analysis studies. The plots of plastic potentials suggest that an associative flow rule is appropriate for a wide range of cases and the associated V-H stability envelopes e.g. see Section 5.2 and 5.3. The lack of generality in the large strain V-H

loading problem does not lend itself to a parametric study with large strain analysis techniques, although this type of analysis may still be useful for site specific analysis. However, use of the existing small strain stability envelopes and an associative flow rule offers an efficient way to investigate some important aspects of large displacement behaviour.

A review of the stability envelopes and associated plastic potentials, as presented in Section 5.2 and 5.3, shows the importance of the vertical load case during horizontal displacement. Three broad categories of pipeline behaviour under large displacement V-H loading can be identified, ride-in behaviour, ride-out behaviour and a third steady state behaviour where the pipeline displaces at constant depth and constant horizontal resistance.

Ride-in behaviour occurs when the V load case during horizontal displacement is towards the bottom half of the V-H stability envelope, an area of the envelope where the plastic potentials point downwards into the seabed. This could occur if installation forces are small or if the pipeline gets heavier post installation e.g. due to flooding with product. During ride-in behaviour a pipeline will penetrate further into the seabed in conjunction with horizontal displacement. This additional pipeline embedment will also increase the resistance to horizontal displacement.

A pipeline exhibiting ride-out behaviour will occur when the V load case during horizontal displacement is in the upper part of the V-H stability envelope. In this area of the stability envelope plastic potentials have an uplift angle, out of the seabed. This case could occur when installation forces are large relative to the self weight of the pipeline. A pipeline experiencing ride-out behaviour will reduce in embedment during horizontal displacement. This reduction in embedment will also reduce the resistance to horizontal displacement.

The third behaviour is a steady state behaviour where the vertical load is equal to the vertical load at which H_{max} occurs. At this point on the V-H stability envelope the plastic potential is horizontal. For this case a displaced pipeline will stay at the same embedment depth during displacement and within this small strain problem definition resistance to horizontal displacement will be constant. It is unlikely that this steady state behaviour will occur during an initial displacement. However, at a larger displacement after a previous episode of ride-in or ride-out behaviour this case can be expected.

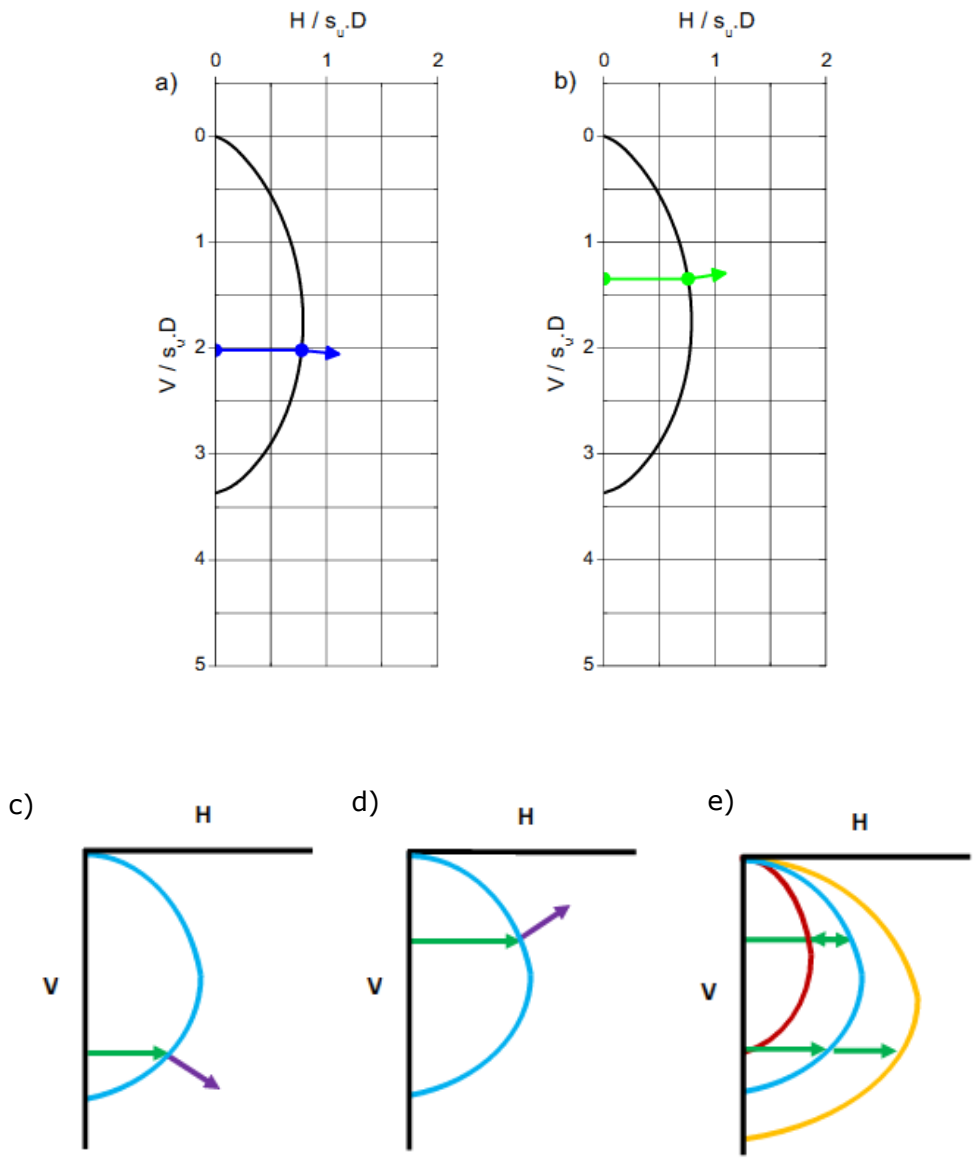

Figure 5.32 a,b,c,d,e *- Example load paths for a) ride-in and b) ride-out behaviour smooth pipeline at an embedment depth of z=0.2D. c), d), e), Sketch of changes in V-H stability envelope with rider-in and ride-out behaviour.*

Figure 5.32 shows an example of two load cases for a pipeline subjected to large displacement V-H loading. These form the starting condition for the analysis presented later in this section. In Figure 5.32a the pipeline is subjected to a constant vertical load of 60% of V_{max}. As can be seen from the plastic potential this will result in ride-in behaviour. Figure 5.32b shows the case of a constant V load of 40% of V_{max}, which will result in ride out behaviour. Analyses were

undertaken for these two cases within a spread sheet program, with analyses progressed to steady state behaviour.

Figure 5.32 c, d, e, also shows a sketch of how a pipelines V-H stability envelope may change with ride-in and ride-out behaviour. For the ride-in case the stability envelope expands (from the blue envelope to the yellow envelope) and is associated with an increase in H capacity due to this large stability envelope at a deeper pipeline embedment depth. For the ride-out behaviour the envelope contracts (from the blue envelope to the red envelope) in association with a reduction in pipeline embedment depth, with this small stability envelope also providing a reduced capacity to H loading. The analysis results later in this section can be reviewed relative to this expected behaviour.

The first analysis step for the ride-in case, V = 60% of V_{max}, was displacement at an angle of 5.9°. This is the angle of the normal plastic potential where a H load of 60% of V_{max} intersects with the V-H stability envelope for a smooth interface pipeline at a wished in place embedment depth of z=0.2D. After a small displacement, 10mm horizontal and ~1mm vertical for this case, the V-H stability envelope is recalculated along with a new plastic potential. For this first analysis step the plastic potential rotated by 0.1° to 5.8°. Analysis was progress over a series of small steps until the plastic potential was at an angle of <0.4°, at which point it was deemed that analysis had progressed sufficiently towards the stead state behaviour mode. The results of this analysis are plotted in Figure 5.33.

In Figure 5.33 pipeline penetration (z_p) is normalised by pipeline diameter (D) to give the dimensionless group z_p/D. Horizontal resistance is expressed in terms of the previously used dimensionless load group $H/s_u.D$. Both parameters are plotted against a lateral displacement along the x coordinate axis, which is also expressed in dimensionless form relative to pipeline diameter, giving x/D.

Figure 5.33 shows a distinct pattern of ride-in behaviour. Penetration occurs at a greater rate during initial displacement, with the rate of penetration gradually reducing with lateral displacement. Analysis was progressed to x/D=5.17, beyond this point additional penetration would be negligible with a plastic potential of <0.4°. Ride in behaviour for this load case has resulted in a significant increase in pipeline embedment, increasing from the initial z_p=0.2D to z_p=0.37D. This increase in embedment is also associated with a significant increase in resistance to lateral displacement, as described by the $H/s_u.D$ term, with an increase in resistance of 60%.

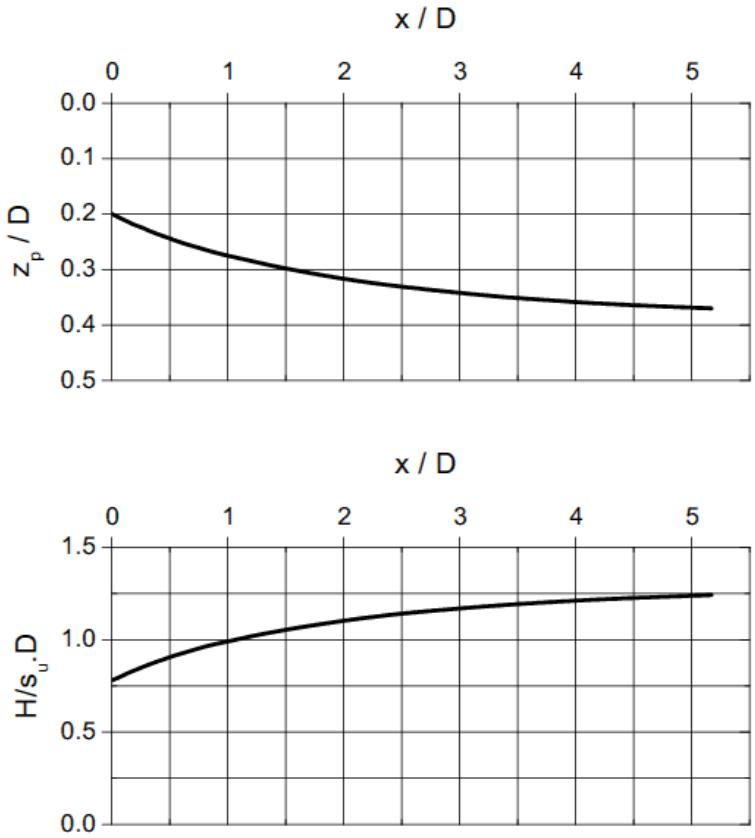

Figure 5.33 *- Change in pipeline embedment depth (z_p) and horizontal resistance ($H/s_u.D$) with ride-in behaviour.*

The analyses undertaken for the ride out load case plotted in Figure 5.32b follows the same process outlined for the ride-in case. Initial displacement was at an angle of -8.8°, a slightly larger angle then the previous case due to slight asymmetry in the envelope. Again analysis was progressed to a displacement angle of <0.4°. The results of this analysis are plotted in Figure 5.34.

Figure 5.34 shows analysis data in terms of the same dimensionless groups as used for the previous plot of ride-out behaviour. Again a significant effect can be observed. For this case pipeline embedment depth reduces from the initial depth of z_p=0.2D to z_p=0.07D. This reduction in depth occurs over a smaller lateral displacement distance then the previous ride-in case, with negligible additional reduction in embedment depth from x/D=2.08. This reduction in embedment results in a reduction of 57% in the horizontal resistance to displacement.

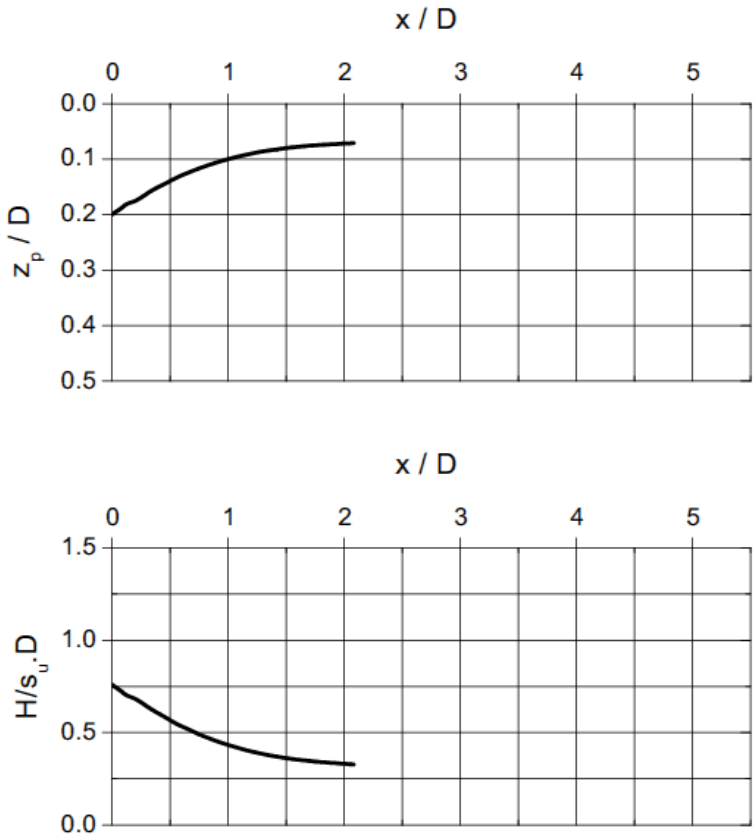

Figure 5.34 *- Change in pipeline embedment depth (z_p) and horizontal resistance ($H/s_u.D$) with ride-out behaviour.*

Although the case of large displacement analysis for a pipeline subjected V-H loading lack generality, a technique to consider ride-in and ride-out behaviour has been demonstrated in this section. These results suggest the change in embedment depth arising from this behaviour, and the associated change in horizontal resistance, could have a significant impact on pipeline behaviour.

5.6 Summary and Discussion

The investigations into pipelines subject to V-H loading reported in this chapter considered the following areas;

- Maximum capacity to horizontal loading (H_{max}) for a homogenous strength weightless seabed
- V-H loading pipeline stability envelopes for a homogenous strength weightless seabed

- The effect of a linear increasing shear strength gradient on maximum capacity to horizontal loading (H_{max})
- The effect of a linear increasing shear strength gradient on pipeline V-H loading stability envelopes
- Seabed slope effects on a V-H loaded pipeline, including the effect of soil unit weight on a sloping seabed
- Large displacement behaviour of a pipeline subjected to V-H loading

It has previously been noted in Chapter 2 that investigations into H_{max} and V-H stability envelopes for a homogenous strength weightless seabed are similar to a study undertaken by Merifield et al. (2008). The scope of this earlier analysis addressed cases up to a pipeline embedment depth of 0.5D. As described in Section 5.2.3; good agreement was found between the analysis reported in this thesis and this previous research. Following this initial analysis and comparisons with previous research this study extended analysis to a pipeline embedment depth of 1.0D. Fitting equations were proposed for these problems including a new relationship to described changes in the V-H stability envelope skew parameters arising from changes in pipeline embedment depth. Soil displacement vector plots were provided to support interpretation of the relationships noted in H_{max} and pipeline stability under combined V-H loading.
The effect of linear increasing shear strength gradient on both H_{max} and pipeline V-H stability envelopes had not been investigated by previous researchers. A parametric study built on the investigations into the effect of linear increasing shear strength gradients on pipeline subjected to V loading reported in Chapter 4, extending this problem definition to pipelines subjected to V-H loading. H_{max} was initial investigated with the reduction in H_{max} in the presence of a linear increasing shear strength gradient noted. Generalised fitting relationships were reported with interpretation supported by vector plots of soil displacement at H_{max}. Full V-H loading in the presence of a linear increasing shear strength gradient was analysed with general fitting equation provided for this problem definition. Pipeline embedment depths of up to 1.0D were investigated as part of this study.

Prior to this study the effect of seabed slopes on a pipeline subjected to V-H loading had not previously been investigated, although some of the results from this study were reported earlier in Morrow and Bransby (2009). This study presented a methodology for rapidly deriving pipeline V-H stability envelopes for a range of slope angles using a stability envelope from a flat seabed case. This methodology we suitable for a weightless soil problem definition up to a pipeline

embedment depth of 0.5D. The effect of soil unit weight on a sloping seabed significantly reduces the generality of the problem. Some cases were investigated with the effect of soil unit weight shown to be strongly influence by the $s_u/\gamma.D$ ratio. Additionally the effect of soil unit weight was limited to specific areas of the pipeline stability envelope. Soil displacement vector plots for positions around the V-H stability envelope aided interpretation of these observations.

Investigations into large displacement behaviour typically lack generality and are computationally intensive. This study demonstrated a method of rapidly assessing ride-in and ride-out behaviour based on small strain V-H stability envelopes and the plastic potentials calculated for these envelopes. The significant effect on pipeline embedment depth and the associated change in horizontal resistance suggested these effects are important at larger displacements.

The application of the analysis reported in this and previous chapters to design practice is summarised in Chapter 7. Conclusions for this study, including potential scope for further research, are also discussed in Chapter 7.

6 Reliability Based Analysis

6.1 Introduction

This chapter reports the results from the application of reliability based analysis techniques to a range of pipe-soil interaction problems. The first case considered with these analysis techniques is a single pipeline subjected to Vertical (V) loading (Section 6.2). A more general vertical loading problem is considered with reliability based analyses of the maximum capacity under vertical loading (V_{max}) for a range of pipeline embedment depths (Section 6.3).

Reliability analysis techniques are extended to general combined vertical and horizontal (V-H) loading with the analysis of the maximum capacity under horizontal loading (H_{max}) for various pipeline embedment depths (Section 6.4). A technique for the application of reliability analysis to V-H stability envelopes is demonstrated in Section 6.5. The results presented in this chapter are summarised in Section 6.6. The implications of this analysis for application of the results of this study to design practice are discussed further in Chapter 7.

Stochastic variation of parameters can be dealt with using the simplified analysis method detailed in Section 3.5.2 or by using Monte Carlo analysis. It can be noted that in the cases considered here only a single stochastic variable is considered, a uniformly distributed s_u with depth. For this type of case a Monte Carlo analysis is not necessary, but it is included as a cross-validation of the simplified method. In all cases the match is almost exact, as would be expected. Use of the Monte Carlo analysis method would allow extension to the consideration of multiple stochastic variables with different CoV, though a suitable expansion of the number of trials undertaken, for example the three parameters required to describe the a general soil profile with a crust considered in Chapter 4.

6.2 A Vertically Loaded Pipeline

The first problem considered with reliability based analysis techniques was the case of a single pipeline subjected to vertical loading on a seabed with a shear strength that is treated as a stochastic variable. A normal distribution of soil undrained shear strength (s_u) with various coefficients of variation (CoV) investigated, see Section 2.6 for background on the technical basis behind the

selection of shear strength distributions. Also see Section 3.2.4 for the problem definition and Section 3.5 for further details of the methodology used for analysis. The case of a single pipeline is a reasonable basis to introduce the use of reliability based analysis within this study and is expected to be representative of a credible design problem for an offshore pipeline project. Considering a single pipeline is a relatively limited scope. Therefore further more general investigations are addressed later in this chapter, including reliability based investigations of V_{max}, H_{max} and V-H stability envelopes.

To increase the relevance of the analysis for a single case some credible analysis parameters were adopted rather than arbitrary parameters for subsequent conversion to dimensionless form. A pipeline of D = 0.4m with the submerged weight of 1.2 kN/m was used. This was similar to one of the example pipelines provided by Clauss et al. (1991), rounded to one decimal place for both variables. A vertical load amplification factor of 2 was applied due to dynamic installation forces, similar to the example provided by Cathie et al. (2005) and consistent with the review by White and Randolph (2007). With the vertical amplification factor this gave V = 2.4 kN/m. A smooth pipeline interface condition was used in analysis. The seabed clay was assigned a uniform mean undrained shear strength ($s_{u\mu}$) of 2.5 kPa which was simplified to a weightless soil for this example.

V_{max} under vertical load was based on Equation [4.5] and the coefficients for a smooth pipeline over the depth range from z = 0.05D to z = 1.0D presented in Table 4.3. This V_{max} relationship was used with the simplified reliability analysis method. For Monte Carlo analysis it was more convenient to use the alternative formulation of this relationship, where penetration is related to vertical load. This used Equation [4.6] and the coefficients for a smooth pipeline over the depth range z = 0.05D to z = 1.0D provided in Table 4.5. Both simplified and MC analysis was undertaken for three coefficients of variation (CoV) of s_u, 0.10, 0.15 and 0.20. Demonstrating the use of two different techniques for this simplified problem.

The results of MC analysis are plotted in Figure 6.1. Three s_u CoV are plotted in this figure commencing at a) CoV= 0.10 and increasing s_u CoV through b) CoV= 0.15 to c) CoV= 0.20. The first plot, for each CoV, shows a histogram of pipeline penetration results for vertical load and analysis conditions considered. The second plot shows a cumulative percentage plot of pipeline penetration. The number of simulations, N, required for each analysis case varied with s_u CoV.

This requirement is related to the range of P_F associated with each CoV for the depth range considered. There was a trend of an increasing N requirement with decreasing CoV, see Table 6.1. This is associated with a lower P_F for a given embedment depth with a lower CoV. The guidance for the likely N requirement described in Section 3.5.3 was found useful, with confirmation of N being suitable by convergence to a particular P_F.

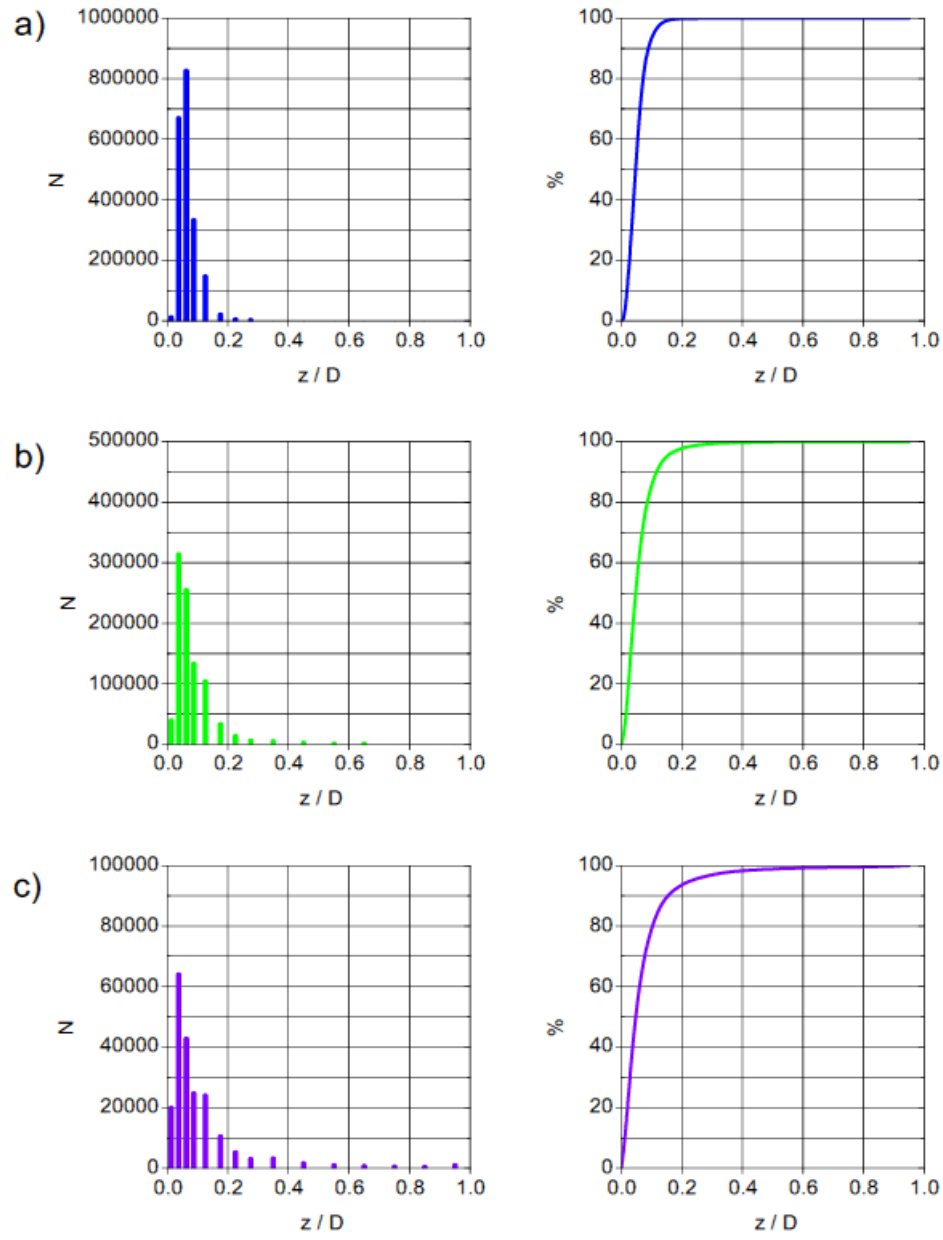

Figure 6.1 *- Monte Carlo analysis statistics for single V loading case. CoV = a) 0.10, b) 0.15, c) 0.20.*

s_u CoV	N
0.20	200,000
0.15	900,000
0.10	2E6

***Table 6.1**: N for MC analysis by s_u CoV.*

In addition to the observations on the changing MC analysis requirements with CoV, the effect of CoV can also be seen in the analysis results presented in Figure 6.1. For a low CoV, e.g. 0.10, analysis results are concentrated towards a shallow pipeline embedment depth with a low probability of the pipeline penetrating to deeper embedment depths for the V load adopted. With increasing CoV the spread of analysis results increases with a wider range of embedment depths occurring at higher frequencies. The likelihood of a deeper embedment depth for this pipeline also increases with increasing CoV. This is as can be expected, with a greater CoV suggesting a wider range of shear strength and a greater number of lower shear strength values within the shear strength distribution. This is reflected in the pipeline penetration with the other variables such as the pipeline penetration relationship, or V_{max} relationship, pipeline diameter and vertical load remaining constant across these analysis cases. For a single pipeline example the degree to which s_u CoV effects the analysis results is specific to the analysis conditions adopted e.g. mean shear strength ($s_{u\mu}$), pipeline diameter, vertical load, etc. However, a similar trend can be expected for most credible analysis conditions.

Although the format used in Figure 6.1 provides scope for some interesting observations an alternative format can provide additional information, as well as allowing a comparison between MC analysis and the simplified analysis methodology, see Figure 6.2. In place of frequency analysis the MC analysis is converted to a P_F (see Equation [3.1], Section 3.5.3), which is plotted along with the results from the simplified analysis method. Both analysis results are plotted in terms of embedment depth, z/D. For this case P_F is defined as the probability of $V>V_{max}$ for a given z/D. When $V>V_{max}$ then a pipeline will penetrate further until $V=V_{max}$, therefore this relationship is an analogue of probability of pipeline penetration to a given z/D. P_F is plotted on a log scale to allow an adequate representation of the lower P_F and the range of P_F of interest.

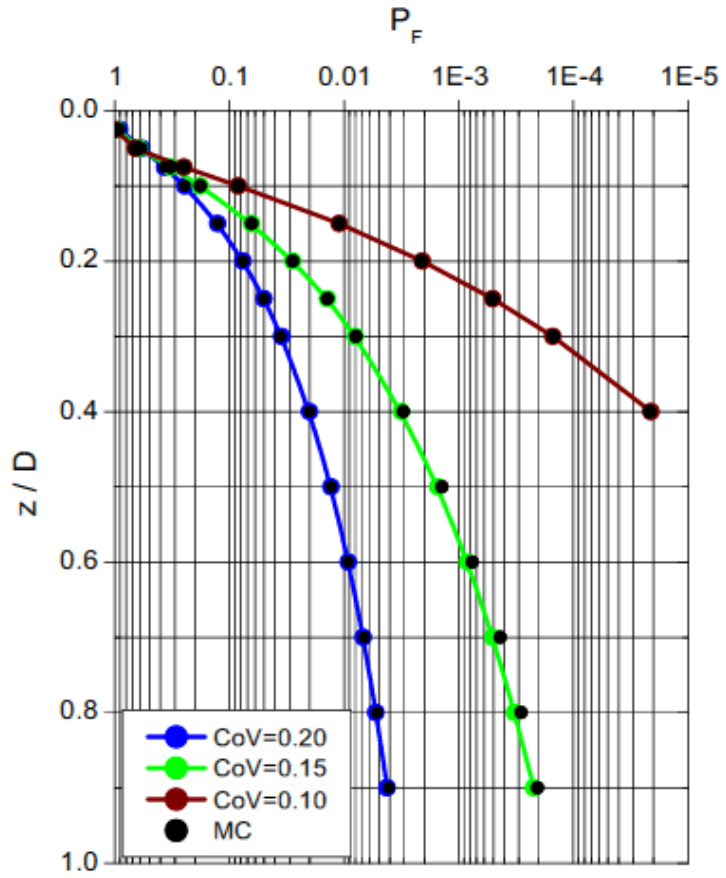

Figure 6.2 *- Probability of failure (P_F) by z/D for simplified and MC analysis.*

From Figure 6.2 it can be seen that at a shallow depth of embedment (e.g. <0.1D) the effect of a change in the CoV of s_u is negligible. This shallow embedment depth is relatively close to the deterministic value for the analysis parameters adopted and it would seem that this, and the combination of the very high P_F, significantly reduces the influence of s_u CoV. As the embedment depth increases the effect of s_u CoV becomes more marked. Consistent with the general observations noted for Figure 6.1, the greater the CoV the higher the P_F for a given embedment depth i.e. the more likely a deeper pipeline embedment will occur for the case being considered. Conversely, at a low CoV, e.g. CoV= 0.1, penetration to the deeper depths is unlikely with a very low P_F i.e. a low probability of $V>V_{max}$ for larger z/D. For CoV= 0.1 the depth range of analysis cases was truncated when the trend to very low P_F was noted from the simplified analysis method.

The steepness of the trend in P_F against z/D can be viewed as a metric of the range of depth of penetration that can be expected. For example a steep line

nearer to a vertical line, as can be noted for CoV = 0.2, shows little difference in P_F for a wide range of embedment depths suggesting a wide range of embedment depths can be expected.

Another interesting observation that can be readily noted from presenting analysis results in the format used in Figure 6.2, is that a change in CoV does not have a proportional effect on P_F. This can be seen in the change in CoV from 0.20 to 0.15 which is relatively minor, especially at shallow depth, as compared to the change from CoV = 0.15 to 0.10 which is dramatic at all but the shallowest embedment depths.

For the higher CoV the trend in the reliability based analysis data shows similarities with the deterministic relationship between vertical load and pipeline embedment depth. For the deterministic case the trend in this relationship relates to the maximum pipe-soil contact width being reached at z = 0.5D, at which point the rate at which greater bearing capacity can be mobilised is reduced for a constant s_u soil. This trend also appears to be reflected in the reliability analysis for higher CoV, where the rate of change in P_F is relatively small at deeper depths. In this example the P_F for a CoV = 0.20 is still quite large even at 0.9D. This suggests a case where very large pipeline penetrations are possible. This may be reasonable for the depth range considered. However, beyond this depth a range of other factors such as a shear strength increase may lead to a rapid reduction in P_F, providing a practical limit on pipeline penetration similar to that which occurs at shallow depth lower CoV, e.g. CoV = 0.10.

The implication of variation in s_u CoV will be discussed in greater detail later in this chapter within the context of more general cases. The implications for application to design practice will also be discussed in Chapter 7.

6.3 Reliability Based Analysis of V_{max}

Reliability based analysis techniques were used to extend the examples considered in the previous section to a more extensive parametric study of vertical loaded pipelines. This analysis addresses V_{max} and probability of failure (P_F) in terms of a dimensionless vertical load term $V/s_u.D$, increasing generality and providing a more comprehensive study of the problem then the single V loading example considered in the previous section. P_F is defined as $V > V_{max}$.

Various $V/s_u.D$ were investigated for a total of seven pre-determined wished in place embedment depths, 0.05D, 0.1D, 0.2D, 0.4D, 0.6D, 0.8D and 1.0D. For each embedment depth a normal distribution of s_u with three coefficients of variation (CoV), CoV = 0.10, 0.15, 0.20 were analysed, see Section 6.1 for additional background. As with previous reliability analysis the reference s_u is the mean soil undrained shear strength ($s_{u\mu}$). Analysis of V_{max} used a combination of the simplified analysis methodology and MC analysis. All cases were investigated using the simplified method, totalling 166 analyses. Slightly over half of the cases, 94, were also investigated with MC analysis. For further details of the analysis variables see Tables 3-2, Appendix C.

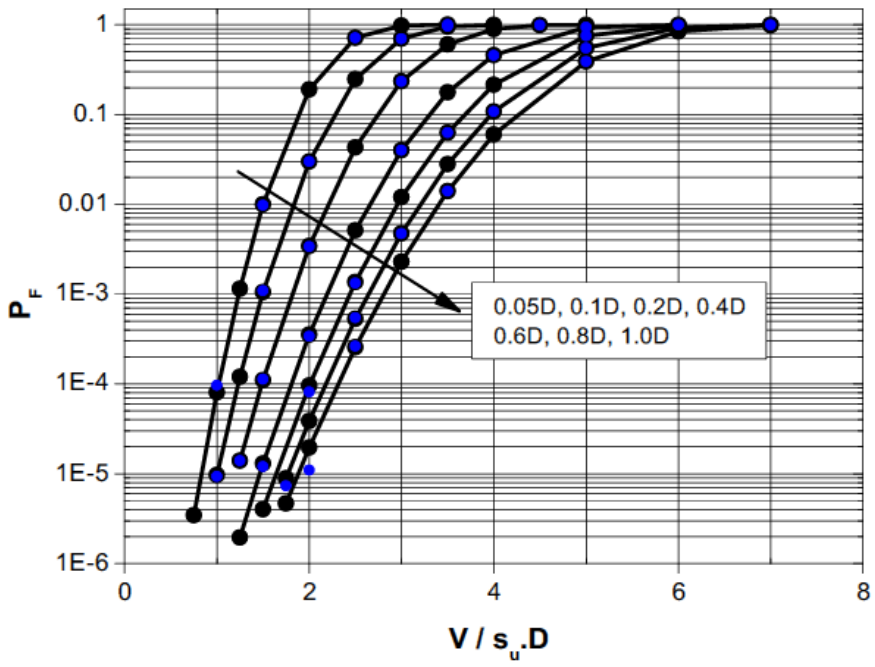

Figure 6.3 *- Reliability analysis of V_{max} for a s_u CoV of 0.15. MC analysis show by blue dots. z = 0.05D, 0.1D, 0.2D, 0.4D, 0.6D, 0.8D, 1.0D.*

Analysis was progressed with V_{max} values derived from Equation [4.4] and the coefficients for a pipeline embedment depth range z = 0.05D to z = 1.0D, presented in Table 4.3. The coefficients for a smooth pipe-soil interface condition were adopted for this analysis and a weightless seabed with uniform mean undrained shear strength was used. $V/s_u.D$ values were selected by adopting arbitrary values of s_u, D and V, and the simplified analysis method was used to ensure a spread of P_F in the range of interest, typically by adjusting V. This range of interest was from P_F>1E-6 to P_F=1.0, ensuring there was always data in the range P_F=3E-5 to P_F=0.07, see discussion related to Fragility Index (I_F) later in the chapter for the rationale behind this target range of P_F. The results obtained from the simplified analysis were plotted and a selection of these cases were investigated further with MC analysis. Figure 6.3 shows the results for analysis with a s_u CoV of 0.15.

Figure 6.3 shows that for a particular P_F an increase in the depth of pipeline embedment is associated with an increase in $V/s_u.D$. In other words, a greater $V/s_u.D$ is required to have the same probability of $V>V_{max}$ and the associated probability additional pipeline penetration into the seabed until $V=V_{max}$. An example of this can be noted by reviewing the $V/s_u.D$ associated with a P_F of 1E-4, which increases from approximately 1.0 to 2.3 over the depth range 0.05D to 1.0D. This trend is to be expected and can be attributed, in part, to the increase in V_{max} with embedment depth. The larger increase in $V/s_u.D$ over a shallower depth range is also consistent with the trend previously discussed for V_{max}, in particular the more rapid increase in V_{max} for embedment depths < 0.5D.

The format adopted in Figure 6.3 and later figures is to present the P_F data on a log scale against load on a standard scale i.e. a semi-log plot. The log scale for P_F allows an adequate representation of the range of P_F of interest, including some relatively small P_F. Typical P_F of interest were know prior to commencing analysis, for example see Figure 6.5. In this semi-log format the relationship between $V/s_u.D$ and P_F exhibits a slight curve. Although it can also be noted that much of the curved section is at higher P_F, with the trend at lower and moderate P_F approximately linear. The steepness of this linear trend can be seen to change with pipeline embedment depth. For example at shallow depth the trend is relatively steep, e.g. 0.05D, followed by a gradual decrease in the gradient towards deeper depths, e.g. 1.0D. The steepness of the V load P_F relationship is an important property as it describes the $V/s_u.D$ required to produce a given change in P_F. This is equivalent to the fragility of the system and has important

implication for the reliability behaviour of the system e.g. appropriate safety factors. This will be discussed further in Section 6.5 as well as in Chapter 7.

The results plotted in Figure 6.3 can also be compared to analysis at different s_u CoV. Figure 6.4 shows the results for a s_u CoV=0.10 and CoV=0.20. The contrast between the plots for CoV=0.10 and CoV=0.20 is significant. To a lesser extent a difference can be noted between each of these plot and CoV=0.15. From a high level review this can be seen as the range of values of $V/s_u.D$ encompassed by the problem domain for a particular CoV and the depth range z = 0.05D to z = 1.0D. A CoV of 0.20 encompasses the largest range and CoV of 0.10 the smallest range, CoV=0.15 represents an intermediate value. This has similarities with the trend noted in the previous section, for a single V loading case. A larger s_u CoV will be associated with a wider shear strength range which when applied to a capacity function, in this case for V_{max}, will result in a wider range of capacity. The magnitude of this effect will be influenced by a combination of the CoV and the form of the capacity function. Associated with this change in range, the gradients for the linear section of the P_F trends can be seen to change with CoV.

An increase in embedment depth results in an increase in the value of $V/s_u.D$ required for a given P_F e.g. reviewing the values at P_F=1E-4. However, the magnitude of this increase varies between these plots i.e. with CoV. While the basis of this increase can be linked to the form of the V_{max} to embedment depth relationship, by considering a range of s_u CoV it can also be seen that the s_u CoV has an important influence on this effect.

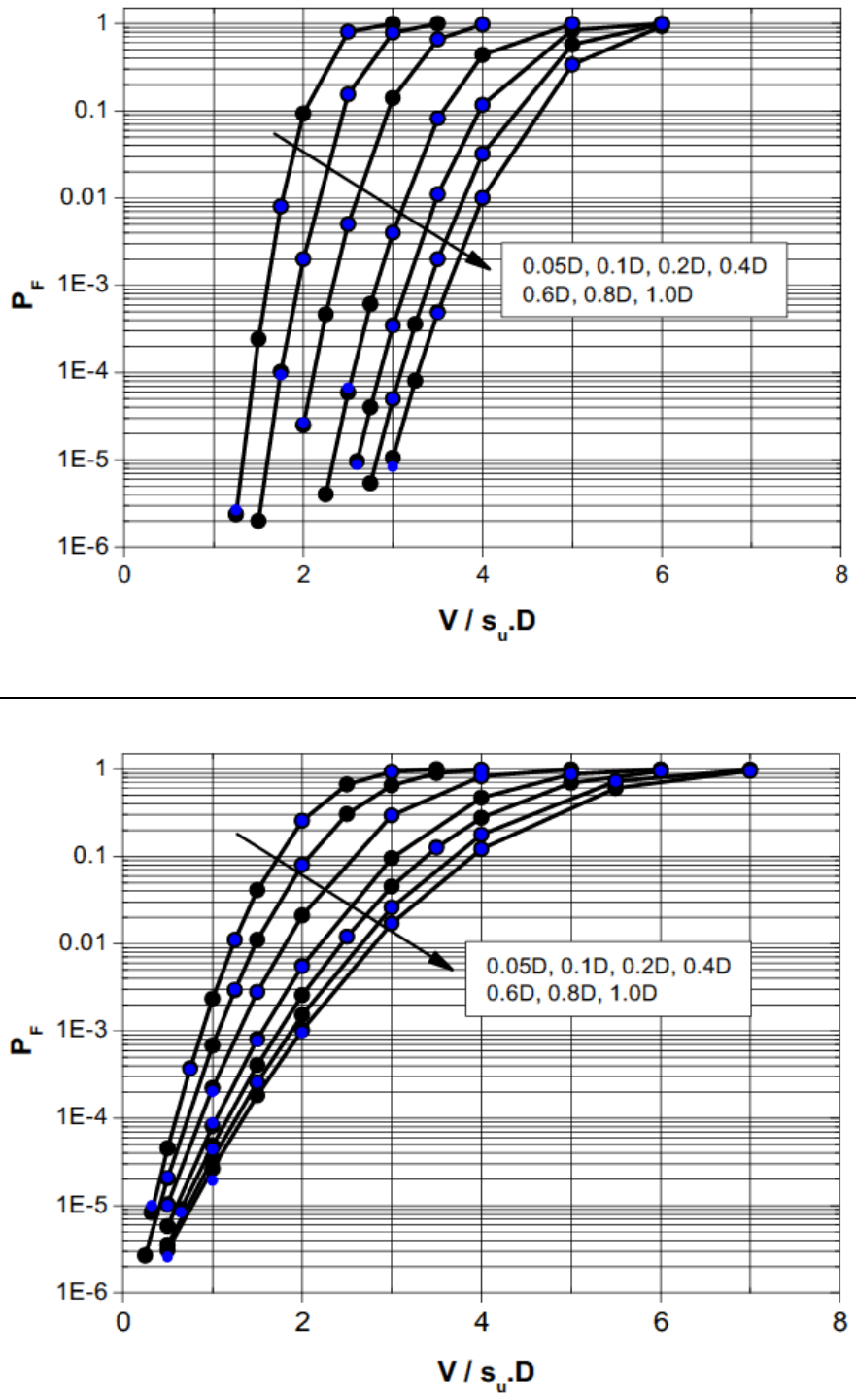

Figure 6.4 *- V_{max} for s_u CoV=0.10 (upper plot) and s_u CoV=0.20 (lower plot) MC analysis show by blue dots. z = 0.05D, 0.1D, 0.2D, 0.4D, 0.6D, 0.8D, 1.0D.*

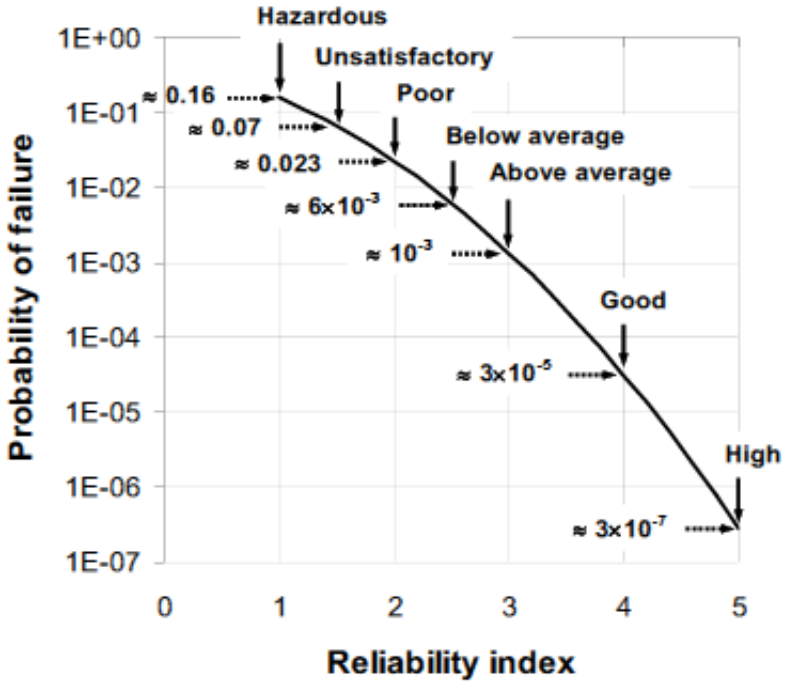

Figure 6.5 *- Probability of failure and reliability index with a description of the* (USACE, 1997) risk categorisation framework. *Extracted from (Phoon, 2004)*

The format used in Figure 6.3 and Figure 6.4 has offered a useful way to represent a large problem domain in a general dimensionless form. A range of observations have been made about this reliability based representation of V_{max}, both for a single s_u CoV and across variation in CoV. To take the interpretation of this problem further alternative methods of representing this data were investigated. The review of variation in $V/s_u.D$ for a single P_F (P_F = 1E-4 was used as an example) has already been noted as a metric of change, both with embedment depth and differences in s_u CoV. A similar metric would be the change in $V/s_u.D$ for a given change in P_F. This has been termed Fragility in this thesis, and although a slightly more complex metric, this fits well with the likely questions a designer would ask e.g. what increase in V will take a problem from a P_F that is acceptable to a P_F that is unacceptable. Fragility can be measured in terms of $V/s_u.D$ and is specific to the range of P_F selected. In deciding on a range of P_F that would be of interest the (USACE, 1997) risk categorisation framework was referred to, see Figure 6.5 for a diagrammatic representation of this framework produced by (Phoon, 2004). The P_F range selected was P_F=3e-5 to P_F=0.07, the $V/s_u.D$ required to go from a good reliability to unsatisfactory reliability within this (USACE, 1997) framework. V_{max} Fragility for this range of P_F has been plotted in Figure 6.6.

In addition to Fragility similar properties were investigated. This lead to development of Index of Fragility (I_F) as part of this study. This is comparable to other curve steepness metrics used in geotechnics e.g. the coefficient of uniformity used in the assessment of particle size distribution curves, see Equation [6.1] for a definition of I_F.

[6.1] $$I_F = \frac{V2}{V1}$$

Where;

I_F = Index of fragility

V1 = Reference Vertical load 1 i.e. $V/s_u.D$ for P_F=0.07

V2 = Reference Vertical load 2 i.e. $V/s_u.D$ for P_F=3E-5

I_F is calculated from the ratio of the V load for the highest P_F of interest (V1) and the V load for the lowest P_F of interest (V2). This implies as a system approaches an I_F of 1 it can be described as a low fragility system; I_F=1 is a deterministic system and decreasing values of I_F relate to increases in fragility. A summary of the calculation results for V_{max} Fragility and I_F is provided in Table 3-3, Appendix C. Figure 6.6 show a plot of Fragility and I_F by embedment depth, z/D, and s_u CoV.

The Fragility plot in Figure 6.6 is consistent with previous observations, with Fragility increasing with an increase in embedment depth. Additionally, for a given embedment depth an increase in s_u CoV leads to an increase in Fragility. This can be attributed to an increase in s_u CoV resulting in an increase in the spread of s_u values. When this wider spread in s_u is combined with a V_{max} function, or other capacity function, this results in an increase in the distance between V1 and V2 in load space, increasing fragility. This increase in fragility with s_u CoV seems to be approximately proportional to the change in CoV. For example an increase in s_u CoV from 0.10 to 0.15 results in a similar change in Fragility as the change from CoV=0.15 to CoV=0.20.

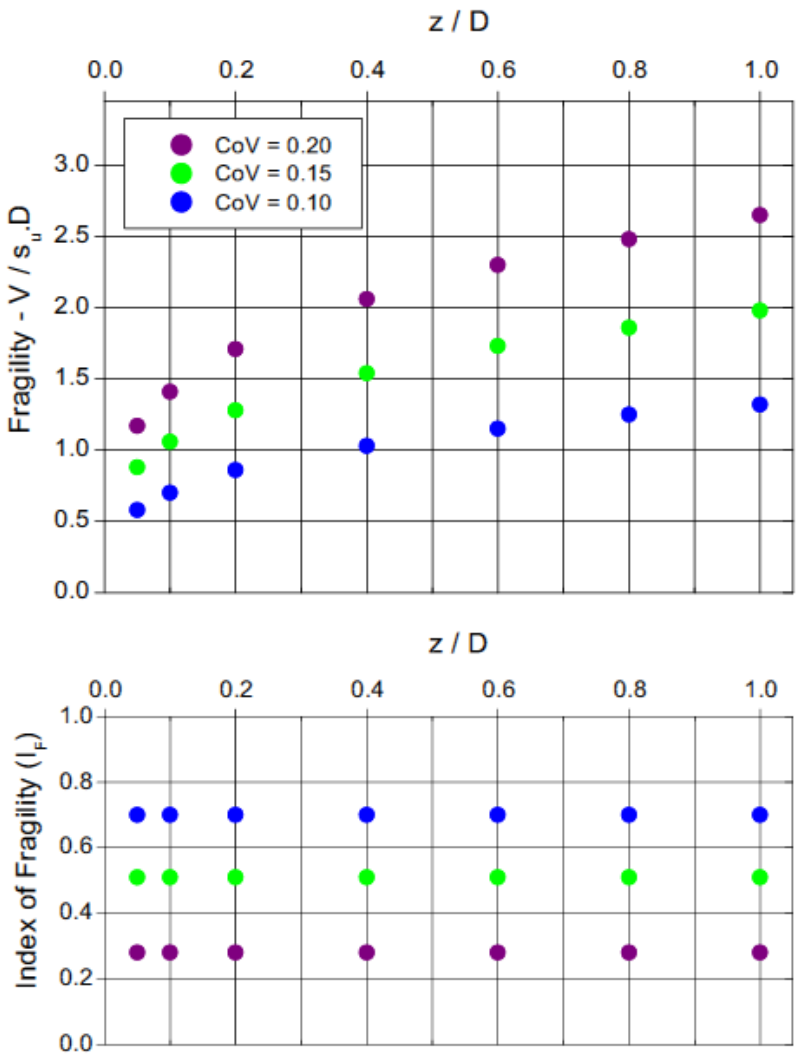

Figure 6.6 - *V_{max} Fragility and Fragility Index for the P_F range* P_F=3e-5 to P_F=0.07.

Perhaps the most significant property that can be observed in Figure 6.6 relates to the trend in I_F. I_F has been plotted against pipeline embedment depth. However, beyond a very small amount of scatter in the data at shallow depth, no change in I_F can be noted with a change in pipeline embedment. The only changes in I_F relate to the change in s_u CoV with an increasing value of I_F with a decrease in CoV i.e. a reduction in fragility. This has important implications for safety factors used in design, suggesting that a safety factor selected on the basis of s_u CoV and P_F would be appropriate for analysis of V_{max} for the problem definition and large pipeline embedment depth range considered in this section. It should be noted that this property arises from the definition of the stochastic system, either within the simplified method or MC method, and that it may not

apply to more complex systems with additional variables. Further discussion of this property is provided in Section 6.5 with links to application in design practice in discussed Chapter 7.

6.4 Reliability Based Analysis of H_{max}

Following on from analysis of V_{max} the same reliability techniques were applied to a study of H_{max}. This allowed initial investigations into a pipeline subject to V-H loading, prior to consideration of full V-H stability envelopes in Section 6.5. The probability of failure (P_F) was investigated with respect to the dimensionless horizontal load term $H/s_u.D$ with failure defined as $H > H_{max}$. A range of $H/s_u.D$ were analysed for seven embedment depth, 0.05D, 0.1D, 0.2D, 0.4D, 0.6D, 0.8D and 1.0D. As with previous reliability analysis three s_u CoV were considered, CoV = 0.10, 0.15, 0.20.

The simplified analysis methodology was applied to all the cases investigated, a total of 167 analyses. Following plotting of the analysis results a proportion of cases were selected for further investigation with MC analysis. The total number of MC analyses undertaken was 91. For further details of this analyses, including a summary of analysis parameters, see Tables 3-4, Appendix C.

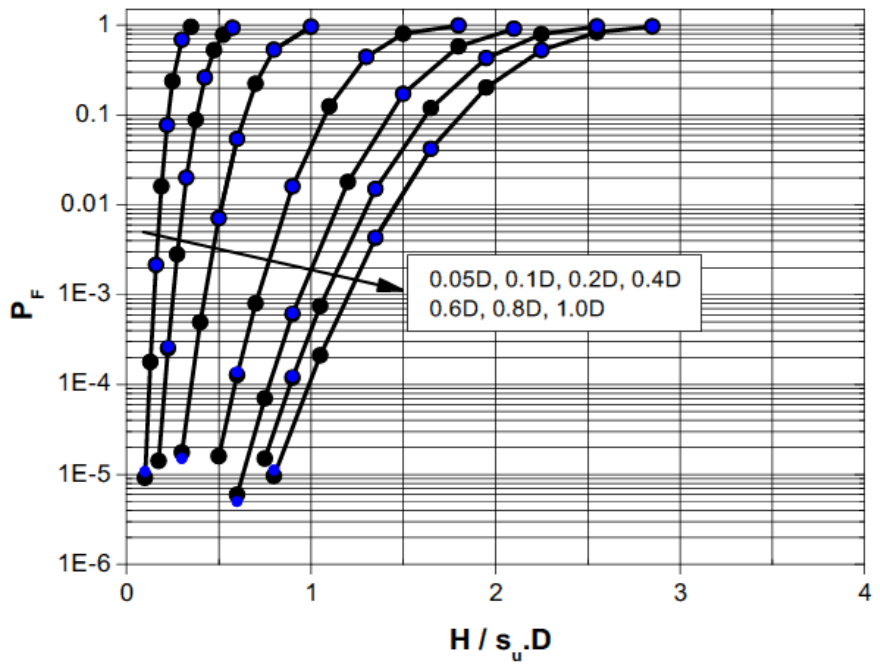

Figure 6.7 *- Reliability analysis of H_{max} for a CoV of 0.15. MC analysis show by blue dots. z = 0.05D, 0.1D, 0.2D, 0.4D, 0.6D, 0.8D, 1.0D.*

The value of H_{max} used in analysis was obtained from Equation [5.1] using coefficients summarised in Table 5.1. Spreadsheets incorporated a logical function to use the coefficients appropriate for the embedment depth being considered, either in the range 0.1D-0.5D or 0.5D to 1.0D. Analysis for z=0.05D was based on the same equation and coefficients i.e. an extrapolation from 0.1D. A smooth pipe-soil interface condition was adopted for this analysis and a weightless seabed with uniform mean undrained shear strength was used.

From Figure 6.7 it can be seen that for a given P_F an increase in pipeline embedment depth leads to an increase in $H/s_u.D$. At shallow depth this relationship appears to be approximately proportional, in that for a given increase in depth a similar increase in $H/s_u.D$ can be noted. This relationship also appears to be proportional at deeper depths, although with a smaller increase in $H/s_u.D$ for an increment of embedment depth. In both case the relationship is not expected to be directly proportional and s_u CoV is expected to be a modifier on the relationship. The latter point will be investigated further later in this section.

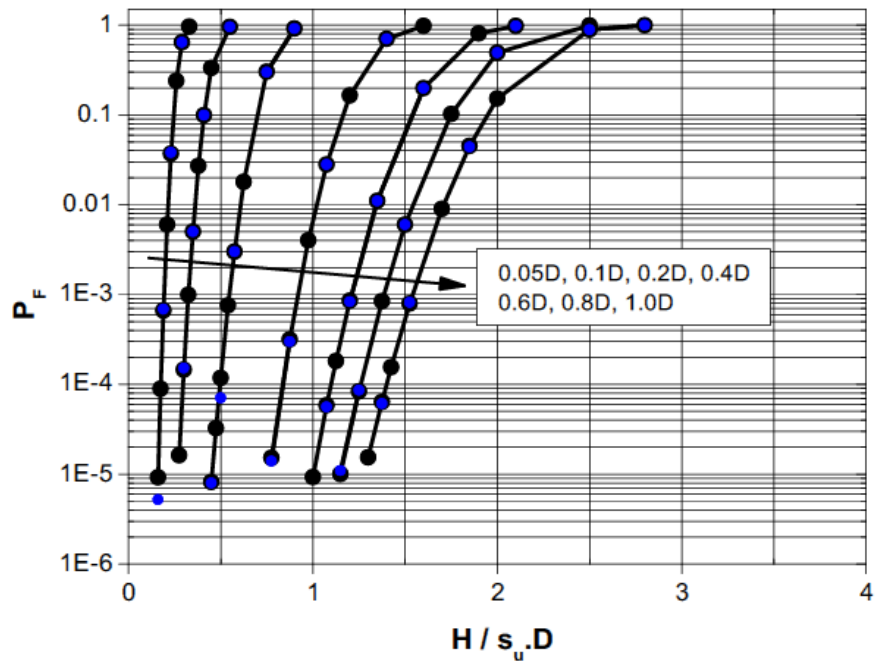

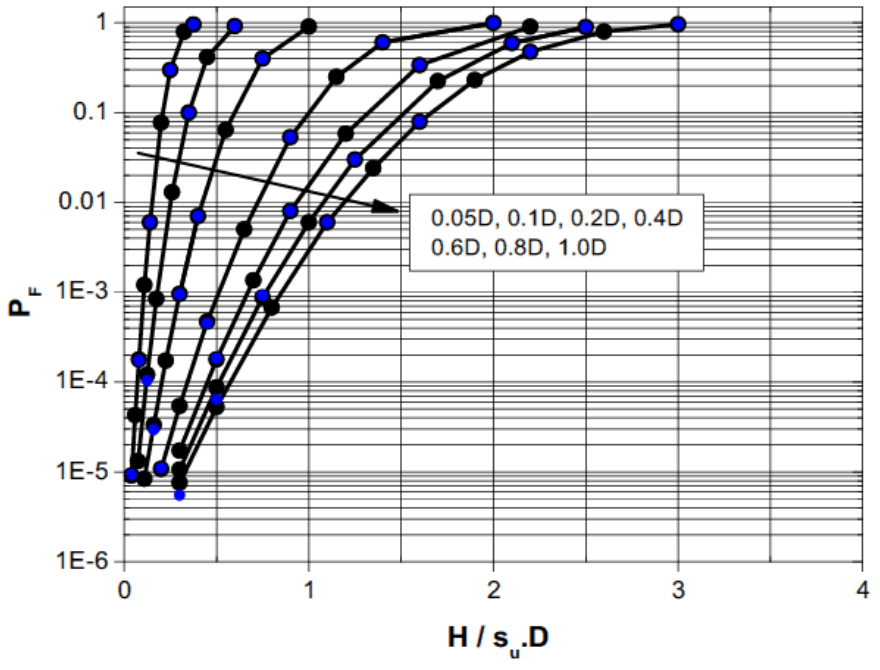

Figure 6.8 *- H_{max} CoV=0.10 (upper plot) and CoV= 0.20 (lower plot)MC analysis show by blue dots. z = 0.05D, 0.1D, 0.2D, 0.4D, 0.6D, 0.8D, 1.0D.*

In order to better display these observations related to Figure 6.7 the increase in $H/s_u.D$ with depth for a fixed P_F were plotted in Figure 6.9. The lines plotted in this figure represent cross sections across Figure 6.7. Four P_F were considered P_F = 3E-5, 1E-4, 1E-3 and 0.07. Additional data points at z/D=0.5 were calculated

using the simplified analysis method to better illustrate the change in trend in the vicinity of 0.5D.

The trends and effects noted in Figure 6.7 and plotted in Figure 6.9 can be attributed to the relatively linear trend in the pipeline embedment to H_{max} relationship, as described earlier in this study e.g. see Figure 5.1. The different gradient in this relationship above and below z=0.5D is also reflected in the reliability based analysis results, although the absolute gradient is dependent on the P_F selected with a steeper gradient (i.e. smaller change in $H/s_u.D$) for lower P_F. This plot format provides some insights into the effect of reliability analysis as a modifier on the H_{max} relationship. The format previously used in Figure 6.7 is more applicable to design applications by representing the full load to P_F relationship including changes with embedment depth.

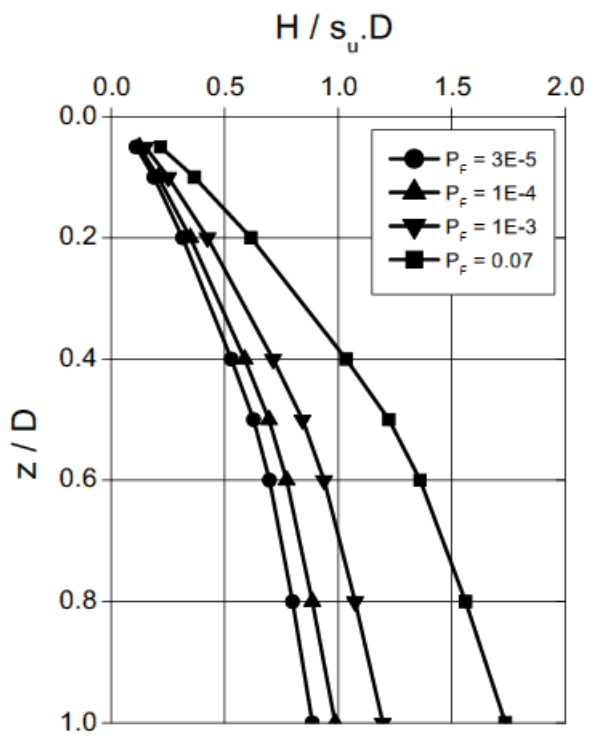

Figure 6.9 *- Change in $H/s_u.D$ with z/D for three P_F. CoV =0.15.*

As with the V_{max} analysis, Figure 6.7 shows a broadly linear trend in the P_F to $H/s_u.D$ relationship at lower P_F, before curving at higher P_F. The gradient of this linear section of the trend can also be noted to change with embedment depth. At shallow pipeline embedment, e.g. 0.05D, the relationship is very steep, near

vertical. This is steeper than previously noted for V_{max} relationships. As embedment depth increases the gradient of the P_F to $H/s_u.D$ relationship decreases. This pattern is equivalent to increasing Fragility with increasing embedment depth.

The effect of CoV on the trends noted in Figure 6.7 can also be reviewed by considering Figure 6.8, which shows analysis data for a s_u CoV of 0.10 and 0.20. This plot shows the same approximately linear section in the P_F to $H/s_u.D$ relationship at lower P_F. For a s_u CoV of 0.10 at shallow depth the P_F to $H/s_u.D$ relationship is the steepest seen in all the reliability analysis undertaken in this study, being only marginally less then vertical. It can also be noted that for the deepest embedment depths at a CoV=0.20 the upper curved section at higher P_F is relatively large, albeit there is still a linear section over the likely zone of interest. Between these two extremes there is a general trend in decreasing P_F to $H/s_u.D$ gradient with increasing CoV and increasing embedment depth. This trend is equivalent to an increase in Fragility with increasing s_u CoV

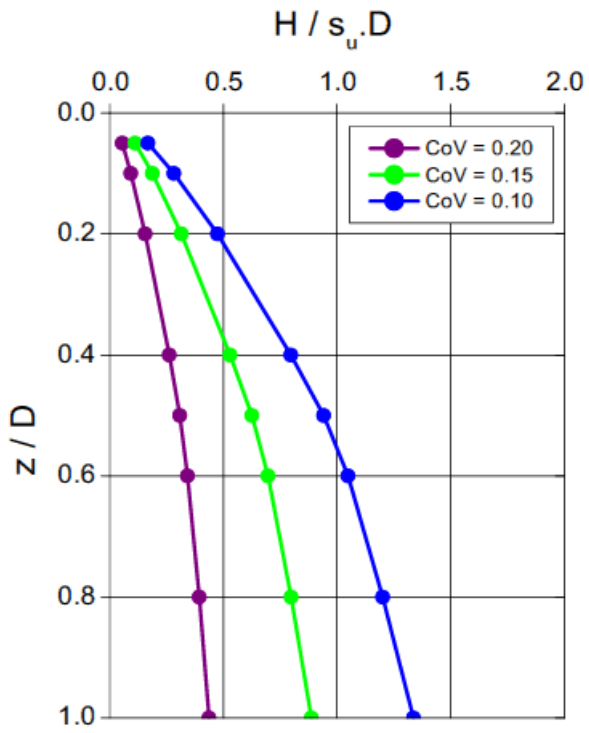

Figure 6.10 *- Effect of s_u CoV on $H/s_u.D$ against z/D relationship, P_F=3E-5.*

As can be expected, similar trends can be seen in the data presented in Figure 6.8 to those in Figure 6.7. It is therefore also of interest to plot cross sections

across Figure 6.8 as was previously done for Figure 6.7. In this case the change with s_u CoV is of particular interest. Figure 6.10 shows the $H/s_u.D$ to z/D relationship for a single P_F, P_F=3E-5, and three s_u CoV. Additional data points were added at z/D = 0.5, using the simplified analysis method. Again the underlying trend can be seen to reflect the H_{max} to depth relationship presented earlier in this study. However, in addition to the effect of changing P_F, noted previously, s_u CoV also has a significant impact on the gradient of the trend. A high s_u CoV has a steeper gradient (smallest change in $H/s_u.D$ with depth) with the gradient reducing with decreasing s_u CoV. Note as this is at a single P_F this does not reflect system fragility, but points to an effect that would work in conjunction with fragility, in particular when failure is taken as an increase in pipeline embedment.

Calculations of Fragility and Fragility Index were also prepared for the H_{max} analysis results. A summary of these calculation is provided in Table 3-5, Appendix C. These results are presented in a graphical format in Figure 6.11.

From a review of Fragility, as plotted in Figure 6.11, the same trends can be noted that have been seen in the plots earlier in this chapter. A trend of increasing Fragility with increasing pipeline embedment depth can be observed. The increase in Fragility with increasing s_u CoV can also be seen. In this format the trend in increasing Fragility with increasing embedment depth can clearly be seen to be approximately linear. The two different gradients in this linear trend, either side of z=0.5D, can also be noted in Figure 6.11.

As with the results for V_{max} plotted in Figure 6.6, the I_F results for H_{max} show an interesting property in the reliability based analysis of H_{max}. With the exception of some minor scatter, particularly at shallow depth, it can be noted that the I_F is independent of pipeline embedment depth. I_F increases with decreasing CoV with effectively the same value of I_F obtained for each value of s_u CoV. The higher degree of scatter for the H_{max} results compared to the results for V_{max} can be attributed to the smaller absolute value of Fragility, as well as some scatter associated with the steep trends in the P_F to $H/s_u.D$ relationship previously noted. In addition I_F being determined by CoV for the H_{max} problem, with a comparison to Figure 6.6 it can also be seen that for a given CoV I_F is the same for both the H_{max} and V_{max} problems considered here. As with analysis of V_{max} it should be noted that this property arises from the definition of the stochastic system, within the simplified method or MC method, and that it may not apply to more complex systems with additional variables. This property has implications for

choice of safety factor for these design problems. A safety factor selected on the basis of s_u CoV would be the same for both V_{max} and H_{max}, albeit a different target P_F may be chosen for these two problems.

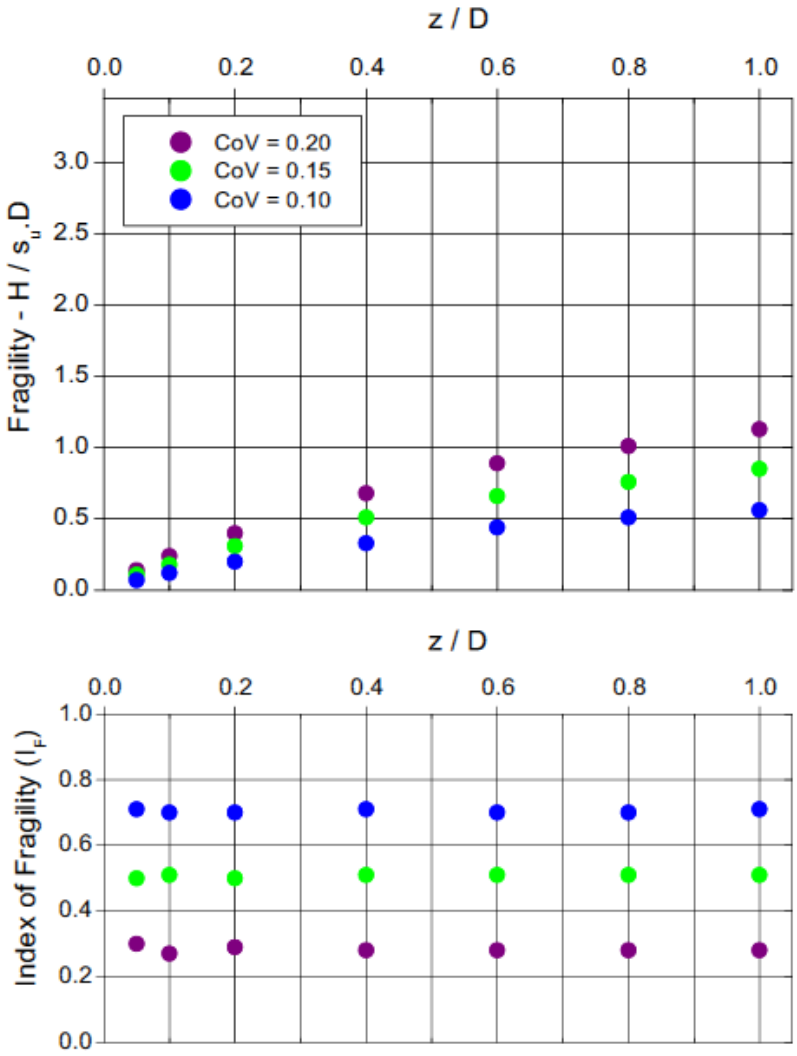

Figure 6.11 *- H_{max} Fragility and Fragility Index for the P_F range* P_F=3E-5 to P_F=0.07.

6.5 Reliability Based Analysis for V-H Loading

As with the deterministic cases investigated earlier in this study, reliability based analysis of V_{max} and H_{max} has provided a significant amount of information on the stability of a subsea pipeline on a clay seabed. However, further information can be gained by applying these reliability based analysis techniques to full V-H stability envelopes. A modification to the simplified reliability based analysis technique, previously detailed, allowed this to be used to investigate V-H stability envelopes by constraining analysis to a fixed V-H ratio reliability probe. Thus reducing the number of dimensions to the problem. This is understood to be the first application of this technique to V-H loading. MC analysis was undertaken, also with a fixed V-H ratio. Analysis results from the simplified analyses and the MC analyses are reported within V-H load space using the dimensionless load terms $V/s_u.D$ and $H/s_u.D$. A resistance term $R/s_u.D$ was also used, representing the total resultant resistance arising along a given load path.

A suite of analyses was undertaken for one pipeline embedment depth, z=0.2D. A smooth pipe-soil interface condition was adopted and a weightless seabed with a uniform mean undrained shear strength was used. Three soil undrained shear strength (s_u) coefficients of variation (CoV) were investigated, CoV = 0.10, 0.15, 0.20. A deterministic V-H stability envelope was also calculated for reference purposes. For each s_u CoV, a series of reliability based V-H stability envelopes were constructed for defined probabilities of failure (P_F). Failure is defined as the probability of the V-H load case exceeding the defined stability envelope.

For a s_u CoV of 0.15 six stability envelopes were produced. These envelopes were P_F = 0.07, 0.01, 1E-3, 1E-4, 3E-5 and the deterministic reference case. For a s_u CoV of 0.10 and 0.20 four envelopes were initially produced, P_F = 0.07, 0.01, 1E-4 as well as the deterministic case. From the analyses of a s_u CoV of 0.15 it was noted that the envelope for a P_F=3E-5 was very close to the adjacent PF=1E-4 envelope. However, for completeness and to bound the problem, analyses using the simplified method only was undertake for a P_F=3E-5 to add to the relevant plots for a CoV of 0.10 and 0.20. For each CoV and P_F an envelope was defined with 10 termination points. Each of these termination points was associated with a fixed V-H ratio reliability based probe, with the V-H ratio defined as an angle in load space δ_{LS}. A total of 130 analysis were undertaken with the simplified analysis methodology. For further details of analysis cases and a summary of analysis results see Table 3-6, Appendix C.

MC analysis was formulated to provide a series of results along a selected V-H ratio reliability probe. This allowed stability envelope termination points to be calculated for each of the P_F of interest along a given probe from a single analysis. Of the 10 δ_{LS} probes investigated with the simplified reliability analysis method 6 were also analysed with MC analysis. With analysis for each of the three s_u CoV this was a total of 18 MC analysis producing 66 stability envelope termination points. The number of simulations (N) for each of these MC analysis was based on the requirements arising from the lowest P_F investigated along the reliability probe. Reliability probes associated with a s_u CoV of 0.15 included stability envelope termination points at P_F=3E-5, N=1.5E6 was used for these cases. For s_u CoV of 0.10 and 0.20 the lowest P_F investigated with MC analysis was a P_F=1E-4, for these cases N=800,000 was used.

Both the simplified analysis and the MC analysis utilised the various deterministic fitting equations previously obtained in this study, as reported in Chapter 4 and 5. As noted in Section 5.2 calculation of a V-H stability envelope requires a value for V_{max}, H_{max}, and parabolic skew parameters β_1, β_2, and β. V_{max} values used in this reliability analysis was based on Equation [4.4] and the fitting coefficients from Table 4.3. H_{max} was obtained from Equation [5.1] and Table 5.1. The skew parameters β_1 and β_2 were obtained from Equation [5.4] and Equation [5.5] with fitting coefficients from Table 5.2. Having obtained β_1 and β_2, β was obtained from Equation [5.3].

Figure 6.12 shows a decrease in the size of the V-H stability envelope and a reduction in the size of the yield surface in association with a decrease in P_F. This was as expected based on previous analysis of V_{max} and H_{max}, albeit this format is a dramatic way of illustrating the combined effect of a reduction in V_{max} and H_{max} when a lower P_F is required. The largest absolute change in envelope size is around V_{max} with a reduced effect towards H_{max}. Vertical uplift, i.e. δ = -90, for a smooth interface condition is zero and represents a constant origin point for all envelopes, regardless of P_F. At a shallow depth such as this case at z=0.2D the soil resistance above H_{max}, i.e. δ = 0 to δ = -90, is relatively small and the effect of a change in P_F is correspondingly small for this portion of the stability envelope. Adding to the information previously obtained for V_{max} and H_{max}, this analysis considers the whole V-H envelope showing the continuity of this trend over a range of load paths and pipeline displacement angles. Another important observation that can be made from Figure 6.12 is that although the stability envelopes decrease in size they keep a constant shape between the points defined by V_{max}, H_{max} and the origin point at zero load. A constant geometry of

yield surface has implications for application to design practice, which will be discussed later in Section 6.6 and Chapter 7.

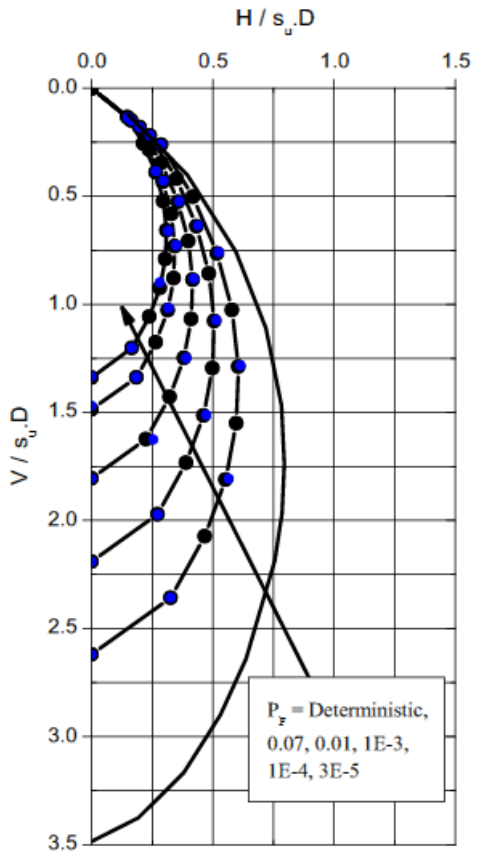

Figure 6.12 *- Reliability based analysis of a V-H stability envelope, s_u CoV=0.15. Blue dots show MC analysis.*

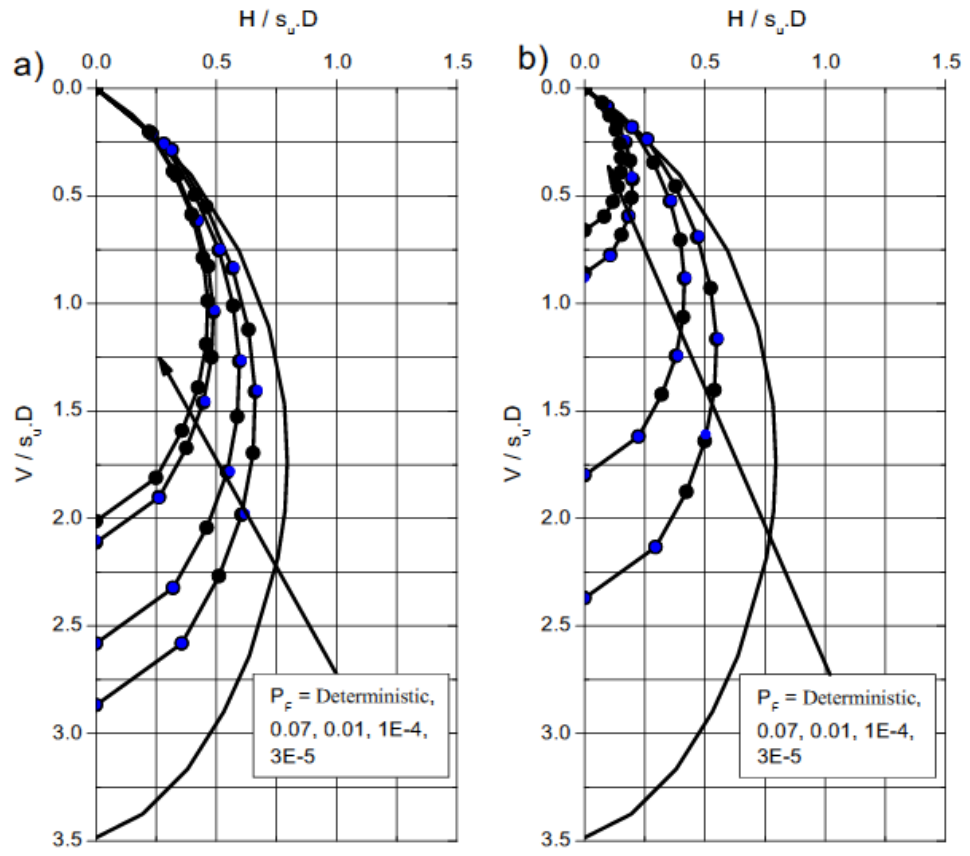

Figure 6.13 *- Reliability based analysis of a V-H stability envelope, s_u CoV=0.10 and 0.20. Blue dots show MC analysis.*

Figure 6.13 shows the effect of s_u CoV on the size of a V-H stability envelope. In all cases a change in P_F produces a significant change to the size of the stability envelope, but not the overall shape as previously noted for Figure 6.12. The difference between the two plots in Figure 6.13 is very marked, showing the large influence of the s_u CoV on the change in the V-H envelope arising from a given variation in P_F. A small s_u CoV such as CoV=0.10 produces the smallest change in the stability envelope whereas for a CoV=0.20 the largest change can be noted. A dramatic example of this can be seen in comparing the size of the P_F=1E-4 envelope for the two s_u CoV presented in Figure 6.13. Comparisons can also be made with Figure 6.11, showing the influence of an intermediate s_u CoV.

Previous observations related to Fragility and Fragility Index (I_F) for V_{max} and H_{max} suggested that the behaviour noted for these principal points would also be applicable to other points on the V-H stability envelope. However, to verify this assumption the data presented in Figure 6.12 was investigated further with Fragility and I_F calculated, as plotted in Figure 6.14.

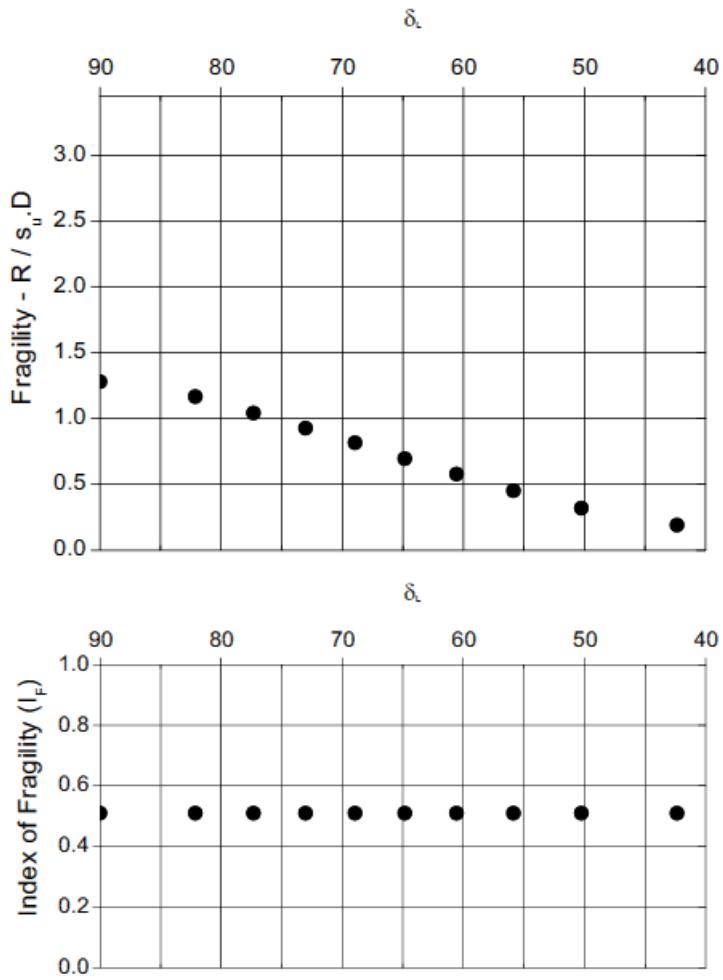

Figure 6.14 *- Fragility and Fragility Index for the data previously presented in Figure 6.12, a s_u CoV of 0.15.*

Figure 6.14 plots Fragility and I_F in terms of the displacement angle in V-H load space, δ_{LS}. The methodology for these calculations is the same as previously used to investigate V_{max} and H_{max} and considers the same P_F range, from P_F=3E-5 to P_F=0.07. Fragility follows a clear decreasing trend across the range of angles considered, consistent with the observations previously made with respect to Figure 6.12.

The most significant point of interest in Figure 6.14 is the constant value of I_F, which is also the essentially the same value obtained for analysis of V_{max} and H_{max} for the same s_u CoV, in this case a CoV=0.15. With respect to application to design practice, this confirms that a safety factor based on s_u CoV will be appropriate for the full V-H stability envelope, assuming a constant design P_F is required in all directions in V-H load space.

The methods used to calculate the pipeline V-H stability envelopes presented in this section provide a set of tools which can be used in pipeline design, either within a P_F framework or to provide guidance on the relevant safety factors to apply to the deterministic envelopes discussed earlier in this thesis. The maintenance of a constant shape for the pipeline V-H stability envelopes with a change in P_F is significant with the plastic potential surface also expected to stay the same over a range of P_F. For further discussion of application to design practice see Chapter 7.

6.6 Discussion

This chapter has reported results from the application of reliability based analysis techniques to pipe-soil interaction on a clay seabed. These studies have varied from example applications, which have still provide some insight into the problem, to more extensive parametric studies. Areas investigated include;

- An example of the application of reliability analysis to a vertically loaded pipeline
- A reliability based parametric study of V_{max} including an assessment of system fragility
- A reliability based parametric study of H_{max} along with an assessment of system fragility
- Application of reliability based analysis techniques to V-H stability envelopes

As has been noted in Chapter 2 no previous research appears to have been reported in this area. Additionally, in the absence of a long history of use for pipe-soil interaction design methods, as is the case with some onshore geotechnical engineering design methods, appropriate safety factors for these design problems are not easily defined from experience alone. The techniques outlined in this chapter provide an alternative to a fixed safety factor whereby the problem is described in terms of a probability of failure (P_F). A selected P_F can be compared to generally accepted norms, e.g. see Figure 6.5, or defined on a project specific basis. These methods also allow these pipe-soil interaction problems to be benchmarked to other geotechnical problems or even problems from other disciplines, such as structural engineering.

An example of the application of reliability analysis to a vertically loaded pipeline has been presented in this chapter. This considered the case of a single pipeline

diameter with one vertical load. For this problem the effect of the soils shear strength coefficient of variation (CoV) on the expected depth of pipeline embedment was seen. This example is also similar to a design problem that might be used on a pipeline project, demonstrating the use of reliability based techniques to a simplified problem.

A more general V loading problem was investigated with reliability based analysis of V_{max}. This showed the effect of s_u COV over a wide problem domain. The fragility of this problem was investigated with a metric developed to quantify fragility, the Index of Fragility (I_F). Index of Fragility allows comparisons in system fragility between this and other problems, for example comparisons with H_{max} later in this chapter and in the wider sense other geotechnical or engineering problems. Investigations into I_F also showed that the same safety factor for pipeline embedment depth was appropriate for the full depth range considered, with I_F only changing with s_u CoV not pipeline embedment. An appropriate safety factor could be selected based on a target P_F and the s_u CoV.

A similar reliability based analysis study was undertaken into a H_{max} problem domain, comparable to the earlier study into V_{max}. In addition to providing an overview of the H_{max} problem within a wide reliability based problem domain investigations were undertaken into system Fragility, including I_F. These investigations into I_F indicated that not only is I_F pipeline embedment depth independent, but also that I_F was the same for both H_{max} and the previous analysis of V_{max}. This suggests an appropriate safety factor can be selected for a wide depth range based on s_u CoV and that this safety factor will be applicable to both V_{max} and H_{max} behaviour.

Following reliability investigations into V_{max} and H_{max} full V-H loading stability envelopes were considered. Techniques were proposed that constrained the problem to a series of fixed V-H ratio reliability based probes, allowing both a simplified analysis method to be used and practical well constrained MC analysis. It is understood this is the first application of the simplified analysis technique to this type of V-H loading problem. The reliability based probes produced termination points on stability envelopes that defined V-H stability for a specific P_F. As with previous analysis in this chapter the simplified analysis method produced useful results which were not only rapid to calculate, but also agreed well with MC analysis techniques. The results from reliability analysis of V-H stability envelopes show the dramatic reduction in the size of the V-H stability envelopes within a reliability based framework, especially for lower target P_F.

Analysis showed how s_u CoV influences this problem. Significantly it was noted that the stability envelopes maintained the same geometry across various P_F and s_u CoV. This would allow these reliability based stability envelopes to be used with the techniques outlined in Section 5.5 to consider large displacement behaviour within a reliability based framework. Investigations into index of fragility also showed the same trend noted for V_{max} and H_{max}. This suggests that a safety factor determined from s_u CoV and a target P_F will be applicable to full V-H pipeline stability.

In this chapter a range reliability based analysis techniques have been demonstrated. This has included the application of a simplified method and the application reliability based techniques to V-H stability envelopes. Observations on the effect of s_u CoV on pipeline stability within a reliability based framework have been made. General guidance on safety factors has been given as well as outlining the tools that can be used to determine a project specific safety factor for pipeline stability. The problem definitions used within this chapter are linked to the deterministic problem definitions addressed earlier in this study, as well as being similar to previous numerical analysis studies in the literature. The analyses reported in this chapter add a reliability based analysis interpretation to these problems. These problem definitions included some simplifications, for example using a constant shear strength and weightless seabed. In some cases this will be a reasonable approach, either because it is sufficiently representative of the field conditions or because it represents a conservative approach. It can be noted the impact of unit weight can be assessed using the techniques outlined in Section 4.5 e.g. the $s_u/\gamma'.D$ ratio.

Consideration of a multivariable problem is considered an important next step from the analysis shown here, to allow reliability techniques to be applied to the more generalised problem of a more complex shear strength distribution e.g. a linearly increasing shear strength gradient or a crust, for which deterministic analyses were conducted in previous chapters. This adds complexity to the reliability problem definition. MC analysis can readily cope with multi variable reliability problems, albeit there are implications for analysis time. The formulation of the simplified reliability method outlined within this chapter is such that it could be applied to cases when the multiple contributions to capacity have the same CoV. In the more likely event that the various variables have different CoV MC analysis would be preferred. Additionally, with the simplified method care would be needed to ensure that this method can readily identify the

capacity in reliability space, a complex failure surface may require integration with an optimisation approach to identify the minimum capacity.

For further discussion with respect to application of the techniques in this chapter to design practice see Chapter 7. The overall conclusions of this study, including potential areas for future research, are also addressed in Chapter 7.

7 Conclusions

7.1 Study Conclusions

This thesis has reported the results of a study investigating pipe-soil interaction on a clay seabed, as relevant to the design of subsea pipeline systems for offshore oil and gas developments. Numerical analysis techniques based on the finite difference code FLAC were used to investigate a range of problems for a pipeline subjected to Vertical (V) loading and combined Vertical (V) and Horizontal (H) loading. Reliability based analysis techniques were also applied to a range of these problems. The aims and objectives of this study, as previously outlined in Section 1.2, have been successfully achieved.

The first objective of this study was to undertake a literature review for pipe-soil interaction on a clay seabed and related areas, as reported in Chapter 2. This literature review provided context and helps to clarify the original contributions made within this study. Additionally this review identified numerical analysis undertaken by previous researchers which provided some useful comparisons and validation for analysis undertaken in the early parts of this study.

The original contributions of this study can be broadly categorised into four areas, as follows;

- Reproduction and validation of earlier research with additional review and interpretation.
- Extension of problem definitions to greater pipeline embedment depths.
- Investigation of new problem definitions.
- Application of reliability based techniques to pipe-soil interaction on a clay seabed.

Chapter 4 reports the results of investigations into a pipeline subjected to V loading, with the scope of these investigations falling into three of the four areas noted in the bullet points above. The final point, reliability based analysis of V loading problems, is reported in Chapter 6.

The case of a pipeline subjected to vertical loading on a homogenous strength weightless seabed has been investigated by Aubeny et al. (2005) and a study limited to a pipeline embedment depth of 0.5D undertaken by Merifield et al. (2008). Analysis undertaken as part of the study reported in this thesis showed good agreement with this earlier research, supporting the conclusions of the

earlier research and validating the methodologies used in this study. Extensive use was made of data presentation tools, such as soil displacement vector plots, to provide a framework for detailed interpretation of analysis results. Displacement vector plots were found to be a useful tool for interpretation of analysis results and these were used extensively throughout this study.

Previous analysis results were also available for a large strain V loading problem definition from a study undertaken by Merifield et al. (2009), although that study was limited to a pipeline embedment depth of 0.5D. This depth limitation obscured effects related to the full diameter of the pipeline coming in to contact with the seabed. The study reported here extended the depth of analysis to 1.0D. Lack of generality at very shallow pipeline embedment depths due to the influence of elastic soil properties was also identified in this study. Analysis results from this study generally agreed well with previous research for depth ranges where comparative data was available. Within this problem definition large strain effects were shown to be relatively small, especially below a pipeline embedment depth of 0.4D to 0.5D.

A new problem definition investigated as part of this study was the case of variation in pipe-soil interface strength. Previous numerical analysis of a pipeline on a clay seabed has been limited to a perfectly smooth or rough pipe-soil interface condition. As part of this study parametric analysis was undertaken to investigate behaviour under vertical loading between these bounds. This analysis showed a relatively complex picture, whereby the effect of interface properties were both non-proportional and varied with pipeline embedment depth. An example of this non-proportionality in interface behaviour is the case of an interface that mobilises half the shear strength of the soil, the capacity under vertical loading for this case does not lie half way between the rough and smooth interface condition. Additionally, the resistance for this and other examples varied relative to the rough and smooth interface condition with changes in pipeline embedment depth.

Pipeline coating, both actual pipeline coating and simulated pipeline interface properties in model testing, is unlikely to behave as either a perfectly smooth or rough interface and different types of coating may behave differently. This area of the study provides useful insights into interface behaviour, emphasising the importance of consideration of interface properties if further refinement in design tools is targeted and if better integration between model testing and numerical analysis is going to be achieved.

The effect of soil unit weight was investigated, including extending the pipeline embedment depth range analysed from that considered by previous researchers and introducing interpretation in terms $s_u/\gamma'.D$ as a tool to assess the impact of soil unit weight effects. A design equation to assess the effect of soil unit weight was provided for the depth range from 0.5D to 1.0D, supplementing previous analysis to a depth of 0.5D. Using $s_u/\gamma'.D$ as a metric it was shown at higher $s_u/\gamma'.D$ soil unit weight effects are negligible, becoming more significant at lower $s_u/\gamma'.D$. The limited effect of soil unit weight at a shallow pipeline embedment depth was also shown, along with the increase in this effect as depth increases.

Previous numerical analysis based research of V loading problems has largely considered uniform soil shear strength conditions. An extensive parametric study was undertaken to investigate a range of non-uniform shear strength problem definitions. Linear increasing shear strength conditions were considered, with a new framework developed to represent the shear strength gradient and strength intercept at mudline. This framework was better suited to pipeline design problems then the generally adopted approach to describing linear increasing shear strength gradients. Fitting equations were provided to describe the behaviour of a pipeline under V loading on a seabed with a range of linear increasing shear strength gradients, showing both a decrease and increase in resistance to V loading depending on depth of embedment, interface conditions and the specifics of the shear strength gradient.

The less general case of a shear strength crust was also investigated, a problem definition not previously considered prior to this study. A range of example crusts were presented. A dramatic reduction in V load capacity associated with a punch through failure mechanism was shown from analysis results, along with examples of how the relationship between pipeline and crust geometry can impact V load capacity.

In addition to investigating the behaviour of pipelines under V loading the more complex case of combined V-H loading was also considered in this study. As with V loading a range of original contributions were made falling into the categories outlined in the earlier bullet points. The results of these investigations are reported in Chapter 5, with the reliability based analysis reported in Chapter 6. As for V loading some of the problem definitions have been considered by previous research, allowing this study to make comparison with this earlier research prior to extending this study to investigate other problems, or a deeper pipeline embedment.

For the case of a uniform shear strength weightless seabed there was good agreement between both H_{max} and the V-H stability envelopes from this study and the work of previous researchers. This study then extended this analysis from a maximum pipeline embedment depth of 0.5D to 1.0D, allowing effects associated with this additional penetration to be investigated. This was considered particularly important as 0.5D is the point at which the full width of the pipeline is in contact with the seabed.

This study also extended analysis of a pipeline subjected to V-H loading to the case of a pipeline on seabed with a linear increasing shear strength gradient. This addressed pipeline embedment depths up to 1.0D. Fitting equations and associated fitting coefficients were provided for this problem.

The case of a pipeline on a sloping clay seabed had not been previously investigated. Two problem definitions were considered within this study. For the case of a weightless seabed a general solution was provided to rapidly assess the effect of any in plane slope angle on a pipelines V-H stability envelope. This method allowed a stability envelope for a given slope angle to be derived from a flat seabed V-H stability envelope by expediently rotating the forces from a local coordinate system parallel to the slope to a global coordinate system. The less general case of a sloping seabed with soil weight was also investigated. As with V loading the effect of $s_u/\gamma'.D$ ratio was demonstrated to be an important metric for assessing the impact of soil unit weight. It was also shown that unit weight effects on a sloping seabed were confined to specific areas of the V-H stability envelope. Interpretation of this pattern was undertaken with support from vector plots of calculated soil displacement for a range of displacement vectors and $s_u/\gamma'.D$ ratio.

Analysis of large strain large displacement behaviour is computationally intensive and lacks generality, additionally previous research in this area has a number of limitations. Ride-in and ride-out behaviour can have a significant effect on resistance to horizontal displacement and is likely to be an important consideration if a more dynamic approach to pipeline stability is adopted e.g. allowable displacement criteria. A demonstration of the effect of ride-in and ride-out effects was presented using a series of small strain V-H stability envelopes and an understanding of the geometry of the plastic potential surface, with previous analysis in this study suggesting associative flow was a reasonable representation of post failure behaviour.

It is a study objective to place the pipe-soil interaction on a clay seabed into a reliability based analysis framework allowing input variables, such as soil undrained shear strength, to be treated stochastically rather than deterministically. This provides an important link between the relationships reported earlier in this study and design practice. In addition to use in this study these reliability methods can also be applied to previous and future research, with the methodologies described in Chapter 3 providing a useful contribution to these problems.

The reliability based methods used in this study provide a link between probability of failure and safety factors, as impacted by a combination of the capacity relationship and load case. Concepts such as fragility, and the fragility index developed as part of this study, provide fundamental information on system behaviour and the influence of parameter uncertainty on system behaviour. The results of investigations with reliability based analysis techniques have been reported in Chapter 6. A review of the literature suggests this is the first application of these techniques to pipe-soil interaction problems, it is also believed that this is the first application of a simplified reliability based analysis method to V-H loading.

Reliability based analysis was initially applied to a relatively limited problem definition, a single pipeline diameter and single V load case. This problem definition lacks generality, but did provide some insight into this simplified case and similar cases. In particular the impact of soil undrained shear strength coefficient of variation was noted. This analysis also demonstrated the use of reliability based techniques for a problem that could be representative of a project specific pipeline design problem.

Following the analysis of a limited V loading problem more general cases were investigated with application of reliability based analysis techniques applied to V_{max} and H_{max}. Cross validation between a simplified spreadsheet based method, modified for use in this study, and a Monte Carlo analysis methodology was confirmed with agreement between these methods. The simplified procedure presented in this study provides a rapid method for analysing a large number of cases and identifying overall trends in system reliability. Fragility was investigated for both V_{max} and H_{max}. The use of index of fragility, developed as part of this study, demonstrated important trends in the data. Index of fragility is independent of pipeline embedment depth only changing with soil undrained shear strength (s_u) coefficient of variation (CoV). Index of fragility is also the

same for V_{max} and H_{max}, again only varying with s_u CoV. This suggests the same probability of failure (P_F) can be achieved for both problems with the same safety factor, where the safety factor required for a target P_F is dependent on s_u CoV.

In addition to V_{max} and H_{max} problems a methodology was developed as part of this study to construct V-H stability envelopes for a defined P_F. This method used a series of fixed V-H ratio reliability probes to define termination points on the V-H stability envelope. This methodology can be implemented in both a simplified spreadsheet based methodology and with MC analysis. Index of fragility was also investigated for a reliability based V-H stability envelopes, again indicating s_u CoV is the controlling variable and determines the required safety factor to provide a target P_F.

Application of the methodologies and findings of this study to design practice are considered in the next section, Section 7.2. Potential areas for future research are discussed in Section 7.3.

7.2 Application to Design Practice

The analysis methods and results reported in this thesis are applicable to design practice for subsea pipelines on a clay seabed. A range of literature describing analysis methods and results for pipe-soil interaction problems on a clay seabed has been summarised in Chapter 2. This provides a good overview of the academic literature, but this is not necessarily fully representative of the current state of design practice. An alternative approach to consider design practice is to review pipeline design codes and recommended practice documents in order to give context to this study.

Two example pipeline design codes that characterise current design practice are BSI (2015) and DNV (2007). BSI (2015) suggests it is common design practice to consider pipe-soil interaction as a friction coefficient, including on a clay seabed. Although it is noted that this is an empirical simplification rather than an accurate physical representation. No design methods are provided, instead a table of "typical effective coefficients" is presented, citing experience of use in the North Sea. The range of friction coefficients is relatively broad from 0.3 to 0.75 and no guidance is given on selecting within this range, or indeed when this range might not be applicable. DNV (2007) also suggest the widespread use of a friction coefficient approach. In this recommended practice some design methods are presented for example for pipeline penetration and lateral resistance. Although poorly referenced it would appear that the analysis methods provided

in DNV (2007) are based on early model testing studies e.g. Wagner et al. (1987), Brennodden et al. (1989) and Verley and Lund (1995).

A review of BSI (2015) and DNV (2007) suggest significant limitations in current design practice. However, it is not believed that these design standards preclude the using of alternative approaches to design. BSI (2015) in particular leaves the option of use of a range of approaches with open statements such as "Soil bearing capacity should be evaluated using soil mechanics theory...". The methods and fitting relationships provided in this study and other similar research referenced in Chapter 2 offer improvements to the state of practice summarised in these two design standards.

Earlier stage design, where there may be limited engineering resources expended, can particularly benefit from fitting relationships to numerical analysis data as presented in this and similar studies. This allows rapid analysis of design problems such as pipeline penetration or V-H stability without the need for the numerical analysis to be repeated. As a design tool these fitting relationships are also readily linked to measurable geotechnical parameters such as soil undrained shear strength, which can also be integrated with reliability analysis techniques to address uncertainty in these parameters, if required. These fitting relationships can then be carried on to more detailed later stage design. Additionally for critical, particularly sensitive applications, or cases that depart somewhat from the problem definition for which fitting relationships are available, a project or site specific suite of numerical analysis can be undertaken. This project specific analysis could be undertaken using similar numerical analysis techniques to those used in this study, adding further refinement to analysis when required, or addressing specific issues.

Various aspects of this study provide tools to assess if a site or project specific pipe-soil analysis is required, or if various fitting relationships are a reasonable representation. For example, study of variation in interface conditions can be used to assess if interface conditions need to be investigated further, or if bounding the problem with a rough and smooth interface condition is reasonable. The concept of $s_u/\gamma'.D$ provides a useful tool to estimate the influence of soil unit weight and to feed into the decision process with regards to any requirement for a more complex analysis that accounts for unit weight effects. The relationships provided for a range of shear strength gradients and examples of some shear strength crusts provided in this study can be used to consider a very wide

variation in soil conditions, or be used in an assessment with respect to if a site specific representation of conditions is needed, say for a later stage design work.

The use of reliability based techniques within this study provides a framework to assess the probability of failure for a given design problem. These methods provide a rational and rigorous approach to accounting for uncertainty in geotechnical design parameters. It is also possible to widen the scope of this analysis to address other uncertainties in the design problem, or integrate with wider reliability based studies. A greater use of reliability based analysis techniques for pipe-soil interaction problems is recommended. Development of simplified reliability based methods for more complex problem definitions, e.g. multi variable problems, is a promising area for future research.

Cassidy (2006) raised the issue of how pipeline design engineers can incorporate increasingly complex analysis techniques, and results, into general purpose finite element analysis used for pipeline structural design. This concern is consistent with the emphasis on simple friction coefficients with the design codes cited earlier in this section. Additionally the pipeline engineer may have little or no background in geotechnics. Cassidy (2006) discussed the use of macro elements, where pipeline behaviour under loading is captured by a macro element similar to the stability envelopes presented in this study. Change in the geometry of the stability envelope is described by a flow rule that describes the plastic potential surface. This is similar to the approach used to assess ride-in and ride-out behaviour in Section 5.5. An additional interesting perspective to this is the reliability based stability envelopes produced in this study. It should be possible to develop reliability based macro elements for use in pipeline design.

If a macro element approach is considered too complex for use in pipeline design, for example for early stage preliminary design, it may still be possible to work within a friction coefficient framework, albeit it is far from ideal. The geotechnical specialist could assess pipeline penetrations under V load and derive representative friction coefficient for V-H loading problems using methods in this and similar studies. Although, as discussed in BSI (2015), it should be noted that a friction coefficient approach would be purely for analytical convenience rather being fully representative of the problem. Care is also needed if even minor changes to the problem occur and the friction coefficients may need to be recalculated as they could change disproportionally.

In addition to, and setting aside, the specifics of how analysis is undertaken by the pipeline engineer; the application of methods and results of this and similar studies to pipe-soil interaction problems is recommended. Deriving pipe-soil interaction from numerical analysis, possibly with future integration with physical modelling techniques, offers a rational and rigorous approach to considering a wide range of pipe-soil interaction problems.

7.3 Potential Areas for Future Research

In undertaking this study a number of potential areas for future research were identified. These areas are summarised in this section.

Correlations and fitting relationships have been produced for a range of problems within this study. The benefit of these relationships for rapid assessment of pipe-soil interaction problems in design practice has also been highlighted in discussions of application to design practice. A potential area for future research may be to establish further fitting relationships for other pipe-soil interaction problem definitions. Some of these problem definitions may be region specific, e.g. to address specific and/or more complex soil conditions. However, provided they occur as a design problem with some regularity and can be described with an appropriate generalised framework it is likely to be beneficial to undertake this further research. The fitting relationships presented in this study for V-H loading followed the sequential approach used by previous researchers i.e. consider V_{max}, consider H_{max} then fit skew parameters. Future research could give consideration to fitting V-H stability envelopes to analyse data as a 2D optimisation problem.

Unfortunately there is limited integration between physical modelling of pipe-soil interaction and recent numerical analysis. The effect of variation in pipe-soil interface strength investigated as part of this study highlights one of the complexities of this further integration. The accuracy of measuring soil shear strength for model testing is another barrier. This represents a promising area for future research with potentially significant benefits. It is likely that this further integration will require physical modelling to be reported in the same format as numerical analysis as well as providing further details of pipe-soil interface conditions. A range of interface roughness model tests may also be needed. Initial linking to numerical analysis may be more readily undertaken for a simplified element test prior to extension to a model pipeline. There may also be a requirement for more complex interface elements in the numerical analysis,

for example one that considers interface normal stress and, or, strain softening. The reliability based techniques used in this study, or similar techniques, may be usefully applied to model test data to quantify uncertainty of variables such as soil shear strength. This may require an extension to multi-variable reliability methods. In a wider sense it would be beneficial if greater details on pipeline coating properties were available in the public domain.

When considering shallow pipeline penetration depths within a large strain analysis problem definition it was noted that a lack of generality was introduced due to soil elastic behaviour. There is scope for further investigations into this and related areas. In particular pipe-soil interaction on high strength clay seabeds would appear to represent a potential area for future research with pipeline penetration on these higher strength seabed expected to be minimal. These higher shear strength soils are likely to have a high over consolidation ratio and may be of glacial origin. The presence of sand and gravel in these soils may also influence these problems.

Two dimensional, plane strain analysis, is an appropriate approach for a wide range of pipeline design problems. The use of full three dimensional numerical analysis is a potential area for future research, although it is expected that this type of analysis would have limited generality. It is also expected to be very computationally intensive. One area where three dimensional analysis could be a promising area of future research is interaction with complex seabed features, including those that result in pipeline free spans. The pipe soil interaction in the vicinity of these features would be of interest including interaction relevant to pipeline fatigue under hydrodynamic loading.

From the perspective of development of pipeline design codes the methods outlined in this and similar studies show promise, including integration with reliability based techniques to establish an appropriate probability of failure. In the longer term databases of typical coefficients of variation in design parameters, possibly on a regional basis, offer potential for further guidance on typical safety factor requirements. The extension of simplified reliability methods to multi-variable problems is also a promising area for future research. For example consideration of combined soil shear strength and unit weight effects, or more complex shear strength distributions such linearly increasing shear strength gradients. This could initially extend the potential for project specific reliability analysis as well as, in the longer term, feeding into pipeline design codes and recommended practice documents.

7.4 Concluding Remarks

The objectives of this study have been achieved. A literature review has been reported for pipe-soil interaction on a clay seabed and building on some of the analysis found in this literature a range of vertical loading and combined vertical and horizontal loading problems were investigated. The depth range for these problems was typically extended to assess the effect beyond half a pipeline diameter, prior to investigating a range of other problem definition not previously considered. Reliability based analysis techniques have been applied to a range or pipe-soil interaction problems including the development of a technique to produce stability envelopes in vertical and horizontal load space for a defined probability of failure. This thesis has concluded by considering application of this and similar studies to design practice and identify potential areas for future research.

AUBENY, C. P., SHI, H. & MURFF, J. D. (2005) Collapse Loads for a Cylinder Embedded in Trench in Cohesive Soil. *International Journal of Geomechanics,* 5**,** 320-325.

BARBOSA-CRUZ, E. R. & RANDOLPH, M. F. (2005) Bearing Capacity and Large Penetration of a Cylindrical Object at Shallow Embedment. *Proceedings of the International Conference on Frontiers in Offshore Geotechnics.* Perth, Australia, Taylor Francis.

BISCAYE, P. E. (1965) Mineralogy and Sedimentation of Recent Deep-Sea Clay in Atlantic Ocean and Adjacent Seas and Oceans. *Geological Society of America Bulletin,* 76**,** 803-832.

BOURG, D. M. (2006) *Excel Scientific and Engineering Cookbook*, O'Reilly.

BRANSBY, F. & RANDOLPH, M. (1998) The effects of skirted foundation shape on behaviour under V-H-M loading. *Proceedings of ISOPE 98.* Montreal, Canada.

BRANSBY, M. F., AMMAN, S. & ZAJAC, P. (2008a) Numerical Analysis of Capacity of On-Bottom Offshore Pipelines. *Proceedings of the 2nd BGA International Conference on Foundations.* Dundee, UK, BRE Press.

BRANSBY, M. F., ZAJAC, P. & AMMAN, S. (2008b) Finite Element Analysis of the Vertical Penetration of On-Bottom Pipelines in Clay. *Proceedings of the Conference of the International Society for Offshore and Polar Engineers.* Vancouver, Canada.

BRENNODDEN, H., SVEGGEN, O., WAGNER, D. A. & MURFF, J. D. (1986) Full Scale Pipe-Soil Interaction Tests. *Proceedings of the Offshore Technology Conference* Houston, USA. OTC Paper No. 5338.

BRENNODDEN, H., LEING, J. T., SOTBURG, T. & VERLEY, R. L. P. (1989) An Energy Based Pipe-Soil Interaction Model. *Proceedings of the Offshore Technology Conference.* Houston, USA. OTC Paper No. 6057.

BRENNODDEN, H. & STOKKELAND, A. (1992) Time Dependent Pipe-Soil Resistance in Soft Clay. *Proceedings of the Offshore Technology Conference.* Houston, USA. OTC Paper No. 6846.

BRIDGES, C., LAVER, K., CLUKEY, E. & EVANS, T. (2004) Steel Caternary Riser Touchdown Point Vertical Interaction Models. *Proceedings of the Offshore Technology Conference.* Houston, USA. OTC Paper No. 16628.

BRUTON, D., WHITE, D. J., CHEUK, C., BOLTON, M. & CARR, M. (2006) Pipe-Soil Interaction Behaviour During Lateral Buckling Including Large Amplitude Cyclic Displacement Tests by the SAFEBUCK JIP. *Proceedings of the Offshore Technology Conference.* Houston, USA. OTC Paper No. 17944.

BSI (2003) Petroleum and Natural Gas Industries - Specific Requirements for Offshore Structures - Part 4: Geotechnical and Foundation Design Considerations ISO 19901-4:2003.

BSI (2015) PD 8010-2:2015 Pipeline Systems - Part 2: Subsea pipelines - Code of practice.

CAMPBELL, J. (2008) Greater Plutonio - Angola Deepwater Project. *Proceedings of the Offshore Technology Conference.* Houston, USA. OTC Paper No. 19672.

CARR, M., SINCLAIR, F. & BRUTON, D. (2006) Pipeline Walking - Understanding the Field Layout Challenges and Analytical Solutions Developed for the SAFEBUCK JIP. *Proceedings of the Offshore Technology Conference.* Houston, USA. OTC Paper No. 17945.

CASSIDY, M. J., HOUSLBY, G. T. & EASTOCK-TAYLOR, R. (2003) Probabilistic models applicable to the short-term extreme response analysis of jack-up platforms. *Journal of Offshore Mechanics and Arctic Engineering,* 125.

CASSIDY, M. J. (2006) Application of Force-Resultant Models to the Analysis of Offshore Pipelines. *Structural Engineering and Mechanics,* 22**,** 511-515.

CASSIDY, M. J., UZIELLI, M. & TIAN, Y. (2013) Probabilistic combined loading failure envelopes of a strip footing on spatially random soil. *Computers and Geotechnics,* 49**,** 191-205.

CATHIE, D. N., JAECK, C., BALLARD, J. C. & WINTGENS, J. F. (2005) Pipeline Geotechnics: State of the Art. *Proceedings of the International Conference on Frontiers in Offshore Geotechnics.* Perth, Australia, Taylor Francis.

CHATTERJEE, S., RANDOLPH, M., WHITE, D. & WANG, D. (2010) Large Deformation Finite Element Analysis of Vertical Penetration of Pipelines in Seabed. *Proceedings of the International Conference on Frontiers in Offshore Geotechnics.* Perth, Australia, Taylor Francis.

CHATTERJEE, S., WHITE, D. & RANDOLPH, M. (2011) Lateral movement of pipelines on a soft clay seabed: large deformation finite element analysis. *Proceedings of the International Conference on Ocean Offshore and Arctic Engineering.* Rotterdam, Netherlands.

CHATTERJEE, S. (2012) Numerical Modelling of Pipe-soil Interactions. *Centre for Offshore Foundation Systems.* Perth, The University of Western Australia.

CHATTERJEE, S., RANDOLPH, M. & WHITE, D. (2012a) The effects of penetration rate and strain softening on the vertical resistance of seabed pipelines. *Geotechnique,* 62**,** 573-582.

CHATTERJEE, S., WHITE, D. & RANDOLPH, M. (2012b) Numerical simulations of pipe-soil interaction during lateral movements on clay. *Geotechnique,* 62**,** 693-705.

CHEUK, C. (2005) Seabed-Pipeline Interaction at the Seabed. University of Cambridge.

CHEUK, C. & BOLTON, M. (2006) A Technique for Modelling the Lateral Stability of On-Bottom Pipelines in a Small Drum Centrifuge. *International Conference on Physical Modelling in Geotechnics.* Hong Kong.

CHEUK, C. Y., WHITE, D. J. & DINGLE, H. R. C. (2008) Upper bound plasticity analysis of a partially-embedded pipe under combined vertical and horizontal loading. *Soils and Foundations,* 48**,** 133-140.

CHING, J. (2011) Practical Monte Carlo Based Reliability Analysis and Design Methods for Geotechnical Problems. IN MORDECHAI, S. (Ed.) *Application of Monte Carlo Methods in Science and Engineering.* InTech.

CLAUSS, G. F., WEEDE, H. & SAROUKH, A. (1991) Offshore Pipelaying: Significance of Motions and Dynamic Stresses During Laying Operations. *Proceedings of the Offshore Technology Conference.* Houston, USA. OTC Paper No. 6760.

DAS, B. M. (2007) *Advanced Soil Mechanics*, Taylor Francis.

DAVIS, E. H. & BOOKER, J. R. (1973) The Effect of Increasing Strength with Depth on the Bearing Capacity of Clays. *Geotechnique,* 23**,** 551-563.

DEAN, E. T. R. (2009) *Offshore Geotechnical Engineering: Principles and Practice*, Thomas Telford.

DEGROOT, D. J., LUNNE, T., ANDERSON, K. H. & BOSCARDIN, A. G. (2012) Laboratory Measurement of the Remoulded Shear Strength of Clays with Application to Design of Offshore Infrastructure. *Proceedings of the Conference of the Offshore Site Investigation Group of the Society of Underwater Technology.* London, UK.

DENDANI, H. & JAECK, C. (2007a) Pipe-Soil Interaction In Highly Plastic Clay. *Proceedings of the Conference of the Offshore Site Investigation Group of the Society of Underwater Technology.* London, UK.

DENDANI, H. & JAECK, C. (2007b) Pipe-Soil Interaction in Soft Clays. *Offshore Mediterranean Conference.* Ravenna, Italy.

DENDANI, H. & JAECK, C. (2008) Flowline and Riser: Soil Interaction in Plastic Clays. *Proceedings of the Offshore Technology Conference.* Houston, USA. OTC Paper No. 19261.

DINGLE, H. R. C., WHITE, D. J. & GAUDIN, C. (2008) Mechanisms of Pipe Embedment and Lateral Breakout on Soft Clay. *Canadian Geotechnical Journal,* 45**,** 636-652.

DNV (1992) Classification Note No. 30.4 - Foundations.

DNV (2007) Recommended Practice DNV-RP-F109 On-Bottom Stability Design of Submarine Pipelines.

DUNLAP, W. A. (1990) Burial of Vertically Loaded Offshore Pipelines in Weak Sediments. *Proceedings of the Offshore Technology Conference.* Houston, USA. OTC Paper No. 6375.

EHLERS, C. J., CHEN, J., ROBERTS, H. H. & LEE, Y. C. (2005) The Origin of Near-Surface Crust Zones in Deepwater. *Proceedings of the International Conference on Frontiers in Offshore Geotechnics.* Perth, Australia, Taylor Francis.

EVANS, T., USHER, N. & MOORE, R. (2007) Management of Geotechnical and Geohazard Risks in the West Nile Delta. *Proceedings of the Conference of the Offshore Site Investigation Group of the Society of Underwater Technology.* London, UK.

FENTON, G. A., ZHOUE, H., JAKSA, M. B. & GRIFFITHS, D. V. (2003) Reliability analysis of a strip footing designed against settlement. *Applications of Statistics and Probability in Civil Engineering.* Rotterdam, Netherlands.

FENTON, G. A. & GRIFFITHS, D. V. (2008) *Risk Assessment in Geotechnical Engineering*, Wiley.

FINCH, M., FISHER, R., PALMER, A. & BAUMGARD, A. (2000) An Integrated Approach to Pipeline Burial in the 21st Century. *Deep Offshore Technology Conference.* New Orleans, USA.

GAO, F. P., CAO, J., HAN, X. T., SHA, Y., ZHANG, E. Y., WU, Y. X. & CUI, J. S. (2011) Full-Scale Physical Modelling of Pipeline Instability on a Slipping Seabed. *Proceedings of the Offshore Technology Conference.* Houston, USA. OTC Paper No. 21260.

GIECK, K. & GIECK, R. (1997) *Engineering Formulas*, Mcgraw-Hill.

GILBERT, R. B., CHOI, S., DANGAYACH, S. S. & NAJJAR, S. S. (2005) Reliability based design considerations for deepwater mooring system foundations. *Proceedings of the International Conference on Frontiers in Offshore Geotechnics.* Perth, Australia, Taylor Francis.

GILBERT, R. B., MURFF, J. D. & CLUKEY, E. (2010) Risk and reliability on the frontier of offshore geotechnics. *Proceedings of the International*

Conference on Frontiers in Offshore Geotechnics. Perth, Australia, Taylor Francis.

GOURVENEC, S. & WHITE, D. (2010) Elastic Solutions for Consolidation Around Seabed Pipelines. *Proceedings of the Offshore Technology Conference.* Houston, USA. OTC Paper No. 20554.

GRIFFITHS, D. V. & FENTON, G. A. (2001) Bearing capacity of spatially random soil: the undrained clay Prandtl problem revisited. *Geotechnique,* 51**,** 351-359.

HEATH, G. R. & PISIAS, N. G. (1979) A Method for the Quantitative Estimation of Clay Minerals in North Pacific Deep Sea Sediments. *Clays and Clay Minerals,* 27**,** 175-184.

HILL, A. J. & JACOB, H. (2008) In-situ Measurement of Pipe-Soil Interaction in Deep Water. *Proceedings of the Offshore Technology Conference.* Houston, USA. OTC Paper No. 19528.

HODDER, M. S., CASSIDY, M. J. & BARRETT, D. (2008) Undrained Response of Shallow Pipelines Subjected to Combined Loading. *Proceedings of the 2nd BGA International Conference on Foundations.* Dundee, UK, BRE Press.

HODDER, M. S. & CASSIDY, M. J. (2010) A Plasticity Model for Predicting the Vertical and Lateral Behaviour of Pipelines in Clay Soils. *Geotechnique,* 60**,** 247-263.

HODDER, M. S., WHITE, D. & CASSIDY, M. J. (2013) An effective stress framework for the variation in penetration resistance due to episodes of remoulding and reconsolidation. *Geotechnique,* 63**,** 30-43.

HOULSBY, G. T. & CASSIDY, M. J. (2011) A Simplified Mechanically Based Model For Predicting Partially Drained Behaviour of Penetrometers and Shallow Foundations. *Geotechnique Letters,* 1**,** 65-69.

HOUSE, A. R., OLIVEIRA, J. R. M. S. & RANDOLPH, M. (2001) Evaluating the Coefficient of Consolidation Using Penetration Tests. *International Journal of Physical Modelling in Geotechnics***,** 17-26.

HOVLAND, M. (1979) Characteristics of Pockmarks in the Norwegian Trench. *Marine Geology,* 39**,** 103-117.

ITASCA (2005) *FLAC 5.0 Users Guide*, Itasca Consulting Group.

ITASCA (2008a) *FLAC 6.0 FISH in FLAC*, Itasca Consulting Group.

ITASCA (2008b) *FLAC 6.0 Theory and Background*, Itasca Consulting Group.

ITASCA (2008c) *FLAC 6.0 User Guide*, Itasca Consulting Group.

JOHNSON, H., RICHARDS, P. C., LONG, D. & GRAHAM, C. C. (1993) *The geology of the northern North Sea*, HMSO.

JUDD, A. G. (2001) Pockmarks in the UK Sector of the North Sea. *Strategic Environmental Assessment - SEA2 - DTI.*

KARAL, K. (1977) Lateral Stability of Submarine Pipelines. *Proceedings of the Offshore Technology Conference.* Houston, USA. OTC Paper No. 2967.

KROST, K., GOURVENEC, S. M. & WHITE, D. J. (2011) Consolidation Around Partially Embedded Seabed Pipelines. *Geotechnique,* 61**,** 167-173.

KULHAWY, F. H. & PHOON, K. K. (2002) Observations on geotechnical reliability-based design development in North America. *Foundation Design Codes and Soil Investigation in view of International Harmonization and Performance.* Kamaura, Japan.

KUO, M. Y. H. & BOLTON, M. (2009) Soil Characterization of Deep Sea West African Clays: Biology a Source of Mechanical Strength. *Proceedings of the Nineteenth International Offshore and Polar Engineering Conference* Oska, Japan.

KUO, M. Y. H., BOLTON, M., HILL, A. J. & RATTLEY, M. J. (2010) New Evidence for the Origin and Behaviour of Deep Ocean Crusts. *Proceedings of the International Conference on Frontiers in Offshore Geotechnics.* Perth, Australia, Taylor Francis.

LAMBRAKOS, K. F. (1985) Marine Pipeline Soil Friction Coefficients From Insitu Testing. *Ocean Engineering,* 12**,** 131-150.

LANGFORD, T., DYVIK, R. & CLEAVE, R. (2007) Offshore Pipeline and Riser Geotechnical Model Testing: Practice and Interpretation. *Proceedings of the International Conference on Ocean Offshore and Artic Engineering.* San Diego, USA.

LEE, Y. S., SMITH, C. C. & CHEUK, C. (2008) Bearing Capacity of Embedded Foundations. *Proceedings of the 2nd BGA International Conference on Foundations.* Dundee, UK, BRE Press.

LEE, Y. S., SMITH, C. C. & CHEUK, C. (2011) Lateral Breakout Resistance of Shallowly Embedded Offshore Pipelines. *Procedia Engineering,* 14**,** 1690-1695.

LEE, Y. S., CHEUK, C. & SMITH, C. C. (2012) Lateral Soil Resistance fo On-bottom Pipeline Design on Clayey Seabed. *Transactions of HKIE,* 19**,** 2-10.

LEMOS, L. J. L. & VAUGHAN, P. R. (2000) Clay-Interface Shear Resistance. *Geotechnique,* 50**,** 55-64.

LOW, B. K. & PHOON, K. K. (2002) Practical First-Order Reliability Computations Using Spreadsheet. *Proceedings of Probabilistics In Geotechnics: Technical and Economic Risk Estimation.* Graz, Austria.

LOW, B. K. (2005) Reliability-based design applied to retaining walls. *Geotechnique,* 55**,** 63-75.

LUND, K. M. (2000) Effects of Increase in Pipeline Soil Penetration from Installation *Proceedings of the International Conference on Ocean Offshore and Artic Engineering.* New Orleans, USA.

LYONS, C. G. (1973) Soil Resistance to Lateral Sliding of Marine Pipelines. *Proceedings of the Offshore Technology Conference.* Houston, USA. OTC Paper No. 1876.

MARTIN, C. (1994) Physical and Numerical Modelling of Offshore Foundations Under Combined Loading. University of Oxford.

MARTIN, C. M. & HOULSBY, G. T. (2001) Combined Loading of Spudcan Foundations on Clay: Numerical Modelling. *Geotechnique,* 51**,** 687-699.

MARTIN, C. & WHITE, D. (2012) Limit analysis of the undrained bearing capacity of offshore pipeline. *Geotechnique,* 62**,** 847-863.

MCCARRON, W. O. (2008) Discussion of "Large-scale modelling of soil-pipe interaction during large amplitude cyclic movements of partially embedded pipelines". *Canadian Geotechnical Journal,* 45**,** 742-743.

MCCARRON, W. O. (2011) *Deepwater Foundation and Pipeline Geomechanics*, J. Ross Publishing.

MEBARKIA, S. (2006) Effect of High-Pressure/High-Temperature Flowlines and Soil Interaction on Deepwater Subsea Development. *Proceedings of the Offshore Technology Conference.* Houston, USA. OTC Paper No. 18107.

MERIFIELD, R., WHITE, D. J. & RANDOLPH, M. F. (2008) The Ultimate Undrained Resistance of Partially Embedded Pipelines. *Geotechnique,* 58**,** 461-470.

MERIFIELD, R. S., WHITE, D. J. & RANDOLPH, M. F. (2009) Effect of Surface Heave on Response of Partially Embedded Pipelines on Clay. *Journal of Geotechnical and Geoenvironmental Engineering,* 135**,** 819-829.

MESSIAS-DOS-SANTOS, L. G. S. (2005) Barracuda and Caratinga Development Project. *Proceedings of the Offshore Technology Conference.* Houston, USA. OTC Paper No. 17052.

MORRIS, D. V., WEBB, R. E. & DUNLAP, W. A. (1986) Self Burial of Laterally Loaded Offshore Pipelines in Weak Sediments. *Proceedings of the Offshore Technology Conference.* Houston, USA. OTC Paper No. 5855.

MORROW, D. R. & LARKIN, P. D. (2007) The Challenges of Pipeline Burial. *Proceedings of the Seventeenth International Offshore and Polar Engineering Conference* Lisbon, Portugal.

MORROW, D. R. & BRANSBY, M. F. (2009) The Influence of Slope on the Stability of Pipelines Subjected to Horizontal and Vertical Loading on Clay Seabeds. *Proceedings of the International Conference on Ocean Offshore and Arctic Engineering.* Honolulu, USA.

MORROW, D. R. & BRANSBY, M. F. (2010) Pipe-Soil Interaction on Clay with a Variable Shear Strength Profile. *Proceedings of the International Conference on Frontiers in Offshore Geotechnics.* Perth, Australia, Taylor Francis.

MURFF, J. D., WAGNER, D. A. & RANDOLPH, M. F. (1989) Pipe Penetration in Cohesive Soil. *Geotechnique,* 39**,** 213-229.

NAJJAR, S. S., GILBERT, R. B., LIEDTKE, E. & MCCARRON, B. (2003) Tilt Table Test For Interface Shear Resistance Between Flowlines and Soils. *Proceedings of the International Conference on Ocean Offshore and Artic Engineering.* Cancun, Mexico.

NAJJAR, S. S., GILBERT, R. B., LIEDTKE, E., MCCARRON, B. & YOUNG, A. G. (2007) Residual Shear Strength for Interfaces Between Pipelines and Clays at Low Effective Normal Stresses. *Journal of Geotechnical and Geoenvironmental Engineering,* 133**,** 695-706.

OLDFIELD, T. (2008) Subsea Umbilicals Risers and Flowlines (SURF): Performance Management of Large Contracts in an Overheated Market - Risk Management and Learnings. *Proceedings of the Offshore Technology Conference.* Houston, USA. OTC Paper No. 19676.

PADFIELD, C. J. & SHARROCK, M. J. (1983) *Settlement of Structures on Clay Soils - CIRIA Special Publication 27*.

PALMER, A. (2008) Touchdown Indentation of the Seabed. *Applied Ocean Research,* 30**,** 235-238.

PARSLOE, N. F. A., MANCHEC, P., DORBEC, A. & YANG, X. (2006) Methods for Assessing Design Issues With HP/HT Pipelines at Early Stages of a Project. *Proceedings of the Offshore Technology Conference.* Houston, USA. OTC Paper No. 17922.

PERINET, D. & FRASER, I. (2006) Mitigation Methods for Deepwater Pipeline Instability Induced by Pressure and Temperature Variation *Proceedings of the Offshore Technology Conference.* Houston, USA. OTC Paper No. 17815.

PHOON, K. K. & KULHAWY, F. H. (1999) Characterization of geotechnical variability. *Canadian Geotechnical Journal,* 36**,** 612-624.

PHOON, K. K., BECKER, D. E., KULHAWY, F. H., HONJO, Y., OVESEN, N. K. & LO, S. R. (2003) Why Consider reliability Analysis for Geotechnical Limit State Design? *International Workshop on Limit State Design in Geotechnical Engineering Practice.* Boston, USA.

PHOON, K.-K. (2004) Towards Reliability-based Design for Geotechnical Engineering. *Special Lecture for Korean Geotechnical Society.* Seoul, Korea.

PHOON, K. K. (Ed.) (2008) *Reliability Based Design In Geotechnical Engineering*, Taylor & Francis.

POTYONDY, J. G. (1961) Skin Friction Between Various soils and Construction Materials. *Geotechnique,* 11**,** 339-353.

PUECH, A., COLLIAT, J. L., NAUROY, J.-F. & MENIER, J. (2005) Some Geotechnical Specificities of Gulf of Guinea Deepwater Sediments. *Proceedings of the International Conference on Frontiers in Offshore Geotechnics.* Perth, Australia, Taylor Francis.

QUIROS, G. W. & LITTLE, R. L. (2003) Deepwater Soil Properties and Their Impact on the Geotechnical Program. *Proceedings of the Offshore Technology Conference* Houston, USA. OTC Paper No. 15262.

RANDOLPH, M. F. & WHITE, D. J. (2008) Upper-Bound Yield Envelopes for Pipelines at Shallow Embedment in Clay. *Geotechnique,* 58**,** 297-301.

RANDOLPH, M. & GOURVENEC, S. (2011) *Offshore Geotechnical Engineering*, Spon Press.

RAO, K. S. S., ALLAM, M. M. & ROBINSON, R. G. (2000) Drained Shear Strength of Fine-Grained Soil-Solid Surface Interfaces. *Proceedings of the Institution of Civil Engineers-Geotechnical Engineering,* 143**,** 75-81.

ROBINSON, R. G. & ALLAM, M. M. (1998) Effect of Clay Mineralogy on Coefficient of Consolidation. *Clays and Clay Minerals,* 46**,** 596-600.

SCHOTMAN, G. J. M. & STORK, F. G. (1987) Pipe-Soil Interaction Model for Laterally Loaded Pipelines in Clay. *Proceedings of the Offshore Technology Conference.* Houston, USA. OTC Paper No. 5588.

SCHULTZ, M. T., GOULDBY, B. P., SIMM, D. & WIBOWO, J. L. (2010) Beyond The Factor of Safety: Developing Fragility Curves to Characterize System Reliability. US Army Corp of Engineers, Washington.

SMITH, C. C. & GILBERT, M. (2007) Application of discontinuity layout optimization to plane plasticity problems *Proceedings of the Royal Society,* 463**,** 2461-2484.

TAIEBAT, H. A. & CARTER, J. P. (2008) Flow rule effects in the Tresca model. *Computers and Geotechnics*, 35, 500-503.

TORNES, K., ZEITOUN, H., CUMMING, G. & WILLCOCKS, J. (2009) A Stability Rationale - A Review of Present Design Approaches. *Proceedings of the International Conference on Ocean Offshore and Arctic Engineering.* Honolulu, USA.

USACE (1997) Introduction to Probability and Reliability Methods for Use In Geotechnical Engineering - Technical Letter No. 1110-2-547. Department of the Army, US Army Corp of Engineers, Washington.

VERLEY, R. L. P. & LUND, K. M. (1995) A Soil Resistance Model for Pipeline Place on Clay Soils. *Proceedings of the International Conference on Ocean Offshore and Arctic Engineering.* Copenhagen, Denmark.

WAGNER, D. A., MURFF, J. D., BRENNODDEN, H. & SVEGGEN, O. (1987) Pipe-Soil Interaction Model. *Proceedings of the Offshore Technology Conference.* Houston, USA. OTC Paper No. 5504.

WANTLAND, G. M., O'NEILL, M. W., REESE, L. C. & KALAJIAN, E. H. (1979) Lateral Stability of Pipelines in Clay. *Proceedings of the Offshore Technology Conference.* Houston, USA. OTC Paper No. 3477.

WANTLAND, G. M., ONEILL, M. W., KALAJIAN, E. H. & REESE, L. C. (1982) Pipeline Lateral Stability in Soft Clay. *Journal of Petroleum Technology,* 34**,** 217-220.

WESTGATE, Z. J., RANDOLPH, M., WHITE, D. & LI, S. (2010) The influence of sea state on as-laid pipeline embedment: A case sudy. *Applied Ocean Research,* 32**,** 321-331.

WHITE, D.J., TAKE, W. A. & BOLTON, M.D. (2003) Soil deformation measurement using particle image velocimetry (PIV) and photogrammetry. *Geotechnique, 53, 619-631.*

WHITE, D. J. & RANDOLPH, M. F. (2007) Seabed Characterisation and Models for Pipe-Soil Interaction. *Proceedings of the Seventeenth International Offshore and Polar Engineering Conference* Lisbon, Portugal.

WHITE, D. J. & CATHIE, D. N. (2010) Geotechnics for Subsea Pipelines. *Proceedings of the International Conference on Frontiers in Offshore Geotechnics.* Perth, Australia, Taylor Francis.

WHITE, D. J. & DINGLE, H. R. C. (2011) The Mechanism of Steady Friction Between Seabed Pipelines and Clay Soils. *Geotechnique,* 61**,** 1035-1041.

WHITE, D., GANESAN, S. A., BOLTON, M., BRUTON, D., BALLARD, J. C. & LANDFORD, T. (2011) SAFEBUCK JIP - Observations of Axial Pipe-Soil Interaction from Testing on Soft Natural Clays. *Proceedings of the Offshore Technology Conference.* Houston, USA. OTC Paper No. 21249.

WILLIS, N. R. T. & WEST, P. T. J. (2001) Interaction between deepwater catenary risers and a soft seabed: Large scale sea trials. *Offshore Technology Conference***,** 13113.

YU, S. & KONUK, I. (2007) Continuum FE Modelling of Lateral Buckling. *Proceedings of the Offshore Technology Conference.* Houston, USA. OTC Paper No. 18934.

YUN, T. S., NARSILO, G. A. & SANTAMARINA, J. C. (2006) Physical Characterization of core samples recovered from the Gulf of Mexico. *Marine and Petroleum Geology,* 23**,** 893-900.

ZEITOUN, H., TORNES, K., CUMMING, G. & BRANKOVIC, M. (2008) Pipeline Stability - State of the Art. *Proceedings of the International Conference on Ocean Offshore and Arctic Engineering.* Estoril, Portugal.

Appendix A

Analysis Summary - Vertical Loading	
Table Number	Description
1-1	Smooth Interface, Shallow Depth (0.05D-0.5D), Uniform s_u, No γ
1-2	Rough Interface, Shallow Depth (0.05D-0.5D), Uniform s_u, No γ
1-3	Smooth Interface, Deeper Depth (0.5D-1.0D), Uniform s_u, No γ
1-4	Rough Interface, Shallow Depth (0.5D-1.0D), Uniform s_u, No γ
1-5	Soil Unit Weight Effect and Calculation of N_{SW}
1-6	Variation in Interface Roughness
1-7	Smooth Interface, Linear Increasing Shear Strength Gradient
1-8	Rough Interface, Linear Increasing Shear Strength Gradient
1-9	Smooth Interface, Shear Strength Crust
1-10	Rough Interface, Shear Strength Crust
1-11	Smooth Interface, Large Strain Analysis
1-12	Rough Interface, Large Strain Analysis

Table Number 1-1

Vertical Penetration - Smooth Interface, Shallow Depth (0.05D-0.5D), Uniform s_u, No γ

s_u (Pa)	D (mm)	z (mm)	z/D	v (m/s)	Number of Zones	Δ_z (mm)	Δ_z/D	R/2 (N)	R (N)	$V/s_u.D$	Analysis No.
5000	300	15	0.05	1.0E-06	1759	10	0.03333	1627	3254	2.169	VC1
5000	300	15	0.05	5.0E-07	2488	7.5	0.02500	1615	3230	2.153	C2
5000	300	15	0.05	2.5E-07	3008	6	0.02000	1608	3216	2.144	M3
5000	**300**	**15**	**0.05**	**5.0E-07**	**5598**	**5**	**0.01667**	**1576**	**3152**	**2.101**	**F4**
5000	300	15	0.05	2.5E-07	9862	3.75	0.01250	1579	3158	2.105	VF5
5000	300	30	0.1	1.0E-06	1752	12	0.04000	2153	4306	2.871	VVC6
5000	**300**	**30**	**0.1**	**1.0E-06**	**2382**	**10**	**0.03333**	**2090**	**4180**	**2.787**	**VC7**
5000	300	30	0.1	5.0E-07	4192	7.5	0.02500	2100	4200	2.800	C8
5000	300	60	0.2	1.0E-06	2079	11.6667	0.03889	2686	5372	3.581	VVC9
5000	**300**	**60**	**0.2**	**1.0E-06**	**2864**	**10**	**0.03333**	**2613**	**5226**	**3.484**	**VC10**
5000	300	60	0.2	1.0E-06	4160	8.75	0.02917	2645	5290	3.527	C11
5000	300	90	0.3	1.0E-06	2246	12.5	0.04167	2963	5926	3.951	VC12
5000	300	90	0.3	1.0E-06	2845	11.25	0.03750	2927	5854	3.903	C13
5000	**300**	**90**	**0.3**	**1.0E-06**	**3509**	**10**	**0.03333**	**2888**	**5776**	**3.851**	**M14**
5000	300	90	0.3	2.5E-07	6240	7.5	0.02500	2916	5832	3.888	F15
5000	300	120	0.4	5.0E-07	1718	16.6667	0.05556	3186	6372	4.248	VVC16
5000	300	120	0.4	2.5E-07	2941	12.5	0.04167	3112	6224	4.149	VC17
5000	**300**	**120**	**0.4**	**2.5E-07**	**4627**	**10**	**0.03333**	**3086**	**6172**	**4.115**	**C18**
5000	300	120	0.4	5.0E-07	6699	8.3333	0.02778	3115	6230	4.153	M19
5000	300	150	0.5	1.0E-07	2421	15	0.05000	3321	6642	4.428	VVC20
5000	**300**	**150**	**0.5**	**1.0E-07**	**5446**	**12**	**0.04000**	**3250**	**6500**	**4.333**	**VC21**
5000	300	150	0.5	1.0E-07	8557	8	0.02667	3289	6578	4.385	C22

Note: The analysis results presented in bold represent a convergence state.

Total	22

Table Number 1-2

Vertical Penetration - Rough Interface, Shallow Depth (0.05D-0.5D), Uniform s_u, No γ

s_u (Pa)	D (mm)	z (mm)	z/D	v (m/s)	Number of Zones	Δ_z (mm)	Δ_z/D	R/2 (N)	R (N)	V/s_u.D	Analysis No.
5000	300	15	0.05	1.0E-06	1759	10	0.03333	1829	3658	2.439	VC23
5000	300	15	0.05	5.0E-07	2488	7.5	0.02500	1791	3582	2.388	C24
5000	**300**	**15**	**0.05**	**5.0E-07**	**3008**	**6**	**0.02000**	**1744**	**3488**	**2.325**	M25
5000	300	15	0.05	5.0E-07	5598	5	0.01667	1767	3534	2.356	F26
5000	300	30	0.1	7.5E-07	2382	10	0.03333	2481	4962	3.308	VC27
5000	**300**	**30**	**0.1**	**1.0E-06**	**4192**	**7.5**	**0.02500**	**2408**	**4816**	**3.211**	C28
5000	300	30	0.1	5.0E-07	6672	6	0.02000	2426	4852	3.235	M29
5000	300	60	0.2	5.0E-07	2079	11.6667	0.03889	3289	6578	4.385	VVC30
5000	300	60	0.2	1.0E-06	2864	10	0.03333	3226	6452	4.301	VC31
5000	**300**	**60**	**0.2**	**5.0E-07**	**4160**	**8.75**	**0.02917**	**3138**	**6276**	**4.184**	C32
5000	300	60	0.2	5.0E-07	5825	7	0.02333	3204	6408	4.272	M33
5000	300	90	0.3	1.0E-06	2246	12.50	0.04167	3757	7514	5.009	VC34
5000	300	90	0.3	1.0E-06	2845	11.25	0.03750	3725	7450	4.967	C35
5000	300	90	0.3	2.5E-07	3509	10.00	0.03333	3733	7466	4.977	M36
5000	**300**	**90**	**0.3**	**2.5E-07**	**6240**	**7.50**	**0.02500**	**3616**	**7232**	**4.821**	F37
5000	300	90	0.3	2.5E-07	11167	5.625	0.01875	3669	7338	4.892	VF38
5000	300	120	0.4	1.0E-06	2941	12.5	0.04167	4120	8240	5.493	VC39
5000	300	120	0.4	5.0E-07	4627	10	0.03333	4087	8174	5.449	C40
5000	300	120	0.4	5.0E-07	6699	8.3333	0.02778	4064	8128	5.419	M41
5000	**300**	**120**	**0.4**	**1.0E-07**	**10311**	**6.6667**	**0.02222**	**3989**	**7978**	**5.319**	F42
5000	300	120	0.4	1.0E-07	18505	5	0.01667	4032	8064	5.376	VF43
5000	300	150	0.5	1.0E-07	5446	10	0.03333	4358	8716	5.811	VC44
5000	300	150	0.5	1.0E-07	8557	8	0.02667	4309	8618	5.745	C45
5000	**300**	**150**	**0.5**	**1.0E-07**	**15129**	**6**	**0.02000**	**4284**	**8568**	**5.712**	M46
5000	300	150	0.5	7.5E-08	21652	5	0.01667	4305	8610	5.740	F47

Note: The analysis results presented in bold represent a convergence state.

Total	25

Table Number **1-3**

Vertical Penetration - Smooth Interface, Deeper Depth (0.5D-1.0D), Uniform s_u , No γ

s_u (Pa)	D (mm)	z (mm)	z/D	v (m/s)	Number of Zones	Δ_z (mm)	Δ_z/D	R/2 (N)	R (N)	V/s_u.D	Analysis No.
5000	300	225	0.75	5.0E-07	6252	12.5	0.04167	3657	7314	4.876	VC48
5000	300	225	0.75	5.0E-07	12213	10	0.03333	3614	7228	4.819	C49
5000	300	225	0.75	5.0E-07	18770	8.06	0.02687	3608	7216	4.811	M50
5000	**300**	**225**	**0.75**	**5.0E-07**	**32837**	**6.09**	**0.02030**	**3601**	**7202**	**4.801**	**F51**
5000	300	300	1	1.0E-06	5003	15.6	0.05200	3922	7844	5.229	VVC52
5000	300	300	1	5.0E-07	6252	12.5	0.04167	3835	7670	5.113	VC53
5000	**300**	**300**	**1**	**5.0E-07**	**12213**	**10**	**0.03333**	**3834**	**7668**	**5.112**	**C54**

Note: The analysis results presented in bold represent a convergence state.

Total	7

Table Number **1-4**

Vertical Penetration - Rough Interface, Deeper Depth (0.5D-1.0D), Uniform s_u, No γ

s_u (Pa)	D (mm)	z (mm)	z/D	v (m/s)	Number of Zones	Δ_z (mm)	Δ_z/D	R/2 (N)	R (N)	V/s_u.D	Analysis No.
5000	300	225	0.75	5.0E-07	6252	12.5	0.04167	5077	10154	6.769	VC55
5000	300	225	0.75	5.0E-07	12213	10	0.03333	4866	9732	6.488	C56
5000	300	225	0.75	5.0E-07	18770	8.06	0.02687	4813	9626	6.417	M57
5000	300	225	0.75	5.0E-07	32837	6.09	0.02030	4743	9486	6.324	F58
5000	**300**	**225**	**0.75**	**5.0E-07**	**48843**	**5**	**0.01667**	**4732**	**9464**	**6.309**	**VF57**
5000	300	300	1	5.0E-07	9344	12.5	0.04167	5126	10252	6.835	VC58
5000	300	300	1	5.0E-07	14596	10.0	0.03333	5072	10144	6.763	C59
5000	300	300	1	2.5E-07	22440	8.06	0.02687	5041	10082	6.721	M60
5000	300	300	1	2.5E-07	39252	6.09	0.02030	4975	9950	6.633	F61
5000	300	300	1	2.5E-07	58393	5	0.01667	4893	9786	6.524	VF62
5000	**300**	**300**	**1**	**2.5E-07**	**91260**	**4**	**0.01333**	**4852**	**9704**	**6.469**	**VVF63**

Note: The analysis results presented in bold represent a convergence state.

Total	11

Table Number **1-5**

Vertical Penetration - Soil Unit Weight Effect and Calculation of N_{sw}

s_u (Pa)	γ' (kN/m^3)	D (mm)	z (mm)	z/D	v (m/s)	Δ_z (mm)	Δ_z/D	R/2 (N)	R (N)	$s_u/\gamma.D$	$V/s_u.D$	$R_{sw}/s_u.D$	Analysis No.
1500	0.0	300	30	0.1	5.0E-07	10	0.03333	627	1254	∞	2.787	-	64
1500	10.0	300	30	0.1	5.0E-07	10	0.03333	645	1290	0.5	2.867	0.40	65
1500	0.0	300	90	0.3	1.0E-06	10	0.03333	866	1732	∞	3.849	-	66
1500	10.0	300	90	0.3	1.0E-06	10	0.03333	955	1910	0.5	4.244	0.66	67
1500	0.0	300	150	0.5	1.0E-07	12	0.04000	975	1950	∞	4.333	-	68
1500	10.0	300	150	0.5	1.0E-07	12	0.04000	1154	2308	0.5	5.129	0.80	69
1500	0.0	300	225	0.75	5.0E-07	6.09	0.02030	1080	2160	∞	4.800	-	70
1500	10.0	300	225	0.75	5.0E-07	6.09	0.02030	1383	2766	0.5	6.147	0.90	71
5000	0.0	300	300	1.0	5.0E-07	10	0.03333	3833	7666	∞	5.111	-	72
5000	10.0	300	300	1.0	5.0E-07	10	0.03333	4264	8528	1.666667	5.685	0.96	73

Note: all analysis uses a smooth interface condition

Total	10

Table Number **1-6**

Vertical Penetration - Variation in Interface Roughness

s_u (Pa)	D (mm)	z (mm)	z/D	v (m/s)	Δ_z (mm)	Δ_z/D	s_{ul}/s_u	R/2 (N)	R (N)	$V/s_u.D$	Analysis No.
5000	300	30	0.1	1.0E-06	7.5	0.02500	0.00	2100	4200	2.800	74C
5000	300	30	0.1	1.0E-06	7.5	0.02500	0.25	2169	4338	2.892	75
5000	300	30	0.1	1.0E-06	7.5	0.02500	0.50	2228	4456	2.971	76
5000	300	30	0.1	1.0E-06	7.5	0.02500	0.75	2279	4558	3.039	77
5000	300	30	0.1	1.0E-06	7.5	0.02500	1.00	2446	4892	3.261	78
5000	300	90	0.3	2.5E-07	7.5	0.02500	0.00	2916	5832	3.888	79F
5000	300	90	0.3	2.5E-07	7.5	0.02500	0.25	3044	6088	4.059	80
5000	300	90	0.3	2.5E-07	7.5	0.02500	0.50	3163	6326	4.217	81
5000	300	90	0.3	2.5E-07	7.5	0.02500	0.75	3268	6536	4.357	82
5000	300	90	0.3	2.5E-07	7.5	0.02500	1.00	3703	7406	4.937	83
5000	300	150	0.5	1.0E-07	6.0	0.02000	0.00	3278	6556	4.371	84M
5000	300	150	0.5	1.0E-07	6.0	0.02000	0.25	3399	6798	4.532	85
5000	300	150	0.5	1.0E-07	6.0	0.02000	0.50	3521	7042	4.695	86
5000	300	150	0.5	1.0E-07	6.0	0.02000	0.75	3619	7238	4.825	87
5000	300	150	0.5	1.0E-07	6.0	0.02000	1.00	4299	8598	5.732	88
5000	300	225	0.75	5.0E-07	5.0	0.01667	0.00	3586	7172	4.781	89VF
5000	300	225	0.75	5.0E-07	5.0	0.01667	0.25	3813	7626	5.084	90
5000	300	225	0.75	5.0E-07	5.0	0.01667	0.50	4000	8000	5.333	91
5000	300	225	0.75	5.0E-07	5.0	0.01667	0.75	4152	8304	5.536	92
5000	300	225	0.75	5.0E-07	5.0	0.01667	1.00	4732	9464	6.309	93
5000	300	300	1.0	2.5E-07	4.0	0.01333	0.00	3829	7658	5.105	94VVF
5000	300	300	1.0	2.5E-07	4.0	0.01333	0.25	4053	8106	5.404	95
5000	300	300	1.0	2.5E-07	4.0	0.01333	0.50	4241	8482	5.655	96
5000	300	300	1.0	2.5E-07	4.0	0.01333	0.75	4383	8766	5.844	97
5000	300	300	1.0	2.5E-07	4.0	0.01333	1.00	4851	9702	6.468	98

Table Number **1-7**

Vertical Penetration - Smooth Interface, Linear Increasing Shear Strength Gradient

s_u @ z_p (Pa)	D (mm)	z (mm)	z/D	v (m/s)	Δ_z (mm)	Δ_z/D	s_{u0} (Pa)	s_{u0} /s_{uzp}	R/2 (N)	R (N)	V/s_u.D	Analysis No.
5000	300	30	0.1	2.5E-07	10	0.03333	0	0.00	2257	4514	3.009	99
5000	300	60	0.2	5.0E-07	10	0.03333	0	0.00	2539	5078	3.385	100
5000	300	90	0.3	5.0E-07	10	0.03333	0	0.00	2719	5438	3.625	101
5000	300	120	0.4	1.0E-07	10	0.03333	0	0.00	2856	5712	3.808	102
5000	300	150	0.5	1.0E-07	10	0.03333	0	0.00	2975	5950	3.967	103
5000	300	225	0.75	2.5E-07	6.09	0.02030	0	0.00	3244	6488	4.325	104
5000	300	300	1.0	2.5E-07	10	0.03333	0	0.00	3432	6864	4.576	105
5000	300	30	0.1	2.5E-07	10	0.03333	1250	0.25	2311	4622	3.081	106
5000	300	60	0.2	5.0E-07	10	0.03333	1250	0.25	2627	5254	3.503	107
5000	300	90	0.3	5.0E-07	10	0.03333	1250	0.25	2816	5632	3.755	108
5000	300	120	0.4	1.0E-07	10	0.03333	1250	0.25	2965	5930	3.953	109
5000	300	150	0.5	1.0E-07	10	0.03333	1250	0.25	3095	6190	4.127	110
5000	300	225	0.75	2.5E-07	6.09	0.02030	1250	0.25	3391	6782	4.521	111
5000	300	300	1.0	2.5E-07	10	0.03333	1250	0.25	3594	7188	4.792	112
5000	300	30	0.1	2.5E-07	10	0.03333	2500	0.50	2310	4620	3.080	113
5000	300	60	0.2	5.0E-07	10	0.03333	2500	0.50	2673	5346	3.564	114
5000	300	90	0.3	5.0E-07	10	0.03333	2500	0.50	2879	5758	3.839	115
5000	300	120	0.4	1.0E-07	10	0.03333	2500	0.50	3042	6084	4.056	116
5000	300	150	0.5	1.0E-07	10	0.03333	2500	0.50	3184	6368	4.245	117
5000	300	225	0.75	2.5E-07	6.09	0.02030	2500	0.50	3503	7006	4.671	118
5000	300	300	1.0	2.5E-07	10	0.03333	2500	0.50	3718	7436	4.957	119
5000	300	30	0.1	2.5E-07	10	0.03333	3750	0.75	2251	4502	3.001	120
5000	300	60	0.2	5.0E-07	10	0.03333	3750	0.75	2674	5348	3.565	121
5000	300	90	0.3	5.0E-07	10	0.03333	3750	0.75	2909	5818	3.879	122
5000	300	120	0.4	1.0E-07	10	0.03333	3750	0.75	3087	6174	4.116	123
5000	300	150	0.5	1.0E-07	10	0.03333	3750	0.75	3240	6480	4.320	124
5000	300	225	0.75	2.5E-07	6.09	0.02030	3750	0.75	3578	7156	4.771	125
5000	300	300	1.0	2.5E-07	10	0.03333	3750	0.75	3801	7602	5.068	126
5000	300	30	0.1	5.0E-07	10	0.03333	5000	1.00	2090	4180	2.787	127
5000	300	60	0.2	1.0E-06	10	0.03333	5000	1.00	2613	5226	3.484	128
5000	300	90	0.3	1.0E-06	10	0.03333	5000	1.00	2888	5776	3.851	129
5000	300	120	0.4	2.5E-07	10	0.03333	5000	1.00	3085	6170	4.113	130
5000	300	150	0.5	1.0E-07	10	0.03333	5000	1.00	3251	6502	4.335	131
5000	300	225	0.75	5.0E-07	6.09	0.02030	5000	1.00	3601	7202	4.801	132
5000	300	300	1.0	5.0E-07	10	0.03333	5000	1.00	3833	7666	5.111	133

Table Number **1-8**

Vertical Penetration - Rough Interface, Linear Increasing Shear Strength Gradient

s_u @ z_p (Pa)	D (mm)	z (mm)	z/D	v (m/s)	Δ_z (mm)	Δ_z/D	s_{u0} (Pa)	s_{u0}/s_{uzp}	R/2 (N)	R (N)	$V/s_u.D$	Analysis No.
5000	300	30	0.1	2.5E-07	7.5	0.02500	0	0.00	3279	6558	4.372	134
5000	300	60	0.2	2.5E-07	8.75	0.02917	0	0.00	3600	7200	4.800	135
5000	300	90	0.3	1.0E-07	7.5	0.02500	0	0.00	3797	7594	5.063	136
5000	300	120	0.4	1.0E-07	6.667	0.02222	0	0.00	3961	7922	5.281	137
5000	300	150	0.5	1.0E-07	6	0.02000	0	0.00	4122	8244	5.496	138
5000	300	225	0.75	2.5E-07	5	0.01667	0	0.00	4462	8924	5.949	139
5000	300	300	1.0	2.5E-07	4	0.01333	0	0.00	4655	9310	6.207	140
5000	300	30	0.1	2.5E-07	7.5	0.02500	1250	0.25	3265	6530	4.353	141
5000	300	60	0.2	2.5E-07	8.75	0.02917	1250	0.25	3670	7340	4.893	142
5000	300	90	0.3	1.0E-07	7.5	0.02500	1250	0.25	3920	7840	5.227	143
5000	300	120	0.4	1.0E-07	6.667	0.02222	1250	0.25	4111	8222	5.481	144
5000	300	150	0.5	1.0E-07	6	0.02000	1250	0.25	4302	8604	5.736	145
5000	300	225	0.75	2.5E-07	5	0.01667	1250	0.25	4646	9292	6.195	146
5000	300	300	1.0	2.5E-07	4	0.01333	1250	0.25	4767	9534	6.356	147
5000	300	30	0.1	2.5E-07	7.5	0.02500	2500	0.50	3160	6320	4.213	148
5000	300	60	0.2	2.5E-07	8.75	0.02917	2500	0.50	3658	7316	4.877	149
5000	300	90	0.3	1.0E-07	7.5	0.02500	2500	0.50	3964	7928	5.285	150
5000	300	120	0.4	1.0E-07	6.667	0.02222	2500	0.50	4180	8360	5.573	151
5000	300	150	0.5	1.0E-07	6	0.02000	2500	0.50	4371	8742	5.828	152
5000	300	225	0.75	2.5E-07	5	0.01667	2500	0.50	4763	9526	6.351	153
5000	300	300	1.0	2.5E-07	4	0.01333	2500	0.50	4886	9772	6.515	154
5000	300	30	0.1	2.5E-07	7.5	0.02500	3750	0.75	2940	5880	3.920	155
5000	300	60	0.2	2.5E-07	8.75	0.02917	3750	0.75	3545	7090	4.727	156
5000	300	90	0.3	1.0E-07	7.5	0.02500	3750	0.75	3921	7842	5.228	157
5000	300	120	0.4	1.0E-07	6.667	0.02222	3750	0.75	4174	8348	5.565	158
5000	300	150	0.5	1.0E-07	6	0.02000	3750	0.75	4399	8798	5.865	159
5000	300	225	0.75	2.5E-07	5	0.01667	3750	0.75	4807	9614	6.409	160
5000	300	300	1.0	2.5E-07	4	0.01333	3750	0.75	4913	9826	6.551	161
5000	300	30	0.1	5.0E-07	7.5	0.02500	5000	1.00	2446	4892	3.261	162
5000	300	60	0.2	5.0E-07	8.75	0.02917	5000	1.00	3230	6460	4.307	163
5000	300	90	0.3	2.5E-07	7.5	0.02500	5000	1.00	3703	7406	4.937	164
5000	300	120	0.4	1.0E-07	6.667	0.02222	5000	1.00	4028	8056	5.371	165
5000	300	150	0.5	1.0E-07	6	0.02000	5000	1.00	4295	8590	5.727	166
5000	300	225	0.75	5.0E-07	5	0.01667	5000	1.00	4732	9464	6.309	167
5000	300	300	1.0	2.5E-07	4	0.01333	5000	1.00	4847	9694	6.463	168

Table Number **1-9**

Vertical Penetration - Smooth Interface, Shear Strength Crust

s_u @ z_p (Pa)	D (mm)	z (mm)	z/D	z_{cp} (mm)	z_{cp}/D	Crust Peak Strength [1]	v (m/s)	Δ_z (mm)	Δ_z/D	s_{u0} (Pa)	s_{u0}/s_{uzp}	R/2 (N)	R (N)	V/s_u.D	Analysis No.
9000	300	90	0.3	-	-	-	5.0E-07	10	0.03333	9000	1.00	5198	10396	3.850	169
9000	300	90	0.3	-	-	-	2.5E-07	10	0.03333	0	0.00	4892	9784	3.624	170
9000	300	90	0.3	300	1.00	x10	2.5E-07	10	0.03333	0	0.00	4892	9784	3.624	171
9000	300	90	0.3	130	0.433	x10	5.0E-07	10	0.03333	0	0.00	3943	7886	2.921	172
9000	300	90	0.3	90	0.30	x10	5.0E-07	10	0.03333	0	0.00	2453	4906	1.817	173
3600	300	90	0.3	60	0.20	x10	5.0E-07	10	0.03333	0	0.00	1288	2576	2.385	174
9000	300	90	0.3	300	1.00	x5	2.5E-07	10	0.03333	0	0.00	4892	9784	3.624	175
9000	300	90	0.3	130	0.433	x5	5.0E-07	10	0.03333	0	0.00	4686	9372	3.471	176
9000	300	90	0.3	90	0.30	x5	5.0E-07	10	0.03333	0	0.00	3170	6340	2.348	177
4200	300	90	0.3	60	0.20	x5	5.0E-07	10	0.03333	0	0.00	1860	3720	2.952	178

Notes: [1] Crust peak strength as a multiple of the underlying linear increasing shear strength gradient.

Table Number **1-10**

Vertical Penetration - Rough Interface, Shear Strength Crust

s_u @ z_p (Pa)	D (mm)	z (mm)	z/D	z_{cp} (mm)	z_{cp}/D	Crust Peak Strength [1]	v (m/s)	Δ_z (mm)	Δ_z/D	s_{u0} (Pa)	s_{u0}/s_{uzp}	R/2 (N)	R (N)	V/s_u.D	Analysis No.
9000	300	90	0.3	-	-	-	5.0E-07	10	0.03333	9000	1.00	6764	13528	5.010	179
9000	300	90	0.3	-	-	-	2.5E-07	10	0.03333	0	0.00	7136	14272	5.286	180
9000	300	90	0.3	300	1.00	x10	2.5E-07	10	0.03333	0	0.00	7136	14272	5.286	181
9000	300	90	0.3	150	0.5	x10	5.0E-07	10	0.03333	0	0.00	4707	9414	3.487	182
9000	300	90	0.3	90	0.30	x10	5.0E-07	10	0.03333	0	0.00	2768	5536	2.050	183
3600	300	90	0.3	60	0.20	x10	5.0E-07	10	0.03333	0	0.00	1790	3580	3.315	184
9000	300	90	0.3	300	1.00	x5	2.5E-07	10	0.03333	0	0.00	7136	14272	5.286	185
9000	300	90	0.3	150	0.5	x5	5.0E-07	10	0.03333	0	0.00	6334	12668	4.692	186
9000	300	90	0.3	90	0.30	x5	5.0E-07	10	0.03333	0	0.00	3746	7492	2.775	187
4200	300	90	0.3	60	0.20	x5	5.0E-07	10	0.03333	0	0.00	2627	5254	4.170	188

Notes: [1] Crust peak strength as a multiple of the underlying linear increasing shear strength gradient.

Table Number **1-11**

Vertical Penetration - Smooth Interface, Large Strain Analysis

s_u (Pa)	D (mm)	z range		z/D range		v (m/s)	Δ_z (mm)	Δ_z/D	R/2 Range		R Range		$V/s_u.D$ Range		Analysis No.
		Min z (mm)	Max z (mm)	Min z/D	Max z/D				Min (N)	Max (N)	Min (N)	Max (N)	Min (N)	Max (N)	
5000	300	0	80	0.00	0.27	1.0E-07	10	0.03333	0	2922	0	5844	0	3.896	189
5000	300	30	110	0.10	0.37	2.5E-07	10	0.03333	0	3141	0	6282	0	4.188	190
5000	300	60	140	0.20	0.47	2.5E-07	10	0.03333	0	3306	0	6612	0	4.408	191
5000	300	90	170	0.30	0.57	2.5E-07	10	0.03333	0	3447	0	6894	0	4.596	192
5000	300	120	210	0.40	0.70	2.5E-07	10	0.03333	0	3618	0	7236	0	4.824	193
5000	300	180	280	0.60	0.93	2.5E-07	10	0.03333	0	3856	0	7712	0	5.141	194
5000	300	225	300	0.75	1.00	2.5E-07	10	0.03333	0	3882	0	7764	0	5.176	195

Table Number **1-12**

Vertical Penetration - Rough Interface, Large Strain Analysis

s_u (Pa)	D (mm)	z range		z/D range		v (m/s)	Δ_z (mm)	Δ_z/D	R/2 Range		R Range		$V/s_u.D$ Range		Analysis No.
		Min z (mm)	Max z (mm)	Min z/D	Max z/D				Min (N)	Max (N)	Min (N)	Max (N)	Min	Max	
5000	300	0	75	0.00	0.25	1.0E-06	5	0.01667	0	3533	0	7066	0	4.711	196
5000	300	50	90	0.17	0.30	1.0E-06	5	0.01667	0	3795	0	7590	0	5.060	197
5000	300	70	110	0.23	0.37	1.0E-06	5	0.01667	0	3892	0	7784	0	5.189	198
5000	300	90	140	0.30	0.47	1.0E-06	5	0.01667	0	4082	0	8164	0	5.443	199
5000	300	120	155	0.40	0.52	1.0E-06	5	0.01667	0	4217	0	8434	0	5.623	200
5000	300	140	193	0.47	0.64	1.0E-06	5	0.01667	0	4404	0	8808	0	5.872	201
5000	300	170	220	0.57	0.73	1.0E-06	5	0.01667	0	4538	0	9076	0	6.051	202
5000	300	200	260	0.67	0.87	1.0E-06	5	0.01667	0	4625	0	9250	0	6.167	203
5000	300	235	300	0.78	1.00	1.0E-06	5	0.01667	0	4719	0	9438	0	6.292	204

Appendix B

Analysis Summary - Combined Vertical and Horizontal Loading	
Table Number	Description
2-1	Horizontal Displacement - Smooth Interface, Uniform s_u, No γ
2-2	V-H Displacement - Smooth Interface, Uniform s_u, No γ
2-3	Horizontal Displacement - Smooth Interface, Linear Increasing Shear Strength Gradient
2-4	V-H Displacement - Smooth Interface, Linear Increasing Shear Strength Gradient
2-5	V-H Displacement on a Sloping Seabed

Table Number 2-1

Horizontal Displacement - Smooth Interface, Uniform s_u, No γ

s_u (Pa)	D (mm)	z (mm)	z/D	u (m/s)	Number of Zones	Δ_z (mm)	Δ_z/D	R_H (N)	H/s_u.D	Analysis No.
5000	300	30	0.1	5.0E-06	3850	12.5	0.04167	697	0.465	VVC1
5000	300	30	0.1	5.0E-06	4762	10	0.03333	667	0.445	VC2
5000	300	30	0.1	5.0E-06	8382	7.5	0.02500	677	0.451	C3
5000	300	60	0.2	5.0E-06	2992	14	0.04667	1244	0.829	EC4
5000	300	60	0.2	5.0E-06	4728	11.66	0.03887	1188	0.792	VVC5
5000	300	60	0.2	5.0E-06	5728	10	0.03333	1193	0.795	VC6
5000	300	90	0.3	5.0E-07	3120	15.0	0.05000	2347	1.565	VVC7
5000	300	90	0.3	5.0E-07	4492	12.50	0.04167	1679	1.119	VC8
5000	300	90	0.3	5.0E-07	5582	11.25	0.03750	1667	1.111	C9
5000	300	90	0.3	5.0E-07	7028	10	0.03333	1666	1.111	M10
5000	300	120	0.4	5.0E-07	9254	10	0.03333	2026	1.351	C11
5000	300	150	0.5	5.0E-07	7042	15	0.05000	2399	1.599	VVC12
5000	300	150	0.5	5.0E-07	11012	12	0.04000	2398	1.599	VC13
5000	300	225	0.75	2.5E-07	99294	6.09	0.02030	2920	1.947	M14
5000	300	300	1.0	5.0E-07	16246	15	0.05000	3409	2.273	VVC15
5000	300	300	1.0	5.0E-07	25466	12	0.04000	3296	2.197	VC16
5000	300	300	1.0	5.0E-07	36692	10	0.03333	3261	2.174	C17
5000	300	300	1.0	5.0E-07	57265	8	0.02667	3306	2.204	M18

Total	18

Table Number 2-2a

VH Displacement - Smooth Interface, Uniform s_u, No γ

s_u (Pa)	D (mm)	z (mm)	z/D	Δ_z (mm)	δ (°)	v (m/s)	u (m/s)	$\bar{v}$ (m/s)	R_H (N)	R_V (N)	R (N)	$H/s_u.D$	$V/s_u.D$	$R/s_u.D$	Analysis No.
5000	300	30	0.1	7.5	-30	2.5000E-06	4.3301E-06	5.00E-06	215	316	382	0.143	0.211	0.255	19
5000	300	30	0.1	7.5	-25	2.1131E-06	4.5315E-06	5.00E-06	370	618	720	0.247	0.412	0.480	20
5000	300	30	0.1	7.5	-15	1.2941E-06	4.8296E-06	5.00E-06	552	1141	1268	0.368	0.761	0.845	21
5000	300	30	0.1	7.5	-10	8.6824E-07	4.9240E-06	5.00E-06	615	1436	1562	0.410	0.957	1.041	22
5000	300	30	0.1	7.5	-5	4.3578E-07	4.9810E-06	5.00E-06	648	1682	1803	0.432	1.121	1.202	23
5000	300	30	0.1	7.5	0	0.0000E+00	5.0000E-06	5.00E-06	667	2102	2205	0.445	1.401	1.470	24
5000	300	30	0.1	7.5	5	-4.3578E-07	4.9810E-06	5.00E-06	651	2434	2520	0.434	1.623	1.680	25
5000	300	30	0.1	7.5	10	-8.6824E-07	4.9240E-06	5.00E-06	607	2761	2827	0.405	1.841	1.885	26
5000	300	30	0.1	7.5	15	-1.2941E-06	4.8296E-06	5.00E-06	522	3156	3199	0.348	2.104	2.133	27
5000	300	30	0.1	7.5	20	-1.7101E-06	4.6985E-06	5.00E-06	435	3426	3454	0.290	2.284	2.302	28
5000	300	30	0.1	7.5	30	-2.5000E-06	4.3301E-06	5.00E-06	235	3871	3878	0.157	2.581	2.585	29
5000	300	30	0.1	7.5	90	-5.0000E-07	0.0000E+00	5.00E-07	0	4180	4180	0.000	2.787	2.787	30
5000	300	60	0.2	10	-45	7.0711E-07	7.0711E-07	1.00E-06	225	183	290	0.150	0.122	0.193	31
5000	300	60	0.2	10	-35	5.7358E-07	8.1915E-07	1.00E-06	592	603	845	0.395	0.402	0.563	32
5000	300	60	0.2	10	-25	2.1131E-06	4.5315E-06	5.00E-06	893	1134	1443	0.595	0.756	0.962	33
5000	300	60	0.2	10	-15	1.2941E-06	4.8296E-06	5.00E-06	1079	1663	1982	0.719	1.109	1.322	34
5000	300	60	0.2	10	-5	4.3578E-07	4.9810E-06	5.00E-06	1175	2204	2498	0.783	1.469	1.665	35
5000	300	60	0.2	10	0	0.0000E+00	5.0000E-06	5.00E-06	1193	2609	2869	0.795	1.739	1.913	36
5000	300	60	0.2	10	5	-4.3578E-07	4.9810E-06	5.00E-06	1177	2951	3177	0.785	1.967	2.118	37
5000	300	60	0.2	10	10	-8.6824E-07	4.9240E-06	5.00E-06	1134	3276	3467	0.756	2.184	2.311	38
5000	300	60	0.2	10	20	-1.7101E-06	4.6985E-06	5.00E-06	955	3960	4074	0.637	2.640	2.716	39
5000	300	60	0.2	10	25	-2.1131E-06	4.5315E-06	5.00E-06	796	4349	4421	0.531	2.899	2.947	40
5000	300	60	0.2	10	35	-5.7358E-07	8.1915E-07	1.00E-06	570	4751	4785	0.380	3.167	3.190	41
5000	300	60	0.2	10	50	-7.6604E-07	6.4279E-07	1.00E-06	290	5063	5071	0.193	3.375	3.381	42
5000	300	60	0.2	10	90	-1.0000E-06	0.0000E+00	1.00E-06	0	5227	5227	0.000	3.485	3.485	43

Table Number 2-2b

VH Displacement - Smooth Interface, Uniform s_u, No γ

s_u (Pa)	D (mm)	z (mm)	z/D	Δ_z (mm)	δ (°)	v (m/s)	u (m/s)	$\bar{v}$ (m/s)	R_H (N)	R_V (N)	R (N)	$H/s_u.D$	$V/s_u.D$	$R/s_u.D$	Analysis No.
5000	300	90	0.3	10	-50	3.8302E-07	3.2139E-07	5.00E-07	580	358	682	0.387	0.239	0.454	44
5000	300	90	0.3	10	-35	2.8679E-07	4.0958E-07	5.00E-07	1052	888	1377	0.701	0.592	0.918	45
5000	300	90	0.3	10	-25	2.1131E-07	4.5315E-07	5.00E-07	1362	1424	1970	0.908	0.949	1.314	46
5000	300	90	0.3	10	-15	1.2941E-07	4.8296E-07	5.00E-07	1547	1933	2476	1.031	1.289	1.651	47
5000	300	90	0.3	10	-10	8.6824E-08	4.9240E-07	5.00E-07	1602	2162	2691	1.068	1.441	1.794	48
5000	300	90	0.3	10	0	0.0000E+00	5.0000E-07	5.00E-07	1667	2824	3279	1.111	1.883	2.186	49
5000	300	90	0.3	10	10	-8.6824E-08	4.9240E-07	5.00E-07	1630	3430	3798	1.087	2.287	2.532	50
5000	300	90	0.3	10	15	-1.2941E-07	4.8296E-07	5.00E-07	1517	3961	4242	1.011	2.641	2.828	51
5000	300	90	0.3	10	25	-2.1131E-07	4.5315E-07	5.00E-07	1274	4619	4791	0.849	3.079	3.194	52
5000	300	90	0.3	10	35	-2.8679E-07	4.0958E-07	5.00E-07	935	5225	5308	0.623	3.483	3.539	53
5000	300	90	0.3	10	45	-3.5355E-07	3.5355E-07	5.00E-07	690	5520	5563	0.460	3.680	3.709	54
5000	300	90	0.3	10	55	-4.0958E-07	2.8679E-07	5.00E-07	491	5679	5700	0.327	3.786	3.800	55
5000	300	90	0.3	10	65	-4.5315E-07	2.1131E-07	5.00E-07	370	5760	5772	0.247	3.840	3.848	56
5000	300	90	0.3	10	90	-1.0000E-06	0.0000E+00	1.00E-06	0	5844	5844	0.000	3.896	3.896	57
5000	300	120	0.4	10	-60	4.3301E-07	2.5000E-07	5.00E-07	581	213	619	0.387	0.142	0.413	58
5000	300	120	0.4	10	-50	3.8302E-07	3.2139E-07	5.00E-07	1024	531	1153	0.683	0.354	0.769	59
5000	300	120	0.4	10	-35	2.8679E-07	4.0958E-07	5.00E-07	1433	990	1742	0.955	0.660	1.161	60
5000	300	120	0.4	10	-25	2.1131E-07	4.5315E-07	5.00E-07	1731	1515	2300	1.154	1.010	1.534	61
5000	300	120	0.4	10	-15	1.2941E-07	4.8296E-07	5.00E-07	1916	2042	2800	1.277	1.361	1.867	62
5000	300	120	0.4	10	-10	8.6824E-08	4.9240E-07	5.00E-07	1977	2326	3053	1.318	1.551	2.035	63
5000	300	120	0.4	10	0	0.0000E+00	5.0000E-07	5.00E-07	2030	2969	3597	1.353	1.979	2.398	64
5000	300	120	0.4	10	10	-8.6824E-08	4.9240E-07	5.00E-07	1972	3652	4150	1.315	2.435	2.767	65
5000	300	120	0.4	10	15	-1.2941E-07	4.8296E-07	5.00E-07	1886	4053	4470	1.257	2.702	2.980	66
5000	300	120	0.4	10	25	-2.1131E-07	4.5315E-07	5.00E-07	1634	4729	5003	1.089	3.153	3.336	67
5000	300	120	0.4	10	35	-2.8679E-07	4.0958E-07	5.00E-07	1234	5423	5562	0.823	3.615	3.708	68
5000	300	120	0.4	10	50	-3.8302E-07	3.2139E-07	5.00E-07	863	5831	5895	0.575	3.887	3.930	69
5000	300	120	0.4	10	65	-4.5315E-07	2.1131E-07	5.00E-07	513	6067	6089	0.342	4.045	4.059	70
5000	300	120	0.4	10	90	-2.5000E-07	0.0000E+00	2.50E-07	0	6166	6166	0.000	4.111	4.111	71

Table Number 2-2c

VH Displacement - Smooth Interface, Uniform s_u, No γ

s_u (Pa)	D (mm)	z (mm)	z/D	Δ_z (mm)	δ (°)	v (m/s)	u (m/s)	$\bar{v}$ (m/s)	R_H (N)	R_V (N)	R (N)	$H/s_u.D$	$V/s_u.D$	$R/s_u.D$	Analysis No.
5000	300	150	0.5	12	-65	4.5315E-07	2.1131E-07	5.00E-07	814	191	836	0.543	0.127	0.557	72
5000	300	150	0.5	12	-50	3.8302E-07	3.2139E-07	5.00E-07	1346	553	1455	0.897	0.369	0.970	73
5000	300	150	0.5	12	-35	2.8679E-07	4.0958E-07	5.00E-07	1819	1092	2122	1.213	0.728	1.414	74
5000	300	150	0.5	12	-25	2.1131E-07	4.5315E-07	5.00E-07	2065	1525	2567	1.377	1.017	1.711	75
5000	300	150	0.5	12	-15	1.2941E-07	4.8296E-07	5.00E-07	2267	2061	3064	1.511	1.374	2.043	76
5000	300	150	0.5	12	-10	8.6824E-08	4.9240E-07	5.00E-07	2332	2332	3298	1.555	1.555	2.199	77
5000	300	150	0.5	12	0	0.0000E+00	5.0000E-07	5.00E-07	2399	3058	3887	1.599	2.039	2.591	78
5000	300	150	0.5	12	10	-8.6824E-08	4.9240E-07	5.00E-07	2329	3810	4465	1.553	2.540	2.977	79
5000	300	150	0.5	12	15	-1.2941E-07	4.8296E-07	5.00E-07	2253	4136	4710	1.502	2.757	3.140	80
5000	300	150	0.5	12	25	-2.1131E-07	4.5315E-07	5.00E-07	2005	4817	5218	1.337	3.211	3.478	81
5000	300	150	0.5	12	35	-2.8679E-07	4.0958E-07	5.00E-07	1605	5516	5745	1.070	3.677	3.830	82
5000	300	150	0.5	12	45	-3.5355E-07	3.5355E-07	5.00E-07	1200	6014	6133	0.800	4.009	4.088	83
5000	300	150	0.5	12	55	-4.0958E-07	2.8679E-07	5.00E-07	907	6262	6327	0.605	4.175	4.218	84
5000	300	150	0.5	12	70	-4.6985E-07	1.7101E-07	5.00E-07	517	6466	6487	0.345	4.311	4.324	85
5000	300	150	0.5	12	90	-1.0000E-07	0.0000E+00	1.00E-07	0	6574	6574	0.000	4.383	4.383	86
5000	300	225	0.75	6.09	-65	2.2658E-07	1.0565E-07	2.50E-07	1201	207	1219	0.801	0.138	0.812	87
5000	300	225	0.75	6.09	-55	2.0479E-07	1.4339E-07	2.50E-07	1577	418	1631	1.051	0.279	1.088	88
5000	300	225	0.75	6.09	-45	1.7678E-07	1.7678E-07	2.50E-07	1981	759	2121	1.321	0.506	1.414	89
5000	300	225	0.75	6.09	-35	1.4339E-07	2.0479E-07	2.50E-07	2287	1127	2550	1.525	0.751	1.700	90
5000	300	225	0.75	6.09	-25	1.0565E-07	2.2658E-07	2.50E-07	2576	1627	3047	1.717	1.085	2.031	91
5000	300	225	0.75	6.09	-15	6.4705E-08	2.4148E-07	2.50E-07	2780	2174	3529	1.853	1.449	2.353	92
5000	300	225	0.75	6.09	-10	4.3412E-08	2.4620E-07	2.50E-07	2853	2492	3788	1.902	1.661	2.525	93
5000	300	225	0.75	6.09	0	0.0000E+00	2.5000E-07	2.50E-07	2920	3160	4303	1.947	2.107	2.868	94
5000	300	225	0.75	6.09	10	-4.3412E-08	2.4620E-07	2.50E-07	2867	3889	4832	1.911	2.593	3.221	95
5000	300	225	0.75	6.09	15	-6.4705E-08	2.4148E-07	2.50E-07	2786	4259	5089	1.857	2.839	3.393	96
5000	300	225	0.75	6.09	25	-1.0565E-07	2.2658E-07	2.50E-07	2526	4987	5590	1.684	3.325	3.727	97
5000	300	225	0.75	6.09	35	-1.4339E-07	2.0479E-07	2.50E-07	2088	5754	6121	1.392	3.836	4.081	98
5000	300	225	0.75	6.09	45	-1.7678E-07	1.7678E-07	2.50E-07	1505	6453	6626	1.003	4.302	4.417	99
5000	300	225	0.75	6.09	55	-2.0479E-07	1.4339E-07	2.50E-07	1089	6812	6898	0.726	4.541	4.599	100
5000	300	225	0.75	6.09	70	-2.3492E-07	8.5505E-08	2.50E-07	550	7100	7121	0.367	4.733	4.748	101
5000	300	225	0.75	6.09	90	-5.0000E-07	0.0000E+00	5.00E-07	0	7203	7203	0.000	4.802	4.802	102

Table Number 2-2d

VH Displacement - Smooth Interface, Uniform s_u, No γ

s_u (Pa)	D (mm)	z (mm)	z/D	Δ_z (mm)	δ (°)	v (m/s)	u (m/s)	$\bar{v}$ (m/s)	R_H (N)	R_V (N)	R (N)	$H/s_u.D$	$V/s_u.D$	$R/s_u.D$	Analysis No.
5000	300	300	1.0	10	-70	4.6985E-07	1.7101E-07	5.00E-07	1253	176	1265	0.835	0.117	0.844	103
5000	300	300	1.0	10	-60	4.3301E-07	2.5000E-07	5.00E-07	1648	350	1685	1.099	0.233	1.123	104
5000	300	300	1.0	10	-50	3.8302E-07	3.2139E-07	5.00E-07	2146	705	2259	1.431	0.470	1.506	105
5000	300	300	1.0	10	-35	2.8679E-07	4.0958E-07	5.00E-07	2603	1212	2871	1.735	0.808	1.914	106
5000	300	300	1.0	10	-25	2.1131E-07	4.5315E-07	5.00E-07	2933	1790	3436	1.955	1.193	2.291	107
5000	300	300	1.0	10	-15	1.2941E-07	4.8296E-07	5.00E-07	3136	2364	3927	2.091	1.576	2.618	108
5000	300	300	1.0	10	-10	8.6824E-08	4.9240E-07	5.00E-07	3205	2682	4179	2.137	1.788	2.786	109
5000	300	300	1.0	10	0	0.0000E+00	5.0000E-07	5.00E-07	3261	3366	4687	2.174	2.244	3.124	110
5000	300	300	1.0	10	10	-8.6824E-08	4.9240E-07	5.00E-07	3198	4110	5208	2.132	2.740	3.472	111
5000	300	300	1.0	10	15	-1.2941E-07	4.8296E-07	5.00E-07	3104	4544	5503	2.069	3.029	3.669	112
5000	300	300	1.0	10	25	-2.1131E-07	4.5315E-07	5.00E-07	2829	5283	5993	1.886	3.522	3.995	113
5000	300	300	1.0	10	35	-2.8679E-07	4.0958E-07	5.00E-07	2380	6060	6511	1.587	4.040	4.340	114
5000	300	300	1.0	10	45	-3.5355E-07	3.5355E-07	5.00E-07	1788	6766	6998	1.192	4.511	4.666	115
5000	300	300	1.0	10	55	-4.0958E-07	2.8679E-07	5.00E-07	1258	7235	7344	0.839	4.823	4.896	116
5000	300	300	1.0	10	62	-4.4147E-07	2.3474E-07	5.00E-07	995	7396	7463	0.663	4.931	4.975	117
5000	300	300	1.0	10	70	-4.6985E-07	1.7101E-07	5.00E-07	665	7543	7572	0.443	5.029	5.048	118
5000	300	300	1.0	10	90	-5.0000E-07	3.0629E-23	5.00E-07	0	7666	7666	0.000	5.111	5.111	119

Total Analysis	101

Table Number 2-3

Horizontal Displacement - Smooth Interface, Linear Increasing Shear Strength Gradient

s_u (Pa)	D (mm)	z (mm)	z/D	s_{u0}/s_{uzp}	u (m/s)	Δ_z (mm)	R_H (N)	$H/s_u.D$	Analysis No.
5000	300	30	0.1	0	5.00E-06	7.5	495	0.330	120
5000	300	30	0.1	0.5	5.00E-06	7.5	610	0.407	121
5000	300	90	0.3	0	5.00E-07	10	1056	0.704	122
5000	300	90	0.3	0.5	5.00E-07	10	1385	0.923	123
5000	300	150	0.5	0	5.00E-07	12	1460	0.973	124
5000	300	150	0.5	0.5	5.00E-07	12	1943	1.295	125
5000	300	300	1.0	0	5.00E-07	10	2235	1.490	126
5000	300	300	1.0	0.5	5.00E-07	10	2790	1.860	127

Total	8

Table Number 2-4a

VH Displacement - Smooth Interface, Linear Increasing Shear Strength Gradient

s_u (Pa)	D (mm)	z (mm)	z/D	Δ_z (mm)	δ (°)	s_{u0}/s_{uzp}	v (m/s)	u (m/s)	$\bar{v}$ (m/s)	R_H (N)	R_V (N)	R (N)	$H/s_u.D$	$V/s_u.D$	$R/s_u.D$	Analysis No.
5000	300	30	0.1	7.5	-30	0	2.5000E-06	4.3301E-06	5.00E-06	67	100	120	0.045	0.067	0.080	128
5000	300	30	0.1	7.5	-25	0	2.1131E-06	4.5315E-06	5.00E-06	160	288	329	0.107	0.192	0.220	129
5000	300	30	0.1	7.5	-15	0	1.2941E-06	4.8296E-06	5.00E-06	320	759	824	0.213	0.506	0.549	130
5000	300	30	0.1	7.5	-10	0	8.6824E-07	4.9240E-06	5.00E-06	410	1169	1239	0.273	0.779	0.826	131
5000	300	30	0.1	7.5	-5	0	4.3578E-07	4.9810E-06	5.00E-06	469	1632	1698	0.313	1.088	1.132	132
5000	300	30	0.1	7.5	0	0	0.0000E+00	5.0000E-06	5.00E-06	495	2204	2259	0.330	1.469	1.506	133
5000	300	30	0.1	7.5	5	0	-4.3578E-07	4.9810E-06	5.00E-06	468	2774	2813	0.312	1.849	1.875	134
5000	300	30	0.1	7.5	10	0	-8.6824E-07	4.9240E-06	5.00E-06	387	3394	3416	0.258	2.263	2.277	135
5000	300	30	0.1	7.5	15	0	-1.2941E-06	4.8296E-06	5.00E-06	300	3780	3792	0.200	2.520	2.528	136
5000	300	30	0.1	7.5	20	0	-1.7101E-06	4.6985E-06	5.00E-06	193	4125	4130	0.129	2.750	2.753	137
5000	300	30	0.1	7.5	30	0	-2.5000E-06	4.3301E-06	5.00E-06	53	4440	4440	0.035	2.960	2.960	138
5000	300	30	0.1	7.5	90	0	-5.0000E-07	0.0000E+00	5.00E-07	0	4506	4506	0.000	3.004	3.004	139
5000	300	30	0.1	7.5	-30	0.5	2.5000E-06	4.3301E-06	5.00E-06	142	209	253	0.095	0.139	0.168	140
5000	300	30	0.1	7.5	-25	0.5	2.1131E-06	4.5315E-06	5.00E-06	271	464	537	0.181	0.309	0.358	141
5000	300	30	0.1	7.5	-15	0.5	1.2941E-06	4.8296E-06	5.00E-06	460	1014	1113	0.307	0.676	0.742	142
5000	300	30	0.1	7.5	-10	0.5	8.6824E-07	4.9240E-06	5.00E-06	535	1365	1466	0.357	0.910	0.977	143
5000	300	30	0.1	7.5	-5	0.5	4.3578E-07	4.9810E-06	5.00E-06	588	1772	1867	0.392	1.181	1.245	144
5000	300	30	0.1	7.5	0	0.5	0.0000E+00	5.0000E-06	5.00E-06	610	2289	2369	0.407	1.526	1.579	145
5000	300	30	0.1	7.5	5	0.5	-4.3578E-07	4.9810E-06	5.00E-06	588	2761	2823	0.392	1.841	1.882	146
5000	300	30	0.1	7.5	10	0.5	-8.6824E-07	4.9240E-06	5.00E-06	515	3315	3355	0.343	2.210	2.237	147
5000	300	30	0.1	7.5	15	0.5	-1.2941E-06	4.8296E-06	5.00E-06	433	3687	3712	0.289	2.458	2.475	148
5000	300	30	0.1	7.5	20	0.5	-1.7101E-06	4.6985E-06	5.00E-06	329	4020	4033	0.219	2.680	2.689	149
5000	300	30	0.1	7.5	30	0.5	-2.5000E-06	4.3301E-06	5.00E-06	144	4426	4428	0.096	2.951	2.952	150
5000	300	30	0.1	7.5	90	0.5	-5.0000E-07	0.0000E+00	5.00E-07	0	4620	4620	0.000	3.080	3.080	151

Table Number 2-4b

VH Displacement - Smooth Interface, Linear Increasing Shear Strength Gradient

s_u (Pa)	D (mm)	z (mm)	z/D	Δ_Z (mm)	δ (°)	s_{u0}/s_{uzp}	v (m/s)	u (m/s)	$\bar{v}$ (m/s)	R_H (N)	R_V (N)	R (N)	$H/s_u.D$	$V/s_u.D$	$R/s_u.D$	Analysis No.
5000	300	90	0.3	10	-50	0	3.8302E-07	3.2139E-07	5.00E-07	135	90	162	0.090	0.060	0.108	152
5000	300	90	0.3	10	-35	0	2.8679E-07	4.0958E-07	5.00E-07	405	397	567	0.270	0.265	0.378	153
5000	300	90	0.3	10	-25	0	2.1131E-07	4.5315E-07	5.00E-07	699	903	1142	0.466	0.602	0.761	154
5000	300	90	0.3	10	-15	0	1.2941E-07	4.8296E-07	5.00E-07	905	1467	1724	0.603	0.978	1.149	155
5000	300	90	0.3	10	-10	0	8.6824E-08	4.9240E-07	5.00E-07	974	1750	2003	0.649	1.167	1.335	156
5000	300	90	0.3	10	0	0	0.0000E+00	5.0000E-07	5.00E-07	1056	2606	2812	0.704	1.737	1.875	157
5000	300	90	0.3	10	10	0	-8.6824E-08	4.9240E-07	5.00E-07	977	3636	3765	0.651	2.424	2.510	158
5000	300	90	0.3	10	15	0	-1.2941E-07	4.8296E-07	5.00E-07	858	4177	4264	0.572	2.785	2.843	159
5000	300	90	0.3	10	25	0	-2.1131E-07	4.5315E-07	5.00E-07	623	4843	4883	0.415	3.229	3.255	160
5000	300	90	0.3	10	35	0	-2.8679E-07	4.0958E-07	5.00E-07	438	5165	5184	0.292	3.443	3.456	161
5000	300	90	0.3	10	45	0	-3.5355E-07	3.5355E-07	5.00E-07	271	5368	5375	0.181	3.579	3.583	162
5000	300	90	0.3	10	55	0	-4.0958E-07	2.8679E-07	5.00E-07	172	5453	5456	0.115	3.635	3.637	163
5000	300	90	0.3	10	65	0	-4.5315E-07	2.1131E-07	5.00E-07	97	5497	5498	0.065	3.665	3.665	164
5000	300	90	0.3	10	90	0	-1.0000E-06	0.0000E+00	1.00E-06	0	5520	5520	0.000	3.680	3.680	165
5000	300	90	0.3	10	-50	0.5	3.8302E-07	3.2139E-07	5.00E-07	360	226	425	0.240	0.151	0.283	166
5000	300	90	0.3	10	-35	0.5	2.8679E-07	4.0958E-07	5.00E-07	737	650	983	0.491	0.433	0.655	167
5000	300	90	0.3	10	-25	0.5	2.1131E-07	4.5315E-07	5.00E-07	1047	1187	1583	0.698	0.791	1.055	168
5000	300	90	0.3	10	-15	0.5	1.2941E-07	4.8296E-07	5.00E-07	1245	1732	2133	0.830	1.155	1.422	169
5000	300	90	0.3	10	-10	0.5	8.6824E-08	4.9240E-07	5.00E-07	1309	1997	2388	0.873	1.331	1.592	170
5000	300	90	0.3	10	0	0.5	0.0000E+00	5.0000E-07	5.00E-07	1385	2796	3120	0.923	1.864	2.080	171
5000	300	90	0.3	10	10	0.5	-8.6824E-08	4.9240E-07	5.00E-07	1313	3693	3919	0.875	2.462	2.613	172
5000	300	90	0.3	10	15	0.5	-1.2941E-07	4.8296E-07	5.00E-07	1206	4175	4346	0.804	2.783	2.897	173
5000	300	90	0.3	10	25	0.5	-2.1131E-07	4.5315E-07	5.00E-07	922	4960	5045	0.615	3.307	3.363	174
5000	300	90	0.3	10	35	0.5	-2.8679E-07	4.0958E-07	5.00E-07	709	5339	5386	0.473	3.559	3.591	175
5000	300	90	0.3	10	45	0.5	-3.5355E-07	3.5355E-07	5.00E-07	488	5604	5625	0.325	3.736	3.750	176
5000	300	90	0.3	10	55	0.5	-4.0958E-07	2.8679E-07	5.00E-07	354	5719	5730	0.236	3.813	3.820	177
5000	300	90	0.3	10	65	0.5	-4.5315E-07	2.1131E-07	5.00E-07	240	5786	5791	0.160	3.857	3.861	178
5000	300	90	0.3	10	90	0.5	-1.0000E-06	0.0000E+00	1.00E-06	0	5839	5839	0.000	3.893	3.893	179

Table Number 2-4c

VH Displacement - Smooth Interface, Linear Increasing Shear Strength Gradient

s_u (Pa)	D (mm)	z (mm)	z/D	Δ_z (mm)	δ (°)	s_{u0}/s_{uzp}	v (m/s)	u (m/s)	$\bar{v}$ (m/s)	R_H (N)	R_V (N)	R (N)	$H/s_u.D$	$V/s_u.D$	$R/s_u.D$	Analysis No.
5000	300	150	0.5	12	-65	0	4.5315E-07	2.1131E-07	5.00E-07	202	62	211	0.135	0.041	0.141	180
5000	300	150	0.5	12	-55	0	4.0958E-07	2.8679E-07	5.00E-07	511	277	581	0.341	0.185	0.387	181
5000	300	150	0.5	12	-35	0	2.8679E-07	4.0958E-07	5.00E-07	856	672	1088	0.571	0.448	0.726	182
5000	300	150	0.5	12	-25	0	2.1131E-07	4.5315E-07	5.00E-07	1094	1096	1549	0.729	0.731	1.032	183
5000	300	150	0.5	12	-15	0	1.2941E-07	4.8296E-07	5.00E-07	1300	1649	2100	0.867	1.099	1.400	184
5000	300	150	0.5	12	-10	0	8.6824E-08	4.9240E-07	5.00E-07	1384	2010	2440	0.923	1.340	1.627	185
5000	300	150	0.5	12	0	0	0.0000E+00	5.0000E-07	5.00E-07	1460	2900	3247	0.973	1.933	2.165	186
5000	300	150	0.5	12	10	0	-8.6824E-08	4.9240E-07	5.00E-07	1385	3727	3976	0.923	2.485	2.651	187
5000	300	150	0.5	12	15	0	-1.2941E-07	4.8296E-07	5.00E-07	1273	4235	4422	0.849	2.823	2.948	188
5000	300	150	0.5	12	25	0	-2.1131E-07	4.5315E-07	5.00E-07	981	5038	5133	0.654	3.359	3.422	189
5000	300	150	0.5	12	35	0	-2.8679E-07	4.0958E-07	5.00E-07	754	5448	5500	0.503	3.632	3.667	190
5000	300	150	0.5	12	45	0	-3.5355E-07	3.5355E-07	5.00E-07	546	5697	5723	0.364	3.798	3.815	191
5000	300	150	0.5	12	55	0	-4.0958E-07	2.8679E-07	5.00E-07	369	5846	5858	0.246	3.897	3.905	192
5000	300	150	0.5	12	70	0	-4.6985E-07	1.7101E-07	5.00E-07	197	5937	5940	0.131	3.958	3.960	193
5000	300	150	0.5	12	90	0	-1.0000E-07	0.0000E+00	1.00E-07	0	5972	5972	0.000	3.981	3.981	194
5000	300	150	0.5	12	-65	0.5	4.5315E-07	2.1131E-07	5.00E-07	508	127	524	0.339	0.085	0.349	195
5000	300	150	0.5	12	-55	0.5	4.0958E-07	2.8679E-07	5.00E-07	930	416	1019	0.620	0.277	0.679	196
5000	300	150	0.5	12	-35	0.5	2.8679E-07	4.0958E-07	5.00E-07	1344	888	1611	0.896	0.592	1.074	197
5000	300	150	0.5	12	-25	0.5	2.1131E-07	4.5315E-07	5.00E-07	1588	1321	2066	1.059	0.881	1.377	198
5000	300	150	0.5	12	-15	0.5	1.2941E-07	4.8296E-07	5.00E-07	1795	1872	2594	1.197	1.248	1.729	199
5000	300	150	0.5	12	-10	0.5	8.6824E-08	4.9240E-07	5.00E-07	1870	2195	2884	1.247	1.463	1.922	200
5000	300	150	0.5	12	0	0.5	0.0000E+00	5.0000E-07	5.00E-07	1943	3011	3583	1.295	2.007	2.389	201
5000	300	150	0.5	12	10	0.5	-8.6824E-08	4.9240E-07	5.00E-07	1871	3812	4246	1.247	2.541	2.831	202
5000	300	150	0.5	12	15	0.5	-1.2941E-07	4.8296E-07	5.00E-07	1776	4240	4597	1.184	2.827	3.065	203
5000	300	150	0.5	12	25	0.5	-2.1131E-07	4.5315E-07	5.00E-07	1475	5069	5279	0.983	3.379	3.519	204
5000	300	150	0.5	12	35	0.5	-2.8679E-07	4.0958E-07	5.00E-07	1108	5725	5831	0.739	3.817	3.887	205
5000	300	150	0.5	12	45	0.5	-3.5355E-07	3.5355E-07	5.00E-07	878	5997	6061	0.585	3.998	4.041	206
5000	300	150	0.5	12	55	0.5	-4.0958E-07	2.8679E-07	5.00E-07	635	6202	6234	0.423	4.135	4.156	207
5000	300	150	0.5	12	70	0.5	-4.6985E-07	1.7101E-07	5.00E-07	365	6347	6357	0.243	4.231	4.238	208
5000	300	150	0.5	12	90	0.5	-1.0000E-07	0.0000E+00	1.00E-07	0	6416	6416	0.000	4.277	4.277	209

Table Number 2-4d

VH Displacement - Smooth Interface, Linear Increasing Shear Strength Gradient

s_u (Pa)	D (mm)	z (mm)	z/D	Δ_z (mm)	δ (°)	s_{u0}/s_{uzp}	v (m/s)	u (m/s)	$\bar{v}$ (m/s)	R_H (N)	R_V (N)	R (N)	$H/s_u.D$	$V/s_u.D$	$R/s_u.D$	Analysis No.
5000	300	300	1.0	10	-70	0	4.6985E-07	1.7101E-07	5.00E-07	548	72	553	0.365	0.048	0.368	210
5000	300	300	1.0	10	-60	0	4.3301E-07	2.5000E-07	5.00E-07	833	196	856	0.555	0.131	0.570	211
5000	300	300	1.0	10	-50	0	3.8302E-07	3.2139E-07	5.00E-07	1209	467	1296	0.806	0.311	0.864	212
5000	300	300	1.0	10	-35	0	2.8679E-07	4.0958E-07	5.00E-07	1587	889	1819	1.058	0.593	1.213	213
5000	300	300	1.0	10	-25	0	2.1131E-07	4.5315E-07	5.00E-07	1902	1443	2387	1.268	0.962	1.592	214
5000	300	300	1.0	10	-15	0	1.2941E-07	4.8296E-07	5.00E-07	2103	2017	2914	1.402	1.345	1.943	215
5000	300	300	1.0	10	-10	0	8.6824E-08	4.9240E-07	5.00E-07	2174	2346	3198	1.449	1.564	2.132	216
5000	300	300	1.0	10	0	0	0.0000E+00	5.0000E-07	5.00E-07	2235	3110	3830	1.490	2.073	2.553	217
5000	300	300	1.0	10	10	0	-8.6824E-08	4.9240E-07	5.00E-07	2152	3987	4531	1.435	2.658	3.020	218
5000	300	300	1.0	10	15	0	-1.2941E-07	4.8296E-07	5.00E-07	2077	4331	4803	1.385	2.887	3.202	219
5000	300	300	1.0	10	25	0	-2.1131E-07	4.5315E-07	5.00E-07	1761	5208	5498	1.174	3.472	3.665	220
5000	300	300	1.0	10	35	0	-2.8679E-07	4.0958E-07	5.00E-07	1300	6014	6153	0.867	4.009	4.102	221
5000	300	300	1.0	10	45	0	-3.5355E-07	3.5355E-07	5.00E-07	1014	6374	6454	0.676	4.249	4.303	222
5000	300	300	1.0	10	55	0	-4.0958E-07	2.8679E-07	5.00E-07	744	6600	6642	0.496	4.400	4.428	223
5000	300	300	1.0	10	62	0	-4.4147E-07	2.3474E-07	5.00E-07	555	6716	6739	0.370	4.477	4.493	224
5000	300	300	1.0	10	70	0	-4.6985E-07	1.7101E-07	5.00E-07	370	6799	6809	0.247	4.533	4.539	225
5000	300	300	1.0	10	90	0	-5.0000E-07	3.0629E-23	5.00E-07	0	6865	6865	0.000	4.577	4.577	226
5000	300	300	1.0	10	-70	0.5	4.6985E-07	1.7101E-07	5.00E-07	911	125	920	0.607	0.083	0.613	227
5000	300	300	1.0	10	-60	0.5	4.3301E-07	2.5000E-07	5.00E-07	1259	277	1289	0.839	0.185	0.859	228
5000	300	300	1.0	10	-50	0.5	3.8302E-07	3.2139E-07	5.00E-07	1701	594	1802	1.134	0.396	1.201	229
5000	300	300	1.0	10	-35	0.5	2.8679E-07	4.0958E-07	5.00E-07	2125	1066	2377	1.417	0.711	1.585	230
5000	300	300	1.0	10	-25	0.5	2.1131E-07	4.5315E-07	5.00E-07	2454	1642	2953	1.636	1.095	1.968	231
5000	300	300	1.0	10	-15	0.5	1.2941E-07	4.8296E-07	5.00E-07	2659	2225	3467	1.773	1.483	2.311	232
5000	300	300	1.0	10	-10	0.5	8.6824E-08	4.9240E-07	5.00E-07	2729	2553	3737	1.819	1.702	2.491	233
5000	300	300	1.0	10	0	0.5	0.0000E+00	5.0000E-07	5.00E-07	2790	3291	4314	1.860	2.194	2.876	234
5000	300	300	1.0	10	10	0.5	-8.6824E-08	4.9240E-07	5.00E-07	2713	4129	4941	1.809	2.753	3.294	235
5000	300	300	1.0	10	15	0.5	-1.2941E-07	4.8296E-07	5.00E-07	2635	4495	5210	1.757	2.997	3.474	236
5000	300	300	1.0	10	25	0.5	-2.1131E-07	4.5315E-07	5.00E-07	2321	5363	5844	1.547	3.575	3.896	237
5000	300	300	1.0	10	35	0.5	-2.8679E-07	4.0958E-07	5.00E-07	1843	6190	6459	1.229	4.127	4.306	238
5000	300	300	1.0	10	45	0.5	-3.5355E-07	3.5355E-07	5.00E-07	1281	6866	6984	0.854	4.577	4.656	239
5000	300	300	1.0	10	55	0.5	-4.0958E-07	2.8679E-07	5.00E-07	1040	7062	7138	0.693	4.708	4.759	240
5000	300	300	1.0	10	62	0.5	-4.4147E-07	2.3474E-07	5.00E-07	782	7221	7263	0.521	4.814	4.842	241
5000	300	300	1.0	10	70	0.5	-4.6985E-07	1.7101E-07	5.00E-07	519	7341	7359	0.346	4.894	4.906	242
5000	300	300	1.0	10	90	0.5	-5.0000E-07	3.0629E-23	5.00E-07	0	7437	7437	0.000	4.958	4.958	243

Total Analysis	116

Table Number 2-5a

VH Displacement on a Sloping Seabed - 10° slope - Smooth Interface, Uniform s_u, Δ_z=5mm

s_u (Pa)	D (mm)	γ' (kN/m^3)	$s_u/\gamma'.D$	δ_L (°)	δ (°)	v_L (m/s)	u_L (m/s)	$\bar{v}_L$ (m/s)	$H/s_u.D$	$V/s_u.D$	Analysis No.
10000	300	9.53	3.50	90	100	-5.0000E-07	0.0000E+00	5.00E-07	0.471	2.668	244
10000	300	9.53	3.50	45	55	-3.5355E-07	3.5355E-07	5.00E-07	0.444	2.657	245
10000	300	9.53	3.50	35	45	-2.8679E-07	4.0958E-07	5.00E-07	0.367	2.586	246
10000	300	9.53	3.50	25	35	-2.1131E-07	4.5315E-07	5.00E-07	0.209	2.398	247
10000	300	9.53	3.50	15	25	-1.2941E-07	4.8296E-07	5.00E-07	0.011	2.053	248
10000	300	9.53	3.50	5	15	-4.3578E-08	4.9810E-07	5.00E-07	-0.157	1.580	249
10000	300	9.53	3.50	0	10	0.0000E+00	5.0000E-07	5.00E-07	-0.193	1.411	250
10000	300	9.53	3.50	-5	5	4.3578E-08	4.9810E-07	5.00E-07	-0.220	1.203	251
10000	300	9.53	3.50	-15	-5	1.2941E-07	4.8296E-07	5.00E-07	-0.218	0.754	252
10000	300	9.53	3.50	-25	-15	2.1131E-07	4.5315E-07	5.00E-07	-0.153	0.398	253
10000	300	9.53	3.50	-35	-25	2.8679E-07	4.0958E-07	5.00E-07	-0.032	0.065	254
10000	300	9.53	3.50	-90	-80	5.0000E-07	0.0000E+00	5.00E-07	0.000	0.000	255
10000	300	9.53	3.50	135	145	-3.5355E-07	-3.5355E-07	5.00E-07	0.499	2.646	256
10000	300	9.53	3.50	145	155	-2.8679E-07	-4.0958E-07	5.00E-07	0.549	2.552	257
10000	300	9.53	3.50	155	165	-2.1131E-07	-4.5315E-07	5.00E-07	0.630	2.328	258
10000	300	9.53	3.50	165	175	-1.2941E-07	-4.8296E-07	5.00E-07	0.691	1.956	259
10000	300	9.53	3.50	175	-175	-4.3578E-08	-4.9810E-07	5.00E-07	0.692	1.444	260
10000	300	9.53	3.50	180	-170	0.0000E+00	-5.0000E-07	5.00E-07	0.668	1.268	261
10000	300	9.53	3.50	-175	-165	4.3578E-08	-4.9810E-07	5.00E-07	0.621	1.061	262
10000	300	9.53	3.50	-165	-155	1.2941E-07	-4.8296E-07	5.00E-07	0.465	0.637	263
10000	300	9.53	3.50	-155	-145	2.1131E-07	-4.5315E-07	5.00E-07	0.281	0.322	264
10000	300	9.53	3.50	-145	-135	2.8679E-07	-4.0958E-07	5.00E-07	0.053	0.050	265

Table Number 2-5b

VH Displacement on a Sloping Seabed - 10° slope - Smooth Interface, Uniform s_u, Δ_z=5mm

s_u (Pa)	D (mm)	γ' (kN/m^3)	$s_u/\gamma'.D$	δ_L (°)	δ (°)	v_L (m/s)	u_L (m/s)	$\bar{v}_L$ (m/s)	$H/s_u.D$	$V/s_u.D$	Analysis No.
5000	300	7.36	2.27	90	100	-5.0000E-07	0.0000E+00	5.00E-07	0.476	2.673	266
5000	300	7.36	2.27	45	55	-3.5355E-07	3.5355E-07	5.00E-07	0.447	2.663	267
5000	300	7.36	2.27	35	45	-2.8679E-07	4.0958E-07	5.00E-07	0.369	2.593	268
5000	300	7.36	2.27	25	35	-2.1131E-07	4.5315E-07	5.00E-07	0.212	2.403	269
5000	300	7.36	2.27	15	25	-1.2941E-07	4.8296E-07	5.00E-07	0.015	2.052	270
5000	300	7.36	2.27	5	15	-4.3578E-08	4.9810E-07	5.00E-07	-0.157	1.581	271
5000	300	7.36	2.27	0	10	0.0000E+00	5.0000E-07	5.00E-07	-0.193	1.411	272
5000	300	7.36	2.27	-5	5	4.3578E-08	4.9810E-07	5.00E-07	-0.220	1.203	273
5000	300	7.36	2.27	-15	-5	1.2941E-07	4.8296E-07	5.00E-07	-0.218	0.755	274
5000	300	7.36	2.27	-25	-15	2.1131E-07	4.5315E-07	5.00E-07	-0.153	0.398	275
5000	300	7.36	2.27	-35	-25	2.8679E-07	4.0958E-07	5.00E-07	-0.032	0.065	276
5000	300	7.36	2.27	-90	-80	5.0000E-07	0.0000E+00	5.00E-07	0.000	0.000	277
5000	300	7.36	2.27	135	145	-3.5355E-07	-3.5355E-07	5.00E-07	0.502	2.652	278
5000	300	7.36	2.27	145	155	-2.8679E-07	-4.0958E-07	5.00E-07	0.553	2.559	279
5000	300	7.36	2.27	155	165	-2.1131E-07	-4.5315E-07	5.00E-07	0.633	2.333	280
5000	300	7.36	2.27	165	175	-1.2941E-07	-4.8296E-07	5.00E-07	0.693	1.967	281
5000	300	7.36	2.27	175	-175	-4.3578E-08	-4.9810E-07	5.00E-07	0.695	1.451	282
5000	300	7.36	2.27	180	-170	0.0000E+00	-5.0000E-07	5.00E-07	0.670	1.274	283
5000	300	7.36	2.27	-175	-165	4.3578E-08	-4.9810E-07	5.00E-07	0.623	1.065	284
5000	300	7.36	2.27	-165	-155	1.2941E-07	-4.8296E-07	5.00E-07	0.466	0.639	285
5000	300	7.36	2.27	-155	-145	2.1131E-07	-4.5315E-07	5.00E-07	0.281	0.323	286
5000	300	7.36	2.27	-145	-135	2.8679E-07	-4.0958E-07	5.00E-07	0.053	0.051	287

Table Number **2-5c**

VH Displacement on a Sloping Seabed - 10° slope - Smooth Interface, Uniform s_u, Δ_z=5mm

s_u (Pa)	D (mm)	γ' (kN/m^3)	$s_u/\gamma'.D$	δ_L (°)	δ (°)	v_L (m/s)	u_L (m/s)	$\bar{v}_L$ (m/s)	$H/s_u.D$	$V/s_u.D$	Analysis No.
1000	300	7.36	0.45	90	100	-5.0000E-07	0.0000E+00	5.00E-07	0.504	2.724	288
1000	300	7.36	0.45	45	55	-3.5355E-07	3.5355E-07	5.00E-07	0.476	2.712	289
1000	300	7.36	0.45	35	45	-2.8679E-07	4.0958E-07	5.00E-07	0.406	2.650	290
1000	300	7.36	0.45	25	35	-2.1131E-07	4.5315E-07	5.00E-07	0.234	2.443	291
1000	300	7.36	0.45	15	25	-1.2941E-07	4.8296E-07	5.00E-07	0.008	2.043	292
1000	300	7.36	0.45	5	15	-4.3578E-08	4.9810E-07	5.00E-07	-0.157	1.585	293
1000	300	7.36	0.45	0	10	0.0000E+00	5.0000E-07	5.00E-07	-0.194	1.415	294
1000	300	7.36	0.45	-5	5	4.3578E-08	4.9810E-07	5.00E-07	-0.220	1.210	295
1000	300	7.36	0.45	-15	-5	1.2941E-07	4.8296E-07	5.00E-07	-0.218	0.759	296
1000	300	7.36	0.45	-25	-15	2.1131E-07	4.5315E-07	5.00E-07	-0.153	0.399	297
1000	300	7.36	0.45	-35	-25	2.8679E-07	4.0958E-07	5.00E-07	-0.032	0.067	298
1000	300	7.36	0.45	-90	-80	5.0000E-07	0.0000E+00	5.00E-07	0.000	0.000	299
1000	300	7.36	0.45	135	145	-3.5355E-07	-3.5355E-07	5.00E-07	0.536	2.695	300
1000	300	7.36	0.45	145	155	-2.8679E-07	-4.0958E-07	5.00E-07	0.592	2.597	301
1000	300	7.36	0.45	155	165	-2.1131E-07	-4.5315E-07	5.00E-07	0.667	2.384	302
1000	300	7.36	0.45	165	175	-1.2941E-07	-4.8296E-07	5.00E-07	0.718	2.074	303
1000	300	7.36	0.45	175	-175	-4.3578E-08	-4.9810E-07	5.00E-07	0.721	1.535	304
1000	300	7.36	0.45	180	-170	0.0000E+00	-5.0000E-07	5.00E-07	0.695	1.330	305
1000	300	7.36	0.45	-175	-165	4.3578E-08	-4.9810E-07	5.00E-07	0.642	1.105	306
1000	300	7.36	0.45	-165	-155	1.2941E-07	-4.8296E-07	5.00E-07	0.478	0.657	307
1000	300	7.36	0.45	-155	-145	2.1131E-07	-4.5315E-07	5.00E-07	0.288	0.328	308
1000	300	7.36	0.45	-145	-135	2.8679E-07	-4.0958E-07	5.00E-07	0.053	0.052	309

Total Analysis 66

Appendix C

Analysis Summary - Reliability Based Analysis	
Table Number	Description
3-1	Vertical Loading Example
3-2	V_{max} Analysis
3-3	V_{max} Fragility
3-4	H_{max} Analysis
3-5	H_{max} Fragility
3-6	V-H Analysis
3-7	V-H Fragility

Table Number **3-1**

V Loading Example

z/D	Probability of Failure (P_F)					
	CoV = 10%		CoV = 15%		CoV = 20%	
	Simplified	MC	Simplified	MC	Simplified	MC
0.025	0.995	0.995	0.958	0.957	0.902	0.902
0.050	0.661	0.661	0.609	0.609	0.582	0.582
0.075	0.250	0.249	0.326	0.326	0.368	0.369
0.100	0.084	0.084	0.179	0.179	0.245	0.247
0.150	0.011	0.011	0.064	0.064	0.127	0.127
0.200	2.081E-03	2.101E-03	0.028	0.028	0.076	0.076
0.250	5.059E-04	5.085E-04	0.014	0.014	0.050	0.050
0.300	1.512E-04	1.495E-04	8.003E-03	7.891E-03	0.035	0.036
0.400	2.106E-05	2.150E-05	3.163E-03	3.044E-03	0.020	0.020
0.500	-	-	1.523E-03	1.398E-03	0.013	0.013
0.600	-	-	8.366E-04	7.589E-04	9.208E-03	9.220E-03
0.700	-	-	5.044E-04	4.344E-04	6.831E-03	6.670E-03
0.800	-	-	3.260E-04	2.844E-04	5.283E-03	5.155E-03
0.900	-	-	2.223E-04	2.056E-04	4.218E-03	4.050E-03

Table Number **3-2a**

V_{max} Analysis - CoV = 10%

z/D	$V/s_u.D$	Simplified	MC	
			N	P_F
0.05	1.25	2.384E-06	4.50E+06	2.667E-06
0.05	1.50	2.418E-04	-	-
0.05	1.75	0.008	300000	8.000E-03
0.05	2.00	0.093	-	-
0.05	2.50	0.802	50000	0.804
0.05	3.00	0.999	-	-
0.1	1.50	1.993E-06	-	-
0.1	1.75	1.020E-04	500000	9.400E-05
0.1	2.00	0.002	300000	0.002
0.1	2.50	0.154	200000	0.154
0.1	3.00	0.781	50000	0.781
0.1	3.50	0.995	-	-
0.2	2.00	2.511E-05	900000	2.667E-05
0.2	2.25	4.640E-04	-	-
0.2	2.50	0.005	300000	0.005
0.2	3.00	0.140	-	-
0.2	3.50	0.657	100000	0.656
0.2	4.00	0.971	50000	0.972
0.4	2.25	4.011E-06	-	-
0.4	2.50	5.917E-05	900000	6.667E-05
0.4	2.75	6.093E-04	-	-
0.4	3.00	0.004	300000	0.004
0.4	3.50	0.082	300000	0.082
0.4	4.00	0.437	-	-
0.4	5.00	0.989	50000	0.989
0.6	2.60	9.609E-06	2.50E+06	8.800E-06
0.6	2.75	4.016E-05	-	-
0.6	3.00	3.459E-04	500000	3.400E-04
0.6	3.50	0.011	300000	0.011
0.6	4.00	0.117	100000	0.116
0.6	5.00	0.844	-	-
0.6	6.00	0.999	-	-
0.8	2.75	5.390E-06	-	-
0.8	3.00	4.973E-05	500000	5.000E-05
0.8	3.25	3.587E-04	-	-
0.8	3.50	0.002	300000	0.002
0.8	4.00	0.032	300000	0.032
0.8	5.00	0.571	-	-
0.8	6.00	0.987	50000	0.987

Table Number **3-2a** **continued**

V_{max} Analysis - CoV = 10%

z/D	$V/s_u.D$	Simplified	MC	
			N	P_F
1.0	3.00	1.055E-05	2.50E+06	8.400E-06
1.0	3.25	8.034E-05	-	-
1.0	3.50	4.921E-04	600000	4.750E-04
1.0	4.00	0.010	300000	0.010
1.0	5.00	0.337	100000	0.335
1.0	6.00	0.932	-	-

Table Number **3-2b**

V_{max} Analysis - CoV = 15%

z/D	$V/s_u.D$	Simplified	MC	
			N	P_F
0.05	0.75	3.453E-06	-	-
0.05	1.00	8.059E-05	2.00E+06	9.650E-05
0.05	1.25	1.145E-03	-	-
0.05	1.50	9.997E-03	600000	9.783E-03
0.05	2.00	0.190	-	-
0.05	2.50	0.715	100000	0.714
0.05	3.00	0.978	-	-
0.05	3.5	1.000	100000	1.000
0.1	1.00	9.685E-06	1.50E+06	9.33E-06
0.1	1.25	1.197E-04	-	-
0.1	1.50	1.053E-03	700000	1.093E-03
0.1	2.00	0.030	600000	0.030
0.1	2.50	0.248	-	-
0.1	3.00	0.697	100000	0.699
0.1	3.50	0.957	100000	0.958
0.1	4.00	0.998	-	-
0.2	1.25	1.398E-05	1.50E+06	1.400E-05
0.2	1.50	1.104E-04	700000	1.129E-04
0.2	2.00	3.435E-03	500000	3.384E-03
0.2	2.50	0.043	-	-
0.2	3.00	0.235	100000	0.233
0.2	3.50	0.606	-	-
0.2	4.00	0.896	-	-
0.2	4.50	0.988	100000	0.989
0.2	5.00	0.999	-	-
0.4	1.25	1.951E-06	-	-
0.4	1.50	1.297E-05	1.50E+06	1.200E-05
0.4	2.00	3.540E-04	900000	3.400E-04
0.4	2.50	5.139E-03	-	-
0.4	3.00	0.040	500000	0.040
0.4	3.50	0.177	-	-
0.4	4.00	0.458	100000	0.456
0.4	5.00	0.937	50000	0.937
0.4	6.00	0.999	50000	0.999
0.6	1.50	4.017E-06	-	-
0.6	2.00	9.568E-05	600000	8.167E-05
0.6	2.50	1.368E-03	600000	1.325E-03
0.6	3.00	0.012	-	-
0.6	3.50	0.063	300000	0.063
0.6	4.00	0.214	-	-
0.6	5.00	0.750	100000	0.750
0.6	6.00	0.984	-	-

Table Number **3-2b** **continued**

V_{max} Analysis - CoV = 15%

z/D	$V/s_u.D$	Simplified	MC	
			N	P_F
0.8	1.75	8.882E-06	1.50E+06	7.330E-06
0.8	2.00	3.876E-05	-	-
0.8	2.50	5.316E-04	500000	5.480E-04
0.8	3.00	4.735E-03	600000	4.707E-03
0.8	3.50	0.028	-	-
0.8	4.00	0.108	300000	0.108
0.8	5.00	0.548	100000	0.548
0.8	6.00	0.930	-	-
0.8	7.00	0.998	50000	0.998
1.0	1.75	4.675E-06	-	-
1.0	2.00	1.958E-05	2.00E+06	1.100E-05
1.0	2.50	2.566E-04	500000	2.640E-04
1.0	3.00	2.289E-03	-	-
1.0	3.50	0.014	500000	0.014
1.0	4.00	0.060	-	-
1.0	5.00	0.389	100000	0.389
1.0	6.00	0.840	-	-
1.0	7.00	0.988	-	-

Table Number **3-2c**

V_{max} Analysis - CoV = 20%

z/D	$V/s_u.D$	Simplified	MC	
			N	P_F
0.05	0.32	8.328E-06	2.00E+06	1.000E-05
0.05	0.50	4.521E-05	-	-
0.05	0.75	3.726E-04	500000	3.62E-04
0.05	1.00	2.328E-03	-	-
0.05	1.25	0.011	300000	0.011
0.05	1.50	0.041	-	-
0.05	2.00	0.255	100000	0.255
0.05	2.50	0.665	-	-
0.05	3.00	0.935	50000	0.935
0.05	3.50	0.995	-	-
0.1	0.25	2.669E-06	-	-
0.1	0.50	2.048E-05	1.00E+06	2.100E-05
0.1	1.00	6.776E-04	-	-
0.1	1.25	2.934E-03	300000	2.977E-03
0.1	1.50	0.011	-	-
0.1	2.00	0.080	150000	0.079
0.1	2.50	0.305	-	-
0.1	3.00	0.651	-	-
0.1	3.50	0.901	-	-
0.1	4.00	0.986	50000	0.986
0.2	0.50	1.037E-05	2.00E+06	1.000E-05
0.2	1.00	2.210E-04	700000	2.029E-04
0.2	1.50	2.799E-03	700000	2.786E-03
0.2	2.00	0.021	-	-
0.2	3.00	0.294	100000	0.295
0.2	4.00	0.828	50000	0.826
0.2	5.00	0.992	-	-
0.4	0.50	5.800E-06	-	-
0.4	1.00	8.165E-05	500000	8.800E-05
0.4	1.50	8.029E-04	600000	7.667E-04
0.4	2.00	5.545E-03	900000	5.431E-03
0.4	3.00	0.095	-	-
0.4	4.00	0.468	-	-
0.4	5.00	0.875	50000	0.875
0.4	6.00	0.991	-	-
0.6	0.65	9.169E-06	2.50E+06	8.400E-06
0.6	1.00	4.833E-05	-	-
0.6	1.50	4.067E-04	-	-
0.6	2.00	2.574E-03	-	-
0.6	2.50	0.012	300000	0.012
0.6	3.00	0.045	-	-
0.6	3.50	0.126	100000	0.125
0.6	4.00	0.276	-	-
0.6	5.00	0.694	-	-
0.6	6.00	0.946	50000	0.947

Table Number **3-2c** **continued**

V_{max} Analysis - CoV = 20%

z/D	$V/s_u.D$	Simplified	MC	
			N	P_F
0.8	0.50	3.545E-06	-	-
0.8	1.00	3.417E-05	1.00E+06	4.400E-05
0.8	1.50	2.574E-04	500000	2.580E-04
0.8	2.00	1.519E-03	-	-
0.8	3.00	0.026	250000	0.026
0.8	4.00	0.177	100000	0.178
0.8	5.50	0.725	50000	0.724
0.8	7.00	0.983	-	-
1.0	0.50	3.076E-06	4.0E+06	2.571E-06
1.0	1.00	2.648E-05	1.5E+06	1.933E-05
1.0	1.50	1.832E-04	-	-
1.0	2.00	1.020E-03	700000	9.586E-04
1.0	3.00	0.017	250000	0.017
1.0	4.00	0.121	150000	0.121
1.0	5.50	0.606	-	-
1.0	7.00	0.956	50000	0.951

Table Number **3-3**

V_{max} Fragility

CoV	z/D	$V/s_u.D$			I_F
		P_F = 3E-5	P_F = 0.07	Fragility	
10%	0.05	1.38	1.96	0.58	0.70
10%	0.10	1.67	2.37	0.70	0.70
10%	0.20	2.01	2.87	0.86	0.70
10%	0.40	2.43	3.46	1.03	0.70
10%	0.60	2.72	3.87	1.15	0.70
10%	0.80	2.94	4.19	1.25	0.70
10%	1.00	3.13	4.45	1.32	0.70
15%	0.05	0.91	1.79	0.88	0.51
15%	0.10	1.11	2.17	1.06	0.51
15%	0.20	1.34	2.62	1.28	0.51
15%	0.40	1.62	3.16	1.54	0.51
15%	0.60	1.81	3.54	1.73	0.51
15%	0.80	1.96	3.82	1.86	0.51
15%	1.00	2.08	4.06	1.98	0.51
20%	0.05	0.45	1.62	1.17	0.28
20%	0.10	0.55	1.96	1.41	0.28
20%	0.20	0.66	2.37	1.71	0.28
20%	0.40	0.80	2.86	2.06	0.28
20%	0.60	0.90	3.20	2.30	0.28
20%	0.80	0.98	3.46	2.48	0.28
20%	1.00	1.03	3.68	2.65	0.28

Table Number **3-4a**

H_{max} Analysis - CoV = 10%

z/D	$H/s_u.D$	Simplified	MC	
			N	P_F
0.05	0.160	9.215E-06	2.50E+06	5.200E-06
0.05	0.175	8.943E-05	-	-
0.05	0.190	6.610E-04	300000	6.867E-04
0.05	0.210	0.006	-	-
0.05	0.230	0.037	100000	0.038
0.05	0.260	0.239	-	-
0.05	0.290	0.641	100000	0.640
0.05	0.330	0.963	-	-
0.1	0.275	1.629E-05	-	-
0.1	0.300	1.455E-04	500000	1.520E-04
0.1	0.325	9.946E-04	-	-
0.1	0.350	0.005	200000	0.005
0.1	0.380	0.027	-	-
0.1	0.410	0.099	100000	0.099
0.1	0.450	0.332	-	-
0.1	0.550	0.955	50000	0.954
0.2	0.450	8.171E-06	1.50E+06	8.000E-06
0.2	0.475	3.253E-05	-	-
0.2	0.500	1.178E-04	600000	7.053E-05
0.2	0.540	7.577E-04	-	-
0.2	0.575	0.003	200000	0.003
0.2	0.625	0.018	-	-
0.2	0.750	0.303	100000	0.299
0.2	0.900	0.916	50000	0.915
0.4	0.775	1.522E-05	1.50E+06	1.400E-05
0.4	0.875	3.155E-04	700000	3.000E-04
0.4	0.975	0.004	-	-
0.4	1.075	0.028	100000	0.028
0.4	1.200	0.165	-	-
0.4	1.400	0.702	50000	0.701
0.4	1.600	0.979	-	-
0.6	1.000	9.305E-06	-	-
0.6	1.075	5.857E-05	800000	5.625E-05
0.6	1.125	1.812E-04	-	-
0.6	1.200	8.530E-04	500000	8.340E-04
0.6	1.350	0.011	300000	0.011
0.6	1.600	0.198	100000	0.198
0.6	1.900	0.807	-	-
0.6	2.100	0.978	25000	0.977

Table Number **3-4a** **continued**

H_{max} Analysis - CoV = 10%

z/D	$H/s_u.D$	Simplified	MC	
			N	P_F
0.8	1.150	1.006E-05	1.00E+06	1.100E-05
0.8	1.250	8.340E-05	800000	8.625E-05
0.8	1.375	8.416E-04	-	-
0.8	1.500	0.006	200000	0.006
0.8	1.750	0.102	-	-
0.8	2.000	0.491	50000	0.492
0.8	2.500	0.993	-	-
1.0	1.300	1.539E-05	-	-
1.0	1.375	6.377E-05	800000	6.125E-05
1.0	1.425	1.550E-04	-	-
1.0	1.525	7.938E-04	400000	8.175E-04
1.0	1.700	0.009	-	-
1.0	1.850	0.045	100000	0.044
1.0	2.000	0.152	-	-
1.0	2.500	0.888	50000	0.889
1.0	2.800	0.995	20000	0.995

Table Number **3-4b**

H_{max} Analysis - CoV = 15%

z/D	$H/s_u.D$	Simplified	MC	
			N	P_F
0.05	0.100	9.152E-06	2.50E+06	1.080E-05
0.05	0.130	1.785E-04	-	-
0.05	0.160	2.149E-03	300000	2.150E-03
0.05	0.190	0.016	-	-
0.05	0.220	0.077	100000	0.077
0.05	0.250	0.238	-	-
0.05	0.300	0.684	100000	0.688
0.05	0.350	0.953	-	-
0.1	0.175	1.414E-05	-	-
0.1	0.225	2.523E-04	500000	2.640E-04
0.1	0.275	2.805E-03	-	-
0.1	0.325	0.020	100000	0.020
0.1	0.375	0.088	-	-
0.1	0.425	0.260	100000	0.261
0.1	0.475	0.526	-	-
0.1	0.525	0.780	-	-
0.1	0.575	0.931	50000	0.931
0.2	0.300	1.754E-05	1.20E+06	1.500E-05
0.2	0.400	4.927E-04	-	-
0.2	0.500	7.110E-03	300000	7.083E-03
0.2	0.600	0.054	100000	0.054
0.2	0.700	0.222	-	-
0.2	0.800	0.531	50000	0.530
0.2	1.000	0.961	50000	0.962
0.4	0.500	1.597E-05	-	-
0.4	0.600	1.272E-04	400000	1.375E-04
0.4	0.700	7.991E-04	-	-
0.4	0.900	0.016	100000	0.016
0.4	1.100	0.125	-	-
0.4	1.300	0.441	50000	0.442
0.4	1.500	0.804	-	-
0.4	1.800	0.991	50000	0.992
0.6	0.600	5.960E-06	3.00E+06	5.000E-06
0.6	0.750	7.029E-05	-	-
0.6	0.900	6.077E-04	300000	6.233E-04
0.6	1.200	0.018	-	-
0.6	1.500	0.172	200000	0.17
0.6	1.800	0.578	-	-
0.6	2.100	0.910	100000	0.909

Table Number **3-4b** **continued**

H_{max} Analysis - CoV = 15%

z/D	$H/s_u.D$	Simplified	MC	
			N	P_F
0.8	0.750	1.506E-05	-	-
0.8	0.900	1.195E-04	300000	1.233E-04
0.8	1.050	7.496E-04	-	-
0.8	1.350	0.015	100000	0.015
0.8	1.650	0.119	-	-
0.8	1.950	0.428	50000	0.432
0.8	2.250	0.793	-	-
0.8	2.550	0.965	50000	0.964
1.0	0.800	9.604E-06	2.50E+06	1.120E-05
1.0	1.050	2.108E-04	-	-
1.0	1.350	4.283E-03	300000	4.343E-03
1.0	1.650	0.042	100000	0.042
1.0	1.950	0.202	-	-
1.0	2.250	0.525	50000	0.525
1.0	2.550	0.832	-	-
1.0	2.850	0.968	50000	0.967

Table Number **3-4c**

H_{max} Analysis - CoV = 20%

z/D	$H/s_u.D$	Simplified	MC	
			N	P_F
0.05	0.040	9.121E-06	1.50E+06	9.330E-06
0.05	0.060	4.281E-05	-	-
0.05	0.080	1.780E-04	500000	1.740E-04
0.05	0.110	1.203E-03	-	-
0.05	0.140	0.006	200000	0.006
0.05	0.200	0.077	-	-
0.05	0.250	0.297	50000	0.299
0.05	0.325	0.790	-	-
0.05	0.375	0.955	10000	0.956
0.1	0.075	1.318E-05	-	-
0.1	0.125	1.206E-04	800000	1.038E-04
0.1	0.175	8.444E-04	-	-
0.1	0.260	0.013	-	-
0.1	0.350	0.100	50000	0.099
0.1	0.450	0.414	-	-
0.1	0.600	0.916	20000	0.917
0.2	0.110	8.367E-06	-	-
0.2	0.160	3.326E-05	2.00E+06	2.950E-05
0.2	0.225	1.735E-04	-	-
0.2	0.300	9.570E-04	400000	9.450E-04
0.2	0.400	0.007	200000	0.007
0.2	0.550	0.064	-	-
0.2	0.750	0.398	50000	0.396
0.2	1.000	0.907	-	-
0.4	0.200	1.080E-05	1.00E+06	1.100E-05
0.4	0.300	5.405E-05	-	-
0.4	0.450	4.707E-04	500000	4.520E-04
0.4	0.650	0.005	-	-
0.4	0.900	0.053	100000	0.053
0.4	1.150	0.250	-	-
0.4	1.400	0.605	30000	0.606
0.4	2.000	0.994	10000	0.994
0.6	0.300	1.720E-05	-	-
0.6	0.500	1.783E-04	600000	1.833E-04
0.6	0.700	1.357E-03	-	-
0.6	0.900	0.008	300000	0.008
0.6	1.200	0.058	-	-
0.6	1.600	0.336	50000	0.339
0.6	2.200	0.902	-	-

Table Number **3-4c continued**

H_{max} Analysis - CoV = 20%

z/D	$H/s_u.D$	Simplified	MC	
			N	P_F
0.8	0.300	1.061E-05	2.00E+06	5.500E-06
0.8	0.500	8.739E-05	-	-
0.8	0.750	8.759E-04	500000	9.220E-04
0.8	1.000	0.006	-	-
0.8	1.250	0.030	100000	0.030
0.8	1.700	0.224	-	-
0.8	2.100	0.594	40000	0.593
0.8	2.500	0.892	40000	0.895
1.0	0.300	7.557E-06	-	-
1.0	0.500	5.257E-05	500000	6.400E-05
1.0	0.800	6.743E-04	-	-
1.0	1.100	0.006	300000	0.006
1.0	1.350	0.024	-	-
1.0	1.600	0.079	100000	0.079
1.0	1.900	0.230	-	-
1.0	2.200	0.474	50000	0.475
1.0	2.600	0.797	-	-
1.0	3.000	0.958	10000	0.959

Table Number **3-5**

H_{max} Fragility

CoV	z/D	$H/s_u.D$			I_F
		P_f = 3E-5	P_f = 0.07	Fragility	
10%	0.05	0.17	0.24	0.07	0.71
10%	0.10	0.28	0.40	0.12	0.70
10%	0.20	0.47	0.67	0.20	0.70
10%	0.40	0.80	1.13	0.33	0.71
10%	0.60	1.05	1.49	0.44	0.70
10%	0.80	1.20	1.71	0.51	0.70
10%	1.00	1.34	1.90	0.56	0.71
15%	0.05	0.11	0.22	0.11	0.50
15%	0.10	0.19	0.37	0.18	0.51
15%	0.20	0.31	0.62	0.31	0.50
15%	0.40	0.53	1.04	0.51	0.51
15%	0.60	0.70	1.36	0.66	0.51
15%	0.80	0.80	1.56	0.76	0.51
15%	1.00	0.89	1.74	0.85	0.51
20%	0.05	0.06	0.20	0.14	0.30
20%	0.10	0.09	0.33	0.24	0.27
20%	0.20	0.16	0.56	0.40	0.29
20%	0.40	0.26	0.94	0.68	0.28
20%	0.60	0.34	1.23	0.89	0.28
20%	0.80	0.40	1.41	1.01	0.28
20%	1.00	0.44	1.57	1.13	0.28

Table Number **3-6a**

VH Analysis - CoV = 10%

z/D	P_F	δ_{LS} (˚)	Simplified		MC	
			$H/s_u.D$	$V/s_u.D$	$H/s_u.D$	$V/s_u.D$
0.2	0.07	90	0.000	2.868	0	2.866
0.2	0.07	82.13	0.357	2.581	0.357	2.580
0.2	0.07	77.31	0.511	2.269	-	-
0.2	0.07	73.03	0.605	1.983	0.619	1.978
0.2	0.07	68.94	0.653	1.696	-	-
0.2	0.07	64.84	0.662	1.410	0.672	1.405
0.2	0.07	60.56	0.634	1.123	-	-
0.2	0.07	55.85	0.567	0.837	0.575	0.832
0.2	0.07	50.24	0.458	0.550	-	-
0.2	0.07	42.34	0.315	0.287	0.315	0.287
0.2	0.01	90	0.000	2.581	0.000	2.580
0.2	0.01	82.13	0.321	2.323	0.321	2.322
0.2	0.01	77.31	0.460	2.043	-	-
0.2	0.01	73.03	0.545	1.785	0.558	1.782
0.2	0.01	68.94	0.588	1.527	-	-
0.2	0.01	64.84	0.596	1.269	0.605	1.265
0.2	0.01	60.56	0.571	1.011	-	-
0.2	0.01	55.85	0.511	0.753	0.517	0.748
0.2	0.01	50.24	0.412	0.495	-	-
0.2	0.01	42.34	0.283	0.258	0.283	0.258
0.2	1.0E-04	90	0.000	2.112	0.000	2.102
0.2	1.0E-04	82.13	0.263	1.901	0.263	1.905
0.2	1.0E-04	77.31	0.376	1.672	-	-
0.2	1.0E-04	73.03	0.446	1.461	0.455	1.455
0.2	1.0E-04	68.94	0.481	1.250	-	-
0.2	1.0E-04	64.84	0.488	1.039	0.493	1.031
0.2	1.0E-04	60.56	0.467	0.827	-	-
0.2	1.0E-04	55.85	0.418	0.616	0.424	0.614
0.2	1.0E-04	50.24	0.337	0.405	-	-
0.2	1.0E-04	42.34	0.232	0.211	0.232	0.212

Table Number **3-6b**

VH Analysis - CoV = 15%

z/D	P_F	δ_{LS} (˚)	Simplified		MC	
			$H/s_u.D$	$V/s_u.D$	$H/s_u.D$	$V/s_u.D$
0.2	0.07	90	0.000	2.619	0.000	2.620
0.2	0.07	82.13	0.326	2.357	0.326	2.358
0.2	0.07	77.31	0.467	2.073	-	-
0.2	0.07	73.03	0.553	1.811	0.566	1.808
0.2	0.07	68.94	0.597	1.550	-	-
0.2	0.07	64.84	0.605	1.288	0.614	1.284
0.2	0.07	60.56	0.579	1.026	-	-
0.2	0.07	55.85	0.518	0.764	0.525	0.760
0.2	0.07	50.24	0.418	0.502	-	-
0.2	0.07	42.34	0.287	0.262	0.287	0.262
0.2	0.01	90	0.000	2.190	0.000	2.191
0.2	0.01	82.13	0.272	1.971	0.273	1.973
0.2	0.01	77.31	0.390	1.733	-	-
0.2	0.01	73.03	0.462	1.515	0.473	1.512
0.2	0.01	68.94	0.499	1.296	-	-
0.2	0.01	64.84	0.506	1.077	0.514	1.074
0.2	0.01	60.56	0.484	0.858	-	-
0.2	0.01	55.85	0.433	0.639	0.439	0.635
0.2	0.01	50.24	0.350	0.420	-	-
0.2	0.01	42.34	0.240	0.219	0.240	0.219
0.2	1.0E-03	90	0.000	1.805	0.000	1.806
0.2	1.0E-03	82.13	0.224	1.624	0.255	1.626
0.2	1.0E-03	77.31	0.322	1.428	-	-
0.2	1.0E-03	73.03	0.381	1.248	0.391	1.249
0.2	1.0E-03	68.94	0.411	1.068	-	-
0.2	1.0E-03	64.84	0.417	0.887	0.422	0.882
0.2	1.0E-03	60.56	0.399	0.707	-	-
0.2	1.0E-03	55.85	0.357	0.526	0.362	0.524
0.2	1.0E-03	50.24	0.288	0.346	-	-
0.2	1.0E-03	42.34	0.198	0.180	0.199	0.181
0.2	1.0E-04	90	0.000	1.486	0.000	1.470
0.2	1.0E-04	82.13	0.185	1.338	0.185	1.338
0.2	1.0E-04	77.31	0.265	1.176	-	-
0.2	1.0E-04	73.03	0.314	1.028	0.318	1.018
0.2	1.0E-04	68.94	0.339	0.880	-	-
0.2	1.0E-04	64.84	0.343	0.731	0.349	0.728
0.2	1.0E-04	60.56	0.329	0.582	-	-
0.2	1.0E-04	55.85	0.294	0.434	0.297	0.429
0.2	1.0E-04	50.24	0.237	0.285	-	-
0.2	1.0E-04	42.34	0.163	0.149	0.165	0.150

Table Number **3-6b** **continued**

VH Analysis - CoV = 15%

z/D	P_F	δ_{LS} (˚)	Equation		MC	
			$H/s_u.D$	$V/s_u.D$	$H/s_u.D$	$V/s_u.D$
0.2	3.0E-05	90	0.000	1.339	0.000	1.334
0.2	3.0E-05	82.13	0.166	1.202	0.166	1.202
0.2	3.0E-05	77.31	0.238	1.057	-	-
0.2	3.0E-05	73.03	0.282	0.924	0.282	0.900
0.2	3.0E-05	68.94	0.304	0.790	-	-
0.2	3.0E-05	64.84	0.309	0.658	0.316	0.661
0.2	3.0E-05	60.56	0.295	0.523	-	-
0.2	3.0E-05	55.85	0.265	0.390	0.266	0.385
0.2	3.0E-05	50.24	0.213	0.256	-	-
0.2	3.0E-05	42.34	0.147	0.134	0.149	0.136

Table Number **3-6c**

VH Analysis - CoV = 20%

z/D	Pf	δ_{LS} (˚)	Simplified		MC	
			$H/s_u.D$	$V/s_u.D$	$H/s_u.D$	$V/s_u.D$
0.2	0.07	90	0.000	2.371	0.000	2.370
0.2	0.07	82.13	0.295	2.134	0.295	2.134
0.2	0.07	77.31	0.423	1.876	-	-
0.2	0.07	73.03	0.500	1.640	0.504	1.610
0.2	0.07	68.94	0.540	1.403	-	-
0.2	0.07	64.84	0.548	1.166	0.557	1.163
0.2	0.07	60.56	0.524	0.929	-	-
0.2	0.07	55.85	0.469	0.692	0.476	0.688
0.2	0.07	50.24	0.378	0.455	-	-
0.2	0.07	42.34	0.260	0.237	0.261	0.237
0.2	0.01	90	0.000	1.799	0.000	1.795
0.2	0.01	82.13	0.224	1.619	0.224	1.620
0.2	0.01	77.31	0.321	1.424	-	-
0.2	0.01	73.03	0.380	1.244	0.389	1.243
0.2	0.01	68.94	0.410	1.064	-	-
0.2	0.01	64.84	0.415	0.884	0.422	0.881
0.2	0.01	60.56	0.398	0.705	-	-
0.2	0.01	55.85	0.356	0.525	0.361	0.522
0.2	0.01	50.24	0.287	0.345	-	-
0.2	0.01	42.34	0.197	0.180	0.198	0.180
0.2	1.0E-04	90	0.000	0.861	0.000	0.881
0.2	1.0E-04	82.13	0.107	0.775	0.108	0.780
0.2	1.0E-04	77.31	0.153	0.681	-	-
0.2	1.0E-04	73.03	0.182	0.595	0.186	0.594
0.2	1.0E-04	68.94	0.196	0.509	-	-
0.2	1.0E-04	64.84	0.199	0.423	0.197	0.412
0.2	1.0E-04	60.56	0.190	0.337	-	-
0.2	1.0E-04	55.85	0.170	0.251	0.167	0.242
0.2	1.0E-04	50.24	0.137	0.165	-	-
0.2	1.0E-04	42.34	0.095	0.086	0.093	0.084

Table Number **3-7**

VH Fragility - CoV = 15%

δ_{LS} (˚)	P_f = 3E-5			P_f = 0.07			Fragility	I_F
	$H/s_u.D$	$V/s_u.D$	$R/s_u.D$	$H/s_u.D$	$V/s_u.D$	$R/s_u.D$		
90	0.000	1.339	1.339	0.000	2.619	2.619	1.280	0.51
82.13	0.166	1.202	1.213	0.326	2.357	2.379	1.166	0.51
77.31	0.238	1.057	1.083	0.467	2.073	2.125	1.041	0.51
73.03	0.282	0.924	0.966	0.553	1.811	1.894	0.927	0.51
68.94	0.304	0.790	0.846	0.597	1.550	1.661	0.815	0.51
64.84	0.309	0.658	0.727	0.605	1.288	1.423	0.696	0.51
60.56	0.295	0.523	0.600	0.579	1.026	1.178	0.578	0.51
55.85	0.265	0.390	0.472	0.518	0.764	0.923	0.452	0.51
50.24	0.213	0.256	0.333	0.418	0.502	0.653	0.320	0.51
42.34	0.147	0.134	0.199	0.287	0.262	0.389	0.190	0.51